University of Alberta

Substituted Cysteine Accessibility Method Analysis of the C-terminal Half of Human Concentrative Nucleoside Transporter 3 (hCNT3)

by

Ras Mulinta

A thesis submitted to the Faculty of Graduate Studies and Research
in partial fulfillment of the requirements for the degree of

Doctor of Philosophy

Department of Physiology

Winter 2010
Edmonton, Alberta

Examining Committee

Dr. James D. Young, Physiology

Dr. Carol E. Cass, Oncology

Dr. Christopher Cheeseman, Physiology

Dr. Joseph Casey, Physiology

Dr. Marek Duszyk, Physiology

Dr. Scott Landfear, Oregon Health & Science University, Department of Molecular Microbiology & Immunology

Abstract

Concentrative nucleoside transporter (CNT) proteins mediate active nucleoside transport using the electrochemical gradient of the coupling cation. The molecular mechanisms underlying interactions with both nucleosides and cations were investigated by heterelogous expression of recombinant CNT family members in *Xenopus* oocytes. Substituted cysteine accessibility method (SCAM) analysis in combination with radioisotope flux assays and electrophysiological studies revealed novel topological features within the C-terminal half of human (h) CNTs and identified residues of functional importance.

The hCNT (SLC28) protein family is represented by three members. hCNT1 and hCNT2 are pyrimidine nucleoside- and purine nucleoside-selective, respectively, while hCNT3 transports both pyrimidine and purine nucleosides. hCNT1 and hCNT2 function exclusively as Na^+-coupled nucleoside transporters and share a 1:1 Na^+:nucleoside stoichiometry. Belonging to a CNT subfamily phylogenetically distinct from hCNT1/2, hCNT3 utilizes electrochemical gradients of Na^+, Li^+ or H^+ to drive nucleoside transport and exhibits 2:1 Na+:nucleoside and 1:1 H^+:nucleoside stoichiometries. Non-mammalian H^+-coupled CNT family members that have been functionally characterized include NupC from *Escherichia coli*. Both Na^+ and H^+ activate CNTs through mechanisms to increase nucleoside apparent binding affinity.

Multiple alignments of CNT family members reveal strong sequence similarities within the C-terminal halves of the proteins, and hCNT1/3 and other chimeric studies have demonstrated that this region determines both nucleoside

and cation interactions with the transporter. In hCNT3, access of *p*-chloromercuribenzene sulfonate (PCMBS) to introduced cysteine residues within putative transmembrane segments (TMs) 7, 8, 9 and 11A revealed novel discontinuous regions within α-helical structures, whereas putative TMs 10, 11, 12 and 13 exhibited conventional α-helical characteristics. Putative TM 11A, which contains the highly conserved CNT family motif (G/A)XKX3NEFVA(Y/M/F), was shown to be membrane associated and, most likely, membrane spanning, TMs 7-11 having a reversed orientation in the membrane compared to previous models of CNT topology. Furthermore, putative TMs 7, 8, 9, 11A and 12 were shown to contribute functional and structural elements to a common nucleoside/cation translocation pore.

These studies, which were extended to TMs 7 and 8 of hCNT1 and to corresponding TMs of *E. coli* NupC, provide important structural and functional insights into the nature of CNT nucleoside/cation cotransport.

Acknowledgements

First and foremost, I would like to thank my supervisor, Dr. James Young, for giving me the opportunity to study in his laboratory and for his continuing guidance and academic mentorship. I also thank past and current members of his laboratory, Amy Ng, Mabel Ritzel, Drs. Sylvia Yao, Kyla Smith and Melissa Slugoski, all whom, befriended, taught and navigated me through the field of nucleoside transporters. I am grateful to Dr. Carol Cass for serving on my supervisory committee and supporting our collaborative research. I am also grateful to Professor Stephen Baldwin for his contributions to our joint manuscripts. I thank Drs. Chris Cheeseman and Joseph Casey for also serving on my supervisory committee and for providing a conducive and open environment for scientific discussion. Additionally, my gratitude extends to Drs. Edward Karpinski and Elaine Leslie, who served on my candidacy examination committee, and to Drs. Marek Duszyk and Scott Landfear, who serve on my thesis defense committee.

I would like to extend my thanks also to the other professors, staff and graduate students of the Department of Physiology and the Membrane Protein Research Group for making my Ph.D. program memorable.

Special mention goes to Mabel and Gary Ritzel for their help and generosity. Last but not least, I would like to acknowledge and express my sincere appreciation to my immediate family members - Mum, Dad, Aida, Andrew and Mike, for their endless kind encouragement, love and support.

Tables of Contents

List of Tables

List of Figures

List of Nomenclature, Abbreviations and Symbols

2-CdA	cladribine
araA	adenine arabinoside
araC	cytarabine
At	*Arabidopsis thaliana*
ATP	adenosine triphosphate
AZT	zidovudine
BLAST	basic logic alignment search tool
Ca	*Candida albicans*
capecitabine	5'-deoxy-5-*N*-[(pentoxy)carbonyl]cytidine
cDNA	complementary deoxyribonucleic acid
C-	Cysteine-less
Ce	*Caenorhabditis elegans*
ChCl	choline chloride
cib	concentrative, insensitive to NBMPR, broadly selective
cif	concentration, insensitive to NBMPR, formycin B-transporting
cit	concentration, insensitive to NBMPR, thymidine-transporting
cladribine	2'-chloro-2'-deoxyadenosine; 2-CdA
clofarabine	2-chloro-9-(2'-deoxy-2'-fluoro-β-D-arabinofuranosyl)adenine
CNT	concentrative nucleoside transporter
cs	concentrative, sensitive to NBMPR
CSF	colony stimulating factor
csg	concentrative, sensitive to NBMPR, guanosine-transporting

cytarabine	1-β-D-arabinofuranosyl cytosine; araC
ddC	zalcitabine
ddI	didanosine
didanosine	2', 3'-dideoxyinosine; ddI
dFdC	gemcitabine
DNA	deoxyribonucleic acid
ei	equilibrative, insensitive
ENT	equilibrative nucleoside transporter
es	equilibrative sensitive
EST	expressed sequence tag
F-araA	fludarabine
FIAU	fialuridine
fialuridine	1-(2-deoxy-2-fluoro-β-D-arabinofuranosyl)-5-iodouracil; FIAU
g	gram
GABA	γ-aminobutyric acid
gemcitabine	2', 2'-difluorodeoxycytidine; dFdC
GFP	green fluorescent protein
h	human
HEPES	4-(2-hydroxyethyl)-1-piperazineethanesulfonic acid
hf	hagfish
HIV	human immunodeficiency virus
IC_{50}	inhibitor concentration at half-maximal unidirectional flux; apparent inhibition constant

I_{max}	maximum current
I-V	current-voltage
K_{50}	permeant concentration at half-maximal unidirectional flux; apparent affinity for cation
K_m	permeant concentration at half-maximal unidirectional flux; apparent affinity for permeant
l	liter
lamivudine	2', 3'-dideoxy-3'-thiacytidine
Ld	*Leishmania donovi*
m	mouse
M	molar
MDCK	Madin-Darby canine kidney
MDR	multidrug resistance
MES	2-(*N*-morpholino)ethanesulfonic acid
MFS	major facilitator superfamily
min	minute
mM	millimolar
mol	mole
mRNA	messenger ribonucleic acid
MTS	methanethiosulfonate
MTSEA	2-aminoethyl methanethiosulfonate hydrobromide
MTSES	2-sulfonatoethyl methanethiosulfonate sodium salt
MTSET	2-(trimethylammonium) ethyl methanethiosulfonate
mV	millivolts
NBMPR	nitrobenzylthioinosine; nitrobenzylmercaptopurine riboside

nd	not determined
NHS	nucleoside:H^+ symporter
NT	nucleoside transporter
NUP	nucleoside permease
OAT	organic anion transporter
OCT	organic cation transporter
PCMBS	*p*-chloromercuribenzene sulfonate
PCR	polymerase chain reaction
Pf	*Plasmodium falciparum*
pK	pig kidney
PKC	protein kinase C
PMA-RE	phorbol myristate acetate response element
RNA	ribonucleic acid
RT-PCR	reverse transcriptase polymerase chain reaction
r	rat
rb	rabbit
ribavirin	1-(β-D-ribofuranosyl)-1*H*-1,2,4-triazole-3-carboxamide; guanosine analog with 1, 2, 4-triazole-3-carboxamide group at C-1' in place of pyrimidine group
SCAM	substituted cysteine accessibility method
SDS	sodium dodecyl sulphate
SE	standard error of the fitted estimate
s	second
SEM	standard error of the mean

serotonin	5-hydroxytryptamine; 5-HT
SGLT	sodium glucose transporter
SNP	single nucleotide polymorphism
SPNT	sodium-dependent purine nucleoside transporter
sulfo-NHS-LC-biotin	sulfosuccinimidyl-6-(biotinamido) hexanoate
Tb	*Trypanosoma brucei*
Tg	*Toxoplasma gondii*
TM	transmembrane domain
Tsx	T6 (six) phage receptor
tubercidin	7-deazaadenosine
V	volt
V_h	holding potential
V_m	membrane potential
V_{max}	maximum transport rate
V_t	test potential
YFP	yellow fluorescent protein
zalcitabine	2', 3'-dideoxycytidine; ddC
zidovudine	3'-azido-3'-deoxythymidine; AZT
^oC	degrees Celcius
Ω	ohms

Chapter 1:
General Introduction

Nucleoside Transport

Nucleosides are an important class of molecules involved in various biochemical and physiological processes. Naturally occurring nucleosides include the purine nucleosides adenosine, guanosine and inosine, and the pyrimidine nucleosides uridine, cytidine and thymidine (Fig. 1-1). Nucleosides are the metabolic precursors of nucleotides, which include energy-rich compounds such as ATP, and which are essential precursors in the formation of DNA and RNA. Some cells which lack glucose transport activity, for example adult pig erythrocytes, embryonic chicken erythrocytes and adult chicken erythrocytes, use purine nucleosides in place of glucose as their primary *in vivo* source of metabolic energy (1-4). The purine nucleoside adenosine acts as a signaling molecule which, by binding to cell-surface purinergic receptors, regulates numerous physiological processes, including the cardiovascular function (5-14), inflammation (15, 16), lipolysis (17), platelet aggregation (18,19), renal function (20, 21), nociception (22, 23) and neurotransmission and neuromodulation (24-27).

Since nucleosides are hydrophilic and therefore unable to passively diffuse across the plasma membrane, specialized nucleoside transporter proteins (NTs) are required to mediate their passage into or out of cells and between intracellular compartments (27-34). Metabolically, NTs are central elements of purine and pyrimidine nucleoside salvage pathways (27-34), which are energetically more favourable than *de novo* purine and pyrimidine biosynthesis, and thus have key roles in nucleoside and nucleotide homeostasis (35-37). Furthermore, some cell types are deficient in purine *de novo* biosynthetic pathways, and are thus entirely dependent upon imported nucleosides (and nucleobases) for purine nucleotide synthesis. In mammals, for example, these include bone marrow cells (38), erythrocytes (39, 40), intestinal enterocytes (41), leukocytes and certain brain cells (42). Similarly, nucleoside salvage pathways are crucial to protozoan and helminth parasites that lack purine *de novo* biosynthetic capability (43-48). Major sources of nucleosides are the diet, reabsorption from the kidney and production by the liver (38, 49-53).

NTs are also involved in providing cytosolic nucleosides to intracellular organelles (30). Conversely, NTs prevent excess accumulation of nucleotide breakdown products by releasing nucleosides from cells and intracellular compartments. This is especially important in lysosomes which are responsible for the intracellular degradation of nucleic acids into nucleosides (54). NTs, moreover, determine the levels of extracellular free nucleosides in the general circulation and, therefore, modulate their physiological effects. For example, NTs regulate the concentration of adenosine available to cell surface purinoreceptors and thus play key roles in the many adenosine-regulated physiological processes mentioned above (28, 31). Clinically, NTs mediate cellular uptake of anticancer and antiviral nucleoside drugs (Fig. 1-2).

Nucleoside Transporter Proteins

In the past 30 years, various nucleoside transport processes have been described functionally in both eukaryotic and prokaryotic cells. The advent of molecular cloning strategies and associated heterologous expression systems combined with genome sequencing and bioinformatic studies have identified a diversity of structurally distinct nucleoside transport proteins. At least six transporter families have been identified that contain members which transport nucleosides. In human and other mammalian cells, these include the equilibrative nucleoside transporter (ENT), concentrative nucleoside transporter (CNT), organic cation transporter (OCT) and organic anion transporter (OAT) families, of which ENTs and CNTs are of primary importance. In lower eukaryotes and prokaryotes, they include the nucleoside:H^+ symporter (NHS), Tsx channel, uracil/allantoin permease and nucleoside permease (NUP) families. Each family has multiple members.

The research presented in this thesis focuses primarily on human CNTs, but also includes an investigation of a prokaryotic CNT family member (NupC) of the bacterium *Escherichia coli*. The remainder of this Introduction centers on CNTs and, more briefly, on ENTs.

Equilibrative nucleoside transporter (ENT) family

Most mammalian cells possess low-affinity, equilibrative nucleoside transport processes, now known in humans to be mediated by members of the SLC29 protein family (reviewed in 4, 28, 34, 55). Initially, equilibrative transport processes were classified on the basis of sensitivity to inhibition by nitrobenzylthioinosine (nitrobenzylmercaptopurine riboside; NBMPR) (Fig. 1-3) as either *es* (equilibrative sensitive) or *ei* (equilibrative insensitive) (31, 55). Subsequently, the archetypal *es* transporter present in human (h) erythrocytes (56, reviewed in 55) was cloned from human placenta and designated as hENT1 (57, reviewed in 55) (Fig. 1-4). Subsequently, cDNA clones encoding the *ei*-type transporter, hENT2, were isolated from the same source by virtue of homology with hENT1 (58, reviewed in 55). Parallel molecular cloning of hENT2 was also achieved by a functional complementation approach (59, reviewed in 55). Recently, two additional human members of the family were cloned and characterized, hENT3 and hENT4 (60 – 67, reviewed in 55). To date, no prokaryote or archeal members of the ENT family have been identified (60, reviewed in 55). A phylogenetic diagram showing the relationships between selected ENT family members is shown in Fig. 1-5.

ENTs are present in most, possibly all, mammalian cell types, and play a central role in absorption, distribution and elimination of nucleosides and nucleoside drugs (27, reviewed in 55). ENT1/2 (along with CNTs) account for the major nucleoside uptake processes of human and other mammalian cells (55). ENT3 possibly corresponds to a previously described low-affinity transport system for nucleosides in lysosomes (54, 55), while ENT4 functional activity remains to be demonstrated. All have been produced and studied in a variety of heterologous expression systems, including *Xenopus* oocytes, yeast and mammalian cells (55, 68). Since the initial molecular cloning of hENT1, homologs of mammalian ENTs have been identified in an increasing diversity of other eukaryotic organisms, including insects, nematodes, protozoa, fungi and plants (Fig. 1-5) (55). However, the majority of these proteins remain functionally uncharacterized. Of the mammalian transporters, ENT1 and ENT2 are the best studied and have been confirmed to function as

bidirectional facilitated diffusion systems. Some other ENTs, however, such as those in *Leishmania* and *Trypanosoma* kinetoplastid protozoa, are active, proton-linked transporters (60, 69, reviewed in 55). Unlike ENT1 and ENT2, ENT3 and ENT4 are activated under acidic conditions, and it remains to be determined whether or not this is associated with proton/nucleoside co-transport (55). All four human ENTs (hENT1-4) transport adenosine (Fig. 1-4), but differ in their abilities to transport other nucleosides and nucleobases (Table 1-1) (55). hENT4 additionally functions as a polyspecific organic cation transporter (63, 65, 66). In general, ENTs have relatively low apparent affinities for their nucleoside permeants, 0.1 – 3.0 mM range (Table 1-2) (55). ENTs from *T. brucei*, however, show high (micromolar) apparent affinities for their permeants (Table 1-2) (55).

Concentrative nucleoside transporter (CNT) family

Concentrative, NBMPR-insensitive and cation-dependent nucleoside transport processes were initially observed in rat, rabbit and bovine renal brush-border membrane vesicles (70-77). Subsequent studies established that transport was mediated by members of the concentrative nucleoside transporter (CNT) family (27-32, 34, 78-80). CNT family members have been identified and characterized in various eukaryote and prokaryote species. A phylogenetic diagram showing the relationships between selected CNT family members is shown in Fig. 1-6.

Mammalian CNT family members

In addition to equilibrative nucleoside transport processes, flux studies of mammalian tissues and cultured cell lines also indicated the presence of concentrative mechanisms of nucleoside transport. This functional activity was both Na^+-dependent and NBMPR-insensitive (70-75, 81). Permeant selectivity was studied using radiolabeled nucleosides in mouse intestinal epithelial cells (82). It was shown that the uptake of formycin B, a non-metabolizable inosine analog, was not inhibited by the presence of thymidine, and the corresponding uptake of thymidine was not

inhibited by formycin B (82). The two transport systems responsible for these fluxes were designated N1 or *cif* (concentrative, insensitive to NBMPR, formycin B-transporting) and N2 or *cit* (concentrative, insensitive to NBMPR, thymidine-transporting), respectively. Additional permeants for *cif* included the purine nucleosides guanosine and inosine and, for *cit*, the pyrimidine nucleoside cytidine (82). Subsequent studies described the existence of the *cit* system in rabbit intestinal mucosa (83) and in guinea pig blood-brain and blood-CSF barriers (84), while the *cif* system was found, for example, in murine splenocytes (85), murine and rat peritoneal macrophages (86), rat hepatocytes (87) and L1210 murine leukemia cells (88). In addition to mouse intestinal epithelial cells (82), coexistence of the *cit* and *cif* systems has been demonstrated in rabbit (75), rat (76) and bovine (77) renal brush border membrane vesicles, rabbit intestinal brush border membrane vesicles (74) and guinea pig intestinal enterocytes (81). Both the *cit* and *cif* systems exhibited an apparent 1:1 Na^+:nucleoside coupling stoichiometry (29, 73, 74, 78).

A third concentrative system was later described, and referred to as the N3 or *cib* (concentrative, NBMPR-insensitive, broadly selective) nucleoside transport process. These studies included experiments in human (89), rat (90) and rabbit renal (75) and rabbit intestinal (74) brush border membrane vesicles, guinea pig intestinal epithelial cells (81) and mouse peritoneal macrophages (91). It was, however, difficult to differentiate these relatively low *cib*-type activities from possible coexistence of systems *cit* and *cif*. The first unambiguous demonstrations of *cib*-type transport activity occurred with isolated leukemic blasts (92), human colon cancer Caco-2 cells (93) and in *Xenopus* oocytes injected with rat jejunum mRNA (94). Subsequently, it was shown in rabbit choroid plexus and rat microglia that the *cib* system differed from the *cif* and *cit* systems not only in permeant selectivity, but also by having an apparent Na^+:nucleoside stoichiometry of 2:1 (versus 1:1 for *cif* and *cit*) (95, 96).

Three additional minor concentrative mechanisms have also been observed functionally in some cells, and have been designated N4, N5 (or *cs*- concentrative, sensitive to NBMPR) and *csg* (concentrative, sensitive to NMBPR, guanosine-transporting) (89, 93, 97). Considered to be a subtype of the *cit* system, N4 was

identified in counter-flux experiments in human renal brush border membrane vesicles, which demonstrated that guanosine, but not inosine, was able to stimulate radiolabeled thymidine uptake (89, 97, 98). The N5 transport process accepts adenosine analogs as permeants and has only been observed in human leukemic cells (93, 99). The guanosine selective *csg* transport process has only been observed in cultured human NB4 acute promyelocytic and murine L1210 leukemic cells (97, 100).

The three major *cit*, *cif* and *cib* concentrative nucleoside transport processes have been identified at the molecular level. The corresponding proteins are designated CNT1 (*cit*), CNT2 (*cif*) and CNT3 (*cib*) (Fig. 1-4). In humans, CNT1/2/3 are designated as the SLC28 family of proteins. No further functional characterization of the three minor systems has been reported in the literature and, the molecular identity of the corresponding proteins is unknown. Identified mammalian members of the concentrative nucleoside transporter family are shown in Table 1-1.

CNT1

The first mammalian member of the CNT family of proteins was identified by expression screening of a size-selected cDNA library from rat jejunum in *Xenopus* oocytes (101). Rat CNT1 (rCNT1) consists of 648 amino acid residues with its hydrophilic N-terminal and glycosylated C-terminal domains located on the intracellular and extracellular faces of the membrane, respectively (101-103). Within the extracellular C-terminal region, two sites of glycosylation have been identified (102, 103). hCNT1, the first CNT to be cloned from human tissues, was subsequently isolated from human kidney by hybridization/RT-PCR cloning and functional expression in *Xenopus* oocytes (104). hCNT1 is 650 amino acids in length and 83% identical in sequence to rCNT1 (104). hCNT1 maps to chromosome 15q25-26 (104). Radiotracer functional characterization in *Xenopus laevis* oocytes and in transiently transfected mammalian COS-1 cells showed rCNT1 and hCNT1 to exhibit Na^+-dependent *cit*/N2-type pyrimidine nucleoside-selective characteristics (101, 104-106). Electrophysiological studies in *Xenopus* oocytes also found h/rCNT1-mediated

transport to be pyrimidine nucleoside-selective in a Na^+- and voltage-dependent manner (107-109).

The purine nucleoside adenosine was also found to be a permeant for both hCNT1 and rCNT1 (104, 106, 109, 110). Kinetic analysis of rCNT1-mediated adenosine transport demonstrated that adenosine binds with high affinity to the transporter, but was transported at low rates (110). As such, adenosine may regulate CNT1 activity *in vivo* by binding to the transporter and inhibiting the transport of pyrimidine nucleosides (111). A summary diagram comparing the permeant selectivity of hCNT1 to those hCNT2 and hCNT3 is shown in Fig. 1-4.

Apparent K_m values for hCNT1-mediated nucleoside transport in various heterologous expression systems are compared to those of other hCNT family members in Table 1-3. For uridine transport in oocytes, the apparent affinity was 45 μM (104) and hCNT1 was partially inhibited by phloridzin (IC_{50} value of 0.2 mM) which putatively exerted its effect by binding after Na^+ to a site different from that of uridine (109). For h/rCNT1-mediated transport, the relationship between nucleoside flux and Na^+ concentration was hyperbolic, with an apparent K_{50} value of ~ 10 mM and calculated Hill coefficient consistent with a 1:1 Na^+:nucleoside stoichiometry (105, 110). Electrophysiological charge/flux ratio studies using *Xenopus* oocytes determined directly that the Na^+:nucleoside coupling ratio of hCNT1 was 1:1 (109). Measurements of hCNT1 presteady-state currents determined that the fraction of the membrane field sensed by Na^+ was 61%, that the average number of transporters present in the oocytes plasma membrane was 6.8×10^{10} per cell, and that the turnover rate was 9.6 molecules of uridine transporter per second at -50 mV (109).

In addition to physiological pyrimidine nucleosides (and adenosine), h/rCNT1 produced in *Xenopus* oocytes were found to mediate uptake of the antiviral nucleoside analogs, AZT (Zidovudine) and ddC (Zalcitabine) (101, 104, 109, 112) (Fig. 1-2). Antineoplastic nucleoside chemotherapeutic agents that are also permeants of hCNT1 include dFdC (gemcitabine) (108, 111, 113, 114) and the uridine analogs 5-fluorouridine, 2'-deoxyuridine, 5-fluoro-2'-deoxyuridine and 5-fluoro-5'-deoxyuridine (108, 109, 115) (Fig. 1-2). Although, 5-deoxy-5'-flourouridine is a hCNT1 permeant, the parent compound capecitabine and its metabolite 5'-fluorouracil

are not (116). 2', 3'-Dideoxy-3'-thiacytidine (lamivudine) was shown to be a poor inhibitor of hCNT1-mediated uridine uptake (117). Although hCNT1 exhibits high-affinity adenosine transport that occurs at low rates, transport of the anticancer adenosine analogs 2-CdA and F-araA was not detected in oocyte or human cell line flux studies (114, 115); however, 2-CdA did induce inward currents in hCNT1-producing *Xenopus* oocytes (109). Similarly, araC (cytarabine) was demonstrated to be a poor permeant of hCNT1 in radiolabeled flux assays (117), but inward currents were apparent in electrophysiology experiments (109).

CNT1 is found in highly differentiated tissues such as epithelial cells of the kidney and intestine, as well as liver, placenta and brain (118, 119, 120). Northern blot analysis revealed rCNT1 transcripts in intestinal and renal tissues (101). rCNT1 protein was present only in the brush border membrane of jejunum and renal cortical tubules (103). Similarly, in human tissues, hCNT1 was localized apically in dudodenum enterocytes and kidney proximal tubular cells (119). An apical location in epithelial cells was also evident for both hCNT1-CFP (cyan fluorescent protein) (121) and rCNT1-GFP (green fluorescent protein) (122) expressed in renal MDCK cells. A wide variation in expression of hCNT1 mRNA was noted in kidney from different individuals, as well as particularly low levels in kidney tumor samples (123). The presence of rCNT1 protein was reported in bile canalicular membranes in rat liver (103) and of hCNT1 protein in human hepatocytes (119). mRNA for rCNT1 was identified throughout the brain, including cerebral cortex, cerebellum, hippocampus, striatum, brain stem, superior colliculus, posterior hypothalamus and choroid plexus (124).

rCNT1 was originally predicted by hydropathy plots to contain 14 TMs with intracellular N- and C-termini (101). However, experiments using endoglycosidase F treatment of rCNT1 produced in *Xenopus* oocytes revealed that the transporter was glycoslyated (103). Since the only two potential sites of *N*-linked glycosylation in rCNT1 are located at the C-terminus, the 14 TM model with an intracellular C-terminus was likely incorrect. Introduction of *N*-glycosylation sites at the N-terminus and in the loop between putative TMs 4 and 5 did not alter the glycosylation status of the protein and, together with studies using predictive algorithims and site-specific

antibodies, led to a revised 13 TM topology model for CNT1 which is depicted in Fig. 1-7 (103).

CNT2

The second mammalian member of the CNT family to be identified was isolated from rat liver and jejunum by expression and homology cloning in *Xenopus* oocytes (110, 125): it was named rCNT2 (SPNT) and was 659 amino acids in length. The human homolog, hCNT2, was later cloned from human kidney and intestine and is a 658 residue protein (126, 127). hCNT2 shares 83% amino acid sequence identity with rCNT2, with the greatest divergence towards the N-terminus, and 72% sequence identity with hCNT1 (126, 127). Subsequently, CNT2 homologs from mouse and rabbit were also cloned and designated mCNT2 (128) and rbCNT2, respectively (129). Electrophysiological charge/flux ratio studies using *Xenopus* oocytes determined that the Na^+:nucleoside coupling ratio of hCNT2, like hCNT1, was 1:1 (109). hCNT2 maps to chromosome 15q15 (127).

Functional studies in *Xenopus* oocytes were consistent with *cif*/N1-type functional activity and demonstrated h/r/rbCNT2 Na^+-dependent transport of the purine nucleosides adenosine, inosine and guanosine and, as well, uridine (110, 126, 127, 129-131). hCNT2 transported inosine and uridine with apparent K_m values of 4.5 and 80 μM, respectively (126). Table 1-3 compares these K_m values to those of other CNT family members.

hCNT2 was also demonstrated to transport uridine analogs such as 5-fluorouridine, 5-fluoro-2'-deoxyuridine and 2'-deoxyuridine (115, 132), as well as 2'-deoxyadenosine (126) and, at low levels, ddI (127). Although adenosine is a substrate for hCNT2, its chemotherapeutic analogs such as 2-CdA and F-araA were poor permeants (115, 132), and AZT and ddC were also not transported (111). Interestingly, while hCNT2 did not transport 2', 3'-dideoxyadenosine, araA, F-araA, 2-CdA and ddI, its rat homolog rCNT2 did (120, 131, 133, 134).

CNT2 transcripts were found in numerous tissue types, including kidney, intestine, liver, heart, skeletal muscle, pancreas, spleen, epididymis, brain, prostate,

cervix, placenta and lung (123, 25-127, 129, 135). Also, it was shown that transcript levels differed between individuals (123). Tagging of rCNT2 with GFP revealed localization primarily to the apical surface of MDCK cells, with some basolateral staining also visible (122, 136). In rat liver, rCNT2 was localized to the basolateral membrane (119). Studies with human tissues located hCNT2 to the apical membranes of the duodenum and kidney proximal tubule (119).

Initial hydropathy analyses of rCNT2 predicted 14 TM domains with both intracellular C- and N-termini (125). In line with rCNT1, this was later revised to 13 TMs as shown in Fig. 1-7 (103).

rCNT2 has three putative sites of glycosylation, but only two, Asn606 and Asn625, are glycosylated, while the third, Asn603, is not (136). All three residues are located in the extracellular C-terminal tail (136). The sites of glycosylation are conserved across species, but not essential for function or polarized trafficking of rCNT2 in stably transfected MDCK cells (136).

CNT3

hCNT3 was identified using BLAST searches of CNT sequences which found overlapping human expressed sequence tags (ESTs) from mammary gland and colon adenocarcinoma (137). Full-length hCNT3 cDNA was cloned by RT-PCR from mammary gland and differentiated HL-60 cells (137). The encoded protein was 691 amino acids in length, and 48% and 47% identical to hCNT1 and hCNT2, respectively (137). Its molecular weight was calculated to be 77 kDA, and the gene mapped to chromosome 9q22.2 (137, 138). Molecular cloning of the murine counterpart (mCNT3) was achieved in a similar manner from liver using ESTs identified from mouse mammary gland (137). The upstream promoter region of the hCNT3 gene expresses a response element for phorbol myristate acetate (ester) (PMA-RE) (137). In HL-60 cells, phorbol ester treatment causes cell differentiation, expression of hCNT3 mRNA and appearance of *cib*-type functional activity (137).

Within the CNT family, and as shown in Fig. 1-6, h/mCNT3 and a closely related transporter from hagfish (hfCNT), form a separate subfamily distinct from that of CNT1 and CNT2 (137, 139).

In a study examining 270 DNA samples, 56 hCNT3 SNPs were identified, of which 16 were in the coding region (140). Ten variants were nonsynonymous. Upon expression in *Xenopus* oocytes, however, all but one revealed wild-type hCNT3-like Na^+-dependent uptake of radiolabeled thymidine and inosine. The exception was G367R, which exhibited only ~ 20% of the uptake seen with hCNT3 (140). In a separate study of 96 DNA samples, 16 SNPs were identified: three of the five coding region variants were nonsynonymous, but retained wild-type hCNT3-like nucleoside transport activity (141). Both these studies suggest a high degree of conservation within the hCNT3 gene. SNPs are also infrequent in hCNT1 and hCNT2. Characterization of 15 nonsynonymous variants in hCNT1 identified only two which were nonfunctional (142). All six of the nonsynonymous variants that have been identified in hCNT2 were functional (143). These findings suggest that all three hCNTs are under high selective pressure and, therefore, individually important.

Xenopus oocytes producing recombinant hCNT3 showed concentrative uptake of radiolabelled nucleosides that was NBMPR-insensitive and Na^+-dependent, findings that paralleled results of electrophysiological experiments using the two-electrode voltage-clamp technique (137). h/mCNT3 were found to transport both pyrimidine and purine nucleosides, but not the nucleobases uracil and hypoxanthine (137, 138). This permeant selectivity was consistent with previous characterization of the native *cib*/N3-type transport process. Purine and pyrimidine nucleosides were transported by hCNT3 with similar kinetic efficiencies, and apparent K_m values ranged between 15 and 53 μM for all of the permeants tested (Table 1-3) (137). Weak inhibition of recombinant hCNT3 transport activity by phloridzin was observed in Cos7L cells (138) and *Xenopus* oocytes (109), with reported IC_{50} values of 0.17 and 0.3 mM, respectively.

Unlike hCNT1/2, the relationship between uridine uptake and Na^+ concentration was sigmoidal for both hCNT3 and mCNT3 (137). In good agreement with *cib* type transport in choroid plexus and microglia (96, 144), the Hill coefficient

for both hCNT3 and mCNT3 was consistent with a 2:1 Na^+:nucleoside coupling ratio (137, 138, 145). Direct measurement of the Na^+:nucleoside coupling ratio for hCNT3 by comparing uridine-induced currents and radiolabeled uridine uptake in the same individual oocytes confirmed a 2:1 stoichiometry (109, 137). In addition to Na^+, and unlike hCNT1/2, h/mCNT3 can also use H^+ as the driving cation for cotransport (109). Unlike Na^+, however, the H^+:nucleoside coupling ratio is 1:1. A recent study has found that H^+ induces a specific conformational state of hCNT3, whereby the transporter acquires sensitivity to inhibition by the mercurial agent *p*-chloromercuribenzene sulfonate (PCMBS) (146). As described below, Na^+- and H^+-activated forms of hCNT3 also exhibit different permeant selectivities for nucleosides and nucleoside drugs (147).

Na^+-coupled hCNT3 transports a broad range of both pyrimidine and purine antineoplastic and antiviral drugs (137). These include the pyrimidine nucleoside analogs 5-fluorouridine, 5-fluoro-2'-deoxyuridine, 3-deazauridine, zebularine, dFdC, AZT and ddC and the purine nucleoside analogs cladribine, fludarabine, clofarabine, ddI and ribavirin (27, 111, 137, 145). H^+-coupled hCNT3, in contrast, does not transport AZT or ddC, and exhibits a narrow uridine-preferring selectivity for physiological nucleosides (147).

hCNT3 transcripts were found to be more ubiquitously expressed than hCNT1/2, with highest abundance in mammary gland, pancreas, bone marrow, trachea, duodenum and the lowest abundance in kidney, liver, lung, placenta, prostrate, testis and regions of the brain and heart (137). Transcripts were also found in fetal tissues and, in low amounts, in cultured cell lines such as K562, HeLa and undifferentiated HL-60 cells (137). In the kidney, hCNT3 transcripts and protein were present in both cortex and medulla, with immunostaining most evident on apical surfaces of proximal tubules and thick ascending loops of Henle (148). Some cytoplasmic staining was also present (148).

h/mCNT3 contain multiple consensus sites for *N*-linked glycosylation which are grouped at the carboxyl terminus (137). hCNT3 has four putative glycosyaltion sites (Asn630, Asn636, Asn664 and Asn678) (137) and treatment of membrane preparations containing hCNT3 with PNGase F or Endo H shifts the electrophoretic

mobility of the transporter on SDS-polyacrylamide gels from 67 to 58 kDa, consistent with hCNT3 being a glycoprotein (138). Two of these putative glycosylation sites are conserved between hCNT1/2/3 (Asn630 and Asn678) (137). Similar to hCNT1 and hCNT2, protein structure algorithms predict a 13 TM topology for hCNT3 (Fig. 1-7) (137).

Non-mammalian eukaryotic CNT family members

Apart from mammals, several representative recombinant CNT transporter proteins have been identified and functionally characterized in other eukaryotes.

Within lower vertebrates, the cDNA encoding a CNT transporter was cloned from the ancient marine prevertebrate the Pacific hagfish *Eptatretus stouti* and named hagfish (hf) CNT (139). hfCNT is 683 amino acids in length and, like its mammalian counterparts, has 13 putative TM domains (139). It has 52, 50 and 57% sequence identity with hCNT1, hCNT2 and hCNT3, respectively. In the region incorporating TMs 4 to 13 the sequence identity is 77% for hCNT3, even though the hagfish diverged from the main line of vertebrate evolution about 550 million years ago (139). A member of the CNT3 subfamily, recombinant hfCNT exhibits *cib*-like transport activity when produced in *Xenopus* oocytes, with Na^+- dependent transport of both purine and pyrimidine nucleosides, as well as the purine and pyrimidine nucleoside analogs AZT, ddC and ddI (139). Unlike hCNT3, however, H^+-dependent transport was not observed. The apparent K_m value for uridine uptake was 10 μM (139) and charge/flux ratio studies revealed a 2:1 Na^+:uridine stoichiometry similar to hCNT3 (139). In contrast to hCNT3, hfCNT exhibited low-affinity binding of Na^+ with an apparent K_{50} value exceeding 100 mM. This is likely an adaptation to the high concentration of Na^+ (about 500 mM) in hagfish extracellular fluids, including the plasma of blood, which are isosmotic with sea water (139).

In nematodes, two CNTs from *Caenorhabditis elegans* have been characterized (149). Encoded by the F27E11.1 and F27E11.2 genes, both full-length cDNAs were cloned, although the F27E11.1 cDNA was not further characterized due to low expression in *Xenopus* oocytes (149). That for F27E11.2 exhibited broad

selectivity for both purine (adenosine, inosine and guanosine) and pyrimidine (only uridine and thymidine) nucleosides (149). Designated CeCNT3 (to reflect its apparent *cib*-like functional phenotype), CeCNT3 has 575 amino acids and exhibits ~ 30% sequence identity to mammalian CNTs (149). Inosine and thymidine apparent K_m values were 15 and 11 μM, respectively (149). Transport mediated by CeCNT3 was not dependent upon Na^+, but activated at acid pH, suggesting that the transporter functions as a H^+/nucleoside symporter (149).

In fungi, a CNT family member was identified by BLAST searches of the genome sequence databank from the pathogenic yeast *Candida albicans*, and its cDNA was cloned by PCR from a *C. albicans* cDNA library (150). *C. albicans* (Ca) CNT is 608 amino acids in length. Potentially containing 13 TM domains, it lacks the long extracellular glycosylated C-terminus of mammalian CNTs (150). CaCNT shares 33, 34 and 38% sequence identity with hCNT1, hCNT2 and hCNT3, respectively (150). Produced in *Xenopus* oocytes, recombinant CaCNT exhibited H^+-dependent transport (and not Na^+-dependent transport) of purine nucleosides (adenosine, inosine and guanosine), as well as uridine, with apparent K_m values ranging from 16 to 64 μM (150). CaCNT also transported the purine nucleoside analogs ddI, F-araA and 2-CdA, and the uridine analogs, 5-fluorouridine, 5-fluoro-2'-deoxyuridine and zebularine (150). Charge to flux ratio experiments revealed a 1:1 H^+:uridine coupling ratio for CaCNT similar to that of hCNT3 (150).

Prokaryotic CNT family members

While ENTs are not found in prokaryotes, CNTs are. A CNT family member from the inner membrane of *Escherichia coli* was isolated by functional rescue studies and named NupC (151). The NupC protein is 400 amino acids in length and, lacking the first three TMs of mammalian and other eukaryote CNTs, contains 10 predicted membrane-spanning domains (151). NupC was functionally characterized following the expression of its cDNA in *Xenopus* oocytes (152). Like native NupC, recombinant NupC produced in oocytes was found to be H^+-dependent for transport of pyrimidine nucleosides and adenosine, but was also capable of low levels of

inosine uptake (152). NupC exhibited a hyperbolic proton-activation curve consistent with a H^+:uridine stoichiometry of 1:1 (152).

Physiological Importance

Nucleoside transport occurs in most tissues and cells via multiple transporter proteins. This redundancy of NTs with overlapping permeant selectivities suggests that the proteins are highly regulated and indicates the potential importance (and existence) of discrete cellular and subcellular localizations. For instance, although both ENTs and CNTs are present in intestinal epithelial cells, CNTs are located in brush border membranes and ENTs are present in basolateral membranes (103, 119, 153-156). Similarly, CNTs are present apically in kidney tubular cells, while ENTs are primarily expressed on the basolateral surface, although hENT1 has recently been reported to be located apically as well (53, 103, 119, 121, 122, 156-158). The relative distributions of ENTs and CNTs in these cells are important for intestinal absorption, renal reabsorption and secretion of nucleosides and nucleoside analogs (119, 157, 159). CNTs have generally higher permeant affinities than ENTs, which aids in the transepithelial movement of nucleosides and nucleoside drugs by increasing the efficiency of initial nucleoside uptake across brush border membranes. The coexistence and differential distribution of ENTs and CNTs in liver cells provides a means to deliver newly synthesized nucleosides into the blood, while at the same time permitting salvage of nucleosides when needed by the liver for regeneration (119, 120, 160).

Aside from hENT3, which is primarily intracellular in localization (64), human ENT and CNT proteins are mostly found in outer plasma membranes of cells, although there is increasing evidence to support additional intracellular localization of hENT1 (mitochondria, nuclear membranes and endoplasmic reticulum) (161, 162), hENT2 (nuclear membranes and endoplasmic reticulum) (162) and hCNT3 (cytoplasmic in chronic lymphocytic leukemia cells) (163). hENT3 tagged with green fluorescent protein co-localizes, in part, with lysosomal markers in cultured human cells (64), while other studies suggest that hENT3 is normally mitochondrial in

location (164). There is only limited information available on how ENT and CNT protein expression and membrane targeting are regulated (118, 160).

Functional differences between transporters complement their different cellular and subcellular localizations. All three CNTs are found in abundance within specialized epithelial cells such as intestine, kidney and liver. This suggests, as described above, important roles for these proteins in absorption, distribution and excretion of physiologic nucleosides and their analogs. In terms of permeant selectivity, hCNT3 transports both purine and pyrimidine nucleosides, and is therefore functionally equivalent to the hCNT1 and hCNT2 transport systems combined, but with the additional capabilities of a 2:1 Na^+:nucleoside coupling ratio, and proton dependence (147). hCNT3 is located on apical surfaces of kidney proximal tubules and thick ascending loops of Henle, where its 2:1 Na^+:nucleoside stoichiometry may help the transporter concentrate nucleosides to a greater extent than hCNT1 or hCNT2, which have 1:1 Na^+:nucleoside coupling ratios (148, 157). The ability of hCNT3 to mediate H^+-nucleoside cotransport may be of particular physiological importance in the acidic environment of the kidney (148, 157). While sodium- and proton-coupled hCNT3 have greatly different permeant selectivities, transport in the presence of both cations (a likely common physiological occurrence) resembles that of the sodium-coupled transporter (*i.e*. *cib*-type activity) (147). CNTs transport in one direction only, while ENTs are bidirectional and can therefore contribute both to cellular uptake and release of nucleosides and nucleoside drugs (55). In kidney proximal tubule, for example, the presence of hENT1 in apical membrane is considered to play a key role in renal secretion of 2'-deoxyadenosine (165). hENT2 complements the other transporters by transporting both nucleosides and nucleobases (55), and the activation of hENT3 at acidic pH is appropriate to its intracellular localization (64).

All three mammalian CNTs transport adenosine and may therefore contribute to the regulation of extracellular concentrations of adenosine available to purinergic receptors. Even though CNTs are not as ubiquitously expressed as the ENTs, their ability to concentrate nucleosides against a concentration gradient may play an important role in the metabolism of adenosine and its analogs. Each hCNT transporter

interacts with adenosine, adenosine analogs and receptor ligands, but with different kinetic profiles that have the potential to be clinically relevant with respect to therapeutic manipulation of adenosine metabolism (115).

Pharmacological Importance

Antineoplastic and antiviral nucleoside drugs – Nucleoside analogs are powerful antimetabolites and have been developed clinically as chemotherapeutic agents for the treatment of both neoplastic and viral diseases, including hematological and solid malignancies, such as leukemias, lymphomas and gastrointestinal tract cancers, as well as human immunodeficiency virus (HIV) and herpes virus infections (27, 111, 118, 153). Nucleoside analogs exert their cytotoxic intracellular actions by undergoing phosphorylation via nucleoside kinases to their corresponding 5'-triphosphate derivatives (68). Examples of therapeutically important nucleoside kinases include thymidine kinases, and 5'-nucleoside monophosphate and 5'-nucleoside diphosphate kinases (68). Conversely, deamination by, for example, adenosine or cytidine deaminase and dephosphorylation by cytoplasmic 5'-nucleotidases will decrease the available concentration of active chemotherapeutic agent (68). The resulting active phosphorylated nucleoside analogs then interfere with nucleotide metabolism and DNA and RNA replication, thus resulting in antiproliferative effects and inhibition of viral replication.

Examples of anticancer purine nucleoside analogs include 2'-chloro-2'-deoxyadenosine (cladribine; 2-CdA) and 9-β-D-arabinosyl-2-fluoroadenine (fludarabine; F-araA) (31, 68, 111, 118, 153). Examples of anticancer pyrimidine nucleoside analogs include 1-β-D-arabinofuranosyl cytosine (cytarabine; araC) and 2', 2'-difluorodeoxycytidine (gemcitabine; dFdC) (31, 68, 111, 118, 153). The structures of these compounds are depicted in Fig. 1-2. Fludarabine is used clinically to treat chronic lymphocytic leukemia, low-grade lymphomas and other hematological malignancies (68, 118). Phosphorylated fludarabine inhibits DNA polymerase, DNA primase, ribonucleotide reductase and DNA ligase I, all of which are enzymes involved in nucleotide synthesis and DNA replication (68, 118). To exert further

cytotoxicity, phosphorylated fludarabine is incorporated into the DNA and RNA structures, thus resulting in premature chain termination (68, 118). In its active phosphorylated form, cladribine, also inhibits DNA replication and repair (118, 153). Cladribine is used clinically to treat hematological malignancies, including low-grade lymphomas, chronic lymphocytic leukemia and hairy cell leukemia (68, 118). The pyrimidine nucleoside drug, cytarabine, is also used clinically against haemotopoietic malignancies, such as acute myelogenous leukemia and non-Hodgkin's lymphoma (68, 118, 166, 167). Its active phosphorylated form, cytarabine inhibits DNA polymerase α and induces chain termination upon incorporation into DNA (68, 118, 166). Gemcitabine is used clinically in the treatment of solid tumors, including pancreatic, breast, non-small cell lung, ovarian, bladder and head and neck cancers (68, 118). Activated, phosphorylated gemcitabine inhibits ribonucleotide reductase, thereby decreasing intracellular concentrations of natural deoxynucleotides (68, 118, 166, 168). It is also incorporated into DNA, followed by the addition of a physiological deoxynucleotide, which then leads to masked chain termination and prevention of repair by proof-reading exonucleases (111, 166, 168).

Examples of antiviral nucleoside analogs include 3'-deoxynucleosides such as 2', 3'-dideoxyinosine (didanosine; ddI), 2', 3'-dideoxycytidine (zalcitabine; ddC) and 3'-azido-3'-deoxythymidine (zidovudine; AZT) (166, 169). These are also depicted in Fig. 1-2. Zidovudine, for example, is used clinically for the treatment of human inmmunodeficiency virus, HIV (166, 170, 171). Similar to antineoplastic nucleoside analogs, these compounds are active in the triphosphate form where incorporation into replicating viral nucleic acid results in chain termination through the inhibition of reverse transcription (166).

Role of NTs in cancer (and antiviral) chemotherapy – Like their naturally occurring physiological nucleoside counterparts, most synthetic nucleoside analogs are hydrophilic molecules, and thus require NTs to cross the plasma membrane and enter intracellular compartments. NTs therefore play critical roles in the cellular uptake, intracellular distribution, metabolism and pharmacological action(s) of these drugs (28, 31, 34, 68, 111, 166). The successful delivery of nucleoside analogs to their intracellular sites of action is thus crucially dependent on functional NTs in

plasma and intracellular membranes, the levels of which have been demonstrated to affect drug toxicity and resistance (111).

The abundance of hENT1 has been correlated with sensitivity to nucleoside analogs such as 5'-deoxy-5-fluorouridine in breast cancer cells (172), 2-CdA and F-araA in acute myelogenous and lymphoblastic leukemia cells (173) and dFdC in pancreatic cancer and non-small cell lung cancer cells (174, 175). In infant acute lymphoblastic leukemia (176) and acute myelogenous and lymphoblastic leukemia in adults (173), increased hENT1 membrane abundance led to increased sensitivity to araC, such that levels of hENT1 have been proposed as a reliable prognostic determinant of araC cytotoxicity (68). For instance, a lack of cell surface hENT1 was related to shorter disease-free survival times in araC-treated acute myeloid leukemia patients (177, 178). A similar retrospective study found that the presence of hENT1 in patient pancreatic adenocarcinoma cells led to a significantly longer survival period following dFdC chemotherapy than those for whom hENT1 was undetectable in a proportion of cells in tumor samples (175). Enhanced clinical outcome in relation to hENT1 abundance levels following dFdC treatment of pancreatic cancer has been reported in multiple centres (179), and recent prospective clinical studies validate the association (180). Patient outcome following dFdC therapy of pancreatic cancer is similarly correlated with hCNT3 tumor abundance, hENT1 and hCNT3 having synergistic effects in this regard (180) Sensitivity to 2-CdA was restored in araC-resistant CEM-ARAC leukemia cells upon *in vitro* stable transfer of hCNT2 cDNA (132). Sensitivity and resistance to dFdC also differed in cultured cell lines depending on the NTs present (181).

Acquired resistance to cytotoxic nucleoside analogs may result from the absence of cell surface transporters and/or down-regulation of transporter produced. In some circumstances, however, increased abundance of cell surface transporters in malignant cells compared to normal cells might also lead to drug resistance (123, 182). For example, the amount of hENT1 is higher in breast cancer cells compared to normal breast epithelia (172), and high abundance of hENT1 has been correlated with dFdC treatment failure in Hodgkin lymphoma patients (183). Since ENTs mediate bidirectional transport, elevated levels of ENTs, especially in cells also producing

CNTs, may lead to drug efflux as a potential mechanism for such resistance to nucleoside drugs. Intracellular localization of NTs may also play a role in resistance and/or toxicity. For example, in a study of chronic lymphocytic leukemia patients, clinical resistance to F-araA was correlated with high levels of intracellular hCNT3 (163). In contrast, a separate study indicated that the presence of hENT1 in mitochondrial membranes enhanced the mitochondrial toxicity of antiviral nucleoside analogs (161, 184). Lysosomal hENT3 has been proposed to contribute to intracellular sequestering of nucleoside drugs and their subsequent degradation (64).

The presence of genetic variation within the patient population, such as SNPs, may also account for some differences in therapeutic outcomes between individuals (118). Additionally, resistance to nucleoside analogs may also arise from gene redundancy because other protein families besides ENTs and CNTs, such as the multidrug resistance (MDR) proteins, are capable of mediating the transport of nucleoside drugs and/or their metabolites, and may therefore play key roles not only in cellular removal but also renal secretion of these compounds (118, 157). It is clear, however, from recent examples that resistance to nucleoside analog chemotherapy could be minimized through the development of better predictive assays to pre-determine the NT profiles of diseased cells and establish in advance their capacities to transport specific nucleoside analogs (68).

While NTs also contribute to nucleoside analog-induced toxicities in normal cells and tissues, NT inhibitors may provide protection against these toxicities and, as well, provide other alternative therapeutic options. Examples of side-effects include hematopoietic toxicity and nephrotoxicity, and many nucleoside drugs produce clinically significant dose-limiting mitochondrial toxicity resulting from their inhibitory actions on mitochondrial DNA replication and repair (157, 166, 185). Mitochondrial toxicity may be linked to the presence of NTs, particularly hENT1 (161, 184), in the mitochondrial membranes. Tissues which consume high levels of ATP, such as kidney, liver, muscle and pancreas, are especially susceptible to mitochondrial toxicity (186). For example, a uridine analog (1-(2-deoxy-2-fluoro-β-D-arabinofuranosyl)-5-iodouracil (fialuridine)) developed for the treatment of hepatitis B, caused severe widespread mitochondrial toxicity resulting in

hepatotoxicity, pancreatitis, neuropathy and myopathy (186). Other nucleoside drugs that can also cause mitochondrial toxicity include F-araA (187), ddI (188, 189), ddC and lamivudine (189, 190). The use of NT inhibitors may lessen these effects. One such study, for example, demonstrated that the ENT inhibitors NBMPR, dilazep and dipyridamole decreased the *in vitro* toxicity of tubercidin against human hematopoietic cells (191). Therefore, use of inhibitors may provide pharmacologic protection to normal tissues, thus minimizing dose-limiting toxicities and side-effects (166). This strategy is likely to be most beneficial in cases where the cancer cells have increased abundance of NTs (111). NT inhibitors may also be administered in parallel with the nucleoside drugs in order to retain the nucleoside analog within cells and therefore maximize cytotoxic actions (31, 111, 166). For example, exposure to NBMPR enhanced the cytotoxicity of 2-CdA in cultured human acute lymphocytic leukemic cells, suggesting that NT inhibition may have prevented drug efflux (192). Those cells with both ENTs and CNTs in their plasma membranes could be exposed to ENT inhibitors as a way to increase cytotoxicity when the nucleoside analog is also a CNT permeant (53). Other than NBMPR, some examples of ENT inhibitors include coronary vasodilator drugs, such as dipyridamole, dilazep and draflazine, some protein kinase inhibitors, including rapamycin, and inhibitors of tyrosine kinase, PKC (protein kinase C) and cyclin-dependent kinase (193). Further studies of nucleoside transport inhibitors, including the design of new compounds and investigation of currently known inhibitors of other target proteins, will be beneficial in the exploitation of these strategies and would also become valuable tools in mechanistic and physiological studies of nucleoside transport proteins. Of special value would be inhibitors specific to each individual transporter isoform. Presently, there are no known specific high-affinity inhibitors of CNTs.

Parasitic protozoa – These pathogens are unable to undergo *de novo* purine synthesis and therefore depend on scavenging mechanisms using NTs for the uptake of host purine nucleosides for growth and survival (194, 195). This presents an opportunity for pharmacologic intervention (194, 195). Examples of parasitic protozoa include *Trypanosomatidae* species responsible for Chagas' disease and African sleeping sickness, *Leishmania* species responsible for leishmaniasis and

Plasmodium species causing malaria (194, 196). It would be clinically beneficial to develop nucleoside analog drugs which are specifically transported by the NTs of such parasites, or to develop specific inhibitors of parasite transporters. Examples of nucleoside analogs in current clinical use to treat parasitic protozoan infections include the nucleobase hypoxanthine analog allopurinol and the inosine analog formycin B, which have selective activity against African trypanosomes and/or *Leishmania* species (reviewed in 197). Helminth parasites, such as hookworm or pinworm, present parallel opportunities for pharmacologic intervention.

Adenosine – This purine nucleoside is an important signaling molecule that also makes it a valuable pharmacological target. For example, adenosine itself is used in the treatment of supraventricular tachycardia, and adenosine agonists and antagonists have well defined clinical roles in the treatment of other human diseases including hypertension, renal failure and epilepsy (8, 52). By inhibiting NTs, the local concentrations of adenosine can be affected (8, 52, 198, 199). For example, under normal conditions in the heart, the net flux of adenosine is intracellularly-directed into cardiomyocytes and endothelial cells (200). Administration of nucleoside transport inhibitors, such as dipyridamole, dilazep or draflazine (Fig. 1-3), prevent influx of adenosine across cell membranes, and thereby increase extracellular adenosine concentrations, resulting in elevated adenosine binding to its receptors and potentiation of adenosine-mediated cardiovascular effects, such as vasodilation (8, 201, 202). Inhibitor studies have functionally implicated ENTs in the regulation of adenosine metabolism and adenosine availability to purinoreceptors in the brain (203, 204) and heart (6, 65, 205-207). A corresponding role is yet to be established for CNTs, although all three mammalian CNTs transport adenosine and CNT transcripts have been located in both brain and heart tissue.

Nucleoside Transporter Protein Structure-Function Studies

Crystal structures for a number of bacterial membrane transport proteins have been solved. These include the nucleobase cation symporter Mhp1 from *M. liquefaciens* (208), *E. coli* glycerol-3-phophate transporter GlpT (209), lactose

permease LacY (210), and Na^+/H^+ antiporter NhaA (211), the *Pyrococcus horikoshii* glutamate transporter Glt_{Ph} (212), the *Aquifex aeolicus* Na^+/Cl^--dependent leucine transporter $LeuT_{Aa}$ (213), and *Vibrio parahaemolyticus* Na^+/galactose symporter vSGLT1 (214). Current understanding of NT structures is generally limited to topology, with additional 3-D information on ENTs provided by low-resolution homology modeling and other approaches. Studies to elucidate ENT and CNT molecular mechanisms have focused mainly on protein-protein chimeras, amino acid substitutions and chemical modification of permeants.

ENT family members

Within ENTs, sequence alignments reveal greatest sequence homology in TMs (53, reviewed in 55), with conservation of overall membrane topology amongst all family members (90, reviewed in 55). This common membrane topology consists of 11 TMs with cytoplasmic N-terminal and extracellular C-terminal regions, and large extracellular and cytoplasmic loops between TMs 1 and 2 and TMs 6 and 7, respectively (60, 215). Glycosylation-defective (aglyco) mutants engineered by site-directed mutagenesis revealed that both hENT1 (215, 216) and hENT2 (217) were glycosylated in the extracellular loop between TMs 1 and 2, although glycosylation was not required for function of either transporter. Glycosylation-scanning mutagenesis has confirmed the 11 TM topology of hENT1 (215).

Using human and rat ENT chimeras, regions which are functionally important for ENT permeant and inhibitor interactions have been identified. For example, h/rENT1 and rENT1/2 chimeras revealed that ENT interactions with the inhibitors dipyridamole, dilazep and NBMPR, all of which compete with permeant for the outward-facing conformation of the nucleoside binding site, involves the TM 3 to 6 region of the transporter (218, 219). Additionally, rENT1/2 chimeras determined that TMs 3 to 4 and TMs 5 to 6 both contribute to NBMPR binding affinity (219). The same chimeras also established a role for TMs 1 to 6 in ENT2 transport of the 3'-deoxynucleosides AZT, ddI and ddC (220), and for TMs 5 to 6 in ENT2 transport of nucleobases (221).

Individual amino acid residues contributing to ENT permeant and inhibitor interactions have been identified and characterized by both random and site-directed mutagenesis approaches. Random mutagenesis of recombinant hENT1 produced in yeast identified Met33 in TM 1 to be involved the binding of dipyridamole and dilazep (222). hENT1 mutant M33I exhibited decreased sensitivity to both inhibitors in the absence of changes to NBMPR or uridine affinity (222). The role of this residue is conserved in hENT2, and the reciprocal mutation in hENT2 (I33M) exhibited increased sensitivity to dipyridamole and dilazep inhibition while retaining insensitivity to NBMPR inhibition (222, 223). hENT2 I33M also displayed an increased apparent affinity for uridine (222, 223). Mutation of hENT2 Ile33 to cysteine conferred sensitivity to PCMBS inhibition in a nucleoside and inhibitor protectable manner, suggesting that this residue is accessible from the extracellular medium and directly involved in permeant and inhibitor binding (225). Mutation of hENT1 Gly154 in TM 4 to the corresponding residure in hENT2 (serine), resulted in decreased sensitivity to NBMPR, dilazep and dipyridamole inhibition, as well as decreased affinity for cytidine and adenosine (60, 224). The corresponding residue in rENT2 is a cysteine, Cys140, which is PCMBS-sensitive and nucleoside protectable, suggesting a key location within the inhibitor-nucleoside binding domain (225). Mutation of highly conserved residues Trp29 (TM 1) and Gly179 (TM 5) in hENT1 were both shown to inhibit transport activity and affect inhibitor binding (68, 226). Additionally, Gly184 in hENT1 TM 5 was found to be important for targeting to the plasma membrane (226). Random mutagenesis and functional complementation also identified four additional residues, hENT1 Trp29 (TM 1), Met89 (TM 2), Leu92 (TM 2) and Ser160 (TM 4), to be important for interactions with both inhibitors and nucleoside permeants (68, 227, 228). Recently, two hENT1 TM 8 residues (Phe334 and Asn338) were reported to participate in interactions with inhibitors, protein folding and catalytic turnover (68, 229).

Using recombinant hENT1 and hENT2 produced in *S. cerevisiae*, inhibition profiles of uridine and cytidine analogs were used to identify key structural determinants responsible for transporter-permeant interactions (230, 231). For example, halogen modification of uridine at the 5 position of the base and the 2' and

5' positions of the ribose moiety are tolerated by both hENT1 and hENT2 (230), in contrast to the hydroxyl group at the 3' position of the ribose moiety which is essential for recognition by both transporters (230). For hENT1, both the 2'- and 3'-hydroxyl groups are important determinants for interaction of cytidine, whereas hENT2 displays an overall lower ability to interact with cytidine and cytidine analogs than hENT1 (230). hENT2 was shown to be more tolerant of sugar modifications than hENT1: strong interactions were apparent with the 3'-hydroxyl group for both hENT1 and hENT2, and moderate interactions were evident with the 2'- and 5'-hydroxyl groups for hENT1, whereas hENT2 showed weak interactions with the 5'-hydroxyl group only (231). Using pharmacophore models, the nucleoside affinity of hENT1 was determined to be dependent largely upon electrostatic and steric features (232).

In addition to studies of mammalian ENTs, further insights to ENT transport mechanisms have been contributed by studies of non-mammalian family members. For example, site-directed mutagenesis studies in *Leishmania donovani* have identified residues influencing permeant recognition and transport in TM 5 (Gly183) and TM 7 (Cys337) of LdNT1.1 (235), and in the TM 4 - 5 loop (Asn175) (234) and TM 5 (Ser189) (235) and TM 8 (Asp389) (236) of LdNT2. Subsequent studies of *L. donovani* LdNT1.1 TM 5 using substituted cysteine accessibility method (SCAM) analysis strongly predicted the involvement of this helix in the translocation pathway (47, 237). Furthermore, site-directed mutagenesis of charged residues in *L. donovani* ENTs has also identified other key residues in nucleoside binding and translocation, including LdNT1.1 Glu94, Lys153 and Asp374 in TMs 2, 4 and 8, respectively (238). *C. elegans* CeENT1 binds dipyridamole with high affinity similar to hENT1 (239), and random mutagenesis and functional screening of CeENT1 for reduced sensitivity to dipyridamole identified the TM 11 residue Ile429 as critical for this interaction (240). Mutagenesis studies of this residue, which corresponds to hENT1 Leu442, and of the previously identified hENT1 TM 1 residue Met33 (222, 241) in three different protein backgrounds (hENT1, hENT2 and CeENT1) confirmed the importance of these residues in both dipyridamole inhibition and nucleoside transport, and suggested close proximity integration of TMs 1 and 11 within the permeant translocation pore (240).

To date, TMs 1, 2, 4, 5, 7, 8 and 11 have been implicated in involvement in inhibitor interactions and/or nucleoside transport, suggesting that they form part of the inhibitor and/or nucleoside binding domain(s) and translocation pore across the membrane. Additionally, 3-D homology models of ENTs (194, 234, 242) based upon distant similarities with MFS transporters have been generated from the crystal structures of *E. coli* GlpT (209) and LacY (210). An *ab initio* structural model of LdNT1.1 has also recently been proposed (243).

CNT family members

Initial models of mammalian CNTs predicted a 14 TM topology (101, 125, 126). Subsequent studies, which investigated sites of *N*-glycosylation and antipeptide antibody binding, revealed an extracellular C-terminus for rCNT1, which indicated a protein with an odd number of TM domains in order to preserve the intracellular location of the N-terminal tail (103). C-terminal glycosylation was also demonstrated in rCNT2 (136) and hCNT3 (138). Computational algorithms indicated a protein with 13 TMs (103), with two other regions (TMs 5A and 11A in Fig. 1.7) weakly predicted to be membrane spanning. Within region 11A there is a highly conserved sequence motif, (A/G)XXXGXKXXXNEFVAYXXLXXY, present in all CNT family members (103). The central conserved glutamate residue (E519) in this motif is critical to CNT function. In hCNT3, mutation to aspartate, glutamine and cysteine yielded mutants (E519D, E519Q and E519C) with altered nucleoside and cation-activation kinetics, loss or impairment of H^+-dependence and, in the case of E519C, a shift in Na^+:nucleoside stoichiometry from 2:1 to 1:1 (244). Effects of mutation of the corresponding glutamate residue in hCNT1 are addressed in the Appendix 1 (245). Consistent with possible pore-lining status, hCNT3 E519C was sensitive to inhibition by PCMBS and partly protected by uridine (244), a finding confirmed by full SCAM analysis of the entire TM 11A region which established it to be membrane spanning with multiple residues contributing to the translocation pore [Chapter 8 (246)]. These studies suggested that a residue within TM 11A of hCNT3 (Glu519) could be the residue involved in accepting the H^+ ion (244). Residues within TM 12 were also

revealed to be potentially pore lining: hCNT3 Cys561, for example, exhibits a H^+-mediated conformational shift that results in sensitivity of the transporter to PCMBS inhibition (146). Subsequent analysis of same residue, Cys561, revealed that its mutation was responsible for the altered Na^+-binding phenotype of hCNT3C-, the engineered cysteine-free protein that served as the template for all of the SCAM analyses described in this thesis [Chapter 3 (247)].

The bacterial CNT, NupC, lacks the first 3 TMs of mammalian and other eukaryote CNTs, suggesting that this region may not be necessary for CNT function (151). Truncation studies confirmed this, by removing the N-terminal region and the first three TMs of rCNT1 and hCNT1 (residues 1 to 173, and 1 to 174, respectively) (103). Both truncated proteins remained functional, but with reduced activity (103). Highlighting the functional importance of the C-terminal half of CNTs, a 50:50 chimera between hfCNT (TMs 1 – 6) and hCNT1 (TMs 7 – 13) produced a protein that adopted a hCNT1-like phenotype, including selectivity for pyrimidine nucleosides (and adenosine), an apparent K_{50} for Na^+ activation of 10 mM, and a Hill coefficient indicative of 1:1 Na^+:nucleoside coupling stoichiometry (139). Corresponding chimeric studies between hCNT1 and hCNT3 similarly located hCNT3-specific permeant and cation interactions to the C-terminal half of hCNT3 (147), a 50:50 chimera between hCNT3 (TMs 1 – 6) and hCNT1 (TMs 7 – 13) exhibiting hCNT1-like substrate selectivity when produced in *Xenopus* oocytes that was Na^+-dependent, but H^+-independent, with a Na^+:nucleoside coupling stoichiometry of 1:1 (147).

Chimeric and mutagenesis studies were also performed between rCNT1-rCNT2 (126, 248, 249) and hCNT1-hCNT2 (250). For rCNT1/2, a chimeric protein consisting of rCNT1, but with TM 7 replaced by that of rCNT2 displayed a broad selectivity for both purine and pyrimidine nucleosides and, hence, a CNT3 (*cib*)-like phenotype (126), while at the same time retaining a Hill coefficient for Na^+-activation consistent with a 1:1 Na^+:nucleoside stoichiometry (248). Subsequent site-directed mutagenesis of a single residue, Ser318, in rCNT1 to the corresponding amino acid in rCNT2 (glycine) showed similar results, indicating this residue as the principal determinant of the observed phenotype (249). A second chimeric construct, in which

TM 8 of rCNT1 was replaced by that of rCNT2, showed compromised thymidine and inosine transport activity (126). For hCNT1/2, replacement TMs 7 – 9 in hCNT1 with those of hCNT2 changed the selectivity of the transporter from pyrimidine nucleoside-selective to purine nucleoside-selective, and thus a hCNT2 (*cif*)-like phenotype (250). Site-directed mutagenesis studies identified two pairs of adjacent residues in TMs 7 and 8 of hCNT1 (Ser319/Gln320 and Ser353/Leu354, respectively) that, when converted to the corresponding residues in hCNT2 (Gly313/Met314 and Thr347/Val348), mediated the change of phenotype. Mutation of the two TM 7 residues alone, resulted in a protein which transported both purine and pyrimidine nucleosides (250). Corresponding mutation of the two TM 8 residues alone resulted in a novel uridine-preferring transport phenotype (251). An investigation of two allelic isoforms of *C. albicans* CaCNT found that a single amino acid substitution in TM 7 altered the apparent affinity for uridine transport by this H^+-coupled NT by ~ 10-fold (252), further highlighting the importance of this TM in CNT function.

Other mutagenesis studies of CNT family members have further highlighted the importance of the C-terminal half of the protein. These include studies of a conserved glutamate residue in TM 7 of hCNT1 (Glu322) and hCNT3 (Glu343), where mutation to the neutral amino acid glutamine resulted in features consistent with uncoupled Na^+ transport, manifested by disproportionately high uridine-induced Na^+ currents causing variable Na^+/nucleoside charge:flux ratios in excess of the expected wild-type value of 2:1 [(244) and Appendix 1 (245)]. When each was converted to cysteine, the mutants were sensitive to PCMBS inhibition, suggesting pore-lining status for this residue [(244) and Appendix 1 (245)]. From a mechanistic standpoint, its location is consistent with a role for this glutamate residue in stabilizing the internal gate of the transporter vestibule [(244) and Appendix 1 (245)]. Corresponding potential gating functions of negatively charged residues within a common cation/solute translocation pore can be found in the recently solved 3-D crystal structure of the Aquifex aeolicus $LeuT_{Aa}$ Na^+/Cl^- dependent leucine transporter, where a leucine residue stabilizes the transporter in a closed conformation that occludes closely associated Na^+- and leucine-binding sites halfway across the membrane lipid bilayer (213, 244). Using SCAM methodology (see section below) to

probe a cysteine-less form of hCNT3 (hCNT3C-) produced in yeast, residues in TMs 11, 12 and 13 were individually mutated to cysteine and tested for inhibition by methanethiosulfonate (MTS) reagents (253). These experiments provided evidence for participation of TMs 11 and 12, but not TM 13, in formation of the nucleoside translocation pathway (253). Findings from the yeast study are corroborated and expanded upon in the SCAM analyses of hCNT3C- TMs 11-13 in *Xenopus* oocytes described in Chapter 8 of this thesis [Chapter 8 (246)].

Using recombinant hCNT1 and hCNT3 produced in *S. cerevisiae*, inhibition profiles of uridine analogs were determined to identify key structural determinants responsible for transporter-permeant interactions (254). For example, hCNT1 and hCNT3 recognized uridine through distinguishable binding motifs (254). hCNT1 was sensitive to modifications at C(3), less sensitive at C(5') or N(3), and much less sensitive at C(2') (254). hCNT3, in contrast, was sensitive to modifications at C(3'), but much less sensitive at N(3), C(5') or C(2') (254). The changes of binding energies between the transporters and different uridine analogs suggested that hCNT1 formed hydrogen bonds (H-bonds) with C(3')-OH, C(5')-OH, or N(3)-H of uridine, but not with C(2')-OH, whereas hCNT3 formed H-bonds with C(3')-OH, but not with N(3)-H, C(5')-OH and C(2')-OH (254). Both transporters barely tolerated modifications at C(3') or inversion of configurations at C(2') or C(3') (254).

In contrast to ENTs, it has not proved possible to thread CNTs onto any of the known bacterial transporter crystal structures. Presently, therefore, no 3-D information is available for this transporter family.

Cysteine Scanning Mutagenesis and Sulfhydryl-Specific Protein Chemistry

In the absence of a crystal structure, substituted cysteine accessibility method (SCAM) analysis is the powerful methodology of choice to analyze the detailed membrane architecture and function of membrane transporter proteins (255-258). SCAM uses the specificity of sulfhydryl chemistry and was first introduced by Akabas *et al* in 1992 (255). Since then, numerous mammalian and bacterial transmembrane protein structures have been probed by this technique, including the

glucose transporter Glut1 (259), the Cl^-/HCO_3^- exchanger AE1 (260, 261), the Na^+/H^+ exchanger NHE1 (262), the glutamate transporter EAAT1 (263), the glutamate transporter GltT (264), the lactose permease LacY (265), the Na^+/H^+ antiporter NhaA (266) and the Na^+/glucose co-transporter SGLT1 (267). The basis of SCAM is that cysteine residues contain sulfhydryl groups that avidly react with a variety of sulfhydryl-specific reagents. Coupled with site-directed mutagenesis to sequentially introduce single cysteine residues into a protein, SCAM can precisely locate the position of the introduced cysteine residue, test the consequences of its chemical modification, and evaluate the functional importance of the replaced amino acid (255-258). Therefore, whole regions of the protein can be systematically scanned with SCAM in order, for example, to identify domains exposed to the external membrane surface, map gating and pore-lining residues, and identify residues involved in permeant and/or cation binding.

The sulfhydryl (–SH) group of a cysteine residue in a membrane protein may be in one of three environments: a water accessible surface, a lipid accessible surface, or the protein interior (258). If located in the lipid environment or within the protein interior, it is generally unresponsive to sulfhydryl reagents because sulfhydryl reagents react with ionized –SH (S^-) ~ 5 x 10^9 times faster than with un-ionized –SH (268) and, due to the low dielectric constant of those environments, ionization of sulphydryl groups is usually minimal (255-258). Native cysteine residues (or those introduced by mutagenesis) that line the translocation pore or are located on the periphery of protein surfaces are water accessible and hence more reactive towards sulfhydryl reagents (258). If located within the transporter translocation pore, for example, this may lead to the alteration (usually inhibition) of function (255-258). If located within or closely adjacent to the permeant binding pocket of the translocation pathway, addition of permeant during exposure to the sulfhydryl reagent may protect against that inhibition (255-258).

For SCAM to work, a protein background lacking endogenous sulfhydryl groups is usually necessary, although a wild-type protein insensitive to the effects of sulfhydryl reagents may be used, even if “silent” endogenous cysteine residues are present. Generally, however, endogenous cysteine residues are removed by mutation,

and the resulting cysteine-free construct should retain wild-type functional characteristics (258). In SCAM analysis of a series of cysteine mutants, results will typically show inhibition by the sulfhydryl reagent, or no observable effect. Caution should be noted when interpreting the latter, which could either indicate lack of reaction, or reaction that had no detectable effect on function (258). Reaction between a sulfhydryl group and sulfhydryl reagent depends on numerous factors in addition to –SH dissociation, including accessibility to reagent, steric constraints on the formation of an activated complex and, for charged reagents, the electric fields along the path to the residue (258).

Sulfhydryl-specific reagents

The most commonly used reagents are mercurial compounds and methanethiosulfonates. An example of the former, PCMBS (Fig. 1-8) is a hydrophilic, negatively-charged, membrane-impermeant sulfhydryl reagent that has been employed extensively in the literature for probing sulfhydryl groups in proteins (259). It is also the reagent used in this thesis. There are several reasons why PCMBS is an ideal choice for SCAM. It is small, stable in aqueous solution and slowly reactive. In the presence of permeant, the latter feature of slow reactivity enhances the possibility of detecting permeant protection against inhibition.

Methanethiosulfonates are sulfhydryl-specific reagents that have a range of permeability, charge and size, all useful characteristics for the probing protein structure. The most commonly used are MTSET (2-(trimethylammonium) ethyl methanethiosulfonate), MTSES (2-sulfonatoethyl methanethiosulfonate sodium salt) and MTSEA (2-aminoethyl methanethiosulfonate hydrobromide) (Fig. 1-8). The first two, MTSET and MTSES, are membrane-impermeant, and positively and negatively charged, respectively, while MTSEA is neutral at physiological pH and able to cross the lipid bilayer (255, 258).

Reliability of cysteine scanning mutagenesis

In recent years, advances in membrane protein crystallography have enabled a growing number of channel and transporter protein structures to be determined. A number of these proteins have also previously been characterized by SCAM. Generally, the topological and other structural information provided by SCAM is in good agreement with the crystal structures, LacY and Glt_{Ph} perhaps providing the best examples of correspondence between the two methodologies (210, 212). Hence, SCAM is a viable means of obtaining structural information for membrane transporter proteins for which a crystal structure is not yet available. An important added advantage of SCAM is that the technique also identifies residues of functional importance.

Thesis Objectives

CNTs have been studied less extensively than ENTs with respect to their structures and the functions of specific amino acid residues. To better understand CNT structure-function relationships and mechanism(s) of transport, it is necessary to identify and characterize regions and residues within the translocation pore, as well as those contributing to, and participating in, the nucleoside permeant and cation coupling binding sites. The objective of the research described in this thesis was to undertake structure-function investigations of representative eukaryotic and prokaryotic CNTs, focusing, in particular, on the human transporter hCNT3. The rationale for using hCNT3 as template for most of this research was its phylogenetic relationship to other CNTs and its unique transport properties. hCNT3 (and mCNT3) are more closely related to prevertebrate hfCNT than to the mammalian CNT1 and CNT2 proteins, despite approximately 550 million years of vertebrate evolution (167), suggesting that the physiological functions of *cib*-type NTs have particular importance. This is further highlighted by the low frequency of hCNT3 SNPs. Mammalian CNT3 is also different from both CNT1/2 in terms of nucleoside selectivity and cation coupling. hCNT1 and hCNT2 are exclusively Na^+-dependent and selective for transport of pyrimidine and purine nucleosides, respectively (109), whereas hCNT3 uses both Na^+ and H^+ electrochemical gradients and mediates

transport of both purine and pyrimidine nucleosides (137). Additionally, hCNT3 exhibits 2:1 Na^+:nucleoside and 1:1 H^+:nucleoside coupling ratios, while hCNT1 and hCNT2 share a common 1:1 Na^+:nucleoside stoichiometry (137). Studies of hCNT3 will therefore be mechanistically relevant to the full spectrum of Na^+- and/or H^+-coupled CNTs. Clinically, hCNT3 transports both antineoplastic and antiviral nucleoside drugs (27, 111, 137, 145), and tumor hCNT3 abundance correlates with patient outcome following nucleoside drug chemotherapy (180).

Xenopus oocytes which lack endogenous nucleoside transport systems, were used exclusively as the heterologous expression system for all of the experiments described in this thesis. Following production of recombinant wild-type and mutant transporters in *Xenopus* oocytes, nucleoside transport was characterized using radioisotope flux assays and, in some instances, electrophysiological techniques (Chapter 2). hCNT3 is the only wild-type mammalian CNT transporter reactive to PCMBS (146). This occurs only in H^+-enriched medium, and results from a conformational shift that exposes a cysteine residue in TM 12 (Cys561) to PCMBS inhibition (146). The functional importance of this TM 12 residue in cation coupling was analyzed in the studies described in Chapter 3, which also describes the characterization of a cysteine-less version of hCNT3 (hCNT3C-) as a suitable template for subsequent PCMBS SCAM analysis of CNT structure and function. Since truncation, chimeric and previous mutagenesis studies have emphasized the functional importance of TMs 7 – 13 (103, 126, 147, 248-251), SCAM analysis began with hCNT3C- TMs 7 and 8, and extended to the entire C-terminal half of the protein. Chapter 4 describes the analyses of hCNT3C- TMs 7 and 8, which revealed the presence of putative discontinuous regions within both transmembrane helices. Since this finding was novel and unexpected, Chapter 5 describes corresponding SCAM analysis of TMs 7 and 8 in wild-type hCNT1. The equivalent TMs in *E. coli* NupC were investigated in the studies of Chapter 6. The studies of chapters 4 and 5 additionally provided evidence that both transmembrane segments have a reversed orientation in the membrane, providing key evidence for a new revised model of CNT topology. The studies of chapter 7 extended the analysis to hCNT3C- TMs 9 and 10. Similar to TMs 7 and 8, TM 9 was also shown to be discontinuous, while SCAM

analysis of TM 10, in contrast, suggested a conventional α-helical conformation. Here, too, TMs 9 and 10 are proposed to be in a reverse orientation consistent with a new revised model of CNT topology. Completing the study, Chapter 8 describes a SCAM analysis of hCNT3C- TMs 11, 11A, 12 and 13. Enabling the reversed orientation of TMs 7 – 10, region TM 11A was shown to be membrane-spanning and, like TMs 7, 8 and 9, discontinuous in nature. TMs 11, 12 and 13, in contrast, exhibited conventional α-helical structures. Reviewed collectively in the General Discussion of Chapter 9, the data generated from these experiments fundamentally revise our understanding of CNT structure, provide insight into the molecular mechanism(s) of CNT cation/permeant coupling, and identify new residues of functional importance

Appendix 1 (245) describes an investigation of the roles of hCNT1 glutamate residues.

Table 1-1. Mammalian nucleoside transporters.

Equilibrative/ Concentrative nucleoside transporter (ENT/CNT) family member	Number of residues	Permeant selectivity	Transport mode
hENT1	465	Purine and pyrimidine nucleosides	Facilitative
hENT2	465	Purine and pyrimidine nucleosides and nucleobases	Facilitative
hENT3	475	Purine and pyrimidine nucleosides and adenine (at pH 5.5)	H^+-dependent
hENT4	530	Adenosine (at pH 5.5) and organic cations, including serotonin	H^+-dependent;
mENT1.1	460	Purine and pyrimidine nucleosides	Facilitative
mENT1.2	458	Purine and pyrimidine nucleosides	Facilitative
mENT2	456	Purine and pyrimidine nucleosides and adenine	Facilitative
mENT3	475	Purine and pyrimidine nucleosides and nucleobases	nd
mENT4	528	Adenosine and adenine (at pH 5.5), organic cations not tested	H^+-dependent
rENT1	457	Purine and pyrimidine nucleosides	Facilitative
rENT2	456	Purine and pyrimidine nucleosides and nucleobases except cytosine	Facilitative
rbENT2	456	Purine and pyrimidine nucleosides and hypoxanthine	Facilitative
rbENT2A	415	Purine and pyrimidine nucleosides and hypoxanthine	Facilitative
hCNT1	649	Pyrimidine nucleosides and adenosine	Na^+-dependent
hCNT2	658	Purine nucleosides and uridine	Na^+-dependent
hCNT3	691	Purine and pyrimidine nucleosides	Na^+/H^+-dependent
rCNT1	648	Pyrimidine nucleosides and adenosine	Na^+-dependent
rCNT2	659	Purine nucleosides and uridine	Na^+-dependent
mCNT1	648	nd	nd
mCNT2	660	Purine nucleosides and uridine	Na^+-dependent
mCNT3	703	Purine and pyrimidine nucleosides	Na^+/H^+-dependent
rbCNT2	658	Purine nucleosides and uridine	Na^+-dependent
pkCNT1	647	Pyrimidine nucleosides	Na^+-dependent

Note: h, human; r, rat; m, mouse; rb, rabbit; pk, pig. ENT properties adapted from (55). CNT properties adapted from (270).

Table 1-2. Kinetic properties of recombinant ENT proteins.

Transporter	Permeant	Apparent K_m value (mM)
hENT1	Uridine	0.24
hENT1	Adenosine	0.12
hENT1	Cytidine	0.60
hENT2	Uridine	0.20
hENT2	Hypoxanthine	0.70
hENT2	Adenine	1.1
hENT2	Thymine	1.7
hENT2	Uracil	2.6
hENT3	Adenosine	1.9
hENT3	Uridine	2.0
hENT4	Adenosine	0.78
hENT4	Serotonin	1.9
mENT1	Adenosine	0.13*
mENT2	Adenosine	0.27*
mENT4	Adenosine	0.13
mENT4	Adenine	2.6
rENT1	Uridine	0.15
rENT2	Uridine	0.30
rENT2	Hypoxanthine	1.0
rENT2	Adenine	2.5
rENT2	Thymine	1.3
rENT2	Uracil	1.8
CeENT1	Uridine	0.67
CeENT1	Adenosine	0.55
CeENT2	Uridine	0.88
CeENT2	Adenosine	0.21
PfENT1	Adenosine	0.32
PfENT1	Adenine	0.32
PfENT1	Hypoxanthine	0.41
TbNT2/5/6/7	Adenosine	<0.005
TbNT2/5/6/7	Inosine	<0.005
TgAT	Adenosine	0.11

Notes: K_m values are for recombinant proteins produced in *Xenopus* oocytes. * IC_{50} values. h, Human; r, rat; m, mouse; Ce, *Caenorhabditis elegans*; Pf, *Plasmodium falciparum*; Tb, *Trypanosoma brucei*; Tg, *Toxoplasma gondii*. V_{max} values are not included because of variable levels of cell surface expression. These data are adapted from (55).

Table 1-3. Kinetic properties of recombinant CNT proteins.

Transporter	Permeant	Apparent K_m value (μM)					
		Xenopus oocytes	Ref.	*S. cerevisiae*	Ref.	Cultured cells	Ref.
hCNT1	Uridine	45	104	9	233	34	115
		22	109			59	117
	Cytidine					140	117
hCNT2	Uridine	80	126			46	132
		40	127			120	130
	Adenosine	8	127	11	68		
	Inosine	5	126			14	130
hCNT3	Uridine	22	137	9	255	1.1	138
	Cytidine	15	137			3.4	138
	Thymidine	21	137			3.7	138
	Adenosine	15	137			4.6	138
	Inosine	53	137			4.3	138
	Guanosine	43	137			5.1	138
rCNT1	Adenosine	26	110			15	106
	Uridine	37	110			21	106
	Thymidine					13	106
rCNT2	Adenosine	6	125				
	Thymidine	13	125				
mCNT1	nd						
mCNT2	Purine nucleosides ; uridine	nd	128				
mCNT3	Purine and pyrimidine nucleosides	15-53	137				
rbCNT2	Uridine	nd	129				
	Inosine	nd	129				
pkCNT1	Uridine	9	105				
hfCNT	Uridine	10	139				
	Thymidine	45	139				
	Inosine	35	139				
CeCNT	Inosine	11	149				
	Thymidine						

Transporter	Permeant	Apparent K_m value (μM)	
		Xenopus oocytes	Ref.
CaCNT	Uridine	16	159
	Adenosine	57	159
	Inosine	64	159
	Guanosine	4	159
NupC	Uridine	2	152
	Adenosine	nd	152
YeiJ	nd		
YeiM	nd		

Notes: K_m values are compared for recombinant proteins produced in three heterologous expression systems, *Xenopus* oocytes, yeast and mammalian cells. V_{max} values are not included because of variable levels of cell surface expression. h, Human; r, rat; m, mouse; rb, rabbit; pk, pig; hf, hagfish; Ce, *Caenorhabditis elegans*; Ca, Candida *albicans*. NupC, YeiJ and YeiM are CNTs from *Escherichia coli*.

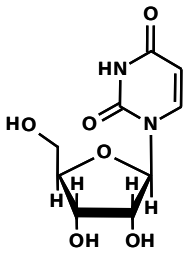

Uridine

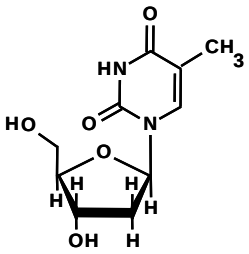

Thymidine

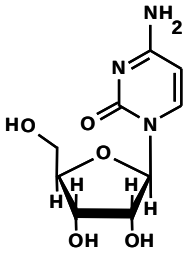

Cytidine

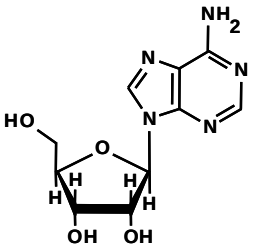

Adenosine

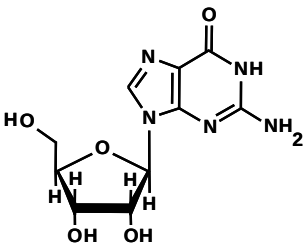

Guanosine

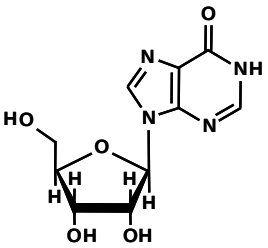

Inosine

Hypoxanthine

Figure 1-1. Chemical structures of physiological nucleosides and the nucleobase hypoxanthine.

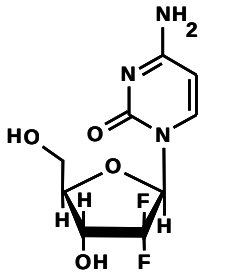

Gemcitabine (dFdC)

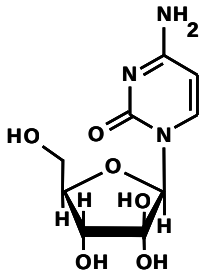

Cytarabine (araC)

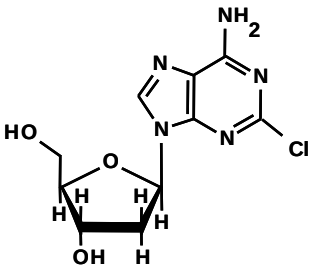

Cladribine (2-CdA)

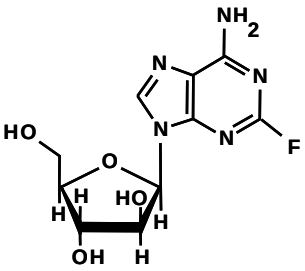

Fludarabine (F-araA)

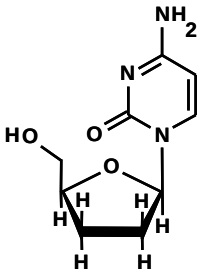

Zalcitabine (ddC)

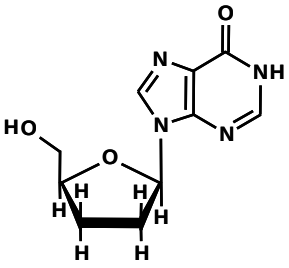

Didanosine (ddI)

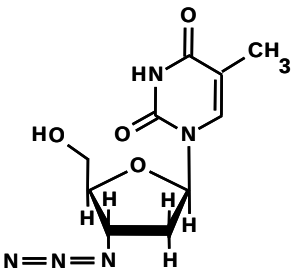

Zidovudine (AZT)

Figure 1-2. Chemical structures of chemotherapeutic nucleoside analogs.

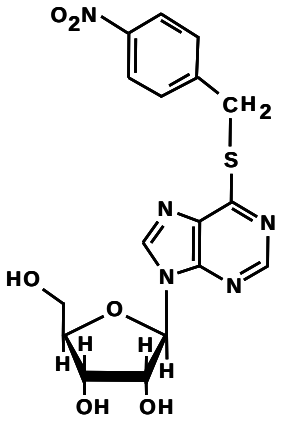

Nitrobenzylthioinosine

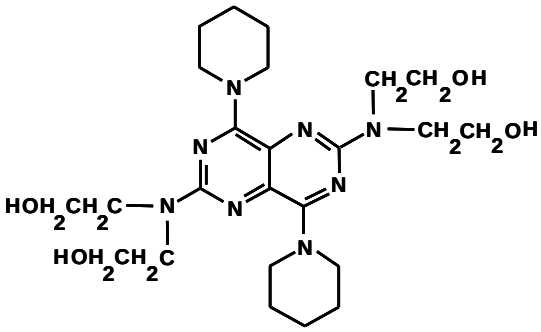

Dipyridamole

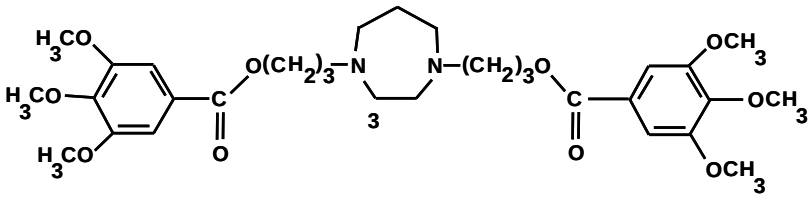

Dilazep

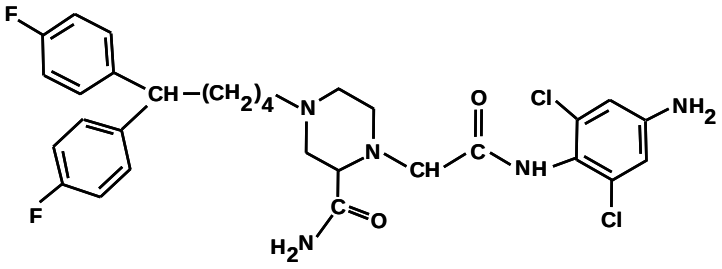

Draflazine

Figure 1-3. Chemical structures of ENT inhibitors.

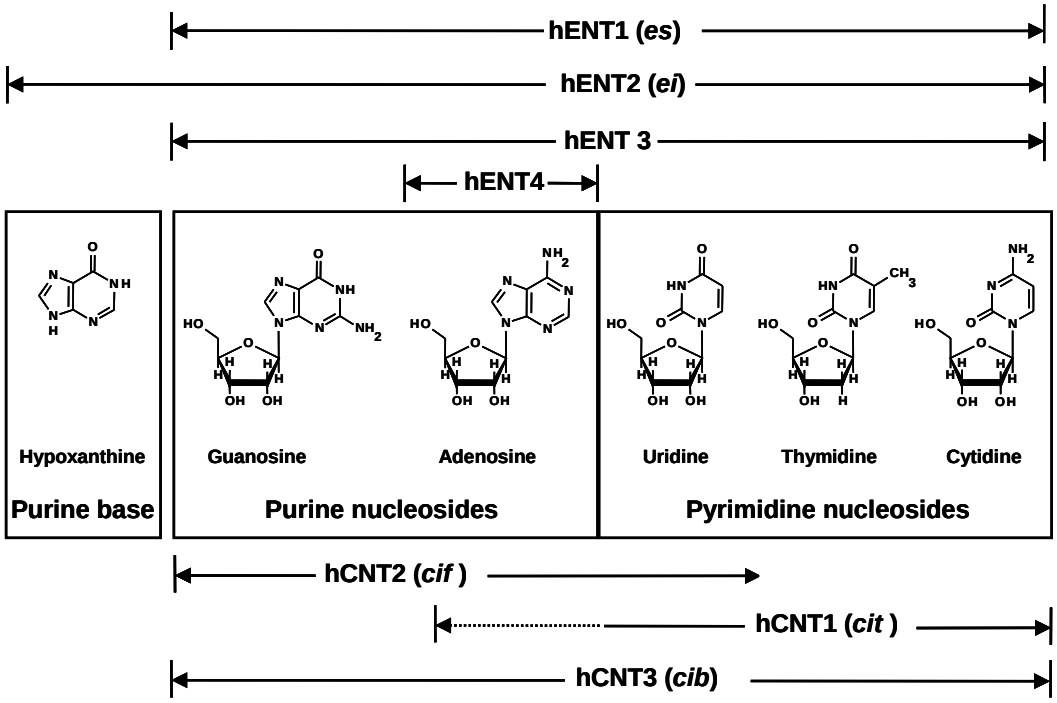

Figure 1-4. Permeant selectivities of human ENT and CNT nucleoside transporter proteins.

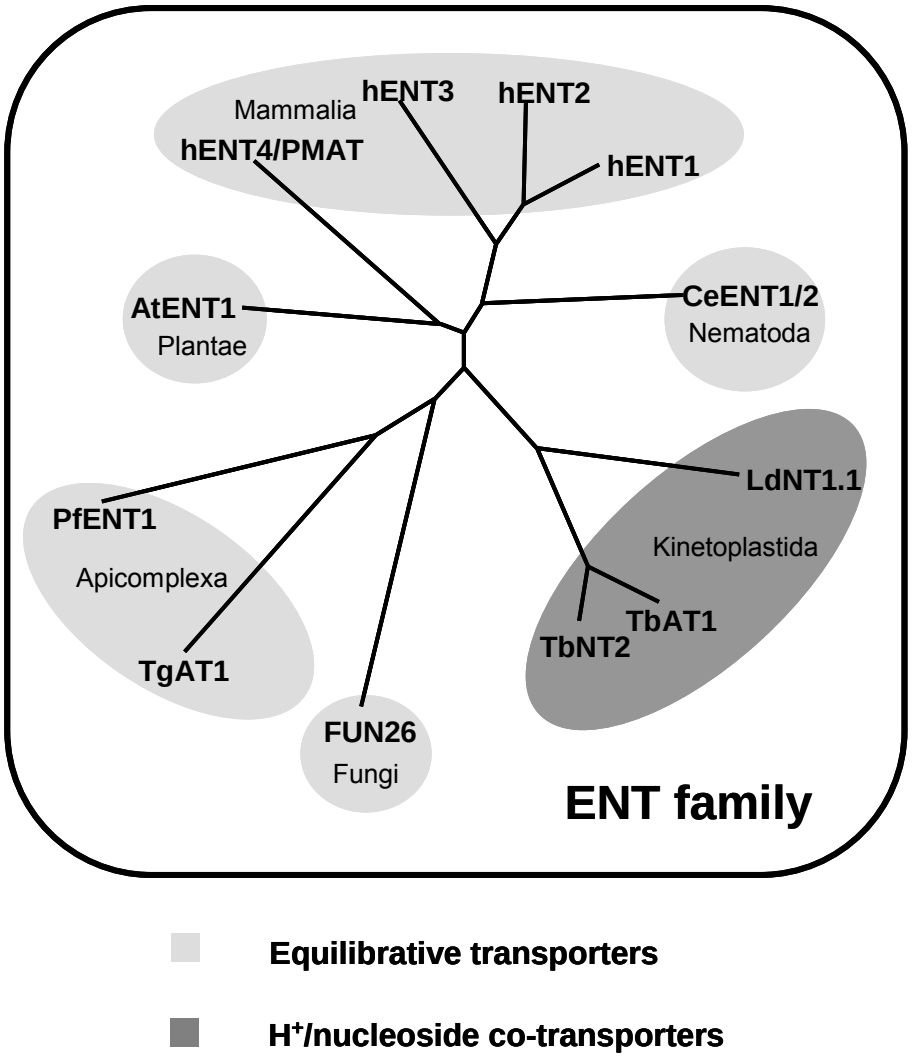

Figure 1-5. Phylogenetic relationships within the ENT family of nucleoside transporter proteins. At, *Arabidopsis thaliana*; Ce, *Caenorhabditis elegans*; FUN, function unknown now; h, human; Ld, *Leishmania donovani*; Pf, *Plasmodium falciparum*; Tb, *Trypanosoma brucei*; Tg, *Toxoplasma gondii* (55).

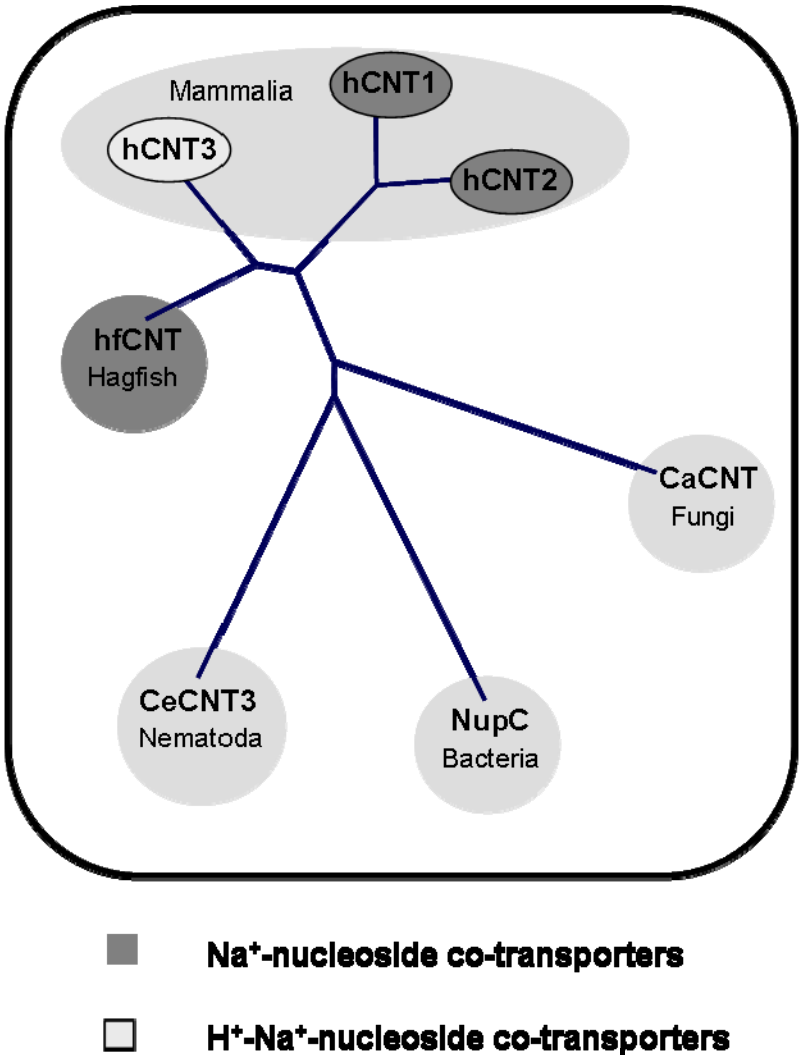

Figure 1-6. Phylogenetic relationships within the CNT family of nucleoside transporter proteins. h, human; hf, *Eptatretus stouti* (hagfish); Ce, *Caenorhabditis elegans*.; NupC, *Escherichia coli* CNT; Ca, *Candida albicans*.

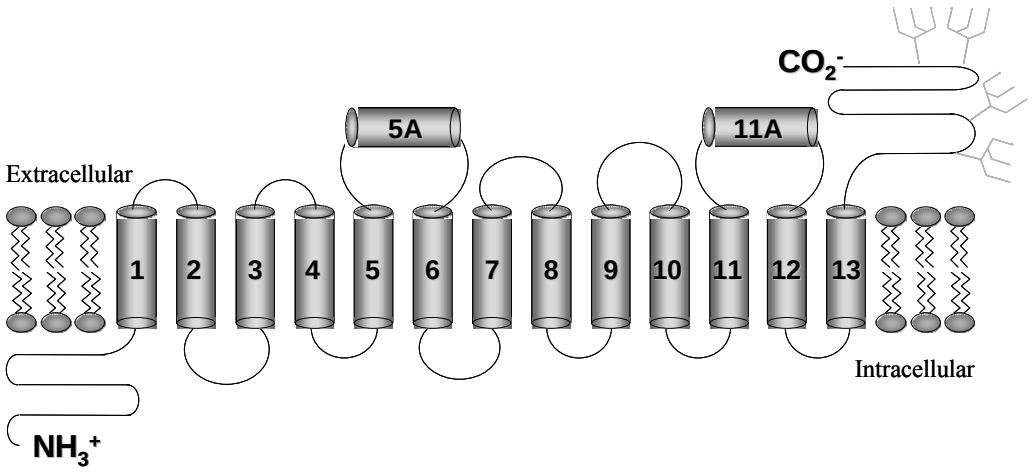

Figure 1-7. Putative model of CNT topology. Potential transmembrane helices are numbered and the sites of *N*-glycosylation in hCNT3 (137) are indicated by the ψ symbol.

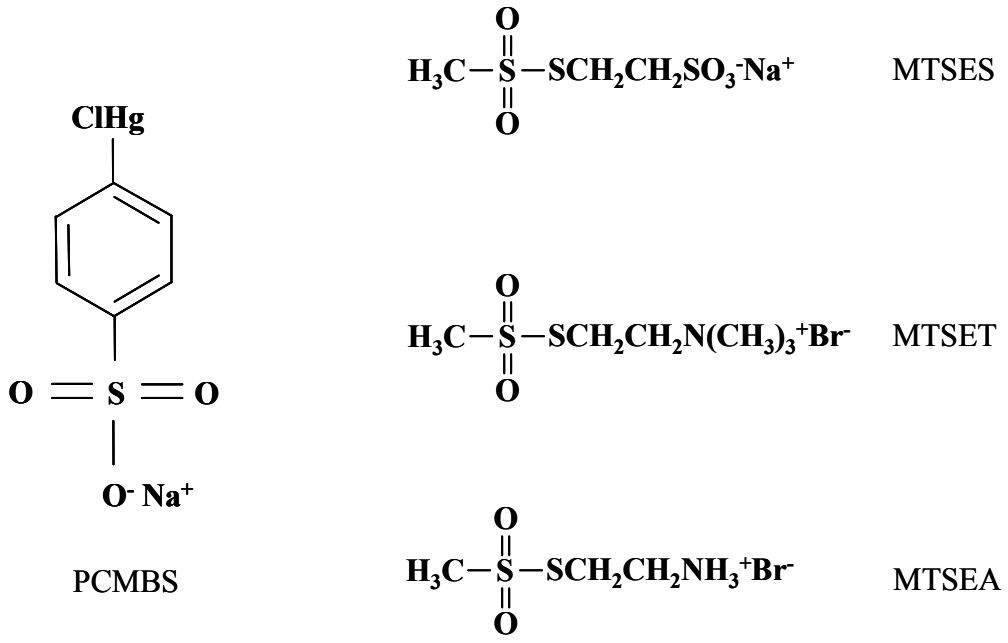

Figure 1-8. Structure of *para*-chloromercuribenzene sulfonate (PCMBS) and methanethiosulfonate (MTS) reagents.

Bibliography

1. Young, J. D., and Jarvis, S. M. (1983) Nucleoside transport in animal cells. *Biosci. Rep.* **3**: 309-322.

2. Young, J. D., Paterson, A. R., and Henderson, J. F. (1985) Nucleoside transport and metabolism in erythrocytes from the Yucatan miniature pig. Evidence that inosine functions as an in vivo energy substrate. *Biochim. Biophys. Acta.* **842**: 214-224.

3. Mathew, A., Grdisa, M., and Johnstone, R. M. (1993) Nucleosides and glutamine are primary energy substrates for embryonic and adult chicken red cells. *Biochem. Cell Biol.* **71**: 288-295.

4. Mathew, A., Grdisa, M., Robbins, P. J., White, M. K., and Johnstone, R. M. (1994) Loss of glucose transporters is an early event in differentiation of HD3 cells. *Am. J. Physiol.* **266**: C1222-C1230.

5. Mubagwa, K., Mullane, K., and Flameng, W. (1996) Role of adenosine in the heart and circulation. *Cardiovasc. Res.* **32**: 797-813.

6. Mubagwa, K., and Flameng, W. (2001) Adenosine, adenosine receptors and myocardial protection: an updated overview. *Cardiovasc. Res.* **52**: 25-39.

7. West, G. A., and Belardinelli, L. (1985) Sinus slowing and pacemaker shift caused by adenosine in rabbit SA node. *Pflugers Arch.* **403**: 66-74.

8. Belardinelli, L., Linden, J., and Berne, R. M. (1989) The cardiac effects of adenosine. *Prog. Cardiovasc. Dis.* **32**: 73-97.

9. Zaza, A., Rocchetti, M., and DiFrancesco, D. (1996) Modulation of the hyperpolarization-activated current (I_f) by adenosine in rabbit sinoatrial myocytes. *Circulation* **94**: 734-741.

10. Shryock, J. C., and Belardinelli, L. (1997) Adenosine and adenosine receptors in the cardiovascular system: biochemistry, physiology, and pharmacology. *Am. J. Cardiol.* **79**: 2-10.

11. de Jong, J. W., de Jonge, R., Keijzer, E., and Bradamante, S. (2000) The role of adenosine in preconditioning. *Pharmacol. Ther.* **87**: 141-149.

12. Baxter, G. (2002) Role of adenosine in delayed preconditioning of myocardium. *Cardiovasc. Res.* **55**: 483-494.

13. Riksen, N. P., Smits, P., and Rongen, G. A. (2004) Ischaemic preconditioning: from molecular characterization to clinical application - part I. *Neth. J. Med.* **62**: 353-363.

14. Loffler, M., Morote-Garcia, J. C., Eltzschig, S. A., Coe, I. R., and Eltzschig, H. K. (2007) Physiological roles of vascular nucleoside transporters. *Arterioscler. Thromb. Vasc. Biol.* **27**: 1004-1013.

15. Cronstein, B. N. (1994) Adenosine, an endogenous anti-inflammatory agent. *J. Appl. Physiol.* **76**: 5-13.

16. Linden, J. (2001) Molecular approach to adenosine receptors: receptor-mediated mechanisms of tissue protection. *Annu. Rev. Pharmacol. Toxicol.* **41**: 775-787.

17. Koszalka, P., Ozűyaman, B., Huo, Y., Zernecke, A, Flőgel, U., Braun, N., Buchheiser, A., Decking, U. K., Smith, M. L., Sévigny, J., Gear, A., Weber, A. A., Molojavyi, A., Ding, Z., Weber, C., Ley, K., Zimmermann, H., Gődecke, A., and Schrader, J. (2004) Targeted disruption of cd73/ecto-5'-nucleotidase alters thromboregulation and augments vascular imflammatory response. *Circ. Res.* **95**: 814-821.

18. Jennings, L. K., White, M. N., and Mandrell, T. D. (1995) Interspecies comparison of platelet aggregation, LIBS expression and clot retraction: observed differences in GPIIb-IIIa functional activity. *Thromb. Haemost.* **74**: 1551-1556.

19. Birk, A. V., Broekman, M. J., Gladek, E. M., Robertson, H. D., Drosopoulos, J. H., Marcus, A. J., and Szeto, H. H. (2002) Role of extracellular ATP metabolism in regulation of platelet reactivity. *J. Lab. Clin. Med.* **140**: 166-175.

20. Spielman, W. S., and Arend, L. J. (1991) Adenosine receptors and signaling in the kidney. *Hypertension* **17**: 117-130.

21. Navar, L. G., Inscho, E. W., Majid, D. S. A., Imig, J. D., Harrison-Bernard, L. M., and Mitchell, K. D. (1996) Paracrine regulation of the renal microcirculation. *Physiol. Rev.* **76**: 425-536.

22. Poon, A., and Sawynok, J. (1998) Antinociception by adenosine analogs and inhibitors of adenosine metabolism in an inflammatory thermal hyperalgesia model in the rat. *Pain* **74**: 235-245.

23. Sawynok, J. (1998) Adenosine receptor activation and nociception. *Eur. J. Pharmacol.* **347**: 1-11.

24. Fox, I. H., and Kelley, W. N. (1978) The role of adenosine and 2'-deoxyadenosine in mammalian cells. *Annu. Rev. Biochem.* **47**: 655-686.

25. Dunwiddie, T. V., and Masino, S. A. (2001) The role and regulation of adenosine in the central nervous system. *Annu. Rev. Neurosci.* **24**: 31-55.

26. Latini, S., and Pedata, F. (2001) Adenosine in the central nervous system: release mechanisms and extracellular concentrations. *J. Neurochem.* **79**: 463-484.

27. King, A. E., Ackley, M. A., Cass, C. E., Young, J. D., and Baldwin, S. A. (2006) Nucleoside transporters: from scavengers to novel therapeutic targets. *Trends Pharmacol. Sci.* **27**: 416-425.

28. Cass, C. E. (1995) Nucleoside transport, in *Drug Transport in Antimicrobial and Anticancer Chemotherapy* (Georgopapadakou, N. H., Ed.), pp 403-451, Marcel Deker, New York.

29. Griffith, D. A., and Jarvis, S. M. (1996) Nucleoside and nucleobase transport systems of mammalian cells. *Biochim. Biophys. Acta* **1286**: 153-181.

30. Cass, C. E., Young, J. D., and Baldwin, S. A. (1998) Recent advances in the molecular biology of nucleoside transporters of mammalian cells. *Biochem. Cell Biol.* **76**: 761-770.

31. Baldwin, S. A., Mackey, J. R., Cass, C. E., and Young, J. D. (1999) Nucleoside transporters: molecular biology and implications for therapeutic development. *Mol. Med. Today* **5**: 216-224.

32. Cass, C. E., Young, J. D., Baldwin, S. A., Cabrita, M. A., Graham, K. A., Griffiths, M., Jennings, L. L., Mackey, J. R., Ng, A. M., Ritzel, M. W., Vickers, M. F., and Yao, S. Y. (1999) Nucleoside transporters of mammalian cells. *Pharm. Biotechnol.* **12**: 313-352.

33. Cheeseman, C. I., Mackey, J. R., Cass, C. E., Baldwin, S. A., and Young, J. D. (2000) Molecular mechanisms of nucleoside and nucleoside drug transport, in *A Volume of Current Topics in Membranes*, pp 330-379, Academic Press, San Diego.

34. Young, J. D., Cheeseman, C., Mackey, J. R., Cass, C. E., and Baldwin, S. A. (2000) In *Current Topics in Membranes, 50* (Barrett, K. E., and Donowitz, M., eds.) pp 329-378, Academic Press, San Diego.

35. Moyer, J. D., Oliver, J. T., and Handschumacher, R. E. (1981) Salvage of circulating pyrimidine nucleosides in the rat. *Cancer Res.* **41**: 3010-3017.

36. Holstege, A., Manglitz, D., and Gerok, W. (1984) Depletion of blood plasma cytidine due to increased hepatocellular salvage in D-galactosamine-treated rats. *Eur. J. Biochem.* **141**: 339-344.

37. Karle, J. M., Anderson, L. W., and Cysyk, R. L. (1984) Effect of plasma concentrations of uridine on pyrimidine biosynthesis in cultered L1210 cells. *J. Biol. Chem.* **259**: 67-72.

38. Lajtha, L. G., and Vane, J. R. (1958) Dependence of bone marrow cells on the liver for purine supply. *Nature* **182**: 191-192.

39. Fontenelle, L. J., and Henderson, J. F. (1969) An enzymatic basis for the inability of erythrocytes to synthesize purine ribonucleotides *de novo*. *Biochim. Biophys. Acta.* **177**: 175-176.

40. Plagemann, P. G., Wohlheuter, R. M., and Kraupp, M. (1985) Adenine nucleotide metabolism and nucleoside transport in human erythrocytes under ATP depletion conditions. *Biochim. Biophys. Acta.* **817**: 51-60.

41. Mackinnon, A. M., and Deller, D. J. (1973) Purine nucleotide biosynthesis in gastrointestinal mucosa. *Biochem. Biophys. Acta.* **319**: 1-4.

42. Murray, A. W. (1971) The biological significance of purine salvage. *Annu. Rev. Biochem.* **40**: 811-826.

43. Marr, J. J., Berens, R. L., and Nelson, D. J. (1978) Purine metabolism in *Leishmania donovani* and *Leishmania braziliensis*. *Biochim. Biophys. Acta* **544**: 360-371.

44. Krug, E. C., Marr, J. J., and Berens, R. L. (1989) Purine metabolism in *Toxoplasma gondii*. *J. Biol. Chem.* **264**: 10601-10607.

45. Berens, R. L., Krug, E. C., and Marr, J. J. (1995) in *Biochemistry of Parasitic Organisms and Its Molecular Foundations* (Marr, J. J., and Muller, M., eds) pp. 89-117, Academic Press, London

46. Landfear, S. M. (2001) Molecular genetics of nucleoside transporters in Leishmanian and African trypanosomes. *Biochemical Parmacology* **63**: 149-155.

47. Landfear, S. M., Ullman, B., Carter, N. S., and Sanchez, M. A. (2004) Nucleoside and nucleobase transporters in parasitic protozoa. *Eukaryot. Cell* **3**: 245-254.

48. Bellofatto, V. (2007) Pyrimidine transport activities in tyrpanosomes. *Trends Parasitol.* **23**: 187-189.

49. Lerner, M. H., and Lowy, B. A. (1974) The formation of adenosine in rabbit liver and its possible role as a direct precursor of erythrocyte adenine nucleotides. *J. Biol. Chem.* **249**: 959-966.

50. Pritchard, J. B., O'Connor, N., Oliver, J. M., and Berlin, R. D. (1975) Uptake and supply of purine compounds by the liver. *Am. J. Physiol.* **229**: 967-972.

51. Monks, A., and Cysyk, R. L. (1982) Uridine regulation by the isolated rat liver: perfusion with an artificial oxygen carrier. *Am. J. Physiol.* **242**: R465-R470.

52. Thorn, J. A., and Jarvis, S. M. (1996) Adenosine transporters. *Gen. Pharmcol.* **27**: 613-620.

53. Baldwin, S. A., Beal, P. R., Yao, S. Y. M., King, A. E., Cass, C. E., and Young, J. D. (2004) The equilibrative nucleoside transporter family, SLC29. *Pflugers Arch.* **447**: 735-743.

54. Pisoni, R. L., and Thoene, J. G. (1989) Detection and characterization of a nucleoside transport system in human fibroblast lysosomes. *J. Biol. Chem.* **264**: 4850-4856.

55. Young, J. D., Yao, S. Y. M., Sun, L., Cass, C. E., and Baldwin, S. A. (2008) The ENT family of nucleoside and nucleobase transporter proteins. *Xenobiotica* **38**:995-1021.

56. Young, J. D., Yao, S. Y. M., Cass, C. E., and Baldwin, S. A. (2003) Equilibrative nucleoside transport proteins. In *Red Cell Transport in Health and Disease* pp 321-337. Springer Verlag, Berlin.

57. Griffiths, M., Beaumont, N., Yao, S. Y. M., Sundaram, M., Bouman, C. E., Davies, A., Kwong, F. Y. P., Coe, I. R., Cass, C. E., Young, J. D., and Baldwin, S. A. (1997) Cloning of a human nucleoside transporter implicated in the cellular uptake of adenosine and chemotherapeutic drugs. *Nat. Med.* **3**: 89-93.

58. Griffiths, M., Yao, S. Y. M., Abidi, F., Phillips, S. E. V., Cass, C. E., Young, J. D., and Baldwin, S. A. (1997) Molecular cloning and characterization of a nitrobenzylthioinosine-insensitive (*ei*) equilibrative nucleoside transporter from human placenta. *Biochem. J.* **328**: 739-743.

59. Crawford, C. R., Patel, D. H., Naeve, C., and Belt, J. A. (1998) Cloning of the human equilibrative, nitrobenzylmercaptopurine riboside (NBMPR)-insensitive nucleoside transporter *ei* by functional expression in a transport-deficient cell line. *J. Biol. Chem.* **273**: 5288-5293.

60. Hyde, R. J., Cass, C. E., Young, J. D., and Baldwin, S. A. (2001) The ENT family of eukaryote nucleoside and nucleobase transporters: recent advances in the investigation of structure/function relationships and the identification of novel isoforms. *Mol. Membr. Biol.* **18**: 53-63.

61. Acimovic, Y., and Coe, I. R. (2002) Molecular evolution of the equilibrative nucleoside transporter family: identification of novel family members in prokaryotes and eukaryotes. *Mol. Biol. Evol.* **19**: 2199-2210.

62. Engel, K., Zhou, M., and Wang, J. (2004) Identification and characterization of a novel monomamine transporter in the human brain. *J. Biol. Chem.* **279**: 50042-50049.

63. Engel, K., and Wang, J. (2005) Interaction of organic cations with a newly identified plasma membrane monoamine transporter. *Mol. Pharmacol.* **68**: 1397-1407.

64. Baldwin, S. A., Yao, S. Y. M., Hyde, R. J., Ng, A. M. L., Foppolo, S., Barnes, K., Ritzel, M. W. L., Cass, C. E., and Young, J. D. (2005) Functional characterization of novel human and mouse equilibrative nucleoside transporters (hENT3 and mENT3) located in intracellular membranes. *J. Biol. Chem.* **280**: 15880-15887.

65. Barnes, K., Dobrzynski, H., Foppolo, S., Beal, P. R., Ismat, F., Scullion, E. R., Sun, L., Tellez, J., Ritzel, M. W. L., Claycomb, W. C., Cass, C. E., Young, J. D., Billeter-Clark, R., Boyett, M. R., and Baldwin, S. A. (2006) Distribution and functional characterization of equilibrative nucleoside transporter-4, a novel cardiac adenosine transporter activated at acidic pH. *Circ. Res.* **99**: 510-519.

66. Xia, L., Engel, K., Zhou, M., and Wang, J. (2006) Membrane localization and pH-dependent transport of a newly cloned organic cation transporter (PMAT) in kidney cells. *Am. J. Physiol. Renl Physiol.* **292**: F682-F690.

67. Zhou, M., Engel, K., and Wang, J. (2006) Evidence for significant contribution of a newly identified monomamine transporter (PMAT) to serotonin uptake in the human brain. *Biochem. Pharm.* **73**: 147-154.

68. Zhang, J., Visser, F., King, K. M., Baldwin, S. A., Young, J. D., and Cass, C. E. (2007) The role of nucleoside transporters in cancer chemotherapy with nucleoside drugs. *Cancer Metastasis Rev.* **26**: 85-110.

69. de Koning, H. P., Bridges, D. J., and Burchmore, R. J. (2005) Purine and pyrimidine transport in pathogenic protozoa: From biology to therapy. *FEMS Microbiology Reviews* **29**: 987-1020.

70. Le Hir, M., and Duback, U. C. (1984) Sodium gradient-energized concentrative transport of adenosine in renal brush border vesicles. *Pflugers Arch.* **401**: 58-63.

71. Le Hir, M., and Duback, U. C. (1985) Concentrative transport of purine nucleosides in brush border vesicles of the rat kidney. *Eur. J. Clin. Invest.* **15**: 121-127.

72. Le Hir, M., and Duback, U. C. (1985) Uphill concentraive transport of pyrimidine nucleosides in renal brush border vesicles. *Pflugers Arch.* **404**: 238-243.

73. Lee, C. W., Cheeseman, C. I., and Jarvis, S. M. (1988) Na^+- and K^+-dependent uridine transport in rat renal brush-border membrane vesicles. *Biochim. Biophys. Acta.* **942**: 139-149.

74. Jarvis, S. M. (1989) Characterization of sodium-dependent nucleoside transport in rabbit intestinal brush-border membrane vesicles. *Biochem. Biophys. Acta.* **979**: 132-138.

75. Williams, T. C., Doherty, A. J., Griffith, D. A., and Jarvis, S. M. (1989) Characterization of sodium-dependent and sodium-independent nucleoside transport systems in rabbit brush-border and basolateral plasma-membrane vesicles from the renal outer cortex. *Biochem. J.* **264**: 223-231.

76. Le Hir, M. (1990) Evidence for separate carriers for purine nucleosides and for pyrimidine nucleosides in the renal brush border membrane. *Ren. Physiol. Biochem.* **13**: 154-161.

77. Williams, T. C., and Jarvis, S. M. (1991) Multiple sodium-dependent nucleoside transport systems in bovine renal brush-border membrane vesicles. *Biochem. J.* **274**: 27-33.

78. Cabrita, M. A., Baldwin, S. A., Young, J. D., and Cass, C. E. (2002) Molecular biology and regulation of nucleoside and nucleobase transporter proteins in eukaryotes and prokaryotes. *Biochem. Cell Biol.* **80**: 623-638.

79. Kong, W., Engel., K., and Wang, J. (2004) Mammalian nucleoside transporters. *Current Drug Metabolism* **5**: 63-84.

80. Gray, J. H., Owen, R. P., and Giacomini, K. M. (2004) The concentrative nucleoside transporter family, SLC28. *Pflugers Arch.* **447**: 728-734.

81. Schwenk, M., Hegazy, E., and del Pino, V. L. (1984) Uridine uptake by isolated intestinal epithelial cells of guinea pig. *Biochim. Biophys. Acta* **805**: 370-374.

82. Vijayalakshmi, D., and Belt, J. A. (1988) Sodium-dependent nucleoside transport in mouse intestinal epithelial cells. *J. Biol. Chem.* **263**: 19419-19423.

83. Jarvis, S. M., and Griffith, D. A. (1991) Expression of the rabbit intestinal N2 Na^+/nucleoside transporter in *Xenopus laevis* ocoytes. *Biochem. J.* **278**: 605-607.

84. Thomas, S. A., and Segal, M. B. (1997) Saturation kinetics, specificity and NBMPR sensitivity of thymidine entry into the central nervous system. *Brain Res.*, **760:** 59-67.

85. Plagemann, P. G. W., and Woffendin, C. (1989) Na^+-dependent and -independent transport of uridine and its phosphorylation in mouse spleen cells. *Biochim. Biophys. Acta* **981**: 315-325.

86. Plagemann, P. G. W., and Aran, J. M. (1990) Characterization of Na^+-dependent, active nucleoside transport in rat and mouse peritoneal macrophages, a mouse macrophage cell line and normal rat kidney cells. *Biochim. Biophys. Acta* **1028**: 289-298.

87. Che, M., Nishida, T., Gatmaitan, Z., and Arias, I. M. (1992) A nucleoside transporter is functionally linked to ectonucleotidases in rat liver canalicular membrane. *J. Biol. Chem.* **267**: 9684-9688.

88. Crawford, C. R., Ng, C. Y. C., Noel, L. D., and Belt, J. A. (1990) Nucleoside transport in L1210 murine leukemia cells. Evidence for three transporters. *J. Biol. Chem.* **265**: 9732-9736.

89. Gutierrez, M. M., Brett, C. M., Ott, R. J., Hui, A. C., and Giacomini, K. M. (1992) Nucleoside transport in brush border membrane vesicles from human kidney. *Biochim. Biophys. Acta* **1105**: 1-9.

90. Franco, R., Centelles, J. J., and Kinne, R. K. H. (1990) Further characterization of adenosine transport in renal brush-border membranes. *Biochim. Biophys. Acta* **1024**: 241-248.

91. Baer, H. P.,and Moorji, A. (1990) Sodium-dependent and inhibitor-insensitive uptake of adenosine by mouse peritoneal exudate cells. *Biochim. Biophys. Acta* **1026**: 241-247.

92. Belt, J. A., Harper, E. H., Byl, J. A., and Noel, L. D. (1992) Na^+-dependent nucleoside transport in human myeloid leukemic cell lines and freshly isolated myeloblasts. *Proc. Am. Assoc. Cancer Res.* **33**: 20.

93. Belt, J. A., Marina, N. M., Phelps, D. A., and Crawford, C. R. (1993) Nucleoside transport in normal and neoplastic cells. *Adv. Enzyme Regul.* **33**: 235-252.

94. Huang, Q., Harvey, C. M., Paterson, A. R. P., Cass, C. E., and Young, J. D. (1993) Functional expression of Na^+-dependent nucleoside transport systems of rat intestine in isolated oocytes of *Xenopus laevis*. Demonstration that rat jejunum expresses the purine-selective system N1 (*cif*) and a second, novel system N3 having broad specificty for purine and pyrimidine nucleosides. *J. Biol. Chem.* **268**: 20613-20619.

95. Wu, X., Yuan, G., Brett, C. M., Hui, A. C., and Giacomini, K. M. (1992) Sodium-dependent nucleoside transport in choroid plexus from rabbit. Evidence for a single transporter for purine and pyrimidine nucleosides. *J. Biol. Chem.* **267**: 8813-8818.

96. Hong, M., Schlichter, L., and Bendayan, R. (2000) A Na^+-dependent nucleoside transporter in microglia. *J. Pharmacol. Exp. Ther.* **292**: 366-374.

97. Gutierrez, M. M., and Giacomini, K. M. (1994) Expression of a human renal nucleoside transporter in *Xenopus laevis* oocytes. *Biochem. Pharmacol.* **48**: 2251-2253.

98. Gutierrez, M. M., and Giacomini, K. M. (1993) Substrate selectivity, potential sensitivity and stoichiometry of Na^+-nucleoside transport in brush border membrane vesicles from human kidney. *Biochim. Biophys. Acta* **1149**: 202-208.

99. Paterson, A. R., Gati, W. P., Vijayalakshmi, D., Cass, C. E., Mant, M. J., Young, J. D., and Belch, A. R. (1993) Inhibitor-sensitive, Na^+-linked transport of nucleoside analogs in leukemic cells from patients. *Proc. Am. Assoc. Cancer Res.* **34**: A84.

100. Flanagan, S. A., Gandhi, V., Secrist, J. A. 3rd, and Meckling, K. A. (2003) The novel nucleoside transport system exhibited by NB4 cells, *csg*, transports deoxyguanosine analogues, including ara-G. *Biochem. Pharmacol.* **66**: 733-737.

101. Huang, Q. Q., Yao, S. Y. M., Ritzel, M. W. L., Paterson, A. R. P., Cass, C. E., and Young, J. D. (1994) Cloning and functional expression of a complementary DNA encoding a mammalian nucleoside transport protein. *J. Biol. Chem.* **269**: 17757-17760.

102. Hamilton, S. R., Yao, S. Y., Ingram, J. C., Henderson, P. J. F., Gallagher, M. P., Cass, C. E., Young, J. D., and Baldwin, S. A. (1997) Anti-peptide antibodies as probes of the structure and subcellular distribution of the sodium-dependent nucleoside transporter, rCNT1. *J. Physiol. (Lond)* **499**: 50-51.

103. Hamilton, S. R., Yao, S. Y., Ingram, J. C., Hadden, D. A., Ritzel, M. W., Gallagher, M. P., Henderson, P. J., Cass, C. E., Young, J. D., and Baldwin, S. A. (2001) Subcellular distribution and membrane topology of the mammalian concentrative Na^+-nucleoside cotransporter, rCNT1. *J. Biol. Chem.* **276**: 27981-27988.

104. Ritzel, M. W. L., Yao, S. Y. M., Huang, M. Y., Elliot, J. F., Cass, C. E., and Young, J. D. (1997) Molecular cloning and functional expression of cDNAs encoding a human Na^+-nucleoside cotransporter (hCNT1). *Am. J. Physiol.* **272**: C707-C714.

105. Pajor, A. M. (1998) Sequence of a pyrimidine-selective Na^+-nucleoside cotransporter from pig kidney, pKCNT1. *Biochim. Biophys. Acta.* **1415**: 266-269.

106. Fang, X., Parkinson, F. E., Mowles, D. A., Young, J. D., and Cass, C. E. (1996) Functional characterization of a recombinant sodium-dependent nucleoside transporter with selectivity for pyrimidine nucleosides (cNT1rat) by transient expression in cultured mammalian cells. *Biochem. J.* **317**: 457-465.

107. Dresser, M. J., Gerstin, K. M., Gray, A. T., Loo, D. D., and Giacomini, K. M. (2000) Electrophysiological analysis of the substrate selectivity of a sodium-coupled nucleoside transporter (rCNT1) expressed in *Xenopus laevis* oocytes. *Drug Metab. Dispos.* **28**: 1135-1140.

108. Larráyoz, I. M., Casado, F. J., Pastor-Anglada, M., and Lostao, M. P. (2004) Electrophysiological characterization of the human Na^+/nucleoside cotransporter

1 (hCNT1) and role of adenosine on hCNT1 function. *J. Biol. Chem.* **279**: 8999-9007.

109. Smith, K. M, Ng, A. M., Yao, S. Y. M., Labedz, K. A., Knauss, E. E., Wiebe, L. I., Cass, C. E., Baldwin, S. A., Chen, X.-Z., Karpinski, E., and Young, J. D. (2004) Electrophysiological characterization of a recombinant human Na^+-coupled nucleoside transporter (hCNT1) produced in *Xenopus* oocytes. *J. Physiol.* **558**: 807-823.

110. Yao, S. Y. M., Ng, A. M. L., Ritzel, M. W. L., Gati, W. P., Cass, C. E., and Young, J. D. (1996) Transport of adenosine by recombinant purine- and pyrimidine-selective sodium/nucleoside cotransporters from rat jejunum expressed in *Xenopus laevis* oocytes. *Mol. Pharmacol.* **50**: 1529-1535.

111. Mackey, J. R., Baldwin, S. A., Young, J. D., and Cass, C. E. (1998) Nucleoside transport and its significance for anticancer drug resistance. *Drug Resist. Updat.* **1**: 310-324.

112. Yao, S. Y. M., Cass, C. E., and Young, J. D. (1996) Transport of the antiviral nucleoside analogs 3'-azido-3'-deoxythimidine and 2',3'-dideoxycytidine by a recombinant nucleoside transporter (rCNT1) expressed in *Xenopus laevis* oocytes. *Mol. Pharmacol.* **50**: 388-393.

113. Mackey, J. R., Yao, S. Y., Smith, K. M., Karpinski, E., Baldwin, S. A., Cass, C. E., and Young, J. D. (1999) Gemcitabine transport in *Xenopus* oocytes expressing recombinant plasma membrane mammalian nucleoside transporters. *J. Natl. Canc. Institute* **91**: 1876-1881.

114. Lostao, M. P., Mata, J. F., Larrayoz, I. M., Inzillo, S. M., Casado, F. J., and Pastor-Anglada, M. (2000) Electrogenic uptake of nucleosides and nucleoside-derived drugs by the human nucleoside transporter 1 (hCNT1) expressed in *Xenopus laevis* oocytes. *FEBS Lett.* **481**: 137-140.

115. Lang, T. T., Young, J. D., and Cass, C. E. (2004) Interactions of nucleoside analogs, caffeine, and nicotine with human concentrative nucleoside transporters 1 and 2 stably produced in a transport-defective human cell line. *Mol. Pharm.* **65**: 925-933.

116. Mata, J. F., Garcia-Manteiga, J. M., Lostao, M. P., Fernández-Veledo, S., Guillén-Gómez, E., Larrayoz, I. M., Lloberas, J., Casado, F. J., and Pastor-Anglada, M. (2001) Role of the human concentrative nucleoside tranpsorter

(hCNT1) in the cytotoxic action of 5'-deoxy-5-fluorouridine, an active intermediate metabolite of capecitabine, a novel oral anticancer drug. *Mol. Pharm.* **59**: 1542-1548.

117. Graham, K. A., Leithoff, J., Coe, I. R., Mowles, D., Mackey, J., R., Young, J. D., and Cass, C. E. (2000) Differential transport of cytosine-containing nucleosides by recombinant human concentrative nucleoside transporter protein hCNT1. *Nucleosides Nucleotides Nucleic Acids* **19**: 415-434.

118. Damaraju, V. L., Damaraju, S., Young, J. D., Baldwin, S. A., Mackey, J., Sawyer, M. B., and Cass, C. E. (2003) Nucleoside anticancer drugs: the role of nucleoside transporters in resistance to cancer chemotherapy. *Oncogene* **22**: 7524-7536.

119. Govindarajan, R., Bakken, A. H., Hudkins, K. L., Lai, Y., Casado, F. J., Pastor-Anglada, M., Tse, C. M., Hayashi, J., and Unadkat, J. D. (2007) *In situ* hybridization and immunolocalization of concentrative and equilibrative nucleoside transporters in the human intestine, liver, kidneys and placenta. *Am. J. Physiol. Regul. Integr. Comp. Physiol.* **293**: R1809-1822.

120. Felipe, A., Valdes, R., Santo., B., Lloberas, J., Casado, J., and Pastor-Anglada, M. (1998) Na^+-dependent nucleoside transport in liver: Two different isoforms from the same gene family are expressed in liver cells. *Biochem. J.* **330**: 997-1001.

121. Lai, Y. R., Bakken, A. H., and Unadkat, J. D. (2002) Simultaneous expression of hCNT1-CFP and hENT1-YFP in Madin-Darby canine kidney cells - localization and vectorial transport studies. *J. Biol. Chem.* **277**: 37711-37717.

122. Mangravite, L. M., Lipschutz, J. H., Mostov, K. E., and Giacomini, K. M. (2001) Localization of GFP-tagged concentrative nucleoside transporters in a renal polarized epithelial cell line. *Am. J. Physiol. Renal Physiol.* **280**: F879-F885.

123. Pennycooke, M., Chaudary, N., Shuralyova, I., Zhang, Y., and Coe, I. R. (2001) Differential expression of human nucleoside transporters in normal and tumor tissue. *Biochem. Biophys. Res. Commun.* **280**: 951-959.

124. Anderson, C. M., Xiong, W., Young, J. D., Cass, C. E., and Parkinson, F. E. (1996) Demonstration of the existence of mRNAs encoding N1/*cif* and N2/*cit* sodium/nucleoside cotransporters in rat brain. *Mol. Brain Res.* **42**: 358-361.

125. Che, M., Ortiz, D. F., and Arias, I. M. (1995) Primary structure and functional expression of a cDNA encoding the bile canalicular, purine-specific Na^+-nucleoside cotransporter. *J. Biol. Chem.* **270**: 13596-13599.

126. Wang, J., Su, S. F., Dresser, M. J., Schaner, M. E., Washington, C. B., and Giacomini, K. M. (1997) Na^+-dependent purine nucleoside transporter from human kidney: cloning and functional characterization. *Am. J. Physiol.* **273**: F1058-F1065.

127. Ritzel, M. W. L., Yao, S. Y. M., Ng, A. M. L., Mackey, J. R., Cass, C. E., and Young, J. D. (1998) Molecular cloning, functional expression and chromosomal localization of a cDNA encoding a human Na^+/nucleoside cotransporter (hCNT2) selective for purine nucleosides and uridine. *Mol. Membr. Biol.* **15**: 203-211.

128. Patel, D., Crawford, C., Naeve, C., and Belt, J. (1997) Molecular cloning and characterization of a mouse purine-selective concentrative nucleoside transporter. *Proc. Am. Assoc. Cancer Res.* **38**: 60.

129. Gerstin, K. M., Dresser, M. J., Wang, J., and Giacomini, K. M. (2000) Molecular cloning of a Na^+-dependent nucleoside transporter from rabbit intestine. *Pharm. Res.* **17**: 906-910.

130. Schaner, M. E., Wang, J., Zhang, L., Su, S. F., Gerstin, K. M., and Giacomini, K. M. (1999) Functional characterization of a human purine-selective, Na^+-dependent nucleoside transporter (hSPNT1) in a mammalian expression system. *J. Pharm. Exp. Ther.* **289**: 1487-1491.

131. Gerstin, K., M., Dresser, M. J., and Giacomini, K. M. (2002) Specificity of human and rat orthologs of the concentrative nucleoside transporter, SPNT. *Am. J. Phys. Renal Phys.* **283**: F344-F349.

132. Lang, T. T., Selner, M., Young, J. D., and Cass, C. E. (2001) Acquisition of human concentrative nucleoside transporter 2 (hcnt2) activity by gene transfer confers sensitivity to fluoropyrimidine nucleosides in drug-resistance leukemia cells. *Mol. Pharmacol.* **60**: 1143-1152.

133. Li, J. Y., Boado. R. J., and Pardridge, W. M. (2001) Differential kinetics of transport of 2', 3'-dideoxyinosine and adenosine via concentrative Na^+ nucleoside transporter CNT2 cloned from rat blood-brain barrier. *J. Pharm. Exp. Ther.* **299**: 735-740.

134. Larráyoz, I. M., Fernández-Nistal, A., Garcés, A. Gorraitz, E., and Lostao, M. P. (2006) Characterization of the rat Na^+/nucleoside cotransporter 2 and transport of nucleoside-derived drugs using electrophysiological methods. *Am. J. Physiol. Cell Physiol.* **291**: C1395-C1404.

135. Leung, G. P., Ward, J. L., Wong, P. Y., and Tse, C. T. (2001) Characterization of nucleoside transport systems in cultured rat epididymal epithelium. *Am. J. Physiol. Cell. Physiol.* **280**: C1076-C1082.

136. Mangravite, L. M., and Giacomini, K. M. (2003) Sorting of rat SPNT in renal epithelium is independent of N-glycosylation. *Pharm. Res.* **20**: 319-323

137. Ritzel, M. W. L., Ng, A. M. L., Yao, S. Y. M., Graham, K., Loewen, S. K., Smith, K. M., Ritzel, R. G., Mowles, D. A., Carpenter, P., Chen, X.-Z., Karpinski, E., Hyde, R. J., Baldwin, S. A., Cass, C. E., and Young, J. D. (2001) Molecular identification and characterization of novel human and mouse concentrative Na^+-nucleoside cotransporter proteins (hCNT3 and mCNT3) broadly selective for purine and pyrimidine nucleosides (system *cib*). *J. Biol. Chem.* **276**: 2914-2927.

138. Toan, S. V., To, K. K., Leung, G. P., de Souza, M. O., Ward, J. L., and Tse, C. M. (2003) Genomic organization and functional characterization of the human concentrative nucleoside transporter-3 isoform (hCNT3) expressed in mammalian cells. *Pflugers Archiv.* **447**: 195-204.

139. Yao, S. Y., Ng, A. M., Loewen, S. K., Cass, C. E., Baldwin, S. A., and Young, J. D. (2002) An ancient prevertabrate Na^+-nucleoside cotransporter (hfCNT) from the Pacific hagfish (*Eptatretus stouti*). *Am. J. Phys. Cell Phys.* **283**: C155-C168.

140. Badagnani, I., Chan, W., Castro, R. A., Brett, C. M., Huang, C. C., Stryke, D., Kawamoto, M., Johns, S. J., Ferrin, T. E., Carlson, E. J., Burchard, E. G., and Giacomini, K. M. (2005) Functional analysis of genetic variants in the human concentrative nucleoside transporter 3 (CNT3; SLC28A3). *Pharmacogenomics J.* **5**: 157-165.

141. Damaraju, V. L., Zhang, J., Visser, F., Tackaberry, T., Dufour, J., Smith, K. M., Slugoski, M. D., Ritzel, M. W., Baldwin, S. A., Young, J. D., and Cass, C. E. (2005) Identification and functional characterization of variants in human concentrative nucleoside transporter 3, hCNT3 (SLC28A3), arising from single nucleotide polymorphisms in coding regions of the hCNT3 gene. *Pharmacogenet. Genomics* **15**: 173-182.

142. Gray, J. H., Mangravite, L. M., Owen, R. P., Urban, T. J., Chan, W., Carlson, E. J., Huang, C. C., Kawamoto, M., Johns, S. J., Stryke, D., Ferrin, T. E., and Giacomini, K. M. (2004) Functional and genetic diversity in the concentrative nucleoside transporter, CNT1, in human populations. *Mol. Pharmacol.* **65**: 512-519.

143. Owen, R. P., Gray, J. H., Taylor, T. R., Carlson, E. J., Huang, C. C., Kawamoto, M., Johns, S. J., Stryke, D., Ferrin, T. E., and Giacomini, K. M. (2005) Genetic analysis and functional characterization of polymorphisms in the human concentrative nucleoside transporter, CNT2. *Pharmacogenet. Genomics* **15**: 83-90.

144. Wu, X., Gutierrez, M. M., and Giacomini, K. M. (1994) Further characterization of the sodium-dependent nucleoside transporter (N3) in choroid plexus from rabbit. *Biochim. Biophys. Acta* **1191**: 190-196.

145. Hu, H., Endres, C. J., Chang, C., Umpathy, N. S., Lee, E. W., Fei, Y. J., Itagaki, S., Swann, P. W., Ganapathy, V., and Unadkat, J. D. (2006) Electrophysiological characterization and modeling of the structure activity relationship of the human concentrative nucleoside transporter 3 (hCNT3). *Mol. Pharmacol.* **69**: 1542-1553.

146. Slugoski, M. D., Ng, A. M., Yao, S. Y., Smith, K. M., Lin, C. C., Zhang, J., Karpinski, E., Cass, C. E., and Baldwin, S. A., and Young, J. D. (2008) A proton-mediated conformational shift identifies a mobile pore-lining cysteine residue (Cys-561) in human concentrative nucleoside transporter 3. *J. Biol. Chem.* **283**: 8496-8507.

147. Smith, K. M., Slugoski, M. D., Loewen, S. K., Ng, A. M., Yao, S. Y., Chen, X.-Z., Karpinski, E., Cass, C. E., Baldwin, S. A., and Young, J. D. (2005) The broadly selective human Na^+/nucleoside cotranpsorter (hCNT3) exhibits novel cation-coupled nucleoside transport characteristics. *J. Biol. Chem.* **280**: 25436-25449.

148. Damaraju, V. L., Elwi, A. N., Hunter, C., Carpenter, P., Santos, C., Barron, G. M., Sun, X., Baldwin, S. A., Young, J. D., Mackey, J. R., Sawyer, M. B., and Cass, C. E. (2007) Localization of broadly selective equilibrative and concentrative nucleoside transporters, hENT1 and hCNT3, in human kidney. *Am. J. Physiol. Renal Physiol.* **293**: F200-F211.

149. Xiao, G., Wang, J., Tangen, T., and Giacomini, K. M. (2001) A novel proton-dependent nucleoside transporter, CeCNT3, from *Caenorhabditis elegans*. *Mol. Pharmacol.* **59**: 339-348.

150. Loewen, S. K., Ng, A. M. L., Mohabir, N. M., Baldwin, S. A., Cass, C. E., and Young, J. D. (2003) Functional characterization of a H^+/nucleoside co-transporter (CaCNT) from *Candida albicans*, a fungal member of the concentrative nucleoside transporter (CNT) family of membrane proteins. *Yeast* **20**: 661-675.

151. Craig, J. E., Zhang, Y., and Gallagher, M. P. (1994) Cloning of the nupC gene of *Escherichia coli* encoding a nucleoside transport system, and identification of an adjacent insertion element, IS 186. *Mol. Micr.* **11**: 1159-1168.

152. Loewen, S. K., Yao, S. Y., Slugoski, M. D., Mohabir, N. N., Turner, R. J., Mackey, J. R., Gallagher, M. P., Henderson, P. J., Baldwin, S. A., Cass, C. E., and Young, J. D. (2004) Transport of physiological nucleosides and anti-viral and anti-neoplastic nucleoside drugs by recombinant *Escherischia coli* nucleoside-H^+ cotransporter (NupC) produced in *Xenopus laevis* oocytes. *Mol. Membr. Biol.* **21**: 1-10.

153. Lum, P. Y., Ngo, L. K., Bakken, A. H., and Unadkat, J. D. (2000) Human intestinal *es* nucleoside transporter: molecular characterization and nucleoside inhibitory profiles. *Cancer Chemother. Pharmacol.* **45**: 273-278.

154. Mun, E. C., Tally, K. J., and Matthews, J. B. (1998) Characterization and regulation of adenosine transport in T84 intestinal epithelial cells. *Am. J. Physiol.* **274**: G261-G269.

155. Patil, S. D., and Unadkat, J. D. (1997) Sodium-dependent nucleoside transport in the human intestinal brush-border membrane. *Am. J. Physiol.* **272**: G1314-G1320.

156. Chandrasena, G., Giltay, R., Patil, S. D., Bakken, A., and Unadkat, J. D. (1997) Functional expression of human intestinal Na^+-dependent and Na^+-independent nucleoside transporters in *Xenopus laevis* oocytes. *Biochem. Pharmacol*. **53**: 1909-1918.

157. Elwi, A. N., Damaraju, V. L., Baldwin, S. A., Young, J. D., Sawyer, M. B., and Cass, C. E. (2006) Renal nucleoside transporters: physiological and clinical implications. *Biochem. Cell. Biol.* **84**: 844-858.

158. Mangravite, L. M., Xiao, G., Giacomini, K. M. (2003) Localization of human equilibrative nucleoside transporters, hENT1 and hENT2, in renal epithelial cells. *Am. J. Physiol.* **284**: F902-910.

159. Pastor-Anglada, M., Errasti-Murugarren, E., Aymerich, I., and Casado, F. J. (2007) Concentrative nucleoside transporters (CNTs) in epithelia: from absorption to cell signaling. *J. Physiol. Biochem.* **63**: 97-110.

160. Pastor-Anglada, M., Casado, F. J., Valdes, R., Mata, J., Garcia-Manteiga, J., and Molina, M. (2001) Complex regulation of nucleoside transproter expression in epithelial and immune system cells. *Mol. Memb. Biol.* **18**: 81-85.

161. Lai, Y., Tse, C.-M., and Unadkat, J. D. (2004) Mitochondrial expression of the human equilibrative nucleoside transporter 1 (hENT1) results in enhanced mitochondrial toxicity of antiviral drugs. *J. Biol. Chem.* **279**: 4490-4497.

162. Mani, R. S., Hammond, J. R., Marjan, J. M. J., Graham, K. A., Young, J. D., Baldwin, S. A., and Cass, C. E. (1998) Demonstration of equilibrative nucleoside transporters (hENT1 and hENT2) in nuclear envelopes of cultured human choriocarcinoma (BeWo) cells by functional reconstitution in proteoliposomes. *J. Biol. Chem.* **273**: 30818-30825.

163. Mackey, J. R., Galmarini, C. M., Graham, K. A., Joy, A. A., Delmer, A., Dabbagh, L., Glubrecht, D., Jewell, L. D., Lai, R., Lang, T., Hanson, J., Young, J. D., Merle-Béral, H., Binet, J. L., Cass, C. E., and Dumontet, C. (2005) Quantitative analysis of nucleoside transporter and metabolism gene expression in chronic lymphocytic leukemia (CLL): identification of fludarabine-sensitive and -insensitive populations. *Blood* **105**: 767-774.

164. Govindarajan, R., Leung, G. P., Zhou, M., Tse, C. M., Wang, J., and Unadkat, J. D. (2009) Facilitated mitochondrial import of antiviral and anticancer nucleoside drugs by human equilibrative nucleoside transporter-3. *Am J Physiol Gastrointest Liver Physiol* **4**: G910-922.

165. Elwi, A. N., Damaraju, V. L., Kuzma, M. L., Mowles, D. A., Baldwin, S. A., Young, J. D., Sawyer, M. B, and Cass, C. E. (2009) Transepithelial fluxes of adenosine and 2'-deoxyadenosine across human renal proximal tubule cells: roles of nucleoside transporters hENT1, hENT2, and hCNT3. *Am. J. Physiol. Renal. Physiol*. **296**: F1439-1451.

166. Pastor-Anglada, M., Felipe A., and Casado, F. J. (1998) Transport and mode of action of nucleoside derivatives used in chemical and antiviral therapies. *Trends Pharmacol. Sci.* **19**: 424-430.

167. Grant, S. (1998) Ara-C: cellular and molecular pharmacology. *Adv. Cancer Res.* **72**: 197-233.

168. Plunkett, W., Huang, P., and Gandhi, V. (1995) Preclinical characteristics of gemcitabine. *Anticancer Drugs* **6**: 7-13.

169. Rosenblum, L. L., Patton, G., Grigg, A. R., Frater, A. J., Cain, D., Erlwein, O., Hill, C. L., Clarke, J. R., and McClure, M. O. (2001) Differential susceptibility of retroviruses to nucleoside analogues. *Antivir. Chem. Chemother.* **12**: 91-97.

170. Giaquinto, C., Rampon, O., Penazzato, M., Fregonese, F., de Rossi, A., and D'Elia, R. (2007) Nucleoside and nucleotide reverse transcriptase inhibitors in children. *Clin. Drug Investig.* **27**: 509-531.

171. Sturmer, M., Staszewski, S., and Doerr, H. W. (2007) Quadruple nucleoside therapy with zidovudine, lamivudine, adacavir and tenofovir in the treatment of HIV. *Antivir. Ther.* **12**: 695-703.

172. Mackey, J. R., Jennings, L. L., Clarke, M. L., Santos, C. L., Dabbagh, L., Vsianska, M., Koski, S. L., Coupland, R. W., Baldwin, S. A., Young, J. D., and Cass, C. E. (2002) Immunohistochemical variation of human equilibrative nucleoside transporter 1 protein in primary breast cancers. *Clin. Cancer Res.* **8**: 110-116.

173. Gati, W. P., Paterson, A. R., Belch, A. R., Chlumecky, V., Larratt, L., M., Mant, M. J., and Turner, A. R. (1998) *Es* nucleoside transporter content of acute leukemia cells: role in cell sensitivity to cytarabine (araC). *Leuk. Lymph.* **32**: 45-54.

174. Achiwa, H., Oguri, T., Sato, S., Maeda, H., Niimi, T., and Ueda, R. (2004) Determinants of sensitivity and resistance to gemcitabine: the roles of human equilibrative nucleoside transporter 1 and deoxycytidine kinase in non-small cell lung cancer. *Cancer Sci.* **95**: 753-757.

175. Spratlin, J., Sangha, R., Glubrecht, D., Dabbagh, L., Young, J. D., Dumontet, C., Cass, C. E., Lai, R., and Mackey, J. R. (2004) The absence of human

equilibrative nucleoside transporter 1 is associated with reduced survival in patients with gemcitabine-treated pancreas adenocarcinoma. *Clin. Cancer Res.* **10**: 6956-6961.

176. Stam, R. W., den Boer, M. L., Meijerink, J. P., Ebus, M. E., Peters, G. J., Noordhuis, P., Janka-Schaub, G. E., Armstrong, S. A., Korsmeyer, S. J., and Pieters, R. (2003) Differential mRNA expression of Ara-C-metabolizing enzymes explains Ara-C sensitivity in MLL gene-rearranged infant acute lymphoblastic leukemia. *Blood* **101**: 1271-1276.

177. Galmarini, C. M., Thomas, X., Calvo, F., Rousselot, P., El Jafaari, A., Cros, E., and Dumontet, C. (2002) Potential mechanisms of resistance to cytarabine in AML patients. *Leuk. Res.* **26**: 621-629.

178. Galmarini, C. M., Thomas, X., Calvo, F., Rousselot, P., Rabilloud, M., El Jaffari, A., Cros, E., and Dumontet, C. (2002) *In vivo* mechanisms of resistance to cytarabine in acute myeloid leukaemia. *Br. J. Haematol.* **117**: 860-868.

179. Giovannetti, E., del Tacca, M., Mey, V., Funel, N., Nannizzi, S., Ricci, S., Orlandini, C., Boggi, U., Campani, D., del Chiaro, M., Iannopollo, M., Bevelacqua, G., Mosca, F., and Danesi, R. (2006) Transcription analysis of human equilibrative nucleoside transporter-1 predicts survival in pancreas cancer patients treated with gemcitabine. *Cancer Res.* **66**: 3928-3935.

180. Marechal, R., Mackey, J. R., Lai, R., Demetter, P., Peeters, M., Polus, M., Cass, C. E., Young, J. D., Salmon, I., Deviere, J., and Van Laethem, J. L. (2009) Human equilibrative nucleoside transporter 1 and human concentrative nucleoside transporter 3 predict survival after adjuvant gemcitabine therapy in resected pancreatic adenocarcinoma. *Clin Cancer Res* **15**: 2913-1919.

181. Mackey, J. R., Mani, R. S., Selner, M., Mowles, D., Young, J. D., Belt, J. A., Crawford, C. R., and Cass, C. E. (1998) Functional nucleoside transporters are required for gemcitabine influx and manifestation of toxicity in cancer cell lines. *Cancer Res.* **58**: 4349-4357.

182. Reiman, T., Clarke, M. L., Dabbagh, L., Vsianska, M., Coupland, R. W., Belch, A. R., Baldwin, S. A., Young, J. D., Cass, C., E., and Mackey, J. R. (2002) Differential expression of human equilibrative nucleoside transporter 1 (hENT1) protein in the Reed-Sternberg cells of Hodgkins' disease. *Leuk. Lymph.* **43**: 1435-1440.

183. Lai, R., Bartlett, N. L., Mackey, J. R., Jung, S. H., Johnson, J. L., Cook, J. R., Jones, D., Cass, C., E., Young, J. D., Said, J., Cheson, B., and Hsi E. D. (2008) High expression of nucleoside transporter protein hENT1 in Reed-Sternberg cells is associated with treatment failure in relapsed/refractory Hodgkin lymphoma patients treated with gemcitabine, vinorelbine and liposomal doxorubicin – a CALGB 59804 correlative study. *Leuk Lymphoma* **49**: 1202-1205.

184. Lee, E. W., Lai, Y., Zhang, H., and Unadkat, J. D. (2006) Identification of the mitochondrial targeting signal of the human equilibrative nucleoside transporter 1 (hENT1): implications for interspecies differences in mitochondrial toxicity of fialuridine. *J. Biol. Chem.* **281**: 16700-16706.

185. Agarwal, R. P., and Olivero, O. A. (1997) Genotoxicity and mitochondrial damage in human hymphocytic cells chronically exposed to 3'-azido-2', 3'-dideoxythymidine. *Mutat. Res.* **390**: 223-231.

186. McKenzie, R., Fried, M. W., Sallie, R., Conjeevaram, H., Di Bisceglie, A. M., Park, Y., Savarese, B., Kleiner, D., Tsokos, M., Luciano, C., Pruett, T., Stotka, J. L., Straus, S. E., and Hoofnagle, J. H. (1995) Hepatic failure and lactic acidosis due to fialuridine (FIAU), an investigational nucleoside analogue for chronic hepatitis B. *N. Engl. J. Med.* **333**: 1099-1105.

187. Genini, D., Adachi, S., Chao, Q., Rose, D. W., Carrera, C. J., Cottam, H. B., Carson, D. A., and Leoni, L. M. (2000) Deoxyadenosine analogs induce programmed cell death in chronic lymphocytic leukemia cells by damaging the DNA and by directly affecting the mitochondria. *Blood* **96**: 3537-3543.

188. Walker, U. A., Setzer, B., and Volksbeck, S. I. (2000) Toxicity of nucleoside-analogue reverse-transcriptase inhibitors. *Lancet.* **355**: 1096.

189. White, A. J. (2001) Mitochondrial toxicity and HIV therapy. *Sex. Transm. Infect.* **77**: 158-173.

190. Feng, J. Y., Johnson, A. A., Johnson, K. A., and Anderson, K. S. (2001) Insights into the molecular mechanism of mitochondrial toxicity by AIDS drugs. *J. Biol. Chem.* **276**: 23832-23837.

191. Cass, C. E., King, K. M., Montano, J. T., and Janowska-Wieczorek, A. (1992) A comparison of the abilities of nitrobenzylthioinosine, dilazep, and dipyridamole to protect human hematopoietic cells from 7-deazaadenosine (tubercidin). *Cancer Res.* **52**: 5879-5886.

192. Wright, A. M., Gati, W. P., and Paterson, A. R. (2000) Enhancement of retention and cytotoxicity of 2-chlorodeoxyadensoine in cultured human leukemic lymphoblasts by nitrobenzylthioinosine, an inhibitor of equilibrative nucleoside transport. *Leukemia* **14**: 52-60.

193. Huang, M., Wang, Y., Cogut, S. B., Mitchell, B. S., and Graves, L. M. (2003) Inhibition of nucleoside transport by protein kinase inhibitors. *J. Pharmacol. Exp. Ther.* **304**: 753-760.

194. Baldwin, S. A., McConkey, G. A., Cass, C. E., and Young, J. D. (2007) Nucleoside transport as a potential target for chemotherapy in malaria. *Curr. Pharm. Des.* **13**: 569-580.

195. el Kouni, M. H. (2007) Adenosine metabolism in *Toxoplasma gondii*: potential targets for chemotherapy. *Curr. Pharm. Des.* **13**: 581-597.

196. Heby, O., Persson, L., and Rentala, M. (2007) Targeting the polyamine biosynthetic enzymes: a promising approach to therapy of African sleeping sickness, Chaga' disease, and leishmaniasis. *Amino Acids* **33**: 359-366.

197. Landfear, S. M. (2009) Transporters for drug delivery and as drug targets in parasitic protozoa. *Clin Pharmacol Ther* (ahead of print).

198. Dennis, D. M., Raatikainen, P., Martens, J. R., and Belardinelli, L. (1996) Modulation of atrioventricular nodal function by metabolic and allosteric regulators of endogenous adenosine in guinea-pig heart. *Circulation* **94**: 2551-2559.

199. Deussen, A. (2000) Metabolic flux rates of adenosine in the heart. *Naunyn. Schmiedebergs Arch. Pharmacol.* **362**: 351-363.

200. Deussen, A., Stappert, M., Schäfer, S., and Kelm, M. (1999) Quantification of extracellular and intracellular adenosine production: understanding the transmembranous concentration gradient. *Circulation* **99**: 2041-2047.

201. Zhang, Y., Legare, D. J., Geiger, J. D., and Lautt, W. W. (1991) Dilazep potentiation of adenosine-mediated superior mesenteric arterial vasodilation. *J. Pharmacol. Exp. Ther.* **258**: 767-771.

202. Rongen, G. A., Smits, P., Ver Donck, K., Willemsen, J. J., De Abreu, R. A., Van Belle, H., and Thien, T. (1995) Hemodynamic and neurohumoral effects of various grades of selective adenosine transport inhibition in humans. Implications for its future role in cardioprotection. *J. Clin. Invest.* **95**: 658-668.

203. Choi, D. S., Cascini, M. G., Mailliard, W., Young, H., Paredes, P., McMahon, T., Diamond, I., Bonci, A., and Messing, R. O. (2004) The type 1 equilibrative nucleoside transporter regulates ethanol intoxication and preference. *Nat. Neurosci.* **7**: 855-861.

204. Parkinson, F. E., Zhang, Y. W., Shepel, P. N., Greenway, S. C., Peeling, J., and Geiger, J. D. (2000) Effects of nitrobenylthioinosine on adenosine levels and neuronal injury in rat forebrain ischemia. *J. Neurochem.* **75**: 795-802.

205. Meester, B. J., Shankley, N. P., Welsh, N. J., Meijler, F. L., and Black, J. W. (1998) Pharmacological analysis of the activity of the adenosine uptake inhibitor, dipyridamole, on the sinoatrial and antrioventricular nodes of the guinea-pig. *Br. J. Pharmacol.* **124**: 729-741.

206. Musa, H., Dobrzynski, H., Berry, F., Abidi, F., Cass, C. E., Young, J. D., Baldwin, S. A., and Boyett, M. R. (2002) Immunocytochemical demonstration of the equilibrative nucleoside transporter rENT1 in rat sinoatrial node. *J. Histochem. Cytochem.* **50**: 305-309.

207. Martin, B. J., Lasley, R. S., and Mentzer, R. M. (1997) Infarct size reduction with the nucleoside transport inhibitor R-75231 in swine. *Am. J. Physiol.* **41**: J1857-J1865.

208. Weyand, S., Shimamura, T., Yajima, S., Suzuki, S., Mirza, O., Krusong, K., Carpenter, E. P., Rutherford, N. G., Hadden, J. M., O'Reilly, J., Ma, P., Saidijam, M., Patching, S. G., Hope, R. J., Norbertczak, H. T., Roach, P. C. J., Iwata, S., Henderson P. J. F., and Cameron, A. D. (2008) Structure and molecular mechanism of a nucleobase-cation-symport-1 family transporter. *Science*. **322**: 709- 713.

209. Huang, Y., Lemieux, M. J., Song, J., Auer, M., and Wang, D. N. (2003) Structure and mechanism of the glycerol-3-phosphate transporter from *Escherichia coli*. *Science* **301**: 616-620.

210. Abramson, J., Smirnova, I., Kasho, V., Verner, G., Kaback, H. R., and Iwata, S. (2003) Structure and mechanism of the lactose permease of *Escherichia coli*. *Science* **301**: 610-605.

211. Hunte, C., Screpanti, E., Venturi, M., Rimon, A., Padan, E., and Michel, H. (2005) Structure of a Na^+/H^+ antiporter and insights into mechanism of action and regulation by pH. *Nature*. **435**: 1197-1202.

212. Yernool, D., Boudker, O., Jin, Y., and Gouaux, E. (2004) Structure of a glutamate transporter homologue from *Pyrococcus horikoshii*. *Nature* **431**: 811-818.

213. Yamashita, A., Singh, S. K., Kawate, T., Jin, Y., and Gouaux, E. (2005) Crystal structure of a bacterial homolgue of Na^+/Cl^--dependent neurotransmitter transporters. *Nature* **437**: 215-223.

214. Faham, S., Watanabe, A., Besserer, G. M., Cascio D., Specht, A., Hirayama, B., Wright, E. M., and Abramson, J. (2008) The crystal structure of a sodium galactose transporter reveals mechanistic insights into Na^+/sugar symport. *Science*. **321**: 810-814.

215. Sundaram, M., Yao, S. Y., Ingram, J. C., Berry, Z. A., Abidi, F., Cass, C. E., Baldwin, S. A., and Young, J. D. (2001) Topology of a human equilibrative, nitrobenzylthioinosine (NBMPR)-sensitive nucleoside transporter (hENT1) implicated in the cellular uptake of adenosine and anti-cancer drugs. *J. Biol. Chem.* **276**: 45270-45275.

216. Vickers, M. F., Mani, R. S., Sundaram, M., Hogue, D. L., Young, J. D., Baldwin, S. A., and Cass, C. E. (1999) Functional production and reconstitution of the human equilibrative nucleoside transporter (hENT1) in *Saccharomyces cerevisiae*. Interaction of inhibitors of nucleoside transport with recombinant hENT1 and a glycosylation-defective derivative (hENT1/N48Q). *Biochem. J.* **339**: 21-32.

217. Ward, J. L., Leung, G. P., Toan, S. V., and Tse, C. M. (2003) Functional analysis of site-directed glycosylation mutants of the human equilibrative nucleoside transporter-2. *Arch. Biochem. Biophys.* **411**: 19-26.

218. Sundaram, M., Yao, S. Y., Ng, A. M., Griffiths, M., Cass, C. E., Baldwin, S. A., and Young, J. D. (1998) Chimeric constructs between human and rat equilibrative nucleoside transporters (hENT1 and rENT1) reveal hENT1

structural domains interacting with coronary vasoactive drugs. *J. Biol. Chem.* **273**: 21519-21525.

219. Sundaram, M., Yao, S. Y., Ng, A. M., Cass, C. E., Baldwin, S. A., and Young, J. D. (2001) Equilibrative nucleoside transporters: mapping regions of interaction for the substrate analogue nitrobenzylthioinosine (NBMPR) using rat chimeric proteins. *Biochemistry* **40**: 8146-8151.

220. Yao, S. Y., Ng, A. M., Sundaram, M., Cass, C. E., Baldwin, S. A., and Young, J. D. (2001) Transport of antiviral 3'-deoxy-nucleoside drugs by recombinant human and rat equilibrative, nitrobenzylthioinosine (NBMPR)-insensitive (ENT2) nucleoside transporter proteins produced in *Xenopus* oocytes. *Mol. Membr. Biol.* **18**: 161-167.

221. Yao, S. Y. M., Ng, A. M. L., Vickers, M. F., Sundaram, M., Cass, C. E., Baldwin, S. A., and Young, J. D. (2002) Functional and molecular characterization of nucleobase transport by recombinant human and rat equilibrative nucleoside transporters 1 and 2 - Chimeric constructs reveal a role for the ENT2 helix 5-6 region in nucleobse translocation. *J. Biol. Chem.* **277**: 24938-24948.

222. Visser, F., Vickers, M. F., Ng, A. L., Baldwin, S. A., Young, J. D., and Cass, C. E. (2002) Mutation of residue 33 of human equilibrative nucleoside transporters 1 and 2 alters sensitivity to inhibition of transport by dilazep and dipyridamole. *J. Biol. Chem.* **277**: 395-401.

223. Visser, F., Zhang, J., Raborn, R. T., Baldwin, S. A., Young, J. D., and Cass, C. E. (2005) Residue 33 of human equilibrative nucleoside transporter 2 is a functionally important component of both the dipyridamole and nucleoside biding sites. *Mol. Pharmacol.* **67**: 1291-1298.

224. SenGupta, D. J., and Unadkat, J. D. (2004) Glycine 154 of the equilibrative nucleoside transporter, hENT1, is important for nucleoside transport and for conferring sensitivity to the inhibitors nitrobenzylthioinosine, dipyridamole, and dilazep. *Biochem. Pharmacol.* **67**: 453-458.

225. Yao, S. Y. M., Sundaram, M., Chomey, E. G., Cass, C. E., Baldwin, S. A., and Young, J. D. (2001) Identification of Cys_{140} in helix 4 as an exofacial cysteine residue within the substrate-translocation channel of rat equilibrative nitrobenzylthioninosine (NBMPR)-insensitive (ENT2) nucleoside transporter rENT2. *Biochem. J.* **353**: 387-393.

226. SenGupta, D. J., Lum, P. Y., Lai, Y. R., Shubochkina, E., Bakken, A. H., Schneider, G., and Unadkat, J. D. (2002) A single glycine mutation in the equilibrative nucleoside transporter gene, hENT1, alters nucleoside transport activity and sensitivity to nitrobenzylthioinosine. *Biochemistry* **41**: 1512-1519.

227. Endres, C. J., SenGupta, D. J., and Unadkat, J. D. (2004) Mutation of leucine-92 selectively reduces the apparent affinity of inosine, guanosine, NBMPR [S^6-(4-nitrobenzyl)-mercaptopurine riboside] and dilazep for the human equilibrative nucleoside transporter, hENT1. *Biochem. J.* **380**: 131-137.

228. Endres, C. J., and Unadkat, J. D. (2005) Residues Met89 and Ser160 in the human equilibrative nucleoside transporter 1 affect its affinity for adenosine, guanosine, S6-(4-Nitrobenzyl)-mercaptopurine riboside, and dipyridamole. *Mol. Pharm.* **67**: 837-844.

229. Visser, F., Sun, L., Damaraju, V., Tackaberry, T., Peng, Y., Robins, M. J., Baldwin, S. A., Young, J. D., and Cass, C. E. (2007) Residues 334 and 338 in transmembrane segment 8 of human equilibrative nucleoside transporter 1 are important determinants of inhibitor sensitivity, protein folding, and catalytic turnover. *J. Biol. Chem.* **282**: 14148-14157.

230. Vickers, M. F., Kumar, R., Visser, F., Zhang, J., Charania, J., Raborn, R. T., Baldwin, S. A., Young, J. D., and Cass, C. E. (2002) Comparison of the interaction of uridine, cytidine, and other pyrimidine nucleoside analogues with recombinant human equilibrative nucleoside transporter 2 (hENT2) produced in *Saccharomyces cerevisiae*. *Biochem. Cell Biol.* **80**: 639-644.

231. Vickers, M. F., Zhang, J., Visser, F., Tackaberry, T., Robins, M. J., Nielsen, L. P., Nowak, I., Baldwin, S. A., Young, J. D., and Cass, C. E. (2004) Uridine recognition motifs of human equilibrative nucleoside transporters 1 and 2 produced in *Saccharomyces cerevisiae*. *Nucleosides Nucleotides Nucleic Acids* **23**: 361-373.

232. Chang, C., Swaan, P. W., Ngo, L. Y., Lum, P. Y., Patil, S. D., and Unadkat, J. D. (2004) Molecular requirements of the human nucleoside transporters hCNT1, hCNT2, and hENT1. *Mol. Pharmacol.* **65**: 558-570.

233. Vasudevan, G., Ullman, B., and Landfear, S. M. (2001) Point mutations in a nucleoside transporter gene from *Leishmania donovani* confer drug resistance and alter substrate selectivity. *Proc. Natl. Acad. Sci. USA* **98**: 6092-6097.

234. Arastu-Kapur, S., Arendt, C. S., Purnat, T., Carter, N. S., and Ullman, B. (2005) Second-site suppression of a nonfunctional mutation within the *Leishmania donovani* inosine-guanosine transporter. *J. Biol. Chem.* **280**: 2213-2219.

235. Galazka, J., Carter, N. S., Bekhouche, S., Arastu-Kapur, S., and Ullman, B. (2006) Point mutations within the LdNT2 nucleoside transpoter gene from *Leishmania donovani* confer drug resistance and transport deficiency. *Int. J. Biochem. Cell. Biol.* **38**: 1221-1229.

236. Arastu-Kapur, S., Ford, E., Ullman, B., and Carter, N. S. (2003) Functional analysis of an inosine-guanosine transporter from *Leishmania donovani*. The role of conserved residues, aspartate 389 and arginine 393. *J. Biol. Chem.* **278**: 33327-33333.

237. Valdes, R., Vasudevan, G., Conklin, D., and Landfear, S. M. (2004) Transmembrane domain 5 of the LdNT1.1 nucleoside transporter is an amphipathic helix that forms part of the nucleoside translocation pathway. *Biochemistry* **43**: 6793-6802.

238. Valdes, R., Liu, W., Ullman, B., and Landfear, S. M. (2006) Comprehensive examination of charged intramembrane residues in a nucleoside transporter. *J. Biol. Chem.* **281**: 22647-22655.

239. Appleford, P. J., Griffiths, M., Yao, S. Y. M., Ng, A. M., Chomey, E. G., Isaac, R. E., Coates, D., Hope, I. A., Cass, C. E., Young, J. D., and Baldwin, S. A. (2004) Functional redundancy of two nucleoside transporters of the ENT family (CeENT1, CeENT2) required for development of Caenorhabditis elegans. *Mol. Membr. Biol.* **21**: 247-259.

240. Visser, F., Baldwin, S. A., Isaac, R. E., Young, J. D., and Cass, C. E. (2005) Identification and mutational analysis of amino acid residues involved in dipyridamole interactions with human and *Caenorhabditis elegans* equilibrative nucleoside transporters. *J. Biol. Chem.* **280**: 11025-11034.

241. Visser, F., Zhang, J., Raborn, R. T., Baldwin, S. A., Young, J. D., and Cass, C. E. (2005) Residue 33 of human equilibrative nucleoside transporter 2 is a functionally important component of both the dipyridamole and nucleoside biding sites. *Mol. Pharmacol.* **67**: 1291-1298.

242. Papageorgiou, I., de Koning, H. P., Soteriadou, K., and Diallinas, G. (2007) Kinetic and mutational analysis of the *Trypanosoma brucei* NBT1 nucleobase transporter expressed in *Saccharomyces cerevisiae* reveals structural similarities between ENT and MFS transporters. *Int. J. Parasitol.* **38**: 641-653.

243. Valdes, R., Arastu-Kapur, S., Landfear, S. M., and Shinde, U. (2009) An ab initio structural model of a nucleoside permease predicts functionally important residues. *J Biol Chem*. **284**: 19067-19076.

244. Slugoski, M., D., Smith, K., M., Ng, A. M. L., Yao, S. Y. M., Karpinski, E., Cass, C. E., Baldwin, S. A., and Young, J. D. (2009a) Conserved glutamate residues E343 and E519 provide mechanistic insights into cation/nucleoside cotransport by human concentrative nucleoside transporter 3 (hCNT3). *J. Biol. Chem.* **284**:17266-17280.

245. Yao, S. Y. M., Ng, A. M., Slugoski, M. D., Smith, K. M., Mulinta, R., Karpinski, E., Cass, C. E., Baldwin, S. A., and Young, J. D. (2007) Conserved glutamate residues are critically involved in Na^+/nucleoside cotransport by human concentrative nucleoside transporter 1 (hCNT1). *J. Biol. Chem.* **282**: 30607-30617.

246. Slugoski, M., D., Ng, A. M. L., Yao, S. Y. M., Lin, C. C., Mulinta, R., Cass, C. E., Baldwin, S. A., and Young, J. D. (2009b) Substituted cysteine accessibility method analysis of human concentrative nucleoside transporter hCNT3 reveals a novel discontinuous region of functional importance within CNT family motif (G/A)XKX3NEFVA(Y/M/F). *J. Biol. Chem.* **284**:17281-17292.

247. Slugoski, M., D., Smith, K., M., Mulinta, R., Ng, A. M. L., Yao, S. Y. M., Morrison, E. L., Lee, Q., O., T., Zhang, J., Karpinski, E., Cass, C. E., Baldwin, S. A., and Young, J. D. (2008) A conformationally mobile cysteine residue (Cys-561) modulates Na^+ and H^+ activation of human CNT3. *J. Biol. Chem.* **283**:24922-24934.

248. Wang, J., and Giacomini, K. M. (1999) Characterization of a bioengineered chimeric Na^+-nucleoside transporter. *Mol. Pharmacol.* **55**: 234-240.

249. Wang, J., and Giacomini, K. M. (1999) Serine 318 is essential for the pyrimidine selectivity of the N2 Na^+-nucleoside transporter. *J. Biol. Chem.* **274**: 2298-2302.

250. Loewen, S. K., Ng, A. M., Yao, S. Y., Cass, C. E., Baldwin, S. A., and Young, J. D. (1999) Identification of amino acid residues responsible for the pyrimidine and purine nucleoside specificities of human concentrative Na^+ nucleoside cotransporters hCNT1 and hCNT2. *J. Biol. Chem.* **274**: 24475-24484.

251. Slugoski, M. D., Loewen, S. K., Ng, A. M., Smith, K. M., Yao, S. Y., Karpinski, E., Cass, C. E., Baldwin, S. A., and Young, J. D. (2007) Specific mutations in transmembrane helix 8 of human concentrative Na^+/nucleoside cotransporter hCNT1 affect permeant selectivity and cation coupling. *Biochemistry*. **46**: 1684-1693.

252. Slugoski, M. D., Loewen, S. K., Ng, A. M., Baldwin, S. A, Cass, C. E., and Young, J. D. (2004) Allelic isoforms of the H^+/nucleoside co-transporter (CaCNT) from *Candida albicans* reveal separate high- and low-affinity transport systems for nucleosides. *Yeast.* **21**: 1269-1277.

253. Zhang, J., Tackaberry, T., Ritzel, M. W., Raborn, T., Barron, G., Baldwin, S. A., Young, J. D., and Cass, C. E. (2006) Cysteine-accessibility analysis of transmembrane domains 11-13 of human concentrative nucleoside transporter 3. *Biochem. J.* **394**: 389-398.

254. Zhang, J. Visser, F., Vickers, M. F., Lang, T., Robins, M. J., Nielsen, L. P., Nowak, I., Baldwin, S. A., Young, J. D., and Cass, C. E. (2003) Uridine binding motifs of human concentrative nucleoside transporters 1 and 3 produced in *Saccharomyces cerevisiae*. *Mol. Pharmacol.* **64**: 1512-1520.

255. Akabas, M. H., Stauffer, D. A., Xu, M., and Karlin, A. (1992) Acetycholine receptor channel structure probed in cysteine-substitution mutants. *Science*. **258**: 307-310.

256. Akabas, M. H., Kaufmann, C., Archdeacon, P., and Karlin, A. (1994a) Identification of acetycholine receptor channel-lining residues in the entire M2 segment of the alpha subunit. *Neuron*. **13**: 919-927.

257. Akabas, M. H., Kaufmann, C., Cook, T. A., and Archdeacon, P. (1994b) Amino acid residues lining the chloride channel of the cystic fibrosis transmembrane conductance regulator. *J. Biol. Chem*. **269**: 14865-14868.

258. Zhu, Q., and Casey, J. R. (2007) Topology of transmembrane proteins by scanning cysteine accessibility mutagenesis methodology. *Methods*. **41**: 439-450.

259. Mueckler, M., and Makepeace, C. (2009) Model of the exofacial substrate-binding site and helical folding of the human Glut1 glucose transporter based on scanning mutagenesis. *Biochem. J*. Ahead of print.

260. Tang, X. B., Fujinaga, J., Kopito, R., and Casey, J. R. (1998) Topology of the region surrounding Glu681 of human AE1 protein, the erythrocyte anion exchanger. *J. Biol. Chem*. 273: 22545-22553.

261. Zhu, Q., Lee, D. W. K., and Casey, J. R. (2003) Novel topology in C-terminal region of the human plasma membrane anion exchanger, AE1. *J. Biol. Chem*. 278: 3112-3120.

262. Lee, B. L., Li, X., Liu, Y., Sykes, B. D., and Fliegel, L. (2009) Structural and functional analysis of transmembrane XI of the NHE1 isoform of the Na^+/H^+ exchanger. J. *Biol. Chem*. **284**: 11546-11556.

263. Seal, R. P., ShigeriY., Eliasof, S., Leighton, B. H., and Amara, S. G. (2001) Sulfhydryl modification of V449C in the glutamate transporter EAAT1 abolishes substrate transport but not the substrate-gated anion conductance. *Proc. Natl Acad. Sci. USA.* **98**: 15324-15329.

264. Slotboom, D. J., Konings, W. N., and Lolkema, J. S. (2001) Cysteine-scanning mutagenesis reveals a highly amphipathic pore-lining membrane spanning helix in the glutamate transporter GltT. *J. Biol. Chem*. **276**: 10775-10781.

265. Ermolova, N., Madhvani, R. V., and Kaback, H. R. (2006) Site-directed alkylation of cysteine replacements in the lactose permease of Escherichia coli: helices I, III, VI and XI. *Biochem*. **45**: 4182-4189.

266. Rimon, A., Hunte, C., Michel, H., and Padan, E. (2008) Epitope mapping of conformational monoclonal antibodies specific to NhaA Na^+/H^+ antiporter: structural and functional implications. *J. Mol. Biol*. **379**: 471-481.

267. Hirayama, B. A., Loo, D. D., Diez-Sampedro, A., Leung, D. W., Meinild, A. K., Lai-Bing, M., Turk, E., and Wright, E. M. (2007) Sodium-dependent reorganization of the sugar-binding site of SGLT1. *Biochem*. **46**: 13391-13406.

268. Roberts, D. D., Lewis, S. D., Ballou, D. P., Olson, S. T., and Shafer, J. A. (1986) Reactivity of small thiolate anions and cysteine-25 in papain toward methyl methanethiosulfonate. *Biochem. J*. **25**: 5595-5601.

Chapter 2:

Experimental Procedures

Xenopus laevis **Oocyte Expression System**

The *Xenopus laevis* oocyte heterologous expression system was central to the initial cDNA cloning and functional of both human and other mammalian ENT and CNT proteins, and is the expression system used in all of the studies described in this thesis. An important advantage of *Xenopus* oocytes over other heterologous expression systems is the absence of detectable endogenous nucleoside transport activity (1-4). As an example, a putative *Xenopus* CNT protein of 645 amino acids (GenBank™ accession number NP_001086782) had been identified by genomic sequencing (5), but is not functionally expressed in oocytes. Oocytes therefore provide a powerful experimental tool to produce and functionally characterize recombinant nucleoside transport proteins in the absence of other competing transport activities with potentially overlapping permeant preferences (4). In radiolabeled flux experiments, the slow non-mediated uptake of nucleosides that occurs in oocytes by simple diffusion across lipid bilayers is readily identified and quantified by measuring uptake in control water-injected oocytes. The cDNAs encoding human and rodent CNT1 and CNT3 were all initially cloned and characterized in *Xenopus* oocytes (2, 6-11).

Xenopus oocytes robustly translate injected exogenous mRNA, are capable of post-translational modifications, and correctly process transporter proteins to cell surfaces (4, 12). *In vitro* cDNA transcription to produce mRNAs of the cloned transport proteins is required, athough direct injection of cDNA into the nucleus is also possible, but less often employed. There is therefore the possibility of RNA degradation and consequent variability of expression. There is also the possibility of species differences resulting from use of amphibian cells to investigate mammalian proteins, especially with respect to post-translational processing of membrane proteins (3, 4). Nevertheless, despite these potential drawbacks, the characterization of nucleoside transport proteins in *Xenopus* oocytes has, to date, accurately reflected the phenotypes of these proteins characterized in native cell types and tissues.

The characterization of membrane transport mechanisms by radioisotope flux measurements in *Xenopus* oocytes may possibly be compromised by intracellular

metabolism of permeants (3, 4, 13). With respect to nucleosides, both thymidine (1) and uridine (14) have been shown to have slow and insignificant metabolism in mRNA-injected *Xenopus* oocytes. The use of short uptake intervals is beneficial in minimizing the possible effects of nucleoside metabolism on nucleoside transport kinetics (2-4, 14). Because of their large size, equilibrium is reached more slowly in *Xenopus* oocytes than other smaller cells, hence extending the time period before which nucleoside or nucleoside metabolite backflux would occur (4).

An additional advantage of the *Xenopus* oocyte heterologous expression system is that electrogenic transport proteins such as CNTs can also be investigated in electrophysiological experiments using, for example, the two microelectrode voltage clamp. Electrophysiological techniques enable characterization of the movement of charge across the membrane (steady-state currents) as well as transporter-associated charge movements within the membrane (15, 16).

The studies presented in this thesis exploited the ability of *Xenopus* oocytes to effectively translate injected exogenous mRNA and produce post-translationally modified proteins at the oocyte plasma membrane. Using moleculat biology, mRNA was transcribed from wild-type and mutant cDNAs by *in vitro* techniques. Once produced in *Xenopus* oocytes, the presence of these proteins at the cell surface was verified by detection of functional activity and by immunoblotting. Subsequent functional characterization of the proteins was undertaken by radioisotope flux assays and, in some experiments, by electrophysiology.

Molecular Biology

Constructs – The molecular cloning of hCNT1 (9), hCNT3 (11) and NupC (17) have been previously described. cDNAs (GenBank™ accession numbers U62968, AF305210 and NC000913 respectively) were subcloned into the enhanced *Xenopus* plasmid expression vector pGEM-HE (18), as previously described (11). By providing 5′- and 3′-untranslated regions from the *Xenopus* β-globin gene flanking the multiple cloning site, pGEM-HE gave greater functional activity than the pBluescript II KS(+) (Stratagene, USA) vector used in earlier studies (9, 10, 19).

The hCNT1 and hCNT3 cDNAs provided the templates for construction of the corresponding hCNT1 (Chapter 5) and hCNT3 mutants (Chapter 3). The hCNT3 cDNA also provided the template for the construction of a cysteine-less version of hCNT3 (hCNT3C-) with all 14 endogenous cysteine residues converted to serine (20). hCNT3C- was transferred from the yeast *Escherichia coli* shuttle vector pYPGE15 (20) into the *Xenopus* oocyte expression vector pGEM-HE. In pGEM-HE, hCNT3C- was then used as template for the construction of hCNT3C- mutants (Chapters 4, 7 and 8). The NupC cDNA provided the template for construction of a cysteine-less version of NupC (NupC(C-) or C96A) in which the single endogenous cysteine residue in the protein (Cys96) was converted to alanine (Chapter 6).

Site-directed mutagenesis – Individual residue changes were introduced into CNT or NupC cDNA templates by the oligonucleotide-directed technique (21) using reagents from the QuikChange™ multi site-directed mutagenesis kit (Stratagene, USA). All constructs were sequenced in both directions by Taq dyedeoxy-terminator cycle sequencing to ensure that only the correct mutation(s) had been introduced.

In vitro transcription and expression in Xenopus oocytes – Plasmid cDNAs were linearized with *Nhe1*. Following linearization, cDNA was transcribed with T7 polymerase using the mMESSAGE mMACHINE^{TM} (Ambion, USA) *in vitro* transcription system. Remaining template was removed by digestion with RNase-free DNase1. Healthy stage V - VI oocytes were isolated by collagenase treatment (2 mg/ml for 2 hours) of ovarian lobes from female *Xenopus laevis* (Biological Sciences Vivarium, University of Alberta, Canada) that had been anaesthetized by immersion in 0.3% (w/v) tricaine methanesulfonate (pH 7.4). Frogs were humanely killed following collection of oocytes in compliance with guidelines approved by the Canadian Council on Animal Care. The remaining follicular layers were removed by phosphate treatment (100 mM K_2PO_4) and manual defolliculation. Twenty-four hours after defolliculation, oocytes were injected with either 10 - 20 nl of water containing 1 ng/nl of capped RNA transcript or the same volume of water alone. Injected oocytes were then incubated for either 4 days (radioisotope flux studies) or 4 - 7 days (electrophysiology) at 18°C in modified Barth's solution (changed daily) (88 mM NaCl, 1 mM KCl, 0.33 mM $Ca(NO_3)_2$, 0.41 mM $CaCl_2$, 0.82 mM $MgSO_4$, 2.4 mM

$NaHCO_3$, 10 mM Hepes, 2.5 mM sodium pyruvate, 0.1 mg/ml penicillin and 0.05 mg/ml gentamycin sulfate, pH 7.5) prior to the assay of nucleoside transport activity.

Cell Surface Expression and Glycosylation

Production of recombinant wild-type and mutant hCNT3 proteins at the oocyte cell surface was determined by labelling of intact oocytes with EZ-Link sulfosuccinimidyl-6-(biotinamido) hexanoate (sulfo-NHS-LC-biotin) (Pierce, USA) followed by isolation of the resultant biotinylated plasma membrane proteins using immobilized streptavidin resin (Pierce, USA) according to the manufacturer's instructions. Glycosylation status was established by digestion with *N*-Glycosidase-F (Roche Molecular Biochemicals, USA). Identically treated samples omitting enzyme were used as controls.

For immunoblotting, one μg aliquots of plasma membrane proteins or solubilized proteins from approximately 1-2 oocytes/lane were resolved on 4-12% Tris-Bis gels (Invitrogen) or 12% sodium dodecyl sulphate (SDS)-polyacrylamide gels (22). The electrophoresed proteins were transferred to polyvinylidene difluoride membranes and probed with affinity-purified rabbit anti- $hCNT3_{45-69}$ polyclonal antibodies (23). Blots were then incubated with horseradish peroxidase-conjugated anti-rabbit antibodies (Pierce) and developed with enhanced chemiluminescence reagents (Amersham Biosciences).

Transport Media

Na^+-containing transport medium was composed of 100 mM NaCl, 2 mM KCl, 1 mM $CaCl_2$, 1 mM $MgCl_2$ and 10 mM HEPES (for pH values > 6.5) or 10 mM MES (for pH values ≤ 6.5). In Na^+-free, choline-containing transport medium, 100 mM NaCl was replaced with 100 mM choline chloride (ChCl). In cation-activation experiments where the indicated Na^+ or Li^+ concentration was less than 100 mM, Na^+ or Li^+ in the transport medium was replaced by equimolar Ch^+ to maintain isomolarity. Unless otherwise indicated, experiments undertaken in Na^+-containing transport medium

were performed at pH 8.5 to minimize the H^+ concentration. In experiments examining the H^+-dependence of transport, Na^+-free choline-containing transport medium (100 mM ChCl) was used at a pH value of 5.5. Experiments replacing NaCl with equimolar ChCl included a 10 min pre-incubation period and several washes with ChCl-containing transport medium, to ensure complete removal of extracellular Na^+ prior to addition of nucleoside-containing transport medium.

Radioisotope Flux Studies

Radioisotope transport assays were performed as described previously (2, 4, 9-11, 19, 24) on groups of 10 - 12 oocytes at room temperature (20°C) using ^{14}C- or ^{3}H-labeled nucleosides (1 or 2 - 4 μCi/ml, respectively) in 200 μl of the appropriate transport medium. Unless otherwise indicated, nucleoside uptake was determined at a concentration of 10 μM for hCNTs or 1 μM for NupC. Nucleosides were obtained from Moravek Biochemicals (USA), Sigma (Canada) or GE Healthcare Biosciences Inc. (Canada). Transport medium for adenosine uptake experiments also contained 1 μM deoxycoformycin to inhibit adenosine deaminase activity. All uptake values, at both high and low permeant concentrations, represent initial rates of transport (2, 7, 9, 19, 24) determined using an incubation period of 1 min for hCNTs, and 10 min for NupC. For ease of comparison, data in all experiments are presented as pmol/oocyte.min^{-1}.

At the end of the incubation period, the oocytes were rapidly washed 5-6 times with ice-cold Na^+-free 100 mM ChCl transport medium (pH 7.5) to remove extracellular radioactivity and then transferred individually into scintillation vials containing 0.3 - 0.5 ml of 1% (w/v) SDS. Oocyte-associated radioactivity was determined by liquid scintillation counting (LS 6000 IC, Beckman Canada Inc., Canada). The flux values shown are the means ± SEM (standard error of the mean) of 10 - 12 oocytes from representative experiments, and individual experiments were performed on cells from single batches of oocytes used on the same day. Values for the transporter-mediated component of uptake were calculated as uptake in RNA transcript-injected oocytes *minus* uptake in oocytes injected with water alone. Each

experiment was performed at least twice using oocytes from different frogs. Flux values varied in different batches of oocytes by up to 3-fold between experiments.

Inhibition studies with the thiol-reactive reagent PCMBS – Oocytes were pretreated with *p*-chloromercuribenzene sulfonate (PCMBS) on ice for 10 min in 200 µl of the appropriate transport medium and then washed three times with ice-cold transport medium to remove excess organomercurial before the assay of transport activity. The oocytes were then transferred to a clean test tube containing the appropriate uptake buffer at room temperature to rest for 1 min. Control experiments established that 10 min exposure to PCMBS resulted in maximum inhibition of hCNT3 transport activity. In permeant protection experiments, unlabeled 20 mM uridine was included along with PCMBS (25). PCMBS reagent was obtained from Toronto Research Chemicals (Canada).

Electrophysiological Studies

Steady-state and presteady-state membrane currents were measured in oocytes at room temperature (20°C) using the whole-cell, two-electrode voltage clamp technique (GeneClamp 500B, Molecular Devices Corp. (formerly Axon Instruments Inc.), USA) as previously described (16). The GeneClamp 500B was interfaced to a dedicated IBM-compatible computer *via* a Digidata 1322A (Chapter 3) A/D converter and controlled by Axoscope or pCLAMP software (Molecular Devices Corp., USA). The microelectrodes were filled with 3 M KCl and had resistances ranging from 0.5 to 2.5 MΩ (megaohms). Following microelectrode penetration, resting membrane potential was measured over a 10 - 15 min period prior to the start of the experiment. Oocytes exhibiting an unstable membrane potential or a potential more positive than -30 mV were discarded. Unless otherwise indicated, the oocyte membrane potential was clamped at a holding potential (V_h) of -50 mV in the appropriate transport medium.

Presteady-state (transient) currents were studied using a voltage pulse protocol, as described previously (16). Membrane voltage was stepped from the holding potential (V_h) of -50 mV to a range of test potentials (V_t) from -150 to +75 mV in 25 mV

increments (Chapter 3). The voltage rise time of the clamp was adjusted by use of an oscilloscope such that it varied between 200 and 500 μsec. Current signals were filtered at 2 kHz (four-pole Bessel filter) at a sampling interval of 200 μsec/point (corresponding to a sampling frequency of 5 kHz). For data presentation, the current at each test potential was averaged from 5 sweeps and further filtered at 0.75 kHz by pCLAMP software (Version 9.0, Molecular Devices Corp., USA).

Current-voltage (I-V) curves were determined from differences in steady-state currents generated in the presence and absence of permeant during 300 msec voltage pulses to potentials between +60 and -110 mV (10 mV steps). For I-V relations, currents were filtered at 2 kHz (four-pole Bessel filter) and sampled at a rate of 200 μsec/point (corresponding to a sampling frequency of 5 kHz).

Data from individual electrophysiology experiments are presented as nucleoside-evoked currents from single representative cells or as mean values (± SEM) from 4 or more oocytes from the same batch used on the same day. Each experiment was repeated at least twice on oocytes from different frogs. No nucleoside-evoked currents were detected in oocytes injected with water alone, demonstrating that currents in transcript-injected oocytes were transporter specific.

Kinetic Parameters

Kinetic parameters (K_m, K_{50}, V_{max}, IC_{50}, Hill coefficient) derived from radioisotope flux and electrophysiological experiments were calculated using SigmaPlot software (Jandel Scientific Software, USA). Those from radioisotope experiments were derived from curve fits to averaged mediated fluxes from 10 - 12 oocytes, and are presented as means ± SE (standard error of the fitted estimate). Mediated fluxes were determined as uptake in RNA-injected oocytes *minus* uptake in water-injected control oocytes. Kinetic parameters derived from electrophysiological experiments were determined from fits to data from individual oocytes normalized to the I_{max} value obtained for that oocyte, and are presented as values ± SE for single representative oocytes or as means ± SEM of 4 or more cells.

Determination of Stoichiometry

Charge-to-nucleoside stoichiometry – Na^+:nucleoside and H^+:nucleoside coupling ratios were determined by simultaneously measuring radiotracer transport-induced current measurements under voltage clamp conditions in transport medium containing 100 mM NaCl, pH 8.5 or 100 mM ChCl, pH 5.5, respectively, unless otherwise indicated. Stoichiometry was determined for hCNT3C- using 100 μM ^{3}H-uridine (2 μCi/ml) (Chapter 3). Individual oocytes were placed in a perfusion chamber and voltage-clamped at V_h of -30, -50 or -90 mV, as indicated, in the appropriate nucleoside-free medium for a 5 - 10 min period to monitor baseline currents. When the baseline was stable, the perfusion was stopped and medium of the same composition containing unlabeled and radiolabeled nucleoside was manually added to the perfusion chamber. Current was measured for 0.5 - 3 min, and uptake of nucleoside was terminated by washing the oocyte with nucleoside-free medium until the current returned to baseline (< 15 sec). The oocyte was then immediately transferred to a scintillation vial and solubilized with 1% (w/v) SDS for quantitation of oocyte-associated radioactivity. Nucleoside-induced current was obtained as the difference between baseline current and the inward nucleoside-induced current. The total charge translocated into the oocyte during the uptake period was calculated from the current-time integral and correlated with the measured radiolabeled flux for each oocyte to determine the charge:uptake ratio. Basal radiolabeled nucleoside uptake was determined in control water-injected oocytes (from the same donor frog) under equivalent conditions and used to correct for endogenous non-mediated uridine uptake over the same incubation period. Coupling ratios (± SE) were calculated from slopes of least-squares fits of uridine-dependent charge *versus* uridine accumulation for five or more oocytes.

Bibliography

1. Jarvis, S. M., and Griffith, D. A. (1991) Expression of the rabbit intestinal N2 Na^+/nucleoside transporter in *Xenopus laevis* oocytes. *Biochem. J.* **278**: 605-607.

2. Huang, Q. Q., Yao, S. Y. M., Ritzel, M. W., Paterson, A. R., Cass, C. E., and Young, J. D. (1994) Cloning and functional expression of a complementary DNA encoding a mammalian nucleoside transport protein. *J. Biol. Chem.* **269**: 17757-17760.

3. Wang, J., Schaner, M. E., Thomassen, S., Su, S., Piquette-Miller, M., and Giacomini, K. M. (1997) Functional and molecular characteristics of Na^+-dependent nucleoside transporters. *Pharm. Res.* **14**: 1524-1532.

4. Yao, S. Y. M., Cass, C. E., and Young, J. D. (2000) The *Xenopus* oocyte expression system for the cDNA cloning and characterization of plasma membrane transport proteins. In *Membrane Transport. A Practical Approach.* (Baldwin, S. A., ed.) Oxford: Oxford University Press; 47-78.

5. Klein, S. L., Strausberg, R. L., Wagner, L., Pontius, J., Clifton, S. W., and Richardson, P. (2002) Genetic and genomic tools for *Xenopus* research: The NIH *Xenopus* initiative. *Dev. Dyn.* **225**: 384-391.

6. Che, M., Ortiz, D. F., and Arias, I. M. (1995) Primary structure and functional expression of a cDNA encoding the bile canalicular, purine-specific Na^+-nucleoside cotransporter. *J. Biol. Chem.* **270**: 13596-13599.

7. Yao, S. Y. M., Cass, C. E., and Young, J. D. (1996) Transport of the antiviral nucleoside analogs 3'-azido-3'-deoxythimidine and 2', 3'-dideoxycytidine by a recombinant nucleoside transporter (rCNT1) expressed in *Xenopus laevis* oocytes. *Mol. Pharmacol.* **50**: 388-393.

8. Yao, S. Y. M., Ng, A. M. L., Ritzel, M. W. L., Gati, W. P., Cass, C. E., and Young, J. D. (1996) Transport of adenosine by recombinant purine- and pyrimidine-selective sodium/nucleoside cotransporters from rat jejunum expressed in *Xenopus laevis* oocytes. *Mol. Pharmacol.* **50**: 1529-1535.

9. Ritzel, M. W. L., Yao, S.Y.M., Huang, M.Y., Elliot, J. F., Cass, C. E., and Young, J. D. (1997) Molecular cloning and functional expression of cDNAs

encoding a human Na^+-nucleoside cotransporter hCNT1. *Am. J. Physiol.* **272**: C707-C714.

10. Ritzel, M. W. L., Yao, S. Y. M., Ng, A. M. L., Mackey, J. R., Cass, C. E., and Young, J. D. (1998) Molecular cloning, functional expression and chromosomal localization of a cDNA encoding a human Na^+/nucleoside cotransporter (hCNT2) selective for purine nucleosides and uridine. *Mol. Membr. Biol.* **15**: 203-211.

11. Ritzel, M. W. L., Ng, A. M. L., Yao, S. Y. M., Graham, K., Loewen, S. K., Smith, K. M., Ritzel, R. G., Mowles, D. A., Carpenter, P., Chen, X.-Z., Karpinski, E., Hyde, R. J., Baldwin, S. A., Cass, C. E., and Young, J. D. (2001) Molecular identification and characterization of novel human and mouse concentrative Na^+-nucleoside cotransporter proteins (hCNT3 and mCNT3) broadly selective for purine and pyrimidine nucleosides (system *cib*). *J. Biol. Chem.* **276**: 2914-2927.

12. Wang, H. C., Beer, B., Sassano, D., Blume, A. J., and Ziai, M. R. (1991) Gene expression in *Xenopus* oocytes. *Int. J. Biochem.* **23**: 271-276.

13. Hong, M., Schlichter, L., and Bendayan, R. (2000) A Na^+-dependent nucleoside transporter in microglia. *J. Pharmacol. Exp. Ther.* **292**: 366-374.

14. Huang, Q., Harvey, C. M., Paterson, A. R. P., Cass, C. E., and Young, J. D. (1993) Functional expression of Na^+-dependent nucleoside transport systems of rat intestine in isolated oocytes of *Xenopus laevis*. Demonstration that rat jejunum expresses the purine-selective system N1 (*cif*) and a second, novel system N3 having broad specificty for purine and pyrimidine nucleosides. *J. Biol. Chem.* **268**: 20613-20619.

15. Mager, S., Cao, Y., and Lester, H. A. (1998) Measurement of transient currents from neurotransmitter transporters expressed in *Xenopus* oocytes. *Methods Enzymol.* **296**: 551-566.

16. Smith, K. M., Ng, A. M. L., Yao, S. Y. M., Labedz, K. A., Knaus, E. E., Wiebe, L. I., Cass, C. E., Baldwin, S. A., Chen, X.-Z., Karpinski, E., and Young, J. D. (2004) Electrophysiological characterization of a recombinant human Na^+-coupled nucleoside transporter (hCNT1) produced in *Xenopus* oocytes. *J. Physiol.* **558**: 807-823.

17. Loewen, S. K., Yao, S. Y., Slugoski, M. D., Mohabir, N. N., Turner, R. J., Mackey, J. R., Gallagher, M. P., Henderson, P. J., Baldwin, S. A., Cass, C. E., and Young, J. D. (2004) Transport of physiological nucleosides and anti-viral and anti-neoplastic nucleoside drugs by recombinant *Escherischia coli* nucleoside-H^+ cotransporter (NupC) produced in *Xenopus laevis* oocytes. *Mol. Membr. Biol.* **21**: 1-10.

18. Liman, E. R., Tytgat, J., and Hess, P. (1992) Subunit stoichiometry of a mammalian K^+ channel determined by construction of multimeric cDNAs. *Neuron* **9**: 861-871.

19. Loewen, S. K., Ng, A. M., Yao, S. Y., Cass, C. E., Baldwin, S. A., and Young, J. D. (1999) Identification of amino acid residues responsible for the pyrimidine and purine nucleoside specificities of human concentrative Na^+ nucleoside cotransporters hCNT1 and hCNT2. *J. Biol. Chem*. **274**: 24475-24484.

20. Zhang, J., Tackaberry, T., Ritzel, M. W., Raborn, T., Barron, G., Baldwin, S. A., Young, J. D., and Cass, C. E. (2006) Cysteine-accessibility analysis of transmembrane domains 11-13 of human concentrative nucleoside transporter 3. *Biochem. J.* **394**: 389-398.

21. Kirsch, R. D., and Joly, E. (1998) An improved PCR-mutagenesis strategy for two-site mutagensis of sequence swapping between related genes. *Nucleic Acid Res*. **26**: 1848-1850.

22. Laemmli, U. K. (1970) Cleavage of structural proteins during the assembly of the head of bacteriophage T4. *Nature* **277**: 680-685.

23. Damaraju, V. L., Elwi, A. N., Hunter, C., Carpenter, P., Santos, C., Barron, G. M., Sun, X., Baldwin, S. A., Young, J. D., Mackey, J., Sawyer, M. B., and Cass, C. E. (2007) Localization of broadly selective equilibrative and concentrative nucleoside transporters, hENT1 and hCNT3, in human kidney. *Am. J. Physiol. Renal Physiol*. **293**: F200-F211.

24. Loewen, S. K., Ng, A. M. L., Mohabir, N. N., Baldwin, S. A., Cass, C. E., and Young, J. D. (2003) Functional characterization of a H^+/nucleoside co-transporter (CaCNT) from *Candida albicans*, a fungal member of the concentrative nucleoside transporter (CNT) family of membrane proteins. *Yeast* **20**: 661-675.

25. Yao, S. Y. M., Sundaram, M., Chomey, E. G., Cass, C. E., Baldwin, S. A., and Young, J. D. (2001) Identification of Cys^{140} in helix 4 as an exofacial cysteine residue within the substrate-translocation channel of rat equilibrative nitrobenzylthioinosine (NBMPR)-insensitive nucleoside transporters rENT2. *Biochem. J.* **353**: 387-393.

Chapter 3:
A Cysteine-Less Version of Human Na^+/Nucleoside Cotransporter 3 (hCNT3)*

* A version of this chapter has been published.

Slugoski, M. D., Smith, K. M., Mulinta, R., Ng, A. M. L., Yao, S. Y. M., Morrison, E. L., Lee, Q. O. T., Zhang, J., Karpinski, E., Cass, C. E., Baldwin, S. A., and Young, J. D. (2008) A conformationally mobile cysteine residue (C561) modulates Na^+- and H^+-activation of human concentrative nucleoside transporter 3 (hCNT3). *J. Biol. Chem.* **283**: 24922-24934.

Acknowledgements and Contributions

Graduate Student Dr. Melissa D. Slugoski was the principle author and investigator of this study. I contributed to the functional characterization of cysteine-free hCNT3C- and aglyco and other hCNT3 mutants. Research Associate Dr. Kyla M. Smith assisted with the electrophysiology experiments. Technologist Mrs. Amy M. L. Ng constructed the mutants and, together with Research Associate Dr. Sylvia Y. M. Yao, assisted with their functional characterization. Summer Students Ms. Ellen L. Morrison and Ms. Queenie O. T. Lee were involved in the characterization of hCNT3 Cys561 mutants. Graduate Student Dr. Jing Zhang constructed the initial version of hCNT3C- used in previous yeast experiments. Drs. Edward Karpinski, Carol E. Cass and Stephen A. Baldwin are collaborative principal investigators who assisted with research funding and manuscript preparation. This research was funded by the National Cancer Institute of Canada with funds from the Canadian Cancer Society (now the Canadian Cancer Society Research Institute), Alberta Cancer Board (now the Alberta Health Services- Cancer Care), The Alberta Cancer Foundation, and by the Alberta Cancer Prevention Legacy Fund.

Introduction

The human SLC28 concentrative nucleoside transporter (CNT) family has three members. hCNT1 and hCNT2 are pyrimidine and purine nucleoside selective, respectively, and couple Na^+:nucleoside cotransport with a 1:1 stoichiometry (1-7). hCNT3, in contrast, is broadly selective for both pyrimidine and purine nucleosides, and exhibits a 2:1 Na^+:nucleoside coupling ratio (6-8). hCNT3 is also capable of H^+/nucleoside cotransport with a coupling stoichiometry of 1:1, whereby one of the transporter's two Na^+ binding sites also functionally interacts with H^+ (6,7).

In the absence of a crystal structure, molecular strategies employing substituted cysteine accessibility method (SCAM) analysis provides a powerful approach to systematically investigate membrane protein architecture and structure/function relationships (9). Pioneered by studies of *E. coli* LacY lactose permease (10), human transporters investigated by this methodology include the glucose transporter GLUT1 (11), the Cl^-/HCO_3^- exchanger AE1 (12, 13), the Na^+/H^+ exchanger NHE1 (14), the glutamate transporters EAAT1 and GltT (15, 16), the Na^+/H^+ antiporter NhaA (17) and the Na^+/glucose co-transporter SGLT1 (18). Most recently, the TM 11 – 13 region of hCNT3 has also been probed by SCAM (19).

To avoid confounding background reactivity with endogenous cysteine residues, SCAM analysis requires construction of a functional cysteine-less version of the transporter to serve as a template for subsequent cysteine reinsertion at defined positions. In the case of hCNT3, the protein was engineered by mutation of all 14 endogenous cysteine residues to serine, resulting in the cysteine-less construct hCNT3C- (19). Expressed in yeast, hCNT3C- was used to assess residues in TMs 11-13 for accessibility to methanethiosulfonate (MTS) reagents (19). More recently, hCNT3C-, expressed in *Xenopus laevis* oocytes, was used to identify a H^+-mediated conformational shift that allows access of *p*-chloromercuribenzene sulfonate (PCMBS) to specific residues in TM 12 under

acidified conditions (20). One of these conformationally mobile amino acids, native cysteine residue 561, was fully protected against PCMBS inhibition by micromolar concentrations of extracellular uridine, suggesting likely proximity to the nucleoside binding pocket. In this Chapter, heterologous expression in *Xenopus* oocytes, cell-surface biotinylation and site-directed mutagenesis were used in combination with radioisotope flux and presteady- and steady-state electrophysiological kinetic experiments to undertake an in depth functional comparison between wild-type and cysteine-less hCNT3. The investigation validates hCNT3C- as a template for SCAM analyses of hCNTs and reveals that Cys561 modulates Na^+- as well as H^+-coupled modes of hCNT3 nucleoside transport.

Results

As depicted in Fig. 3-1, hCNT3 contains 14 endogenous cysteine residues. Nine of these are located within either the extramembraneous N-terminal (Cys82, Cys91 and Cys94) or C-terminal (Cys621, Cys643, Cys644, Cys673, Cys674 and Cys684) regions of the transporter. Five are positioned in predicted TMs (Cys121 in TM 1, Cys486 in TM 11, Cys561 in TM 12, and Cys602 and Cys607 in TM 13). To enable transmembrane protein topology mapping and structure/function analysis of hCNT3 by SCAM, all 14 cysteine residues of hCNT3 were mutated to serine. The resulting cysteine-less version of hCNT3 (hCNT3C-) was capable of Na^+-dependent nucleoside transport when produced in yeast and has been used as template in an initial series of SCAM analyses of hCNT3 TMs 11 - 13 (19). The current work extended these studies by using the dual radioisotope flux and electrophysiological capabilities of the *Xenopus* oocyte heterologous expression system to undertake a detailed functional characterization of hCNT3C-.

Time course of radiolabeled uridine uptake by oocytes producing hCNT3C- – Fig. 3-2 depicts time courses for uptake of 10 μM ^{14}C-labeled uridine in Na^+-containing transport medium (100 mM NaCl, pH 7.5) by control water-injected oocytes and oocytes producing recombinant hCNT3C-. Uridine uptake by hCNT3C- was rapid and approximately linear with time for the first 3 min. Transport was also

concentrative with the 10 min uptake value exceeding the initial extracellular uridine concentration by ~ 2.5-fold, assuming an intracellular water volume of 1 μl (21, 22). Only basal uptake of uridine was evident in control water-injected oocytes under the same conditions. In all subsequent experiments, an uptake interval of 1 min was used to determine initial rates of transport.

hCNT3C- nucleoside selectivity and cation dependence – The experiment of Fig. 3-3*A* investigated the ability of hCNT3C- to transport a panel of radiolabeled physiological pyrimidine and purine nucleosides. Since wild-type hCNT3 is both Na^+- and H^+-coupled (7, 8, 23) and since Na^+- and H^+-coupled hCNT3 exhibit different nucleoside selectivity profiles (7), the experiment was performed both in the presence of Na^+ and H^+ (100 mM NaCl, pH 7.5 and 100 mM ChCl, pH 5.5, respectively). The flux values shown in this and subsequent experiments depict mediated transport activity, defined as the difference in uptake between RNA transcript-injected and control water-injected oocytes. Nucleoside uptake in water-injected oocytes was < 0.1 pmol/oocyte.min^{-1} under all conditions tested (data not shown).

Similar to wild-type hCNT3 (7, 23), hCNT3C- in Na^+-containing medium transported uridine, adenosine, thymidine, cytidine, guanosine and inosine at equivalent rates (4.8 - 7.0 pmol/oocyte.min^{-1}) (Fig. 3-3*A*). Also similar to the wild-type protein (7), this broad selectivity profile was markedly altered in H^+-containing medium (uridine >> adenosine, thymidine > cytidine > guanosine, inosine) with only uridine showing similar rates of transport in the two media. The different nucleoside selectivity profiles of Na^+- and H^+-coupled hCNT3 and hCNT3C- suggest that Na^+- and H^+-bound versions of the transporters have significantly different conformations of the nucleoside binding pocket and/or translocation channel (7). Only the H^+-coupled form of hCNT3 is susceptible to inhibition by the hydrophilic thiol-reactive agent PCMBS (20).

Fig. 3-3*B* compares the cation-dependence of hCNT3 and hCNT3C- influx of 10 μM ^{14}C-labeled uridine in the presence of Na^+ and/or H^+ (100 mM NaCl or ChCl, pH 7.5 or 5.5, as indicated). Like hCNT3, hCNT3C- displayed high levels of uridine uptake in the presence of Na^+ (NaCl, pH 7.5), H^+ (ChCl, pH 5.5) and both

Na^+ and H^+ (NaCl, pH 5.5). Relative to hCNT3, hCNT3C- exhibited an equivalent rate of uridine transport in the presence of H^+ (ChCl, pH 5.5), but did not show the wild-type increase in uridine influx in the presence of Na^+ (NaCl, pH 7.5) or Na^+ plus H^+ (NaCl, pH 5.5). As a result, the ratio of uridine influx in the presence of Na^+ (NaCl, pH 7.5) to that in the presence of H^+ (ChCl, pH 5.5) decreased from 1.60 for wild-type protein to 0.98 for hCNT3C-. These uridine uptake ratios are in good agreement with that reported previously for hCNT3 (7) and with the other results for hCNT3C- shown in Fig. 3-3*A*. The residual uridine fluxes evident in the absence of Na^+ and at a low H^+ concentration (ChCl, pH 7.5) can be attributed to the small, but significant amount of H^+-activation that occurs under these conditions (7).

Cell-surface expression and glycosylation of hCNT3C- – The equivalent levels of transport activity shown in Fig. 3-3*B* suggest that hCNT3 and hCNT3C- were present in oocyte plasma membranes in similar quantities. This was investigated directly by cell-surface labeling with sulfo-NHS-LC-biotin using immobilized streptavidin resin to separate cell-surface protein (Fig. 3-4*A*) from that associated with total (plasma + intracellular) membranes (Fig. 3-4*B*). Immunoblots of the fractions were probed with hCNT3 polyclonal antibodies (24) directed against amino acid residues 45 - 69 of the extramembraneous N-terminal region of the protein (Fig. 3-1). To evaluate the glycosylation status of hCNT3 and hCNT3C-, the immunoblots in Figs. 3-4*A* and *B* also include aglyco-hCNT3, a construct produced by mutating all four potential N-terminal glycosylation acceptor sites, asparagine residues 630, 636, 664 and 678, to aspartate (Fig. 3-1). For comparison with the electrophoretic mobility of aglyco-hCNT3, Fig. 3-4*B* also shows the same streptavidin fractions of total hCNT3 and hCNT3C- membranes before and after digestion with *N*-glycosidase-F. Antibody specificity was evaluated in membrane fractions prepared from control water-injected oocytes.

Consistent with the presence of multiple possible sites of *N*-linked glycosylation, cell surface hCNT3 and hCNT3C- exhibited three discreet immunobands at 100, 86 and 75 kDa (Fig. 3-4*A*). Total cell surface immunoreactivity was similar for the two transporters, the majority of hCNT3 and hCNT3C- staining being associated with the highest and intermediate molecular

weight forms, respectively (Fig. 3-4*A*). Corresponding patterns of immunoreactivity were apparent in total membranes (Fig. 3-4*B*). Indicative of proper protein folding, therefore, hCNT3C- was processed to the oocyte plasma membrane in amounts similar to wild-type hCNT3. Digestion with *N*-glycosidase-F shifted hCNT3 and hCNT3C- immunoreactivity to the lower molecular weight band at 75 kDa, an electrophoretic mobility identical to that of aglyco-hCNT3 and in good agreement with the molecular weight of hCNT3 calculated from its amino acid sequence (77 kDa). Confirming antibody specificity for hCNT3/hCNT3C-, no immunoreactivity was detected in blots from control water-injected oocytes.

Kinetic characterization of hCNT3C- – To further investigate hCNT3C- function, Fig. 3-5 compares the concentration dependence of radiolabeled uridine (0 - 1 mM) influx by hCNT3 and hCNT3C- measured either in the presence of Na^+ (100 mM NaCl, pH 7.5) or in the presence of H^+ (100 mM ChCl, pH 5.5). The corresponding kinetic parameters are given in Table 3-1. The results demonstrate robust high-affinity transport of uridine by hCNT3C-. Similar to hCNT3, and in agreement with previous kinetic data for the wild-type transporter (7), the apparent K_m value of hCNT3C- for uridine in Na^+-containing transport medium was lower than that in the presence of H^+ (15 and 62 μM, respectively, for hCNT3 compared to 18 and 63 μM, respectively, for hCNT3C-). Calculated uridine V_{max}:K_m ratios, an indicator of transporter efficiency and a kinetic predictor of relative transport rates at permeant concentrations less than K_m values, were consistent with the 10 μM influx data shown in Fig. 3-3*B* [hCNT3(Na^+) > hCNT3(H^+), hCNT3C-(Na^+), hCNT3C-(H^+)].

Cation-activation curves were also determined for both transporters using a radiolabeled uridine concentration of 10 μM. Na^+-activation was measured over the concentration range 0 - 100 mM NaCl in transport medium at pH 7.5 and 8.5 (Figs. 3-6*A* and *B*, respectively), the latter to eliminate the small amount of H^+-activation that occurs at neutral pH (7). Isosmolarity was maintained with ChCl. H^+-activation was measured in 100 mM ChCl transport medium at pH values ranging from 4.5 - 8.5 (Fig. 3-6*C*). Kinetic parameters derived from these data are presented in Tables 3-2 and 3-3 (Na^+ and H^+, respectively). Reflecting previously reported differences in

Na^+ and H^+ coupling by hCNT3 (7, 8), the wild-type protein exhibited saturable Na^+- and H^+-activation curves that were sigmoidal and hyperbolic in nature, respectively, with apparent K_{50} values of 12 (pH 7.5) and 11 mM (pH 8.5) for Na^+ and 690 nM for H^+. Calculated Hill coefficients were consistent with 2:1 (Na^+) and 1:1 (H^+) cation:nucleoside coupling ratios. Validating the subsequent use of pH 8.5 to study Na^+ coupling of hCNT3/hCNT3C- without interference from H^+, there was no difference in hCNT3 Na^+-activation kinetics at pH 7.5 and 8.5.

In marked contrast to wild-type hCNT3, and consistent with the relative decrease in Na^+- *versus* H^+-coupled uridine transport activity noted for the cysteine-less transporter in Fig. 3-3*B* and Table 3-1, the corresponding cation-activation curves for hCNT3C- revealed a marked and specific decrease in apparent affinity for Na^+ (apparent K_{50} > 40 mM). This shift in Na^+ affinity did not extend to H^+, since kinetic parameters for hCNT3C- H^+-activation were comparable to those of hCNT3 (apparent K_{50} value of 550 nM). Similarly, the corresponding Hill coefficient was consistent with a H^+:nucleoside coupling ratio of 1:1. That for Na^+ could not be determined, although the curve appeared sigmoidal (Figs. 3-6*A* and *B*), and therefore potentially consistent with the wild-type Na^+:nucleoside coupling ratio of 2:1. Similar to the wild-type protein, there was no difference in hCNT3C- Na^+-activation kinetics at pH 7.5 and 8.5. All subsequent hCNT3/hCNT3C- Na^+-activation and Na^+-coupling experiments were performed at pH 8.5.

Electrophysiological determination of hCNT3C- Na^+-activation kinetics – Since hCNT3 is electrogenic, the Na^+-activation kinetic parameters of hCNT3C- were also determined by electrophysiology. Fig. 3-7 depicts the relationship between Na^+ concentration and 100 μM uridine-evoked current for oocytes expressing wild-type hCNT3 or hCNT3C- clamped at a membrane holding potential of -90 mV. Oocytes were individually normalized to their predicted I_{max} values and subsequently averaged to produce mean kinetic parameters. In agreement with previous studies (7, 8), the apparent K_{50} value for Na^+-coupled uridine uptake by hCNT3 under these conditions was 2.2 ± 0.1 mM. Similar to the radioisotope flux data in Figs. 3-6*A* and *B*, hCNT3C- exhibited a marked decrease (~ 11-fold) in the apparent affinity for Na^+ in comparison to that of the wild-type protein, with an

increased apparent K_{50} value of 24.7 ± 0.8 mM. The corresponding Hill coefficients for hCNT3C- and hCNT3 were ≥ 1.5, suggesting that the wild-type Na^+:uridine stoichiometry of 2:1 was maintained by hCNT3C-. The apparent K_{50} values for hCNT3 and hCNT3C- as determined by electrophysiology were lower than those derived from radioisotope flux data because of (i) the different uridine concentrations used in the two studies (100 and 10 μM, respectively), and (ii) the difference in membrane potential in the two situations (-90 mV for the voltage-clamped oocytes *versus* ~ -40 mV under radioisotope flux conditions) (5).

Presteady-state electrophysiology of hCNT3C- – Presteady-state electrophysiological experiments were performed on oocytes producing hCNT3C-voltage-clamped at a holding potential (V_h) of -50 mV. Presteady-state currents were activated by voltage steps to a series of test potentials (V_t) in the presence of varying concentrations of Na^+ (0 - 100 mM NaCl, pH 8.5; Figs. 3-8*A*-*E*) and in the presence of both Na^+ and extracellular uridine (100 mM NaCl, pH 8.5 + 500 μM uridine; Fig. 3-8*F*). hCNT3C- exhibited presteady-state currents similar to those previously described for wild-type hCNT3 (7) and wild-type hCNT1 (6), which increased in magnitude upon exposure to extracellular Na^+ and were largely eliminated upon addition of uridine. However, consistent with a reduced binding affinity for Na^+, and different from the wild-type protein, presteady-state currents approached maximum values only at Na^+ concentrations > 50 mM, a behavior also observed for hfCNT, another CNT with low apparent affinity for Na^+ (unpublished observation) Presteady-state currents were absent from control water-injected oocytes (data not shown) (6).

Na^+:uridine and H^+:uridine stoichiometry – The Na^+:uridine and H^+:uridine stoichiometries of hCNT3C- were determined directly by simultaneous measurement of uridine evoked currents and 100 μM radiolabeled uridine uptake under voltage clamp conditions, as described previously (6-8). A representative current trace is depicted in Fig. 3-9*A* for an oocyte expressing hCNT3C-exposed to 100 μM radiolabeled uridine in 100 mM NaCl transport medium, pH 8.5. Presented in Fig. 3-9*B* and *C*, each data point represents a single oocyte, and the coupling ratio is given by the slope of the linear fit of charge (pmol) *versus* uptake (pmol). In 100

mM NaCl transport medium (pH 8.5) and at a holding potential of -90 mV, the linear correlation between uridine-dependent charge and uridine accumulation gave a Na^+:uridine coupling ratio of 2.08 ± 0.11 (Fig. 3-9*B*). The corresponding H^+:uridine stoichiometry was determined in acidified 100 mM ChCl transport medium (pH 5.5) and resulted in a coupling ratio of 1.11 ± 0.06 (Fig. 3-9*C*). Both hCNT3C- stoichiometries agree with previously published values for hCNT3 (7, 8), and with the Hill coefficients derived from hCNT3 and hCNT3C- from Figs. 3-6 and 3-7 (Tables 3-2 and 3-3).

Cation-activation of aglyco-hCNT3 – The experiment of Fig. 3-4 demonstrated that wild-type hCNT3 and hCNT3C- have different patterns of *N*-linked glycosylation. To exclude the possibility that the shift in hCNT3C- Na^+ affinity was secondary to the altered glycosylation status of the protein, the apparent K_{50} and V_{max} values for Na^+- and H^+-activation of aglyco-hCNT3 were determined under conditions identical to those used in Fig. 3-6*B* for hCNT3C-. Kinetic parameters for both cations were not significantly different from those of the wild-type protein measured in parallel in the same experiment (aglyco-hCNT3 and hCNT3 apparent K_{50} and V_{max} values of 10.5 ± 1.1 and 8.8 ± 1.2 mM and 6.8 ± 0.4 and 7.4 ± 0.5 pmol/oocyte.min^{-1}, respectively, for Na^+, and 399 ± 98 and 506 ± 182 nM and 4.7 ± 0.2 and 5.3 ± 0.4 pmol/oocyte.min^{-1}, respectively, for H^+) (cation-activation curves not shown).

Cation-activation of hCNT3C- mutants – The hCNT3C- construct differs from wild-type hCNT3 by the replacement of all 14 endogenous cysteine residues with serine. Five of these substitutions lie within predicted TM regions of the protein (Fig. 3-1). Of these, four reside in the C-terminal half of the protein which corresponds to the region that chimeric studies between hCNT1 and hCNT3 (5) and between hCNT1 and hfCNT (25) have demonstrated to be responsible for Na^+ coupling. Site-directed mutagenesis experiments to identify the residue(s) responsible for the shift in hCNT3C- Na^+-affinity therefore focused on the four C-terminal intramembraneous cysteine residues: Cys486 (TM 11), Cys561 (TM 12), Cys602 (TM 13) and Cys607 (TM 13). In the hCNT3C- background, cysteine residues were individually reintroduced at each of these positions, yielding

constructs S486C(C-), S561C(C-), S602C(C-) and S607C(C-). Measured under conditions identical to those used in Fig. 3-6*B*, Fig. 3-10 shows oocyte Na^+-activation curves for each mutant. Corresponding kinetic parameters are given in Table 3-2. S486C(C-), S602C(C-) and S607C(C-) (Figs. 3-10*A, C, D*) each retained Na^+-activation curves similar to that of hCNT3C- (Fig. 3-6*B*), with apparent K_{50} values > 40 mM. In contrast, the Na^+-activation curve for S561C(C-) (Fig. 3-10*B*) closely resembled that of wild-type hCNT3 (Fig. 3-6*B*) with an apparent K_{50} value of 7.2 ± 0.6 mM. H^+-activation kinetics were also determined for S561C(C-) yielding apparent K_{50} and V_{max} values that were similar to those of both hCNT3C- and hCNT3 (cation-activation curve not shown; Table 3-3).

Cation-activation of hCNT3 mutant C561S – To confirm the role of Cys561 in the shift in Na^+-affinity of hCNT3C-, serine was substituted for cysteine in wild-type hCNT3, creating the mutant protein C561S. Na^+- and H^+-activation kinetics for oocytes producing C561S were determined under identical experimental conditions to those described above for other hCNT3/hCNT3C- constructs and are depicted in Fig. 3-11. Kinetic parameters derived from the curves are presented in Tables 3-2 and 3-3. Similar to hCNT3C- (Figs. 3-6*B* and *C*), C561S exhibited a decreased apparent affinity for Na^+ (> 40 mM) in the absence of a parallel shift in H^+ apparent binding affinity.

Cation-activation of hCNT1 and hCNT1 mutant C540S – In contrast to hCNT3, which is both H^+- and Na^+-coupled and exhibits H^+:nucleoside and Na^+:nucleoside stoichiometries of 1:1 and 2:1, respectively, hCNT1 and hCNT2 are Na^+-specific and have a Na^+:nucleoside stoichiometry of 1:1 (4, 6-8, 23). All three proteins share similar high affinities for Na^+ binding with apparent K_{50} values of ~ 10 mM (4, 6-8). The residue corresponding to hCNT3 Cys561 in hCNT1 is Cys540. To investigate the effects of a cysteine to serine mutation at this position in another CNT family member, the same change was made in hCNT1 to create the mutant protein C540S. Mutant C540S and wild-type hCNT1 were then produced in oocytes, and their Na^+-activation kinetics investigated under experimental conditions identical to those described above for hCNT3/hCNT3C- and mutants (Fig. 3-12). In agreement with previous studies (4, 26) hCNT1 displayed a hyperbolic Na^+-

activation curve with an apparent affinity for Na^+ of 6.6 ± 1.0 mM and a V_{max} of 4.5 ± 0.2 pmol/oocyte.min^{-1} (Fig. 3-12*B*). Similarly, Na^+-activation of C540S was also hyperbolic with apparent K_m and V_{max} values of 8.4 ± 1.1 mM and 4.3 ± 0.1 pmol/oocyte.min^{-1}, respectively (Fig. 3-12*A*). Corresponding Hill coefficients were both 1.0 ± 0.1.

Other amino acid substitutions of hCNT3 residue Cys561 – Sequence comparisons of 126 eukaryotic and prokaryotic CNT family members revealed that the residue corresponding to hCNT3 Cys561 is highly conserved. However, in addition to cysteine (90 family members), the amino acids alanine, valine, threonine and isoleucine were also represented at this position (4, 21, 6 and 5 family members, respectively). Therefore, to further elucidate the role of Cys561 in hCNT3 cation-coupling, hCNT3 mutants C561A, C561V, C561T and C561I were constructed and produced in oocytes. Substitution of hCNT3 Cys561 with glycine, the amino acid with the smallest side chain, was also included in the series (mutant C561G). Functional activity and cation selectivity were compared to wild-type hCNT3 and mutant C561S by measuring 10 μM radiolabeled uridine influx in both Na^+- and H^+-containing transport medium (100 mM NaCl, pH 7.5 and 100 mM ChCl, pH 5.5, respectively) (Fig. 3-13). Similar to these transporters, C561G and C561A exhibited both Na^+- and H^+-coupled influx of radiolabeled uridine. However, relative to transport in the presence of Na^+ and in contrast to C561A, C561G exhibited reduced influx of uridine in H^+-containing medium. Extending this trend, substitution of Cys561 with larger neutral amino acids (mutants C561V, C561T and C561I) led to almost total abolition of uridine influx in H^+-containing medium, a finding that was confirmed for C561I by corresponding measurements of 100 μM uridine-induced steady-state currents (Fig. 3-14).

Kinetic parameters for Na^+-activation of C561G, C561A, C561S, C561T, C561V and C561I, measured as described in Fig. 3-6*B*, are given in Table 3-2. Replacement of Cys561 with residues of a similar size (C561A and C561V) allowed full (C561A) or partial (C561V) recovery of Na^+ apparent affinity (K_{50} values of 10.7 ± 0.7 and 31.3 ± 1.9 mM, respectively). In contrast, C561G, C561T and C561I exhibited reduced affinities for Na^+ similar to that of hCNT3C-

(apparent K_{50} values > 40 mM). The ability of alanine to mimic cysteine at residue position 561 extended to the reciprocal hCNT3C- mutant S561A(C-), which exhibited a partially restored apparent K_{50} value of 20.5 ± 0.9 mM (Na^+-activation curve not shown; Table 3-2).

Corresponding kinetic parameters for H^+ activation of mutants C561G and C561A were also determined. Measured as described in Fig. 3-6*C* and similar to wild-type hCNT3, C561G and C561A displayed apparent K_{50} values for H^+ of 900 ± 90 and 490 ± 100 nM, respectively (H^+ activation curves not shown; Table 3-3).

Complementary to these cation activation analyses, we additionally determined the uridine kinetic parameters of hCNT3 mutants. Values were determined as described in Table 3-1 and are presented in Table 3-4 (concentration dependence curves not shown). In Na^+-containing transport medium (100 mM NaCl, pH 8.5), C561A and C561S exhibited high affinity for uridine similar to wild-type hCNT3 (Fig. 3-5 and Table 3-1), with apparent K_m values of 29.5 ± 2.4 and 26.5 ± 2.5 μM, respectively. In contrast, the other mutants in the series exhibited progressively increasing K_m values for uridine influx: C561G (93.8 ± 16.0 μM), C561T (106 ± 27 μM), C561V (120 ± 11 μM), and C561I (216 ± 17 μM). Similar to wild-type hCNT3 (Table 3-1 and Fig. 3-5), uridine apparent K_m values increased when determined in H^+-containing transport medium (100 mM ChCl, pH 5.5). C561A (65.0 ± 6.3 μM) and C561S (91.0 ± 11.0 μM) were again comparable with the wild-type transporterm whereas C561G was higher (234 ± 32 μM).

Presteady-state Electrophysiology of hCNT3 Cys561 and hCNT3C-S561C(C-) Mutants – In a final series of experiments, presteady-state electrophysiological experiments were performed on oocytes producing the hCNT3 mutants C561A and C561S and the hCNT3C- mutants S561C(C-). As undertaken for hCNT3C- in Fig. 3-8, oocytes were voltage-clamped at a holding potential (V_h) of -50 mV and stepped to a series of test potentials (V_t) in the presence of varying concentrations of Na^+ (0-100 mM NaCl, pH 8.5). C561A, C561S, and S561C(C-) exhibited presteady-state currents, which increased in magnitude upon exposure to

extracellular Na^+ and were eliminated following the addition of uridine (500 μM) (data not shown). Consistent with the flux demonstration that both C561A and S561C(C-) displayed high affinity for Na^+ (Table 3-2 and Fig. 3-10*B*) , the profiles of the presteady-state currents function of Na^+ concentration resembled that of wild-type hCNT3 (7) and approached maximum values at low Na^+ concentrations consistent with their respective apparent K_{50} values for Na^+ activation (Table 3-2). In agreement with the decreased apparent affinity of C561S for Na^+ (Table 3-2 and Fig. 3-11*A*), however, C561S presteady-state currents were similar in profile to hCNT3(C-) (Fig. 3-8) and of hfCNT (hagfish CNT), and maximal only at Na^+ concentrations of >50 mM.

Discussion

hCNT3, the most recently discovered and functionally versatile of three human members of the SLC28 (CNT) protein family, is 691 amino acids in length, has a 13 TM membrane architecture, and utilizes electrochemical gradients of both Na^+ and H^+ to accumulate a broad range of pyrimidine and purine nucleosides and nucleoside drugs within cells (5, 6, 25, 27). Although paralogs hCNT1 and hCNT2 have a similar predicted membrane topology, they function predominantly as Na^+-coupled transporters, and are pyrimidine nucleoside-preferring and purine nucleoside-preferring, respectively (4-6, 8). More widely distributed in cells and tissues than hCNT1 or hCNT2 (23) and with a central role in renal transepithelial nucleoside and nucleoside drug transport (24, 27, 28), the multifunctional capability of hCNT3 makes it the protein of choice for systematic in depth molecular characterization by SCAM. A prerequisite of this approach is the availability of a functional cysteine-less version of the transporter.

Cysteine-less hCNT3C-, in which all 14 endogenous cysteine residues of hCNT3 have been converted to serine, is shown here to have a robust functional phenotype when produced in *Xenopus* oocytes. Similar to wild-type hCNT3, and consistent with correct folding of the cysteine-less transporter, hCNT3C- exhibited broad selectivity for both pyrimidine and purine nucleosides in Na^+-containing

medium (Fig. 3-3*A*), displayed the characteristic narrowing of this permeant selectivity in H^+-containing medium (Fig. 3-3*A*), was processed to the cell surface in amounts equivalent to hCNT3 (Fig. 3-4), exhibited apparent binding affinities for uridine in both Na^+- and H^+-containing medium similar to those of the wild-type transporter (Fig. 3-5), and retained the wild-type Na^+:uridine and H^+:uridine coupling stoichiometries of 2:1 and 1:1, respectively (Fig. 3-9). Recombinant hCNT3C- is also functional in yeast and was used in initial SCAM analyses to screen residues in TMs 11-13 for reactivity to MTS reagents (19). In oocytes, hCNT3C- was previously used in SCAM analysis of TM 12 to test residues for inhibition by PCMBS (20). Consistent with correct folding of the nucleoside binding pocket of hCNT3C-, MTS and PCMBS accessibility to some residues was blocked by exofacial uridine (19, 20). Taken together, these analyses validate use of hCNT3C- as a template for SCAM analyses of CNT structure and function.

Characterization of hCNT3C- revealed an altered apparent affinity for Na^+; hCNT3C- and wild-type hCNT3 exhibited apparent K_{50} values for Na^+-activation of 10 μM radiolabeled uridine influx of > 40 mM and 11 - 12 mM, respectively (Figs. 3-6*A* and *B*). Under voltage clamp conditions of -90 mV with a uridine concentration of 100 μM, Na^+-activation curves for hCNT3 and hCNT3C- were sufficiently shifted to the left to establish that the change in binding affinity for Na^+ between hCNT3 and hCNT3C- was ~ 11-fold (apparent K_{50} values of 2.2 and 25 mM, respectively) (Fig. 3-7). This difference, which was also apparent in presteady-state current measurements (Fig. 3-8), was specific to Na^+ and did not extend to H^+ (Fig. 3-6*C*). The change was also specific to one particular cysteine residue, Cys561 in TM 12. Reintroduction of cysteine at position 561 (hCNT3C- mutant S561C(C-)) restored wild-type Na^+ binding (Fig. 3-10), whereas the reciprocal single cysteine-to-serine substitution in hCNT3 (mutant C561S) produced an altered Na^+ binding affinity corresponding to that found for hCNT3C- (Fig. 3-11). Presteady-state current measurements confirmed the Na^+-binding characteristics of S561C(C-) and C561S.

Recently, a naturally-occurring hCNT3 variant has been described in the Spanish population in which a T/C transition leads to the substitution of cysteine at

position 602 by arginine (29). This single amino acid replacement in TM 13 led to a shift in Hill coefficient consistent with a change in Na^+:nucleoside stoichiometry from 2:1 to 1:1. In agreement with the findings presented here, the C602R phenotype was a consequence of the insertion of arginine at this position rather than the loss of cysteine.

Fully processed to the cell surface, hCNT3C- exhibited an altered pattern of *N*-linked glycosylation relative to that of the wild-type protein. As shown in Fig. 3-4, two glycosylated forms of hCNT3/hCNT3C- were apparent on SDS-polyacrylamide gels (100 and 86 kDa). Most hCNT3C- immunoreactivity was associated with the 86 kDa band, in contrast to hCNT3 for which most immunoreactivty was found in the higher molecular weight band of 100 kDa. Since no less than six of the 14 endogenous cysteine residues of hCNT3 are located alongside the four potential N-terminal glycosylation acceptor sites in the extracellular N-terminal tail of the protein (Fig. 3-1), and since these cysteines likely form intramolecular disulfide bridges within the protein, it is likely that the modified glycosylation status of the cysteine-less transporter is secondary to changes in the secondary/tertiary structure of this extramembraneous region of the protein. The demonstration that aglyco-hCNT3 exhibited normal Na^+-activation kinetics verified that altered glycosylation was not responsible for the shift in hCNT3C- Na^+ affinity.

As well as replacement of hCNT3 Cys561 with serine, each of the alternative amino acids found at position 561 in other CNT family members (alanine, valine, threonine and isoleucine) were introduced into hCNT3. To provide a more complete spectrum of neutral amino acid side chain structures in the analysis, cysteine was also mutated to glycine. In addition to cysteine, only alanine at this position (hCNT3 mutant C561A) elicited wild-type cation binding (Table 3-2 and Fig. 3-13). The rank order of Na^+ binding affinities (cysteine, alanine > valine > glycine, serine, threonine, isoleucine) demonstrated that normal hCNT3 Na^+-activation was critically dependent upon a combination of residue 561 side chain bulk and polarity. Tolerance of alanine at position 561 was confirmed in the hCNT3C- background, in that mutant S561A(C-) exhibited partially recovered Na^+

binding affinity (Table 3-2), thereby providing an alternative to hCNT3C- as template for future SCAM analyses of hCNT3 structure and function.

Despite retaining Na^+-coupled transport capability, albeit with reduced Na^+-binding affinity, substitution of Cys561 by valine, threonine and isoleucine had the additional and unanticipated consequence of dramatically decreasing H^+-coupled uridine transport activity (Figs. 3-13 and 3-14). Relative to Na^+, substitution of cysteine with the smaller amino acid glycine also led to reduced H^+-dependent uridine transport activity. Therefore, the nature of the amino acid side chain at position Cys561 in hCNT3 influences both Na^+- and H^+-coupled nucleoside transport, but with seemingly dissimilar structure-function profiles. For example, whereas the apparent affinity of mutant C561V for Na^+ was only moderately decreased (apparent K_{50} of 31 mM compared to 11 mM for wild-type hCNT3; Table 3-2), H^+-coupled uridine transport was essentially eliminated (Figs. 3-13 and 3-14). In the opposite direction, the apparent affinity of mutant C561G for Na^+ was not measurable (Table 3-2), whereas H^+ activation curves revealed wild-type hCNT3-like high affinity binding of H^+ (apparent K_{50} of 900 nM, Table 3-3). The structural requirements for Na^+ and H^+ binding and/or translocation at this single residue position are not, therefore, the same. At the level of the whole protein, other indications that Na^+ and H^+ binding and/or translocation have different structural requirements include the demonstration that hCNT3 exhibits different Na^+ and H^+ binding stoichiometries (7, 8). Na^+- and H^+-coupled hCNT3 also have markedly different nucleoside and nucleoside drug selectivities, a finding that provides evidence for two distinct cation-dependent conformational states of the protein (7). Independent of changes in cation interactions and consistent with cation/nucleoside cotransport through a common translocation pore, amino acid substitutions at position Cys561 were also found to have a marked influence on uridine transport kinetics, increasing the uridine apparent K_m value up to 15-fold in Na^+-containing transport medium and up to 4-fold in H^+-containing transport medium (Tables 3-1 and 3-4).

In a separate study, Cys561 was independently identified as the cysteine residue responsible for inhibition of wild-type hCNT3 by PCMBS (20). Access of

this membrane-impermeant probe to Cys561 required H^+, but not Na^+, and was blocked by micromolar concentrations of extracellular uridine. Although this cysteine residue is conserved in Na^+-specific hCNT1 and hCNT2, neither transporter is affected by PCMBS. When converted to cysteine, two other residues in hCNT3 adjacent to Cys561 (Ile554 and Tyr558) also led to H^+-activated inhibition by PCMBS (20). These findings suggest that Cys561 is located in the translocation pore in a mobile region within or closely adjacent to the nucleoside binding pocket and that accessibility of PCMBS to this residue reports a specific H^+-induced conformational state of the protein (20). Positioned in the middle of TM 12 (Fig. 3-1), this residue position is now also revealed to be capable of modifying the functionality of the protein, with marked influences on both Na^+:nucleoside and H^+:nucleoside cotransport. Within the plane of the membrane, Cys561 is located at the interface between those residues sensitive to inhibition by PCMBS in H^+-containing medium only and those where inhibition occurs in the presence of both Na^+ and H^+ (20). Remarkably, intolerant to substitution by other amino acids, only cysteine replacement by alanine approached full wild-type kinetic functionality. Matching the previous observation that H^+-induced inhibition by PCMBS is specific to hCNT3 and not found in hCNT1/2 (20) we have similarly found that mutation of hCNT1 Cys540 to serine (the cysteine substitution corresponding to hCNT3 C561S) had no influence on Na^+-binding affinity (Fig. 3-12). hCNT3 has two Na^+-binding sites, one of which may be Na^+-specific and the other of which may be shared functionally with H^+ (7, 20). hCNT3 Cys561 seems to be primarily associated with the site interacting with both cations.

Conclusions – Two independent lines of investigation have converged to identify Cys561 as a key residue that resides in a conformationally mobile region of hCNT3 and is intimately involved in both Na^+/nucleoside and H^+/nucleoside cotransport. With actions seemingly specific to one of two hCNT3 cation binding sites, future investigations of Cys561 and adjacent residues will be central to understanding the molecular intricacies of CNT cation/nucleoside cotransport and, in particular, to functionally separating and structurally identifying the two cation binding domains of hCNT3. Without access to a CNT crystal structure, SCAM-

based approaches employing hCNT3C- as a template will be essential to these endeavours, to identification of other residues of structural and functional importance, and to investigations of transporter topology.

Table 3-1. Uridine kinetic parameters for hCNT3 and hCNT3C-. Radiolabeled 10 μM uridine influx was measured in 100 mM NaCl transport medium, pH 7.5, and in 100 mM ChCl transport medium, pH 5.5, under intial rate conditions (1 min) in oocytes producing hCNT3 and hCNT3C-. Kinetic parameters were calculated from data shown in Fig. 3-5 corrected for basal (non-mediated) uptake in control water-injected oocytes.

		Apparent K_m value (μM)	V_{max} (pmol/oocyte.min^{-1})	V_{max}:K_m ratio
hCNT3	NaCl, pH 7.5[a]	14.7 ± 1.7	22.7 ± 0.7	1.54 ± 0.12
	ChCl, pH 5.5[b]	62.4 ± 5.4	53.1 ± 1.1	0.85 ± 0.11
hCNT3C-	NaCl, pH 7.5[a]	18.4 ± 1.5	12.4 ± 0.2	0.67 ± 0.11
	ChCl, pH 5.5[b]	63.4 ± 5.1	23.2 ± 0.4	0.37 ± 0.11

[a], from Fig. 3-5*A-B* (100 mM NaCl, pH 7.5); [b], from Fig. 3-5*C-D* (100 mM ChCl, pH 5.5).

Table 3-2. Na^+-activation kinetic parameters for hCNT3, hCNT3C- and mutants.

		Apparent K_{50} value (mM)	V_{max} (pmol/oocyte.min^{-1})	Hill Coefficient
hCNT3[a]	pH 7.5	12.0 ± 0.8	11.9 ± 0.5	1.4 ± 0.1
	pH 8.5	10.7 ± 1.0	12.0 ± 0.7	1.4 ± 0.1
hCNT3C-[a]	pH 7.5	> 40	nd[e]	-
	pH 8.5	> 40	nd[e]	-
S486C(C-)[b]	pH 8.5	> 40	nd[e]	-
S561C(C-)[b]	pH 8.5	7.2 ± 0.6	6.0 ± 0.3	1.4 ± 0.1
S602C(C-)[b]	pH 8.5	> 40	nd[e]	-
S607C(C-)[b]	pH 8.5	> 40	nd[e]	-
C561S[c]	pH 8.5	> 40	nd[e]	-
C561G[d]	pH 8.5	> 40	nd[e]	-
C561A[d]	pH 8.5	10.7 ± 0.6	6.9 ± 0.2	1.5 ± 0.1
C561V[d]	pH 8.5	31.3 ± 1.9	9.1 ± 0.4	1.4 ± 0.1
C561T[d]	pH 8.5	> 40	nd[e]	-
C561I[d]	pH 8.5	> 40	nd[e]	-
S561A(C-)[d]	pH 8.5	20.5 ± 0.9	6.0 ± 0.2	1.4 ± 0.1

[a], from Fig. 3-6*A*-*B*; [b], from Fig. 3-10*A*-*D*; [c], from Fig. 3-11*A*; [d], data not shown; [e], nd, could not be determined; in 100 mM transport media with 0 - 100 mM NaCl (pH 7.5 or 8.5, as indicated, isosmolarity maintained by ChCl).

Table 3-3. H^+-activation kinetic parameters for hCNT3, hCNT3C- and mutants.

	Apparent K_{50} value (nM)	V_{max} (pmol/oocyte.min^{-1})	Hill Coefficient
hCNT3[a]	690 ± 200	7.0 ± 0.4	0.8 ± 0.1
hCNT3C-[a]	550 ± 100	4.4 ± 0.2	0.8 ± 0.1
S561C(C-)[b]	830 ± 150	7.1 ± 0.3	0.8 ± 0.1
C561S[c]	870 ± 80	4.7 ± 0.1	0.7 ± 0.1
C561G[b]	900 ± 90	2.5 ± 0.1	1.0 ± 0.1
C561A[b]	490 ± 100	3.5 ± 0.2	0.8 ± 0.1

[a], from Fig. 3-6*C*; [b], data not shown; [c], from Fig. 3-11*B*; in 100 mM ChCl transport media with pH values ranging from 4.5 - 8.5.

Table 3-4. Uridine kinetics parameters for hCNT3 mutants. Radiolabeled 10 μM uridine influx was measured in 100 mM NaCl transport medium, pH 8.5, and 100 mM ChCl transport medium, pH 5.5, under initial rate conditions (1 min) in oocytes producing C561G, C561A, C561S, C561V, C561T, and C561I. Kinetic parameters were calculated from data (not shown) corrected for basal (nonmediated) uptake in control water-injected oocytes.

	NaCl, pH 8.5 Apparent K_m value	NaCl, pH 8.5 V_{max}	ChCl, pH 5.5 Apparent K_m value	ChCl, pH 5.5 V_{max}
	μM	pmol/oocytes min^{-1}	μM	pmol/oocytes min^{-1}
C561G	93.8 ± 16.0	21.2 ± 1.0	234 ± 32	8.4 ± 0.4
C561A	29.5 ± 2.4	27.5 ± 0.5	65.0 ± 6.3	14.3 ± 0.4
C561S	26.5 ± 2.5	22.7 ± 0.5	91.0 ± 11.0	14.0 ± 0.5
C561V	120 ± 11	70.5 ± 2.0		
C561T	106 ± 27	74.0 ± 5.5		
C561I	216 ± 17	62.5 ± 1.7		

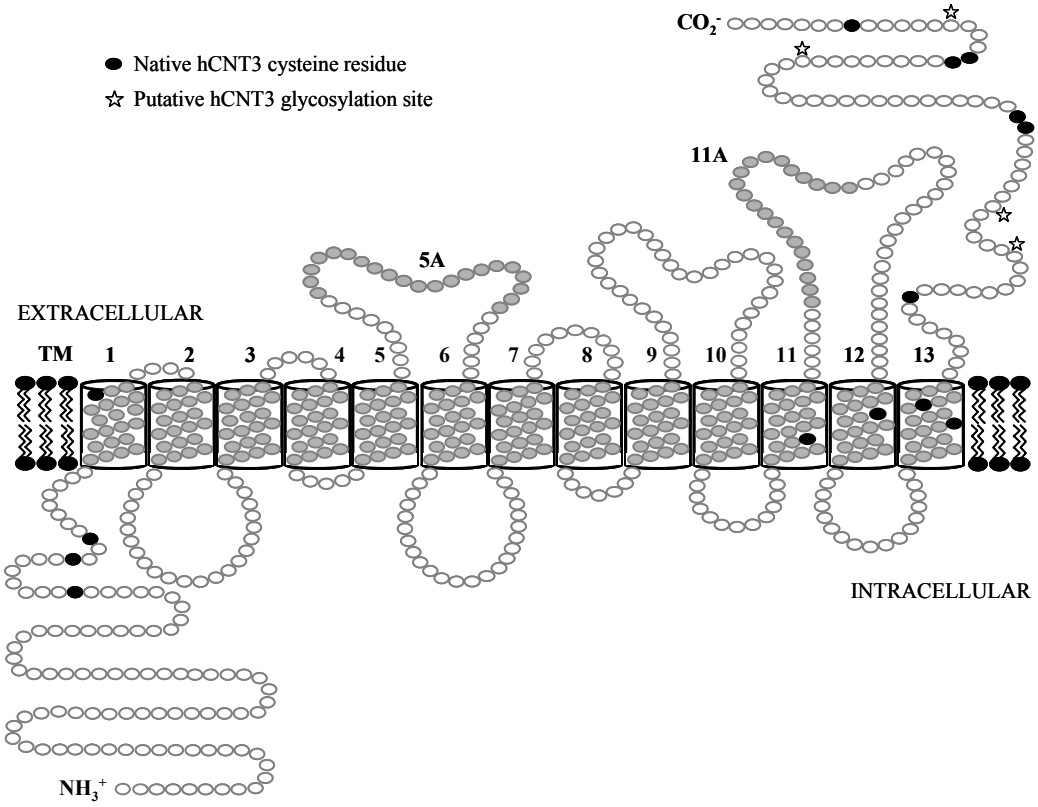

Figure 3-1. Topological model of hCNT3. Membrane-spanning α-helices predicted from bioinformatic analyses of currently identified CNT family members are numbered 1 - 13; 5A and 11A, which are shown as extracellular loops, are weakly predicted to be membrane-spanning α-helices. Cysteine residues and putative glycosylation sites are indicated in *black* and with a *star* symbol, respectively.

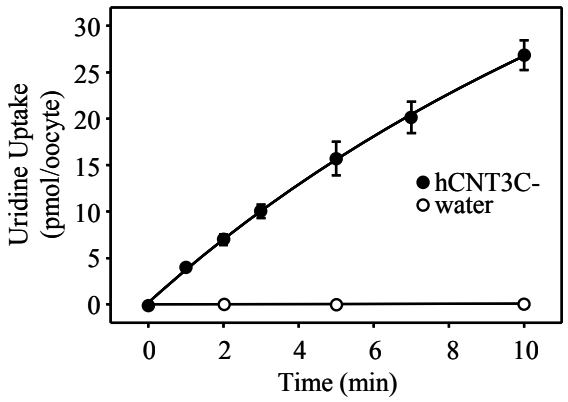

Figure 3-2. Time course of uridine uptake by hCNT3C- in *Xenopus* oocytes. Uptake of 10 μM radiolabeled uridine by oocytes producing hCNT3C- was measured in 100 mM NaCl transport medium (pH 7.5) for various times up to 10 min (*solid* circles) and compared with that of control water-injected oocytes (*open* circles). Each point is the mean ± SEM of 10 - 12 oocytes. Error bars are not shown where values were smaller than that represented by the symbols.

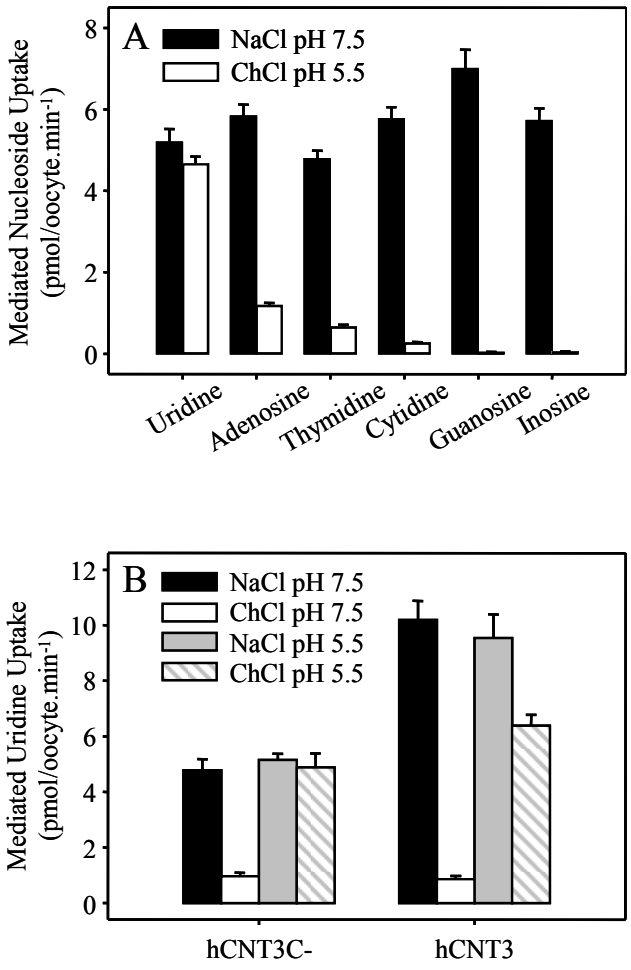

Figure 3-3. Nucleoside and cation selectivity of hCNT3C-. (*A*) Influx of a panel of physiological radiolabeled nucleosides (10 μM) by oocytes producing hCNT3C- was measured under initial rate conditions (1 min flux) in transport medium containing 100 mM NaCl pH 7.5 (*black* bars) or ChCl pH 5.5 (*white* bars). (*B*) Influx (1 min) of 10 μM radiolabeled uridine by wild-type hCNT3 or hCNT3C- was measured in transport medium containing 100 mM NaCl pH 7.5 (*black* bars), ChCl pH 7.5 (*white* bars), NaCl pH 5.5 (*grey* bars) or ChCl pH 5.5 (*hatched* bars). Values (*A* and *B*) were corrected for basal nonmediated uptake in control water-injected oocytes and are means ± SEM of 10 - 12 oocytes.

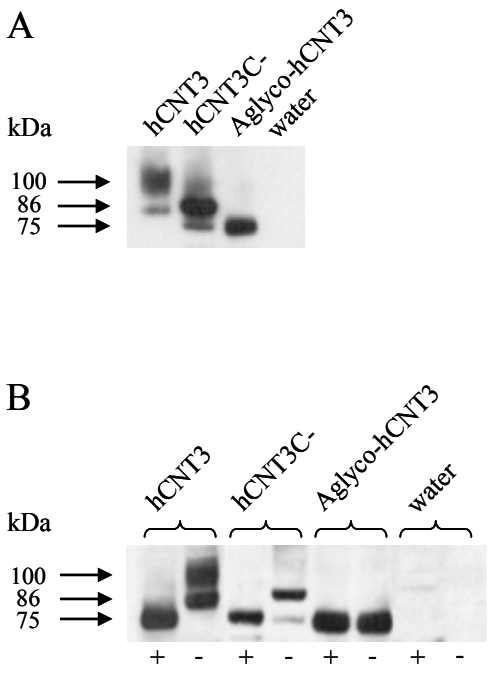

Figure 3-4. Immunoblot analysis of hCNT3, hCNT3C- and aglyco-hCNT3. Labeling of oocytes with sulfo-NHS-LC-biotin was used in conjunction with immobilized streptavidin resin to separate recombinant hCNT3, hCNT3C- and aglyco-hCNT3 cell surface immunoreactivity (*A*) from that associated with total (plasma + intracellular) membranes (*B*). Immunoblots of the fractions were probed with anti-hCNT3 antibodies. In (*B*), (+) and (-) refer to digestion with *N*-glycosidase-F. The positions of molecular weight standards are shown on the left. Water refers to control water-injected oocytes. Blots shown in *A* and *B* are from different gels.

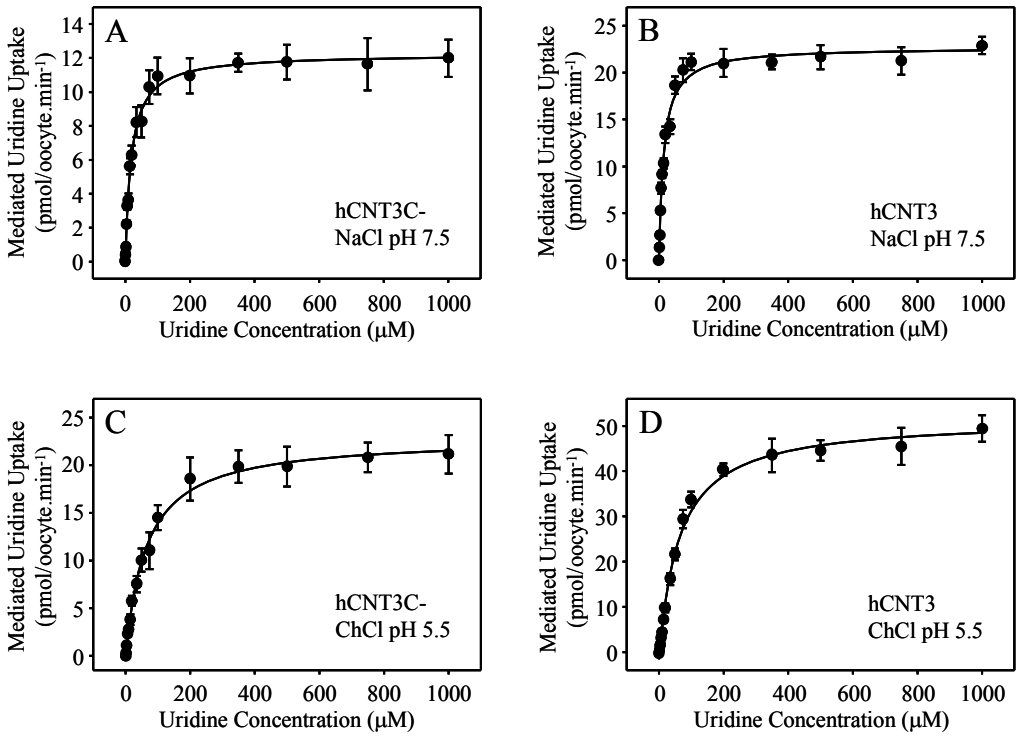

Figure 3-5. Concentration dependence of Na^+- and H^+-coupled uridine uptake by oocytes producing hCNT3 and hCNT3C-. Radiolabeled 10 μM uridine influx was measured in 100 mM NaCl transport medium, pH 7.5 (*A* and *B*) and 100 mM ChCl transport medium, pH 5.5 (*C* and *D*) under initial rate conditions (1 min) in oocytes producing hCNT3 (*B* and *D*) and hCNT3C- (*A* and *C*). Corrected for basal (nonmediated) uptake in control water-injected oocytes, each value is the mean ± SEM of 10 - 12 oocytes. Error bars are not shown where values were smaller than that represented by the symbols. Kinetic parameters calculated from the data are presented in Table 3-1.

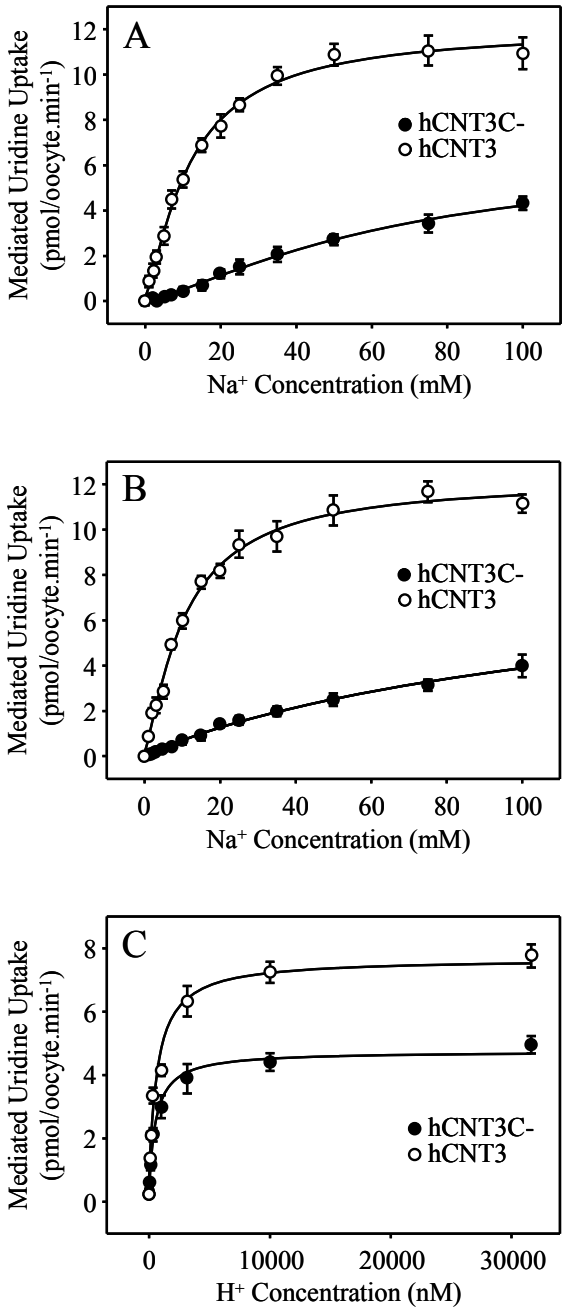
A
Mediated Uridine Uptake (pmol/oocyte.min-1)
hCNT3C-
hCNT3
Na+ Concentration (mM)
B
Mediated Uridine Uptake (pmol/oocyte.min-1)
hCNT3C-
hCNT3
Na+ Concentration (mM)
C
Mediated Uridine Uptake (pmol/oocyte.min-1)
hCNT3C-
hCNT3
H+ Concentration (nM)

Figure 3-6.

Figure 3-6. Na^+- and H^+-activation kinetics of oocytes producing hCNT3 and hCNT3C-. Na^+-activation curves for oocytes producing hCNT3 (*open* circles) and hCNT3C- (*solid* circles) were measured in transport medium containing 0 - 100 mM NaCl at pH 7.5 (*A*) and pH 8.5 (*B*), with isosmolarity maintained by addition of ChCl. Corresponding H^+-activation curves were determined in 100 mM ChCl transport medium at pH values ranging from 4.5 to 8.5 (*C*). The radiolabeled uridine concentration was 10 μM (1 min flux). Corrected for basal (nonmediated) uptake in control water-injected oocytes, each value is the mean ± SEM of 10 - 12 oocytes. Error bars are not shown where values were smaller than that represented by the symbols. Kinetic parameters calculated from the data are presented in Tables 3-2 and 3-3.

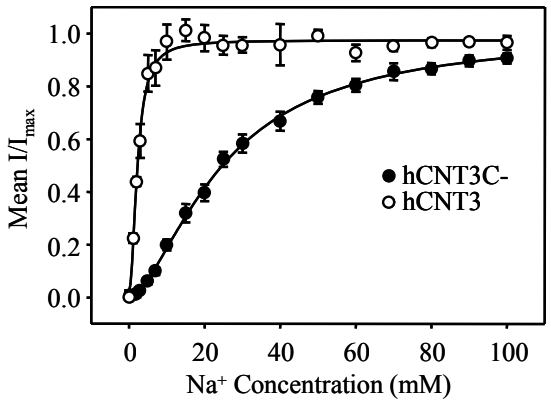

Figure 3-7. Na^+-activation kinetics of hCNT3 and hCNT3C- determined by electrophysiology. Na^+-activation curves for hCNT3 (*open* circles) and hCNT3C- (*solid* circles) were determined at a holding potential of -90 mV in transport media of the same composition used in radioisotope flux studies (Fig. 3-6*B*). The uridine concentration was 100 μM. Uridine-evoked currents at each Na^+ concentration were normalized to the respective fitted I_{max} value and are presented as the mean ± SEM of 6-8 oocytes. Error bars are not shown where values were smaller than that represented by the symbols. No currents were detected in control water-injected oocytes (data not shown).

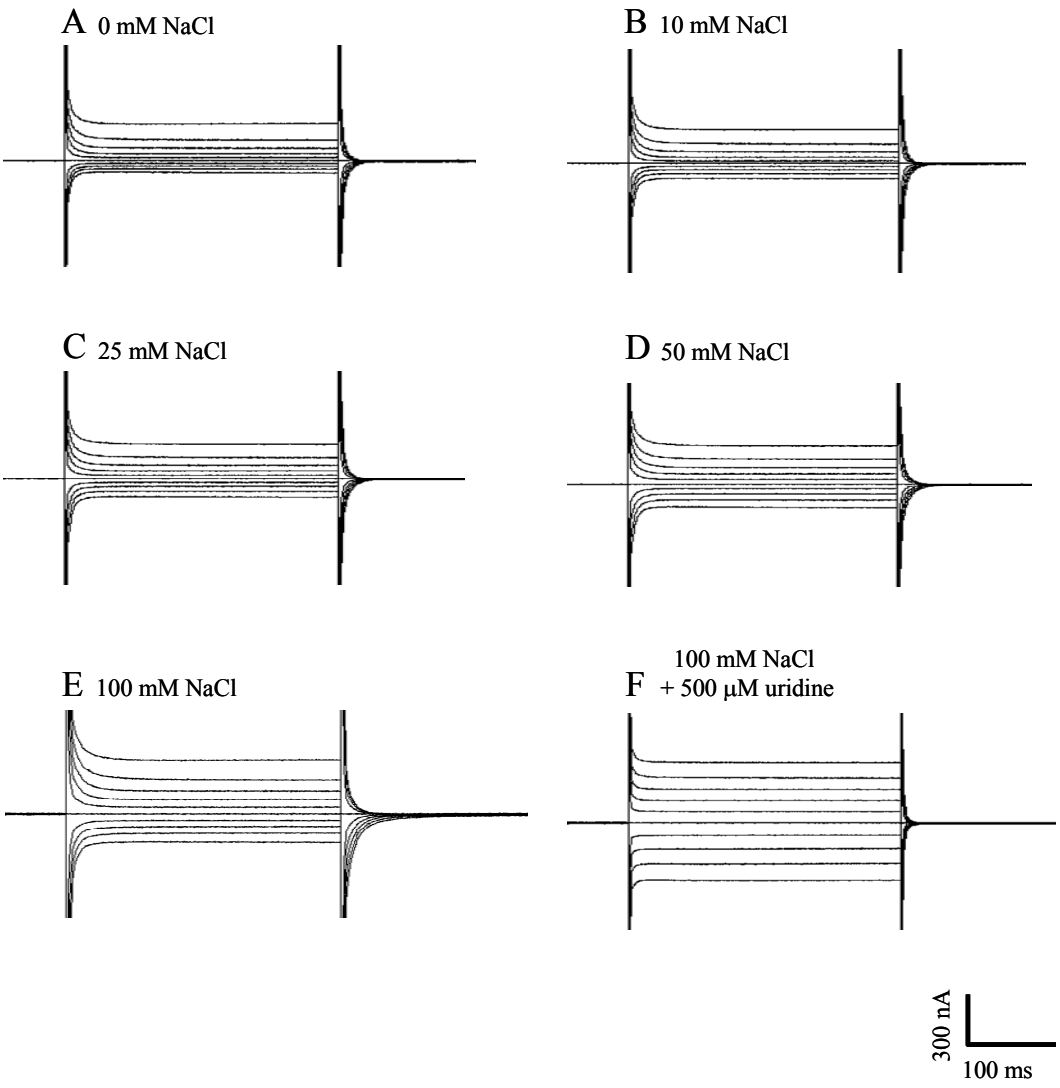

Figure 3-8. Presteady-state currents of hCNT3C-. Oocytes expressing hCNT3C- were held at a holding potential (V_h) of -50 mV and stepped to a range of test potentials (V_t) from -150 to +75 mV in 25 mV increments. Representative traces from a single oocyte are shown in transport medium containing 0 mM NaCl, pH 8.5 (100 mM ChCl, pH 8.5; *A*), 10, 25, 50 and 100 mM NaCl, pH 8.5 (*B*-*E*, respectively) and 100 mM NaCl, pH 8.5 + 500 μM uridine (*F*).

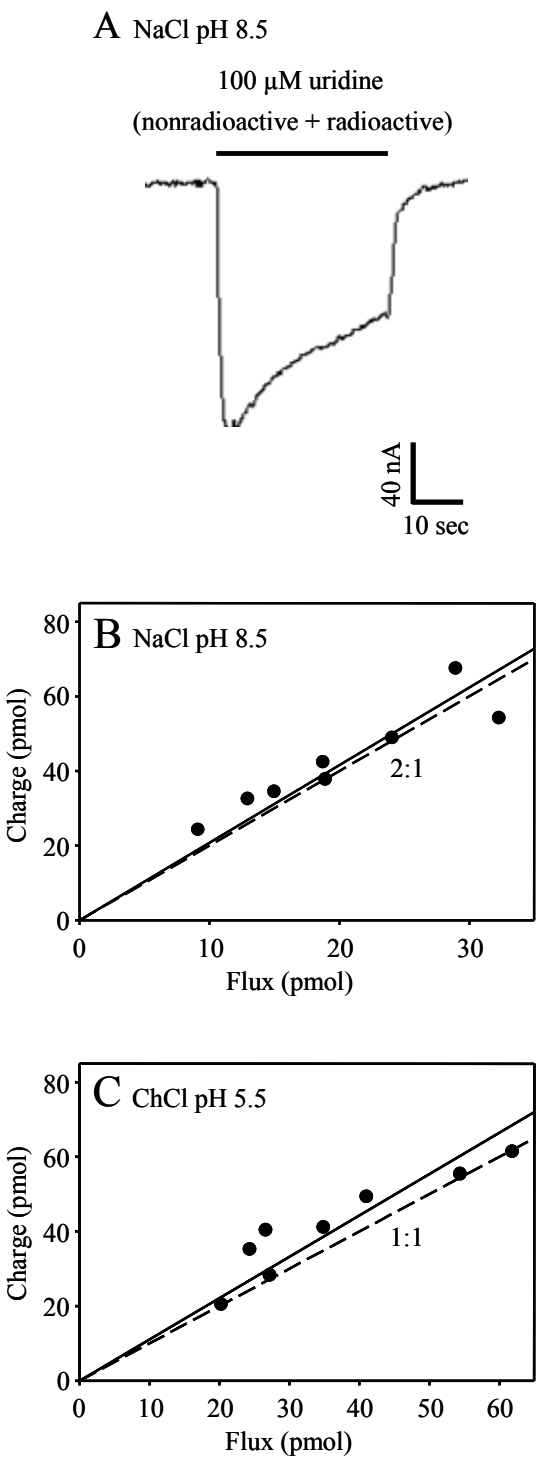
A NaCl pH 8.5
100 µM uridine
(nonradioactive + radioactive)
40 nA
10 sec
B NaCl pH 8.5
Charge (pmol)
Flux (pmol)
2:1
C ChCl pH 5.5
Charge (pmol)
Flux (pmol)
1:1

Figure 3-9.

Figure 3-9. Na^+:uridine and H^+:uridine stoichiometry of hCNT3C-. (*A*) A representative current trace for an oocyte expressing hCNT3C- clamped at a membrane potential of -90 mV and exposed to 100 μM radiolabeled uridine in 100 mM NaCl, pH 8.5. Integration of the uridine-evoked current over the uptake period yielded the charge moved; this charge, representing net cation influx, was correlated to the net uptake (flux) of radiolabeled uridine by the oocyte during the same time interval. Following the same protocol (V_h of -90 mV; 100 μM uridine), (*B*) and (*C*) show charge to flux ratio plots generated for oocytes producing hCNT3C- in either 100 mM NaCl transport medium at pH 8.5 (*B*) or ChCl transport medium at pH 5.5 (*C*). Each point represents a single oocyte. Linear regression fits of both data sets passed through the origin and are indicated by *solid* lines. The *dashed* lines represents theoretical 2:1 (*B*) and 1:1 (*C*) charge:uptake ratios.

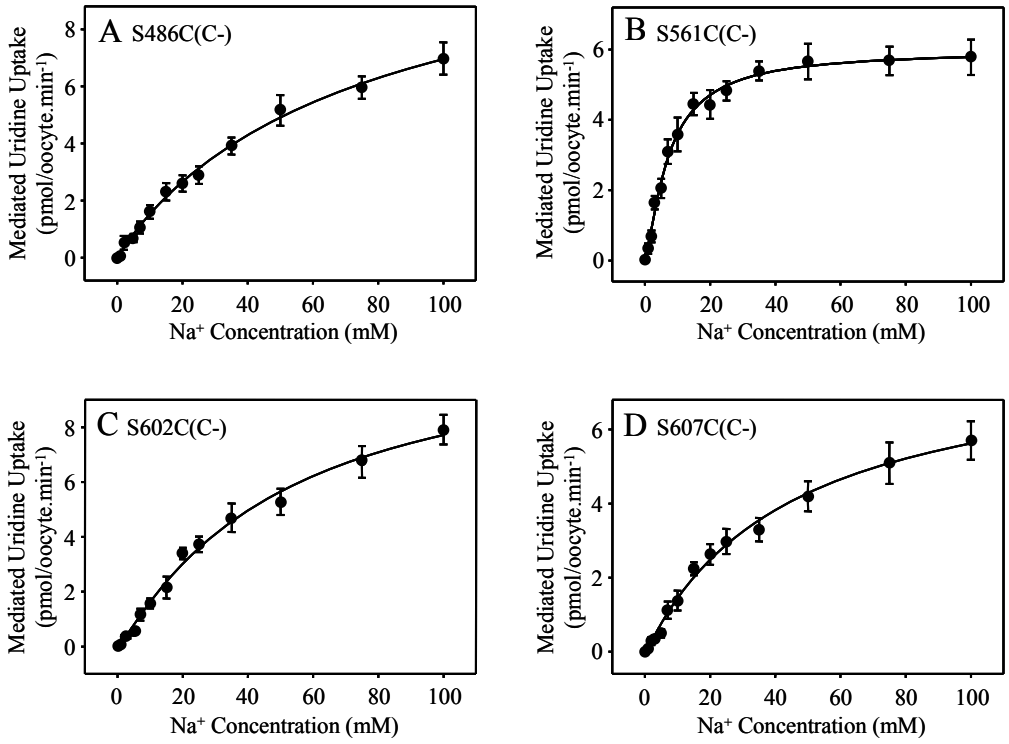

Figure 3-10. Na^+-activation kinetics of oocytes producing hCNT3C- mutants S486C(C-), S561C(C-), S602C(C-) and S607C(C-). Na^+-activation curves were determined as described in Fig. 3-6*B*. The radiolabeled uridine concentration was 10 μM (1 min flux). Corrected for basal (nonmediated) uptake in control water-injected oocytes, each value is the mean ± SEM of 10 - 12 oocytes. Error bars are not shown where values were smaller than that represented by the symbols. Kinetic parameters calculated from the data are presented in Table 3-2.

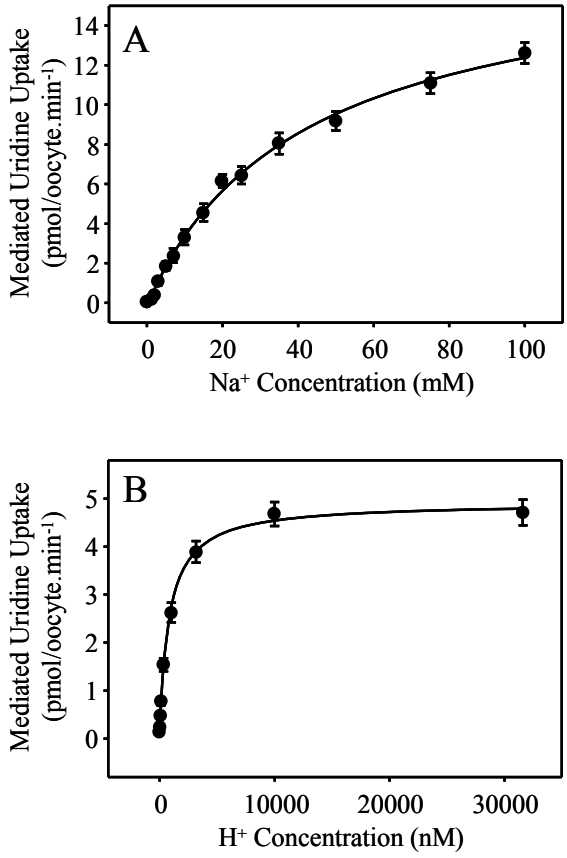

Figure 3-11. Na^+- and H^+-activation kinetics of oocytes producing hCNT3 mutant C561S. Na^+- (*A*) and H^+- (*B*) activation curves were determined as described in Figs. 3-6*B* and *C*, respectively. The radiolabeled uridine concentration was 10 μM (1 min flux). Corrected for basal (nonmediated) uptake in control water-injected oocytes, each value is the mean ± SEM of 10 - 12 oocytes. Error bars are not shown where values were smaller than that represented by the symbols. Kinetic parameters calculated from the data are presented in Tables 3-2 and 3-3.

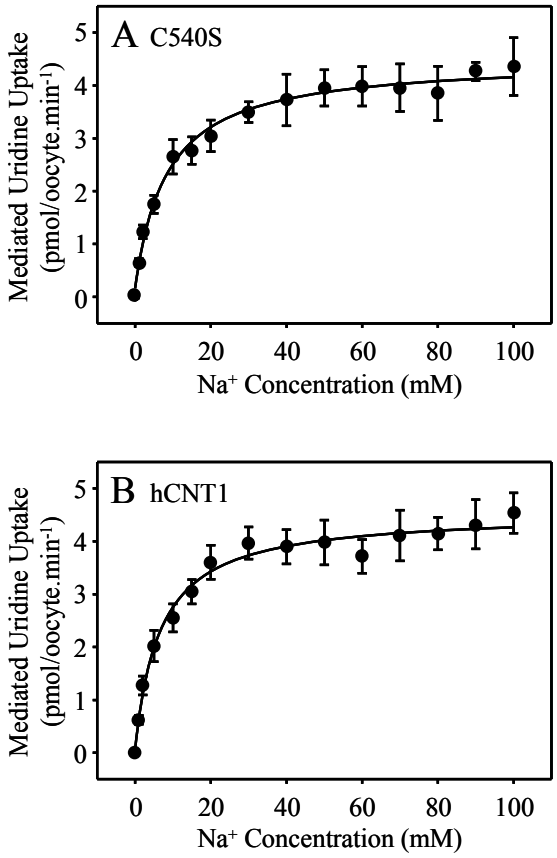

Figure 3-12. Na^+-activation kinetics of oocytes producing hCNT1 and hCNT1 mutant C540S. Na^+-activation curves were determined for oocytes expressing hCNT1 mutant C540S (*A*) and wild-type hCNT1 (*B*) as described in Fig. 3-6*B*. The radiolabeled uridine concentration was 10 μM (1 min flux). Corrected for basal (nonmediated) uptake in control water-injected oocytes, each value is the mean ± SEM of 10 - 12 oocytes. Error bars are not shown where values were smaller than that represented by the symbols.

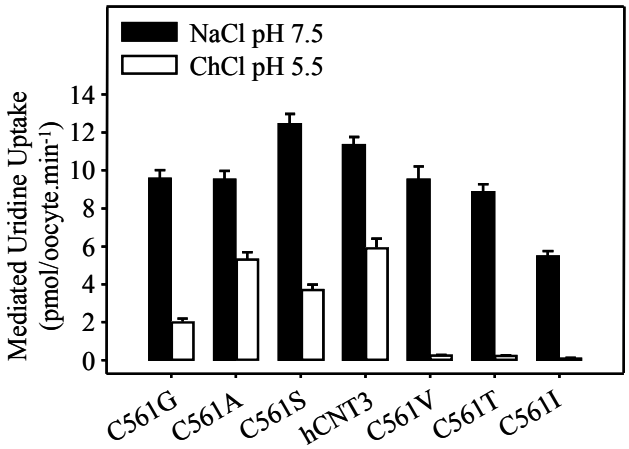

Figure 3-13. Cation selectivity of hCNT3 mutants. Influx of 10 μM radiolabeled uridine by hCNT3 mutants C561G, C561A, C561S, hCNT3, C561V, C561T and C561I was measured under initial rate conditions (1 min flux) in both Na^+-containing (100 mM NaCl, pH 7.5) and H^+-containing (100 mM ChCl, pH 5.5) transport medium (*black* and *white* bars, respectively). Values were corrected for basal nonmediated uptake in control water-injected oocytes and are means ± SEM of 10 - 12 oocytes. Error bars are not shown where values were smaller than that represented by the symbols.

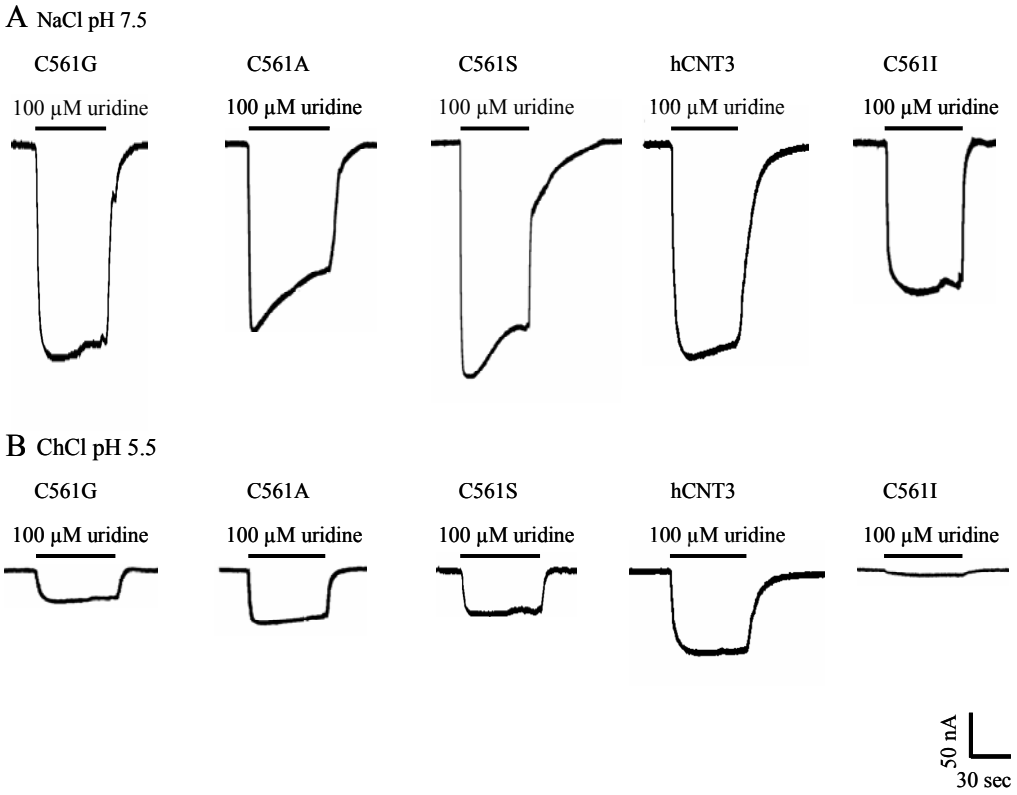

Figure 3-14. Steady-state currents of hCNT3 mutants. Steady-state currents were recorded for wild-type hCNT3 and mutants C561G, C561A, C561S and C561I in oocytes that were voltage-clamped at -90 mV and exposed to 100 µM uridine in transport medium containing 100 mM NaCl, pH 7.5 (*A*) or 100 mM ChCl, pH 5.5 (*B*). No uridine-induced currents were evident in control water-injected oocytes (data not shown).

Bibliography

1. Huang, Q. Q., Yao, S. Y. M., Ritzel, M. W. L., Paterson, A. R. P., Cass, C. E., and Young, J. D. (1994) Cloning and functional expression of a complementary DNA encoding a mammalian nucleoside transport protein. *J. Biol. Chem.* **269**: 17757-17760.

2. Che, M., Ortiz, D. F., and Arias, I. M. (1995) Primary structure and functional expression of a cDNA encoding the bile canalicular, purine-specific Na^+-nucleoside cotransporter. *J. Biol. Chem.* **270**: 13596-13599.

3. Ritzel, M. W. L., Yao, S. Y. M., Huang, M. Y., Elliot, J. F., Cass, C. E., and Young, J. D. (1997) Molecular cloning and functional expression of cDNAs encoding a human Na^+-nucleoside cotransporter (hCNT1). *Am. J. Physiol.* **272**: C707-C714.

4. Wang, J., Su, S. F., Dresser, M. J., Schaner, M. E., Washington, C. B., and Giacomini, K. M. (1997) Na^+-dependent purine nucleoside transporter from human kidney: cloning and functional characterization. *Am. J. Physiol.* **273**: F1058-F1065.

5. Ritzel, M. W. L., Yao, S. Y. M., Ng, A. M. L., Mackey, J. R., Cass, C. E., and Young, J. D. (1998) Molecular cloning, functional expression and chromosomal localization of a cDNA encoding a human Na^+/nucleoside cotransporter (hCNT2) selective for purine nucleosides and uridine. *Mol. Membr. Biol.* **15**: 203-211.

6. Smith, K. M, Ng, A. M., Yao, S. Y. M., Labedz, K. A., Knauss, E. E., Wiebe, L. I., Cass, C. E., Baldwin, S. A., Chen, X.-Z., Karpinski, E., and Young, J. D. (2004) Electrophysiological characterization of a recombinant human Na^+-coupled nucleoside transporter (hCNT1) produced in *Xenopus* oocytes. *J. Physiol.* **558**: 807-823.

7. Smith, K. M., Slugoski, M. D., Loewen, S. K., Ng, A. M., Yao, S. Y., Chen, X.-Z., Karpinski, E., Cass, C. E., Baldwin, S. A., and Young, J. D. (2005) The broadly selective human Na^+/nucleoside cotranpsorter (hCNT3) exhibits novel cation-coupled nucleoside transport characteristics. *J. Biol. Chem.* **280**: 25436-25449.

8. Smith, K. M., Slugoski, M. D., Cass, C. E., Baldwin, S. A, Karpinski, E., and Young, J. D. (2007) Cation coupling properties of human concentrative nucleoside transporters hCNT1, hCNT2 and hCNT3. *Mol Membr Biol*. **24**: 53-64.

9. Zhu, Q., and Casey, J. R. (2007) Topology of transmembrane proteins by scanning cysteine accessibility mutagenesis methodology. *Methods* **41**: 439-450.

10. Ermolova, N., Madhvani, R. V., and Kaback, H. R. (2006) Site-directed alkylation of cysteine replacements in the lactose permease of Escherichia coli: helices I, III, VI and XI. *Biochem*. **45**: 4182-4189.

11. Mueckler, M., and Makepeace, C. (2009) Model of the exofacial substrate-binding site and helical folding of the human Glut1 glucose transporter based on scanning mutagenesis. *Biochem. J*. **48**: 5934-5942.

12. Tang, X. B., Fujinaga, J., Kopito, R., and Casey, J. R. (1998) Topology of the region surrounding Glu681 of human AE1 protein, the erythrocyte anion exchanger. *J. Biol. Chem*. 273: 22545-22553.

13. Zhu, Q., Lee, D. W. K., and Casey, J. R. (2003) Novel topology in C-terminal region of the human plasma membrane anion exchanger, AE1. *J. Biol. Chem*. 278: 3112-3120.

14. Lee, B. L., Li, X., Liu, Y., Sykes, B. D., and Fliegel, L. (2009) Structural and functional analysis of transmembrane XI of the NHE1 isoform of the Na^+/H^+ exchanger. *J. Biol. Chem*. **284**: 11546-11556.

15. Seal, R. P., ShigeriY., Eliasof, S., Leighton, B. H., and Amara, S. G. (2001) Sulfhydryl modification of V449C in the glutamate transporter EAAT1 abolishes substrate transport but not the substrate-gated anion conductance. *Proc. Natl Acad. Sci. USA*. **98**: 15324-15329.

16. Slotboom, D. J., Konings, W. N., and Lolkema, J. S. (2001) Cysteine-scanning mutagenesis reveals a highly amphipathic pore-lining membrane spanning helix in the glutamate transporter GltT. *J. Biol. Chem*. **276**: 10775-10781.

17. Rimon, A., Hunte, C., Michel, H., and Padan, E. (2008) Epitope mapping of conformational monoclonal antibodies specific to NhaA Na^+/H^+ antiporter: structural and functional implications. *J. Mol. Biol*. **379**: 471-481.

18. Hirayama, B. A., Loo, D. D., Diez-Sampedro, A., Leung, D. W., Meinild, A. K., Lai-Bing, M., Turk, E., and Wright, E. M. (2007) Sodium-dependent reorganization of the sugar-binding site of SGLT1. *Biochem*. **46**: 13391-13406.

19. Zhang, J., Tackaberry, T., Ritzel, M. W., Raborn, T., Barron, G., Baldwin, S. A., Young, J. D., and Cass, C. E. (2006) Cysteine-accessibility analysis of transmembrane domains 11-13 of human concentrative nucleoside transporter 3. *Biochem. J.* **394**: 389-398.

20. Slugoski, M. D., Ng, A. M., Yao, S. Y., Smith, K. M., Lin, C. C., Zhang, J., Karpinski, E., Cass, C. E., and Baldwin, S. A., and Young, J. D. (2008) A proton-mediated conformational shift identifies a mobile pore-lining cysteine residue (Cys-561) in human concentrative nucleoside transporter 3. *J. Biol. Chem.* **283**: 8496-8507.

21. Kirsch, R. D., and Joly, E. (1998) An improved PCR-mutagenesis strategy for two-site mutagensis of sequence swapping between related genes. *Nucleic Acid Res*. **26**: 1848-1850.

22. Yao, S. Y. M., Cass, C. E., and Young, J. D. (2000) The *Xenopus* oocyte expression system for the cDNA cloning and characterization of plasma membrane transport proteins. *In Membrane Transport. A Practical Approach.* (Baldwin, S. A., ed.) Oxford: Oxford University Press; 47-78.

23. Ritzel, M. W. L., Ng, A. M. L., Yao, S. Y. M., Graham, K., Loewen, S. K., Smith, K. M., Ritzel, R. G., Mowles, D. A., Carpenter, P., Chen, X.-Z., Karpinski, E., Hyde, R. J., Baldwin, S. A., Cass, C. E., and Young, J. D. (2001) Molecular identification and characterization of novel human and mouse concentrative Na^+-nucleoside cotransporter proteins (hCNT3 and mCNT3) broadly selective for purine and pyrimidine nucleosides (system *cib*). *J. Biol. Chem.* **276**: 2914-2927.

24. Damaraju, V. L., Elwi, A. N., Hunter, C., Carpenter, P., Santos, C., Barron, G. M., Sun, X., Baldwin, S. A., Young, J. D., Mackey, J. R., Sawyer, M. B., and Cass, C. E. (2007) Localization of broadly selective equilibrative and

concentrative nucleoside transporters, hENT1 and hCNT3, in human kidney. *Am. J. Physiol. Renal Physiol.* **293**: F200-F211.

25. Yao, S. Y., Ng, A. M., Loewen, S. K., Cass, C. E., Baldwin, S. A., and Young, J. D. (2002) An ancient prevertabrate Na^+-nucleoside cotransporter (hfCNT) from the Pacific hagfish (*Eptatretus stouti*). *Am. J. Phys. Cell Phys.* **283**: C155-C168.

26. Slugoski, M. D., Loewen, S. K., Ng, A. M., Smith, K. M., Yao, S. Y., Karpinski, E., Cass, C. E., Baldwin, S. A., and Young, J. D. (2007) Specific mutations in transmembrane helix 8 of human concentrative Na^+/nucleoside cotransporter hCNT1 affect permeant selectivity and cation coupling. *Biochem*. **46**: 1684-1693.

27. Elwi, A. N., Damaraju, V. L., Baldwin, S. A., Young, J. D., Sawyer, M. B., and Cass, C. E. (2006) Renal nucleoside transporters: physiological and clinical implications. *Biochem. Cell. Biol.* **84**: 844-858.

28. Pastor-Anglada, M., Errasti-Murugarren, E., Aymerich, I., and Casado, F. J. (2007) Concentrative nucleoside transporters (CNTs) in epithelia: from absorption to cell signaling. *J. Physiol. Biochem.* **63**: 97-110.

29. Errasti-Murugarren, E., Cano-Soldado, P., Pastor-Anglada, M., and Casado, F. J. (2008) Functional characterization of a nucleoside-derived drug transporter variant (hCNT3C602R) showing altered sodium-binding capacity. *Mol. Pharmacol.* **73**: 379-386.

Chapter 4:

Substituted Cysteine Accessibility Method Analysis of Transmembrane Domains 7 & 8 of Human Na^+/Nucleoside Cotransporter 3 (hCNT3)

Acknowledgements and Contributions

Technologist Mrs. Amy M. L. Ng constructed the single cysteine mutants. All of the functional studies were conducted by myself. This research was funded by the National Cancer Institute of Canada with funds from the Canadian Cancer Society (now the Canadian Cancer Society Research Institute), Alberta Cancer Board (now the Alberta Health Services- Cancer Care), The Alberta Cancer Foundation, and by the Alberta Cancer Prevention Legacy Fund.

Introduction

The human SLC28 concentrative nucleoside transporter (CNT) family has three members. hCNT1 and hCNT2 are pyrimidine and purine nucleoside selective, respectively, and couple Na^+:nucleoside cotransport with a 1:1 stoichiometry (1-7). hCNT3, in contrast, is broadly selective for both pyrimidine and purine nucleosides, and exhibits a 2:1 Na^+:nucleoside coupling ratio (6-8). hCNT3 is also capable of H^+/nucleoside cotransport with a coupling stoichiometry of 1:1, whereby one of the transporter's two Na^+ binding sites also functionally interacts with H^+ (6,7).

Current models of CNT topology have 13 putative transmembrane helices (TMs) (3, 5, 8, 9). Two additional TMs (designated 5A and 11A) are weakly predicted by computer algorithms (10), and immunocytochemical experiments with site-specific antibodies and studies of native and introduced glycosylation sites have confirmed an intracellular N-terminus and an extracellular C-terminus (10). Chimeric studies involving human, rat and hagfish members of the CNT protein family have revealed that that the functional domains responsible for nucleoside selectivity and cation coupling reside within the C-terminal TM 7-13 half of the proteins (11-15). In contrast to mammalian and other eukaryotic CNTs, NupC, a H^+-coupled CNT family member from *Escherichia coli*, lacks TMs 1- 3, but otherwise shares a similar predicted membrane topology (12, 13).

A functional cysteine-less version of hCNT3 has been generated by mutagenesis of endogenous cysteine residues to serine, resulting in the cysteine-less construct hCNT3C- employed initially in a yeast expression system for substituted cysteine accessibility method (SCAM) analysis of TMs 11, 12 and 13 using methanethiosulfonate (MTS) reagents (18). Subsequently, hCNT3C- was characterized in *Xenopus* oocytes [Chapter 3 (19)], and SCAM analysis projects initiated in this thesis using the alternative thiol-specific reagent *p*-chloromercuribenzene sulfonate (PCMBS) to systematically investigate the entire C-terminal half of the protein.

Measured by transport inhibition, reactivity of introduced cysteine residues to PCMBS, which is both membrane-impermeant and hydrophilic, indicates pore-lining status and access from the extracellular medium; the ability of permeant to protect against this inhibition indicates location within, or closely adjacent to, the nucleoside binding pocket (20, 21). The present Chapter reports results for hCNT3C- TMs 7 and 8. The results identify residues of functional importance, indicate close proximity cation/nucleoside binding and translocation, provide evidence of novel discontinuous regions within helices, and support a revised model of hCNT membrane topology.

Results

All 14 endogenous cysteine residues of hCNT3 were replaced with serine to produce the cysteine-less hCNT3 construct hCNT3C- [18, Chapter 3 (19)]. hCNT3C- retained wild-type hCNT3 functional activity [Chapter 3 (19)] and was used as a template for the construction of single cysteine mutants for SCAM analysis of functional activity and inhibition by PCMBS. The 64 residues spanning a region between and including TMs 7 and 8 that were investigated in the present Chapter are highlighted in Fig. 4-1.

Functional activity of single cysteine mutants – hCNT3 transports nucleosides using both Na^+ and H^+ electrochemical gradients (7, 8). Therefore, to examine the functional activity of single hCNT3C- cysteine mutants, uptake of 10 μM radiolabeled uridine was determined in both Na^+-containing, H^+-reduced medium (100 mM NaCl, pH 8.5) and in Na^+-free, acidified medium (100 mM ChCl, pH 5.5). The Na^+-containing medium was buffered at a pH of 8.5 to avoid the small but significant H^+ activation of hCNT3 that occurs at pH 7.5 (7, 8). Previously, we have verified that Na^+-coupled uridine transport by hCNT3 at pH 8.5 is kinetically indistinguishable from that at pH 7.5 (22). Initial rates of transport (± S.E.M.) for each mutant, in units of pmol/oocyte.min^{-1}, are given in Table 4-1. The uptake of 10 μM radiolabeled uridine (100 mM NaCl, pH 8.5) by oocytes expressing hCNT3C- varied between experiments in the range 2 to 4

pmol/oocyte.min^{-1} (data not shown). The flux values reported in Table 4-1, and in subsequent Tables and Figures, depict mediated transport activity, defined as the difference in uptake between RNA transcript-injected and control water-injected oocytes, and are from representative experiments. In all studies reported here, uridine uptake in water-injected oocytes was < 0.02 pmol/oocyte.min^{-1} (data not shown).

Mutants exhibiting uridine uptake values < 0.1 pmol/oocyte.min^{-1} were excluded from further analysis (Table 4-1). Only 2 out of the 64 residues investigated fell into this category (3.1%) and, in both cases, the mutation to cysteine resulted in a protein with low functional activity both in Na^+-containing, H^+-reduced and Na^+-free, acidified media (100 mM NaCl, pH 8.5 and 100 mM ChCl, pH 5.5, respectively). The two residues were: Glu343 in TM 7 and Tyr379 TM 8. Cell-surface labeling with sulfo-NHS-LC-biotin and immobilized streptavidin resin were used to distinguish cell-surface proteins from those associated with total (plasma + intracellular) membranes. Both mutants had electrophoretic mobilities similar to hCNT3C-, but were present at cell surfaces in reduced amounts, so that no conclusions could be reached regarding their catalytic activities (data not shown). Although the transport activity of E343C(C-) was < 0.1 pmol/oocyte.min^{-1} and therefore not analyzed in the present study, the transport activity of three Glu343 mutants in the alternative hCNT3 wild-type background (E343D, E343Q and E343C) have previously been characterized (23). Functionally compromised, these mutants displayed altered nucleoside and cation-activation kinetics (all mutants), loss or impairment of H^+-dependence (all mutants) and, similar to the corresponding mutant in Na^+-specific hCNT1, uncoupled Na^+-currents (E343Q) (23).

To facilitate comparisons between the remaining 61 mutants, the uridine transport activity of each construct is presented as the ratio of Na^+-mediated to H^+-mediated uptake (Na^+:H^+) in Table 4-1. The corresponding Na^+:H^+ ratios of uridine uptake (10 μM) for wild-type hCNT3 and for cysteine-less hCNT3C- were ~ 1.7 and 1.0, respectively (averaged results from multiple experiments; data not shown), and were in good agreement with results of previous studies (7, 8, 15, 17).

Residue mutations that resulted in Na^+:H^+ ratios of uridine uptake < 0.5 and > 2.5 (Table 4-1) are highlighted in the hCNT3 topology schematic shown in Fig. 4-2.

Most of the mutants exhibited Na^+:H^+ uptake ratios similar to that of hCNT3/hCNT3C-. In contrast, mutants S334C(C-) and I337C(C-) in TM 7 presented Na^+:H^+ ratios of 0.3 and 0.4 respectively, and eight other TM 7 mutants exhibited Na^+:H^+ ratios > 2.5 (S330C(C-), G335C(C-), N336C(C-), V339C(C-), G340C(C-), Q341C(C-), S344C(C-) and P345C(C-), with ratios equal to 2.7, 3.5, 6.5, 2.9, 10.2, 4.6, 9.4 and 9.2, respectively). One residue in the loop between TMs 7 and 8 and a cluster of residues in TM 8 also exhibited altered cation-coupling characteristics. Mutation of the loop residue Leu352 to cysteine resulted in a Na^+:H^+ uptake ratio of 4.5 and, within TM 8, mutation of residues Ser369, Thr370, and Val375 resulted in Na^+:H^+ ratios of 2.9, 0.2 and 8.0, respectively.

PCMBS inhibition of single cysteine mutants – Wild-type hCNT3 has previously been reported to be sensitive to inhibition by PCMBS under acidic conditions only (*i.e.,* in Na^+-free, acidified medium), there being no corresponding inhibition of transporter exposed to PCMBS in either Na^+-containing, H^+-reduced or in Na^+-free, H^+-reduced media (22). Therefore, single cysteine mutants of hCNT3C- were tested for inhibition by PCMBS both in Na^+-containing, H^+-reduced medium (100 mM NaCl, pH 8.5) and in Na^+-free, acidified medium (100 mM ChCl, pH 5.5). After 10 min exposures to 200 μM PCMBS, uptake of 10 μM radiolabeled uridine was assayed in medium of the same composition. Exposure to PCMBS was performed on ice to minimize its diffusion across oocyte plasma membranes [(22), Chapter 8 (24) and Appendix 1 (25)]. In ascending numerical order of residue position, results for each mutant calculated as a percentage of mediated uridine uptake in the absence of PCMBS are presented in Fig. 4-3. For screening purposes, a residue was considered to be PCMBS-inhibitable upon exhibiting > 20% inhibition of uridine uptake following incubation with PCMBS. Residues that were considered to be PCMBS-sensitive are highlighted in Fig. 4-3. Corresponding numerical flux values are presented in Table 4-2. A schematic of the locations of these PCMBS-inhibitable residues is presented in Fig. 4-4. Fig. 4-3 and Table 4-2 also include control data for wild-type hCNT3 (only inhibited by

PCMBS in Na^+-free, acidified medium) and hCNT3C- (unaffected by PCMBS either in Na^+-containing, H^+-reduced medium or in Na^+-free, acidified medium).

In TM 7, three adjacent residues, Gly340, Gln341 and Thr342, were PCMBS-inhibitable in both Na^+-containing, H^+-reduced and Na^+-free, acidified medium upon conversion to cysteine. Close to Gly340, mutant I337C(C-) was PCMBS-inhibitable only in Na^+-free, acidified medium. In TM 8, nine adjacent mutants (I371C(C-), A372C(C-), G373C(C-), S374C(C-), V375C(C-), L376C(C-), G377C(C-), A378C(C-) and I380C(C-)) were PCMBS-inhibitable in both cation conditions. Next to residue Ile371, Thr370 was PCMBS-inhibitable upon conversion to cysteine only in Na^+-free, acidified medium. Interestingly, a residue which localizes to the predicted intracellular loop following TM 8 (Val384), was sensitive to PCMBS inhibition upon conversion to cysteine in both Na^+-containing, H^+-reduced and Na^+-free, acidified media.

Uridine protection from PCMBS inhibition – Subsequent experiments investigated the ability of extracellular uridine (20 mM) to protect against inhibition by PCMBS for residues that were PCMBS-inhibitable in either or both cation conditions. Results for each individual mutant are presented in Table 4-2, and the uridine-protectable residues are highlighted in the hCNT3 topology schematic of Fig. 4-4.

In TM 7, three residue positions exhibited uridine protection from PCMBS inhibition. Q341C(C-) and T342C(C-), which were PCMBS-inhibitable in both Na^+-containing, H^+-reduced and Na^+-free, acidified media, were fully protected by uridine under both cation conditions. In contrast, G340C(C-), which was also PCMBS-inhibitable under both cation conditions, was protected against PCMBS inhibition in Na^+-containing, H^+-reduced medium only. In TM 8, five residue positions were uridine-protected. T370C(C-), which was PCMBS-sensitive only in Na^+-free, acidified medium, exhibited full uridine protection against that inhibition, while A372C(C-), G373C(C-) and S374C(C-), which were PCMBS-sensitive in both Na^+-containing, H^+-reduced and Na^+-free, acidified media were also fully protected under both cation conditions. In contrast, I371C(C-), which

was also inhibited by PCMBS under both cation conditions, was protected by uridine only in Na^+-containing, H^+-reduced medium.

Permeant selectivity – Subsequent experiments investigated residues within the TM 7 to 8 region of hCNT3 for potential roles in nucleoside selectivity. To do this, I subjected the uridine-protected subset of PCMBS-sensitive hCNT3C- mutants to transport experiments involving a panel of radiolabelled purine and pyrimidine nucleosides (each at 10 μM concentration). Of the 8 hCNT3C- cysteine mutants tested, 5 showed significantly different nucleoside uptake profiles compared to hCNT3 and hCNT3C- and are shown in Fig. 4-5.

As previously reported, wild-type hCNT3 and hCNT3C- exhibited the characteristic broad *cib*-type transport preference for both purine and pyrimidine nucleosides in Na^+-containing, H^+-reduced medium (7) (Figs. 4-5*A* & 4-5*B*). Both also exhibited the characteristic narrowing of nucleoside preference under Na^+-free, acidified conditions (uridine > thymidine, adenosine > cytidine, inosine > guanosine (7) (Figs. 4-5*A* & 4-5*B*).

All five mutants with altered permeant selectivities were located within TMs 7 and 8: G340C(C-), Q341C(C-), T342C(C-), S374C(C-) and V375C(C-). G340C(C-) and V375C(C-) were found to have the greatest differences compared to hCNT3 and hCNT3C-. Relative to uridine, G340C(C-) exhibited markedly reduced uptake of thymidine, adenosine, inosine and guanosine, in Na^+-containing, H^+-reduced medium, while in Na^+-free, acidified medium, uptake was greatly reduced, though measurable, for all nucleosides tested (Fig. 4-5*C*). Similar to hCNT3 and hCNT3C-, V375C(C-) exhibited broadly-selective uptake of both purine and pyrimidine nucleosides in Na^+-containing, H^+-reduced medium, but only very low uptake of uridine, thymidine, adenosine and inosine, and no detectable transport of cytidine and guanosine in Na^+-free, acidified medium (Fig. 4-5*G*). Immediately adjacent to residue Gly340 in TM 7, mutants Q341C(C-) and T342C(C-) showed reduced uptake of cytidine and thymidine (Q341C(C-)) or thymidine and inosine (T342C(C-)) in Na^+-containing, H^+-reduced medium, and reduced uptake of uridine, cytidine, thymidine and adenosine (Q341C(C-)) or cytidine and thymidine (T342C(C-)) in Na^+-free, acidified medium (Figs. 4-5*D* & 4-5*E*). Adjacent to

Val375 in TM 8, mutant S374C(C-) showed a normal uptake profile in Na^+-containing, H^+-reduced medium, but reduced uptake of uridine, cytidine, thymidine and adenosine in Na^+-free, acidified medium (Fig. 4-5*F*). It is noteworthy that residues Gly340, Gln341, Ser374 and Val375 in hCNT3 correspond to the two adjacent pairs of TM 7 and 8 residues in hCNT1 that have previously been shown to determine the differences in permeant selectivity between that transporter and hCNT2 (20, 21).

H^+- mediated PCMBS inhibition of hCNT3C- – Of the 15 hCNT3C-residue positions in the TM 7 – 8 region that were PCMBS-sensitive, 13 were inhibited by PCMBS in both Na^+-containing, H^+-reduced and Na^+-free, acidified media, while 2 were inhibited by PCMBS in Na^+-free, acidified medium only (Table 4-2 and Fig. 4-4). To determine if access of PCMBS to these residues required cation-induced conformational changes within the protein, each of the single cysteine mutants at these positions were re-screened for PCMBS inhibition under the original conditions (Na^+-containing, H^+-reduced and Na^+-free, acidified media) and in both Na^+-free, H^+-reduced medium (100 mM ChCl pH 8.5) and Na^+-containing, acidified medium (100 mM NaCl pH 5.5). Fluxes of 10 μM uridine were then determined under Na^+-free, acidified conditions (Table 4-3).

All of the 13 mutants that were inhibited by PCMBS in both Na^+-containing, H^+-reduced and Na^+-free, acidified media were also inhibited by PCMBS in Na^+-free, H^+-reduced and Na^+-containing, acidified media (Table 4-3), indicating that PCMBS inhibition was not cation-induced. However, the two mutants that exhibited PCMBS inhibition under Na^+-free, acidified conditions only (I337C(C-) in TM 7 and T370C(C-) in TM 8) were unaffected by PCMBS under cation-reduced conditions (Na^+-free, H^+-reduced medium), but strongly inhibited by PCMBS in Na^+-containing, acidified medium. Similar to residues Ile554, Tyr558 and Cys561 in TM 12 of hCNT3 [Chapter 8 (24)], therefore, access of PCMBS to these residue positions reports a specific H^+-induced conformation of the transporter.

Discussion

In previous structure/function studies of hCNTs, two adjacent pairs of residues were identified in TMs 7 and 8 of hCNT1 (Ser319/Gln320 and Ser353/Leu354, respectively) that, when mutated to the corresponding residues in hCNT2 (Gly/Met and Thr/Val, respectively), changed the permeant selectivity of the transporter from pyrimidine nucleoside-selective to purine nucleoside-selective (14). Mutation of hCNT1 TM7 residue Ser319 to Gly enabled transport of purine nucleosides, and co-conversion of Gln320 to Met (which had no effect on its own) augmented this transport. Concurrent mutation of TM8 Ser353 to Thr converted S319G/Q320M to purine nucleoside-selective, but with relatively low adenosine transport activity, while additional mutation of Leu354 to Val (which had no effect on its own) increased the adenosine transport capability of S319G/Q320M/S353T to produce a full hCNT2-like phenotype. Subsequently, it was demonstrated that mutation of the TM8 residues alone generated a unique uridine-preferring phenotype (S353T/L354V) and an increase in apparent binding affinity for Na^+ (L354V) (15). hCNT1 TM 7 residues Glu308 and Glu322 have also been shown to have key roles in Na^+/nucleoside translocation, mutation of the latter residue resulting in uncoupled Na^+ currents, a property also revealed by mutation of the corresponding residue in hCNT3 [(23) and Appendix 1 (25)]. The present Chapter presents a systematic SCAM analysis of the TM 7-8 region of hCNT3C-.

Functional activity of hCNT3C- mutants – Initial characterization of the hCNT3C- single cysteine mutants in the present study measured uridine uptake in both Na^+-containing, H^+-reduced and Na^+-free, acidified media (Table 4-1). Of the 64 mutants examined in the TM 7-8 region of hCNT3C- (Fig. 4-1), two exhibited uridine uptake values < 0.1 pmol/oocyte.min^{-1} under both cation conditions (Table 4-1). One was in TM 7 (E343C(C-)), and the other in TM 8 (Y379C(C-)). Both exhibited reduced quantities in plasma membranes and were excluded from further functional analysis. We have previously characterized the transport activity of TM 7 E343C in the alternate hCNT3 wild-type background (23). Consistent with close-proximity integration of cation/solute binding sites within a

common cation/permeant translocation pore, E343C exhibited altered permeant selectivity, was kinetically compromised with respect to both uridine transport and Na^+/H^+-activation, and was inhibited by PCMBS (23).

hCNT3 couples nucleoside transport to both Na^+ and H^+ electrochemical gradients and exhibits a $Na^+:H^+$ ratio of uridine uptake (10 μM) of ~ 1.7 (7, 8). Similarly, hCNT3C- also mediates both Na^+- and H^+-coupled uridine transport, although the apparent K_{50} for Na^+ is increased ~ 11-fold, decreasing the $Na^+:H^+$ ratio of uridine uptake (10 μM) to ~ 1.0 [Chapter 3 (19)]. Table 4-1 and Fig. 4-2 highlight those residues for which mutation to cysteine in hCNT3C- resulted in $Na^+:H^+$ uridine uptake ratios either < 0.5 (*i.e.*, H^+-preferring) or > 2.5 (*i.e.*, Na^+-preferring). Such characteristics identified residues likely to be involved directly or indirectly in interactions with the coupling cation. Further analysis of the roles of these newly identified amino acids in cation coupling is in progress (Chapter 9).

PCMBS inhibition of hCNT3C- mutants: transmembrane architecture and orientation of TMs 7 & 8 – To summarize the data presented in Table 4-2 and Fig. 4-3, the schematic in Fig. 4-4 highlights those TM 7 – 8 residues identified in hCNT3C- as PCMBS-sensitive and uridine-protected.

In TM 7, PCMBS inhibition was evident for residue Ile337 in Na^+-free, acidified medium only, and for Gly340, Gln341 and Thr342 in both cation conditions. Of these, Gly340 showed uridine protection in Na^+-containing, H^+-reduced medium only, while Gln341 and Thr342 showed uridine protection in both media. This clustering of adjacent PCMBS-inhibitable residues is inconsistent with the patterning anticipated for a conventional α-helix. When plotted on an α-helical projection of TM 7, the residues sensitive to PCMBS inhibition were positioned irregularly around the wheel rather than (as anticipated) down one face of the helix (data not shown). This was apparent even more clearly in TM 8, where a total of nine adjacent residues were sensitive to PCMBS inhibition when mutated to cysteine (Thr370 in Na^+-free, acidified medium only, and Ile371, Ala372, Gly373, Ser374, Val375, Leu376, Gly377 and Ala378 in both cation conditions). Of these, Thr370 showed uridine protection in Na^+-reduced, acidified medium, Ile371 showed uridine protection in Na^+-containing, H^+-

reduced medium only (even though it was inhibited by PCMBS in both cation conditions), while Ala372, Gly373 and Ser374 showed uridine protection in both media. Another residue (Ile380) was also sensitive to PCMBS inhibition in both cation conditions, but was separated from the block of nine consecutive PCMBS-sensitive residues by a low-functioning mutant (Y379C(C-)) whose PCMBS-sensitivity could not be analyzed. Within this region of PCMBS inhibition, Ile380 sits deepest in the membrane at the endofacial boundary of the TM, according to the original 13 TM topology of hCNT3 shown in Fig. 4-1. Altogether, the block of PCMBS-sensitive residues comprises the entire inner half of TM 8. It is proposed that this pattern of inhibition supports a reversed membrane orientation of this region of the protein. As such, the PCMBS-sensitive residues would lie exofacially within the outer half of the membrane, in a position more likely to be accessible to the extracellular medium and available for PCMBS binding. In agreement with this, structure-function studies of negatively charged residues in hCNT1 and hCNT3 also provide evidence for an opposite orientation for TM 7 [(23) and Appendix 1 (25)]. Other evidence supporting the reversed orientation of TM 8 (and 7) is that a residue in the putative internal loop exiting TM 8, Val384, was sensitive to inhibition by PCMBS in both cation conditions: since PCMBS is membrane impermeable, it is predicted that this residue must be extracellular in order to allow access to and binding of PCMBS. It is further concluded, based upon the observed block patterning of PCMBS inhibition seen in Fig.4-4, that TMs 7 and 8 of hCNT3 both contain regions incompatible with conventional α-helical structures.

Mechanistic implications for hCNT3 – Illustrated in Fig. 4-6, the patterns of PCMBS inhibition reported here for TMs 7 and 8 provide important functional evidence of extended structures resembling the discontinuous membrane helices evident in the crystal structures of the recently solved Na^+-coupled bacterial leucine, galactose and hydantoin membrane transporter proteins *Aquifex aeolicus* $LeuT_{Aa}$ (26), *Vibrio parahaemolyticus* SGLT (27), *Escherichia coli* NhaA (28), and *Microbacterium liquefaciens* NCS1 (29). In $LeuT_{Aa}$, non-traditional transmembrane α-helices are disrupted by the insertion of extended regions of

polypeptide that comprise the Na^+ binding sites of the protein and, upon Na^+ binding, favour high-affinity binding of the permeant amino acid leucine (26). A similar feature is also apparent in TM 7 of the glutamate transporter homologue GltPh from *Pyrococcus horikoshii* (30). Reviewed by Screpanti and Hunte (31) and Krishnamurthy *et. al.* (32), such discontinuous membrane helices are proposed to play important mechanistic roles in ion and permeant recognition, binding and translocation in secondary active transporters.

In the case of TMs 7 and 8 of hCNT3, mutation of residues Gly340 (TM 7), Gln341 (TM 7), Ser374 (TM 8) and Val375 (TM 8) to cysteine, resulted in sensitivity to PCMBS inhibition, and protection against that inhibition by uridine. Their mutation to a cysteine also altered the permeant selectivity of the transporter, and Gly340, Gln341 and Val375 exhibited Na^+:H^+ uptake ratios of > 2.5 (*i.e.* Na^+-preferring). The corresponding residues in wild-type hCNT1 have also been shown to be involved in permeant selectiviy and cation binding (14, 15). In good agreement with other Na^+-coupled transporters for which high resolution molecular structures have been solved, including $LeuT_{Aa}$ (26) and GltPh (33), the present results therefore provide further support that TMs 7 and 8 of hCNTs form part of a common nucleoside/cation translocation pore, and that residues contributed by these TMs have locations within or closely adjacent to neighbouring and functionally integrated nucleoside and cation binding pockets.

The present SCAM analysis of hCNT3C- TMs 7 and 8 also contributed insight into cation-dependent conformations adopted by the exofacially-facing form of the protein. In contrast to Na^+-specific hCNT1 and hCNT2, hCNT3 mediates both Na^+- and H^+-coupled nucleoside cotransport (3, 5-9). The cation:nucleoside stoichiometry for hCNT3 H^+-coupled transport is 1:1 compared to 2:1 for Na^+ and, when both cations are present, charge/uptake experiments suggest that hCNT3 binds one Na^+ and one H^+ (7, 8). The nucleoside and nucleoside drug selectivity pattern of hCNT3 in the presence of H^+ also differs from that in the presence of Na^+ (7, 9). Previously, mutation of hCNT3 Cys561 in TM 12 was reported to alter Na^+ and H^+ kinetics and, together with Tyr558 and Ile554, form a face of the helix which becomes extracellularly accessible to

PCMBS only in the presence of H^+, thus reporting a H^+-dependent conformation of the protein (22). Building upon these observations, the present results identify two additional residues in TMs 7 and 8 whose accessibility to PCMBS similarly reports a H^+-dependent conformation of the protein (Table 4-3 and Fig. 4-6), some of which, like the H^+-specific TM 12 Ile554/Tyr558/Cys561 cluster, may involve subdomains within TMs. Other potential conformational differences are even more subtle. The arrows in Figs. 4-4 and 4-6, for example, identify residues in TMs 7 and 8 that were PCMBS-sensitive in both in both Na^+-containing, H^+-reduced and Na^+-free, acidified media, but were uridine-protected only in Na^+-containing, H^+-reduced medium.

Conclusions – The SCAM analysis of TMs 7 and 8 of hCNT3C- presented in this Chapter suggest the presence of novel discontinuous regions within both TMs, indicate their reversed orientation in the membrane, and highlight their functional importance in key cation and nucleoside binding and/or translocation events.

Table 4-1. Na^+- and H^+-mediated uptake of uridine in *Xenopus* oocytes expressing hCNT3C- single cysteine mutants. Influx of 10 μM ^{14}C-uridine or ^{3}H-uridine was measured in both Na^+-containing, H^+-reduced and Na^+-free, acidified media (100 mM NaCl, pH 8.5 or 100 mM ChCl, pH 5.5, respectively). Na^+:H^+ uptake ratios which are < 0.5 or > 2.5 are highlighted with an asterisk (*). Values are corrected for basal non-mediated uptake in control water-injected oocytes. Each value is the mean ± S.E.M. of 10-12 oocytes.

	Mediated Uridine Uptake (pmol/oocyte.min^{-1})		
TM 7	Na^+ (100 mM NaCl, pH 8.5)	H^+ (100 mM ChCl, pH 5.5)	Na^+:H^+ Ratio
I328C(C-)	3.4 ± 0.3	3.7 ± 0.2	0.9
E329C(C-)	1.7 ± 0.2	0.9 ± 0.2	1.9
S330C(C-)	1.6 ± 0.3	0.6 ± 0.1	2.7*
V331C(C-)	2.0 ± 0.2	1.4 ± 0.1	1.5
V332C(C-)	3.8 ± 0.5	1.8 ± 0.3	2.1
A333C(C-)	1.9 ± 0.3	1.1 ± 0.2	1.8
S334C(C-)	0.8 ± 0.1	2.9 ± 0.2	0.3*
G335C(C-)	3.5 ± 0.4	1.0 ± 0.2	3.5*
N336C(C-)	1.3 ± 0.1	0.2 ± 0.1	6.5*
I337C(C-)	0.7 ± 0.1	2.0 ± 0.1	0.4*
F338C(C-)	1.2 ± 0.1	0.6 ± 0.1	2.0
V339C(C-)	4.7 ± 0.1	1.6 ± 0.1	2.9*
G340C(C-)	2.1 ± 0.2	0.2 ± 0.1	10.2*
Q341C(C-)	3.6 ± 0.2	0.8 ± 0.1	4.6*
T342C(C-)	4.0 ± 0.6	3.4 ± 0.2	1.2
E343C(C-)	< 0.1	< 0.1	-
S344C(C-)	4.7 ± 0.2	0.5 ± 0.1	9.4*
P345C(C-)	5.0 ± 0.3	0.5 ± 0.1	9.2*
L346C(C-)	6.2 ± 0.2	3.5 ± 0.3	1.8
L347C(C-)	3.9 ± 0.3	2.2 ± 0.1	1.8
V348C(C-)	4.3 ± 0.2	2.4 ± 0.2	1.8

Table 4-1 continued

TM 7 - 8 Loop	Mediated Uridine Uptake (pmol/oocyte.min^{-1}) Na^+ (100 mM NaCl, pH 8.5)	H^+ (100 mM ChCl, pH 5.5)	Na^+:H^+ Ratio
R349C(C-)	4.9 ± 0.6	4.1 ± 0.6	1.2
P350C(C-)	5.5 ± 0.3	3.1 ± 0.1	1.8
Y351C(C-)	4.6 ± 0.2	3.7 ± 0.2	1.2
L352C(C-)	3.6 ± 0.5	0.8 ± 0.1	4.5*
P353C(C-)	4.0 ± 0.4	3.5 ± 0.1	1.1
Y354C(C-)	5.2 ± 0.4	3.4 ± 0.2	1.5
I355C(C-)	5.4 ± 0.5	2.2 ± 0.2	2.5
T356C(C-)	0.8 ± 0.1	0.6 ± 0.2	1.3
K357C(C-)	2.9 ± 0.5	2.9 ± 0.4	1.0
S358C(C-)	3.6 ± 0.4	2.1 ± 0.4	1.7
E359C(C-)	0.3 ± 0.1	0.2 ± 0.1	1.5

Table 4-1 continued

TM 8	Mediated Uridine Uptake (pmol/oocyte.min^{-1}) Na^+ (100 mM NaCl, pH 8.5)	H^+ (100 mM ChCl, pH 5.5)	Na^+:H^+ Ratio
L360C(C-)	4.5 ± 0.4	1.8 ± 0.2	2.5
H361C(C-)	3.6 ± 0.3	1.5 ± 0.4	2.3
A362C(C-)	6.4 ± 0.3	4.1 ± 0.3	1.5
I363C(C-)	5.3 ± 0.2	2.6 ± 0.1	2.1
M364C(C-)	5.0 ± 0.4	2.6± 0.3	1.9
T365C(C-)	6.3 ± 0.9	4.3 ± 0.4	1.4
A366C(C-)	4.5 ± 0.3	4.6 ± 0.4	1.0
G367C(C-)	3.6 ± 0.3	1.5 ± 0.1	2.4
F368C(C-)	0.3 ± 0.1	0.6 ± 0.1	0.5
S369C(C-)	4.4 ± 0.6	1.5 ± 0.2	2.9*
T370C(C-)	1.5 ± 0.1	7.1 ± 0.5	0.2*
I371C(C-)	1.3 ± 0.1	0.7 ± 0.1	1.9
A372C(C-)	0.7 ± 0.1	0.6 ± 0.1	1.2
G373C(C-)	0.7 ± 0.1	0.5 ± 0.1	1.4
S374C(C-)	4.5 ± 0.4	2.7 ± 0.3	1.7
V375C(C-)	1.6 ± 0.2	0.2 ± 0.1	8.0*
L376C(C-)	1.9 ± 0.1	1.4 ± 0.1	1.4
G377C(C-)	1.9 ± 0.2	1.5 ± 0.2	1.3
A378C(C-)	4.0 ± 0.2	2.3 ± 0.2	1.7
Y379C(C-)	< 0.1	< 0.1	-
I380C(C-)	3.1 ± 0.2	2.1 ± 0.4	1.5

Table 4-1 continued

TM 8 – 9 Loop	Mediated Uridine Uptake (pmol/oocyte.min^{-1}) Na^+ (100 mM NaCl, pH 8.5)	H^+ (100 mM ChCl, pH 5.5)	Na^+:H^+ Ratio
S381C(C-)	3.8 ± 1.0	2.4 ± 0.2	1.6
F382C(C-)	2.0 ± 0.2	1.1 ± 0.1	1.7
G383C(C-)	3.0 ± 0.3	1.2 ± 0.1	2.5
V384C(C-)	0.9 ± 0.1	0.6 ± 0.1	1.4
P385C(C-)	1.4 ± 0.2	1.3 ± 0.1	1.2
S386C(C-)	2.5 ± 0.2	2.1 ± 0.2	1.3
S387C(C-)	1.7 ± 0.1	2.3 ± 0.2	0.7

Table 4-2. Effects of PCMBS on uridine uptake in *Xenopus* oocytes expressing hCNT3C- single cysteine mutants. Influx of 10 μM ^{14}C-uridine or ^{3}H-uridine was measured in both Na^+-containing, H^+-reduced and Na^+-free, acidified media (100 mM NaCl, pH 8.5 or 100 mM ChCl, pH 5.5, respectively) following 10 min incubation on ice in the absence or presence of 200 μM PCMBS or 200 μM PCMBS + 20 mM uridine in media of the same composition used to determine uptake. Values are corrected for basal non-mediated uptake in control water-injected oocytes and are presented as a percentage of mediated uridine influx in the absence of inhibitor for each individual mutant. Each value is the mean ± S.E.M. of 10-12 oocytes. The symbol * indicates substrate protection.

		Na^+ (100 mM NaCl, pH 8.5)		H^+ (100 mM ChCl, pH 5.5)	
TM		+ PCMBS[a] (%)	+ PCMBS + uridine (%)	+ PCMBS[a] (%)	+ PCMBS + uridine (%)
7	I337C(C-)	73 ± 10	78 ±7	40 ± 4	43 ± 4
	G340C(C-)	16 ± 2	*105 ± 9	48 ± 5	57 ± 10
	Q341C(C-)	23 ± 3	*86 ± 14	48 ± 2	*83 ± 6
	T342C(C-)	32 ± 3	*76 ± 4	18 ± 2	*75 ± 6
8	T370C(C-)	104 ± 12	104 ± 10	4 ± 1	*64 ± 4
	I371C(C-)	7 ± 2	*85 ± 10	9 ± 1	19 ± 3
	A372C(C-)	17 ± 3	*100 ± 10	30 ± 4	*115 ± 17
	G373C(C-)	8 ± 1	*56 ± 4	43 ± 10	*96 ± 14
	S374C(C-)	22 ± 5	*89 ± 17	42 ± 7	*87 ± 10
	V375C(C-)	16 ± 3	25 ± 3	8 ± 5	11 ± 4
	L376C(C-)	56 ± 11	60 ± 14	27 ± 2	27 ± 3
	G377C(C-)	48 ± 11	66 ± 10	33 ± 6	57 ± 10
	A378C(C-)	27 ± 11	32 ± 11	22 ± 1	23 ± 3
	I380C(C-)	42 ± 7	62 ± 10	42 ± 3	45 ± 4
8 – 9 Loop	V384C(C-)	19 ± 20	38 ± 19	55 ± 12	53 ± 11
Control					
	hCNT3	101 ± 6	101 ± 9	20 ± 3	*104 ± 9
	hCNT3C-	109 ± 15	109 ± 16	111 ± 7	101 ± 4

[a], mediated uridine influx in the absence of inhibitor is given in pmol/oocytes.min^{-1} in Table 4-1 for each of the individual mutants.

Table 4-3. Effects of cations on PCMBS inhibition of hCNT3C- single cysteine mutants. Influx of 10 μM ^{3}H-uridine was measured in Na^+-free, acidified medium (100 mM ChCl, pH 5.5) following 10 min incubation on ice in the absence or presence of PCMBS in either Na^+-free, H^+-reduced medium (100 mM ChCl, pH 8.5), Na^+-containing, H^+-reduced medium (100 mM NaCl, pH 8.5), Na^+-free, acidified medium (100 mM ChCl, pH 5.5) or Na^+-containing, acidified medium (100 mM NaCl, pH 5.5). Values are corrected for basal non-mediated uptake in control water-injected oocytes and are normalized to the respective influx of uridine in the absence of inhibitor. Each value is the mean ± S.E.M. of 10-12 oocytes.

	Uptake (%) (100 mM ChCl, pH 5.5)			
	PCMBS in Na^+-free, H^+-reduced medium	PCMBS in Na^+-containing, H^+-reduced medium	PCMBS in Na^+-free, acidified medium	PCMBS in Na^+-containing, acidified medium
TM 7				
I337C(C-)	94 ± 8	104 ± 11	55 ± 9	35 ± 5
G340C(C-)	29 ± 4	18 ± 4	35 ± 5	38 ± 6
Q341C(C-)	48 ± 7	53 ± 6	55 ± 3	51 ± 3
T342C(C-)	56 ± 4	53 ± 4	52 ± 3	61 ± 9
TM 8				
T370C(C-)	97 ± 5	91 ± 11	45 ± 3	32 ± 4
I371C(C-)	26 ± 6	23 ± 3	27 ± 8	18 ± 4
A372C(C-)	25 ± 1	19 ± 3	26 ± 3	22 ± 3
G373C(C-)	27 ± 3	28 ± 2	28 ± 3	22 ± 2
S374C(C-)	51 ± 6	35 ± 4	54 ± 8	47 ± 7
V375C(C-)	49 ± 6	44 ± 11	37 ± 10	43 ± 4
L376C(C-)	27 ± 3	12 ± 4	13 ± 3	33 ± 4
G377C(C-)	21 ± 3	21 ± 3	29 ± 4	43 ± 3
A378C(C-)	24 ± 4	33 ± 3	24 ± 2	33 ± 2
I380C(C-)	50 ± 8	63 ± 5	64 ± 6	73 ± 6
TM 8-9 Loop				
V384C(C-)	47 ± 6	24 ± 4	36 ± 3	45 ± 8
hCNT3	102 ± 6	107 ± 23	33 ± 3	54 ± 5

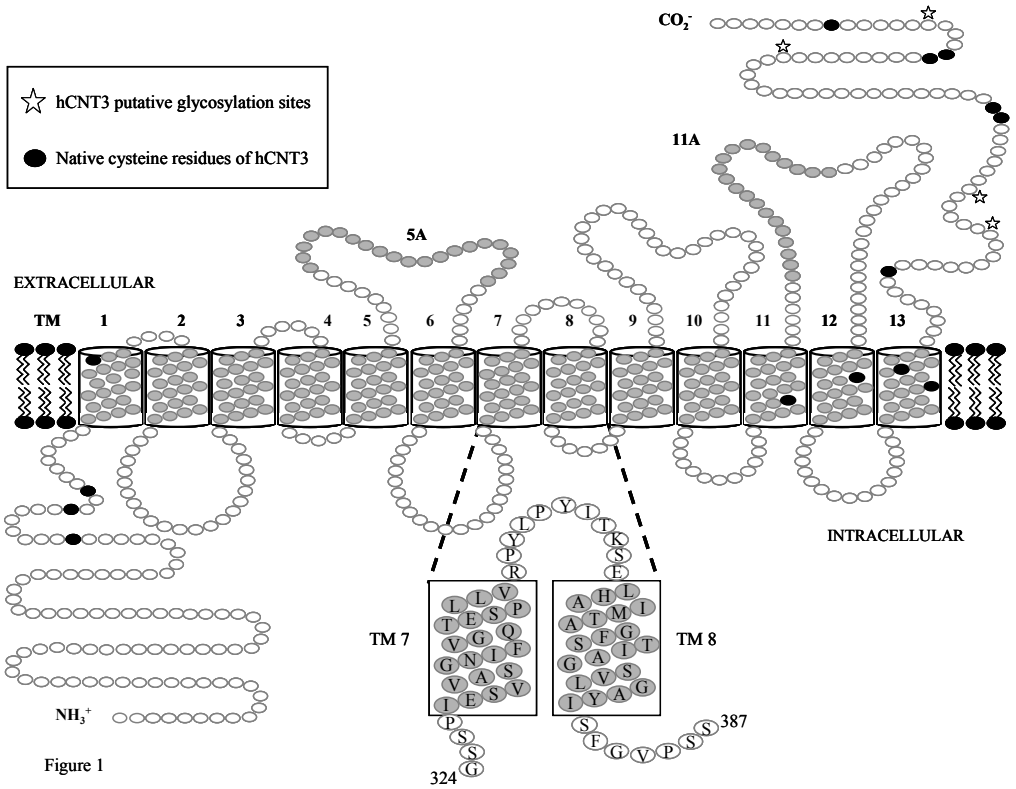

Figure 1

Figure 4-1. Original hCNT3 topology. Schematic of original hCNT3 (GenBank™ accession number AF305210) topology with 13 TMs. Insertion of TMs 5A and 11A into the membrane was weakly predicted and will result in opposite orientations of TMs 6 - 11. The position of endogenous cysteine residues are indicated as *black* residues, and putative glycosylation sites are highlighted with a *star* symbol. Residues studied by SCAM analysis in the present Chapter are depicted in the *inset*.

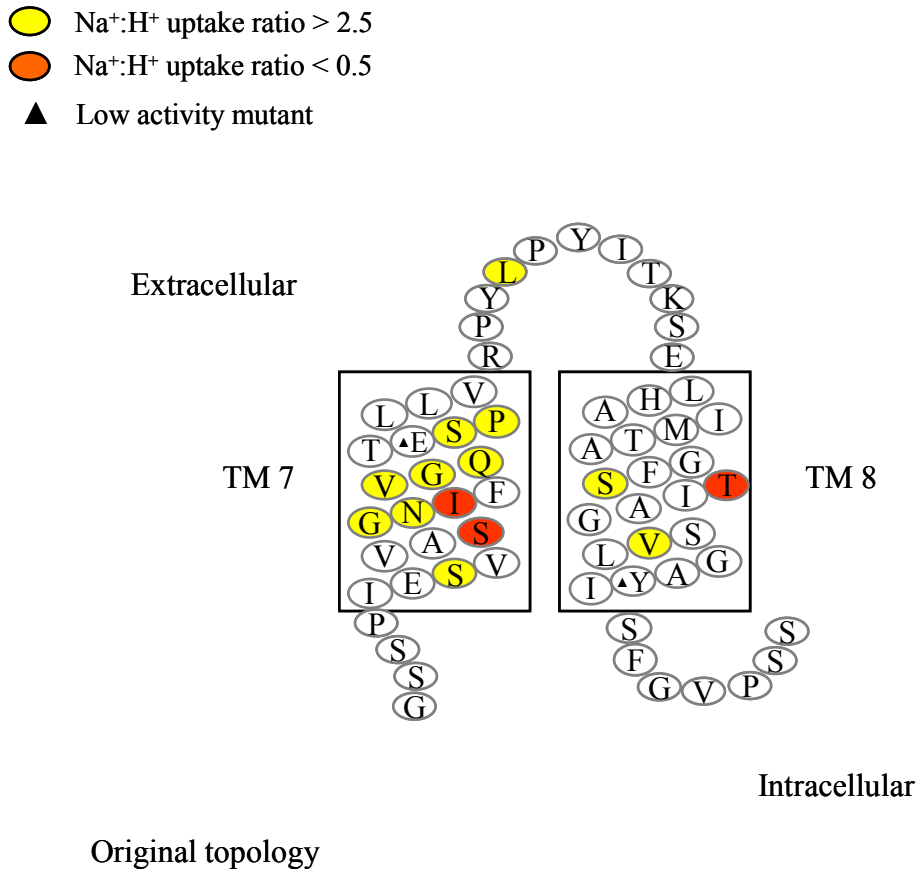

Figure 4-2. hCNT3 residues in the TM 7 - 8 region with altered Na^+:H^+ uridine uptake ratios. hCNT3C- mutants exhibiting Na^+:H^+ uridine uptake ratios > 2.5 are shown in *yellow*, and those with uptake ratios < 0.5 are shown in *orange*. Low activity mutants with uridine transport rates < 0.1 pmol/oocyte.min^{-1} in both Na^+-containing, H^+-reduced and Na^+-free, acidified media (100 mM NaCl, pH 8.5 and ChCl, pH 5.5, respectively) are indicated by the ▲ symbol. Corresponding numerical values are given in Table 4-1.

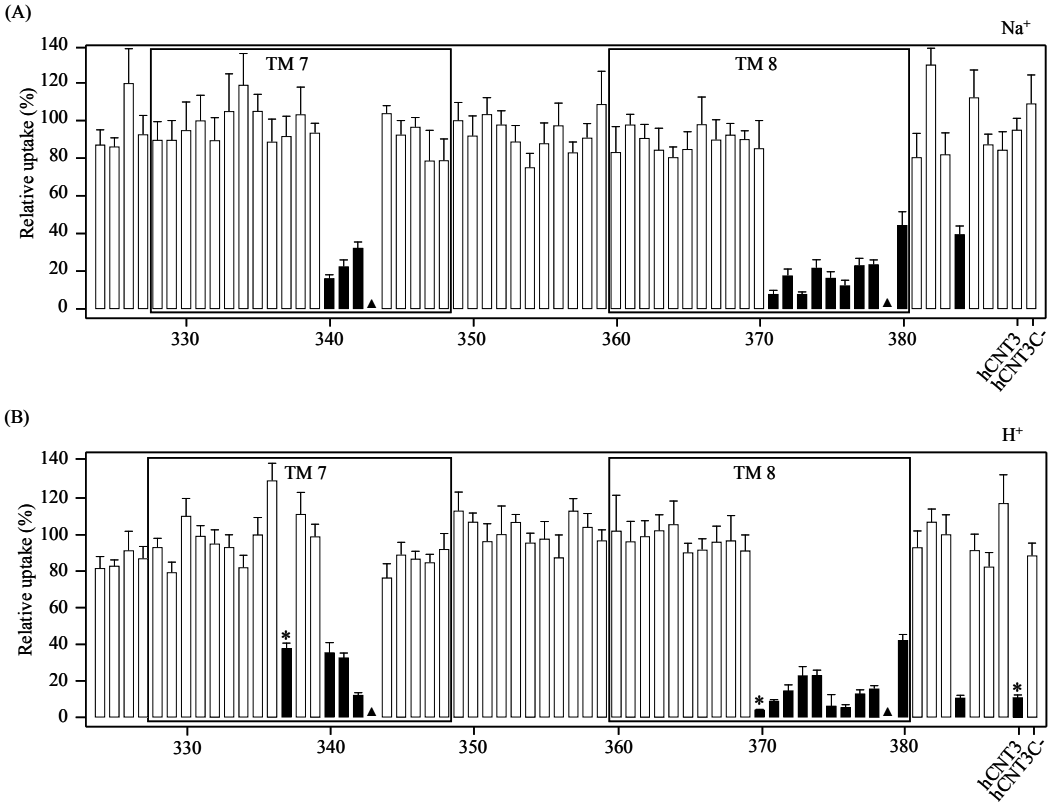

Figure 4-3. PCMBS inhibition of residues in the TM 7 – 8 region of hCNT3C-. Mediated influx of 10 μM radiolabeled uridine in Na^+-containing, H^+-reduced (*A*) or Na^+-free, acidified (*B*) medium (100 mM NaCl, pH 8.5 or 100 mM ChCl, pH 5.5, respectively) was measured following 10 min incubation on ice in the same medium (*A* or *B*, respectively) in the presence of 200 μM PCMBS. *Solid* columns indicate residue positions inhibited by PCMBS; the * symbol identifies those residues that exhibited differential inhibition by PCMBS in the two media. Low activity mutants for which inhibition was not determined are indicated by the ▲ symbol. Data are presented as mediated transport, calculated as uptake in RNA-injected oocytes *minus* uptake in water-injected oocytes, and are normalized to influx of uridine in the absence of inhibitor. Each value is the mean ± S.E.M. of 10-12 oocytes. hCNT3 and hCNT3C- were included as controls in all experiments. Corresponding numerical values are given in Table 4-2.

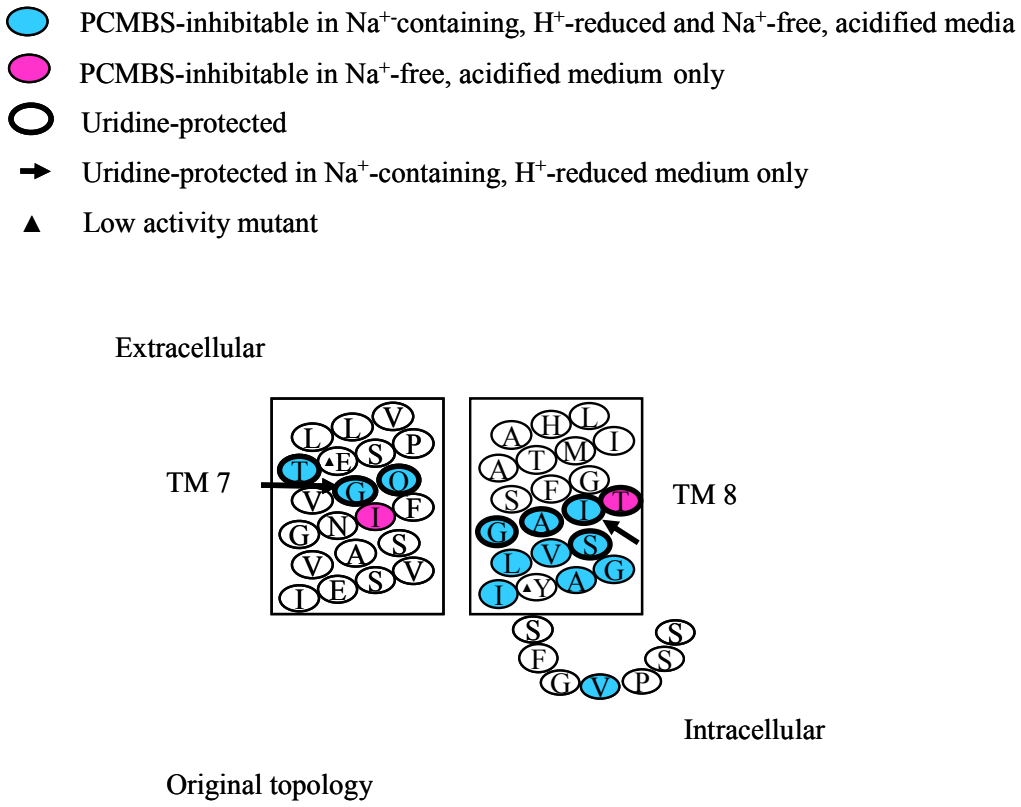

Figure 4-4. hCNT3 TM 7 – 8 region depicting PCMBS-inhibited and uridine-protected residues. hCNT3C- mutants exhibiting inhibition of uridine uptake following incubation with PCMBS in both Na^+-containing, H^+-reduced and Na^+-free, acidified media are indicated in *blue*, and those that were inhibited only in Na^+-free, acidified medium are indicated in *red*. Residues protected from PCMBS inhibition by excess unlabeled uridine are outlined in *black*. The two residues, Gly340 in TM 7 and Ile371 in TM 8, which were inhibited by PCMBS in both media, but protected from that inhibition only in the presence of Na^+- containing, H^+-reduced medium are indicated by a *black arrow*. Low activity mutants are indicated by the ▲ symbol. Corresponding numerical values are given in Table 4-2.

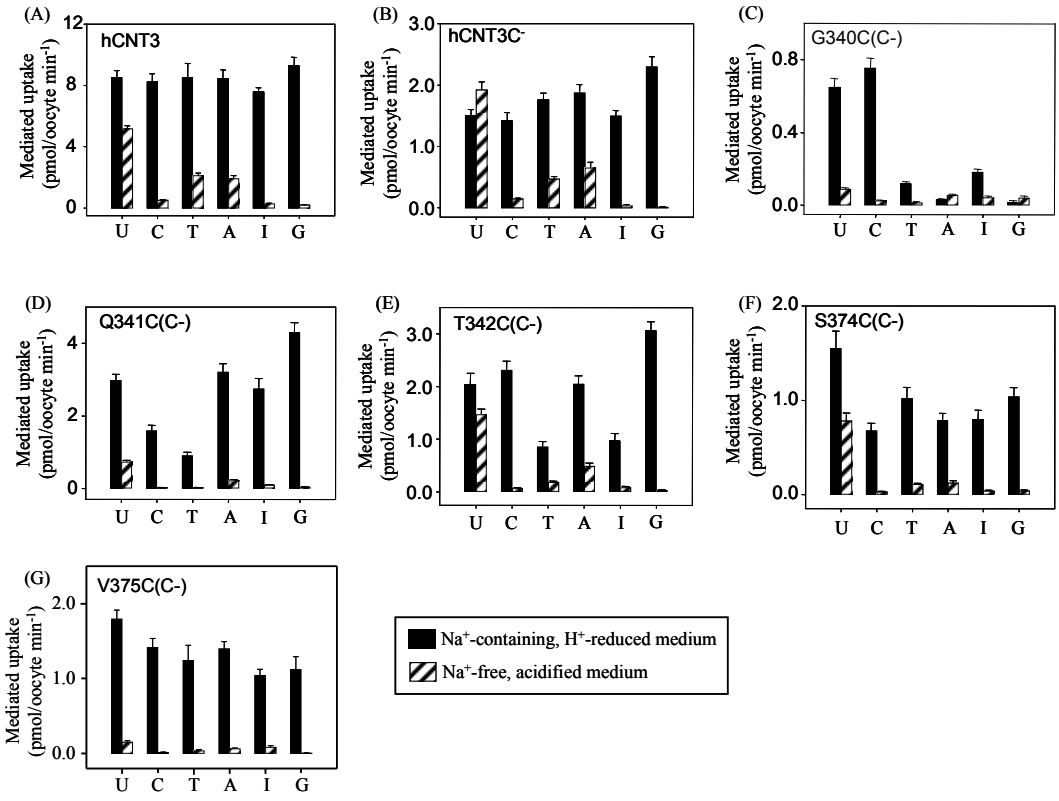

Figure 4-5. Permeant selectivity of wild-type hCNT3, hCNT3C- and hCNT3C single cysteine mutants G340C(C-), Q341C(C-), T342C(C-), S374C(C-) and V375C(C-). Oocytes producing wild-type hCNT3, hCNT3C- or hCNT3C- single cysteine mutants were incubated with 10 μM nucleosides: **U**: Uridine, **C**: Cytidine, **T**: Thymidine, **A**: Adenosine, **I**: Inosine, **G**: Guanosine, and initial rates of uptake measured in either Na^+-containing, H^+-reduced or Na^+-free, acidified media, at 20 °C. Data are presented as mediated transport, calculated as uptake in RNA-injected oocytes *minus* uptake in water-injected oocytes. Each value is the mean ± S.E.M. of 10-12 oocytes.

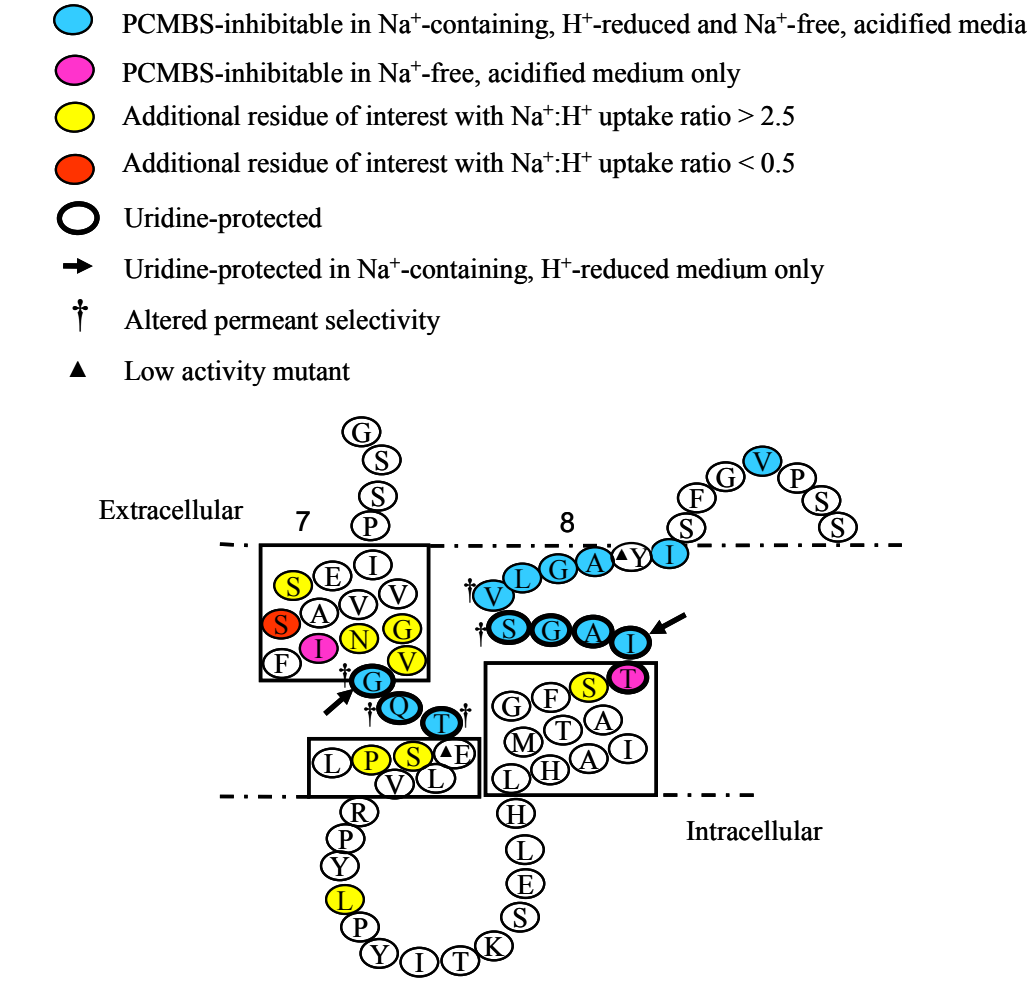

Proposed new topology

Figure 4-6

Figure 4-6. Revised topology of hCNT3 TMs 7 and 8 depicting discontinuous regions within each transmembrane segment. This schematic depicts a reversal in orientation for the TM 7 – 8 region, and non-conventional helical arrangements for both TMs. PCMBS-sensitive and uridine-protected residues, as well as additional residues of interest with Na^+:H^+ uridine uptake ratios > 2.5 or < 0.5, but not inhibited by PCMBS, are highlighted according to Figs. 4-2 and 4-4. The two residues, Gly340 in TM 7 and Ile371 in TM 8, which were inhibited by PCMBS in both media, but were protected from that inhibition only in Na^+-containing, H^+-reduced medium are indicated by a *black arrow*. Low activity mutants are indicated by the ▲ symbol. Corresponding numerical values are given in Tables 4-1 and 4-2. The five residues, Gly340, Gln341 and Thr342 in TM 7 and Ser374 and Val375 in TM 8, which exhibited altered permeant selectivity when mutated to cysteine (Fig. 4-5), are indicated by the † symbol.

Bibliography

1. Huang, Q. Q., Yao, S. Y. M., Ritzel, M. W. L., Paterson, A. R. P., Cass, C. E., and Young, J. D. (1994) Cloning and functional expression of a complementary DNA encoding a mammalian nucleoside transport protein. *J. Biol. Chem.* **269**: 17757-17760.

2. Che, M., Ortiz, D. F., and Arias, I. M. (1995) Primary structure and functional expression of a cDNA encoding the bile canalicular, purine-specific Na^+-nucleoside cotransporter. *J. Biol. Chem.* **270**: 13596-13599.

3. Ritzel, M. W. L., Yao, S. Y. M., Huang, M. Y., Elliot, J. F., Cass, C. E., and Young, J. D. (1997) Molecular cloning and functional expression of cDNAs encoding a human Na^+-nucleoside cotransporter (hCNT1). *Am. J. Physiol.* **272**: C707-C714.

4. Wang, J., Su, S. F., Dresser, M. J., Schaner, M. E., Washington, C. B., and Giacomini, K. M. (1997) Na^+-dependent purine nucleoside transporter from human kidney: cloning and functional characterization. *Am. J. Physiol.* **273**: F1058-F1065.

5. Ritzel, M. W. L., Yao, S. Y. M., Ng, A. M. L., Mackey, J. R., Cass, C. E., and Young, J. D. (1998) Molecular cloning, functional expression and chromosomal localization of a cDNA encoding a human Na^+/nucleoside cotransporter (hCNT2) selective for purine nucleosides and uridine. *Mol. Membr. Biol.* **15**: 203-211.

6. Smith, K. M, Ng, A. M., Yao, S. Y. M., Labedz, K. A., Knauss, E. E., Wiebe, L. I., Cass, C. E., Baldwin, S. A., Chen, X.-Z., Karpinski, E., and Young, J. D. (2004) Electrophysiological characterization of a recombinant human Na^+-coupled nucleoside transporter (hCNT1) produced in *Xenopus* oocytes. *J. Physiol.* **558**: 807-823.

7. Smith, K. M., Slugoski, M. D., Loewen, S. K., Ng, A. M., Yao, S. Y., Chen, X.-Z., Karpinski, E., Cass, C. E., Baldwin, S. A., and Young, J. D. (2005) The broadly selective human Na^+/nucleoside cotranpsorter (hCNT3) exhibits novel cation-coupled nucleoside transport characteristics. *J. Biol. Chem.* **280**: 25436-25449.

8. Smith, K. M., Slugoski, M. D., Cass, C. E., Baldwin, S. A, Karpinski, E., and Young, J. D. (2007) Cation coupling properties of human concentrative nucleoside transporters hCNT1, hCNT2 and hCNT3. *Mol Membr Biol*. **24**: 53-64.

9. Ritzel, M. W. L., Ng, A. M. L., Yao, S. Y. M., Graham, K., Loewen, S. K., Smith, K. M., Ritzel, R. G., Mowles, D. A., Carpenter, P., Chen, X.-Z., Karpinski, E., Hyde, R. J., Baldwin, S. A., Cass, C. E., and Young, J. D. (2001) Molecular identification and characterization of novel human and mouse concentrative Na^+-nucleoside cotransporter proteins (hCNT3 and mCNT3) broadly selective for purine and pyrimidine nucleosides (system *cib*). *J. Biol. Chem.* **276**: 2914-2927.

10. Hamilton, S. R., Yao, S. Y., Ingram, J. C., Hadden, D. A., Ritzel, M. W., Gallagher, M. P., Henderson, P. J., Cass, C. E., Young, J. D., and Baldwin, S. A. (2001) Subcellular distribution and membrane topology of the mammalian concentrative Na^+-nucleoside cotransporter, rCNT1. *J. Biol. Chem.* **276**: 27981-27988.

11. Yao, S. Y., Ng, A. M., Loewen, S. K., Cass, C. E., Baldwin, S. A., and Young, J. D. (2002) An ancient prevertabrate Na^+-nucleoside cotransporter (hfCNT) from the Pacific hagfish (*Eptatretus stouti*). *Am. J. Phys. Cell Phys.* **283**: C155-C168.

12. Smith, K. M., Slugoski, M. D., Loewen, S. K., Ng, A. M., Yao, S. Y., Chen, X.-Z., Karpinski, E., Cass, C. E., Baldwin, S. A., and Young, J. D. (2005) The broadly selective human Na^+/nucleoside cotranpsorter (hCNT3) exhibits novel cation-coupled nucleoside transport characteristics. *J. Biol. Chem.* **280**: 25436-25449.

13. Wang, J., and Giacomini, K. M. (1999) Serine 318 is essential for the pyrimidine selectivity of the N2 Na^+-nucleoside transporter. *J. Biol. Chem.* **274**: 2298-2302.

14. Loewen, S. K., Ng, A. M., Yao, S. Y., Cass, C. E., Baldwin, S. A., and Young, J. D. (1999) Identification of amino acid residues responsible for the pyrimidine and purine nucleoside specificities of human concentrative Na^+ nucleoside cotransporters hCNT1 and hCNT2. *J. Biol. Chem.* **274**: 24475-24484.

15. Slugoski, M. D., Loewen, S. K., Ng, A. M., Smith, K. M., Yao, S. Y., Karpinski, E., Cass, C. E., Baldwin, S. A., and Young, J. D. (2007) Specific mutations in transmembrane helix 8 of human concentrative Na^+/nucleoside cotransporter hCNT1 affect permeant selectivity and cation coupling. *Biochemistry*. **46**: 1684-1693.

16. Craig, J. E., Zhang, Y., and Gallagher, M. P. (1994) Cloning of the nupC gene of *Escherichia coli* encoding a nucleoside transport system, and identification of an adjacent insertion element, IS 186. *Mol. Micr.* **11**: 1159-1168.

17. Loewen, S. K., Yao, S. Y., Slugoski, M. D., Mohabir, N. N., Turner, R. J., Mackey, J. R., Gallagher, M. P., Henderson, P. J., Baldwin, S. A., Cass, C. E., and Young, J. D. (2004) Transport of physiological nucleosides and anti-viral and anti-neoplastic nucleoside drugs by recombinant *Escherischia coli* nucleoside-H^+ cotransporter (NupC) produced in *Xenopus laevis* oocytes. *Mol. Membr. Biol.* **21**: 1-10.

18. Zhang, J., Tackaberry, T., Ritzel, M. W., Raborn, T., Barron, G., Baldwin, S. A., Young, J. D., and Cass, C. E. (2006) Cysteine-accessibility analysis of transmembrane domains 11-13 of human concentrative nucleoside transporter 3. *Biochem. J.* **394**: 389-398.

19. Slugoski, M., D., Smith, K., M., Mulinta, R., Ng, A. M. L., Yao, S. Y. M., Morrison, E. L., Lee, Q., O., T., Zhang, J., Karpinski, E., Cass, C. E., Baldwin, S. A., and Young, J. D. (2008) A conformationally mobile cysteine residue (Cys-561) modulates Na^+ and H^+ activation of human CNT3. *J. Biol. Chem.* **283**:24922-24934.

20. Yan, R. T., and Maloney, P. C. (1993) Identification of a residue in the translocation pathway of a membrane carrier. *Cell.* **75**: 37-44.

21. Yan, R. T., and Maloney, P. C. (1995) Residues in the pathway through a membrane transporter. *Proc Natl Acad Sci U.S.A.* **92**: 5973-5976.

22. Slugoski, M. D., Ng, A. M., Yao, S. Y., Smith, K. M., Lin, C. C., Zhang, J., Karpinski, E., Cass, C. E., and Baldwin, S. A., and Young, J. D. (2008) A proton-mediated conformational shift identifies a mobile pore-lining cysteine residue (Cys-561) in human concentrative nucleoside transporter 3. *J. Biol. Chem.* **283**: 8496-8507.

23. Slugoski, M., D., Smith, K., M., Ng, A. M. L., Yao, S. Y. M., Karpinski, E., Cass, C. E., Baldwin, S. A., and Young, J. D. (2009a) Conserved glutamate residues E343 and E519 provide mechanistic insights into cation/nucleoside cotransport by human concentrative nucleoside transporter 3 (hCNT3). *J. Biol. Chem.* **284**:17266-17280.

24. Slugoski, M., D., Ng, A. M. L., Yao, S. Y. M., Lin, C. C., Mulinta, R., Cass, C. E., Baldwin, S. A., and Young, J. D. (2009b) Substituted cysteine accessibility method analysis of human concentrative nucleoside transporter hCNT3 reveals a novel discontinuous region of functional importance within CNT family motif (G/A)XKX3NEFVA(Y/M/F). *J. Biol. Chem.* **284**:17281-17292.

25. Yao, S. Y. M., Ng, A. M., Slugoski, M. D., Smith, K. M., Mulinta, R., Karpinski, E., Cass, C. E., Baldwin, S. A., and Young, J. D. (2007) Conserved glutamate residues are critically involved in Na^+/nucleoside cotransport by human concentrative nucleoside transporter 1 (hCNT1). *J. Biol. Chem.* **282**: 30607-30617.

26. Yamashita, A., Singh, S. K., Kawate, T., Jin, Y., and Gouaux, E. (2005) Crystal structure of a bacterial homolgue of Na^+/Cl^--dependent neurotransmitter transporters. *Nature* **437**: 215-223.

27. Faham, S., Watanabe, A., Besserer, G. M., Cascio D., Specht, A., Hirayama, B., Wright, E. M., and Abramson, J. (2008) The crystal structure of a sodium galactose transporter reveals mechanistic insights into Na^+/sugar symport. *Science*. **321**: 810-814.

28. Hunte, C., Screpanti, E., Venturi, M., Rimon, A., Padan, E., and Michel, H. (2005) Structure of a Na^+/H^+ antiporter and insights into mechanism of action and regulation by pH. *Nature*. **435**: 1197-1202.

29. Weyand, S., Shimamura, T., Yajima, S., Suzuki, S., Mirza, O., Krusong, K., Carpenter, E. P., Rutherford, N. G., Hadden, J. M., O'Reilly, J., Ma, P., Saidijam, M., Patching, S. G., Hope, R. J., Norbertczak, H. T., Roach, P. C., Iwata, S., Henderson, P. J., and Cameron, A. D. (2008) Structure and molecular mechanism of a nucleobase-cation-symport-1 family transporter. *Science*. **322**: 709-713.

30. Yernool, D., Boudker, O., Jin, Y., and Gouaux, E. (2004) Structure of a glutamate transporter homologue from *Pyrococcus horikoshii*. *Nature* **431**: 811-818.

31. Screpanti, E., and Hunte, C. (2007) Discontinuous membrane helices in transport proteins and their correlation with function. *J. Struct. Biol.* **159**: 261-267.

32. Krishnamurthy, H., Piscitelli, C. L., and Gouaux, E. (2009) Unlocking the molecular secrets of sodium-coupled transporters. *Nature* **459**: 347- 355.

33. Boudker, O., Ryan, R. M., Yernool, D., Shimamoto, K., and Gouaux, E. (2007) Coupling substrate and ion binding to extracellular gate of a sodium-dependent aspartate transporter. *Nature* **445**: 387-393.

Chapter 5:

Substituted Cysteine Accessibility Method Analysis of Transmembrane Domains 7 & 8 of Human Na^+/Nucleoside Cotransporter 1 (hCNT1)

Acknowledgements and Contributions

All of the hCNT1 cysteine mutants were constructed by myself. I also undertook all functional studies. This research was funded by the National Cancer Institute of Canada with funds from the Canadian Cancer Society (now the Canadian Cancer Society Research Institute), Alberta Cancer Board (now the Alberta Health Services- Cancer Care), The Alberta Cancer Foundation, and by the Alberta Cancer Prevention Legacy Fund.

Introduction

hCNT1 is the first of three members of the human SLC28 concentrative nucleoside transporter (CNT) family to be identified (1). hCNT1 is pyrimidine nucleoside selective, but also transports adenosine, while hCNT2 has a reciprocal selectivity for purine nucleosides and uridine (1, 2). Both are Na^+-specific, and couple Na^+:nucleoside cotransport with a 1:1 stoichiometry (1-7). hCNT3, in contrast, is broadly selective for both pyrimidine and purine nucleosides, and exhibits a 2:1 Na^+:nucleoside coupling ratio (6-8). hCNT3 is also capable of H^+/nucleoside cotransport with a coupling stoichiometry of 1:1, whereby one of the transporter's two Na^+ binding sites also functionally interacts with H^+ (6,7). All three transporters have a similar predicted 13 TM membrane topology, with two additional TMs (designated 5A and 11A) weakly predicted by computer algorithms (3, 5, 8, 9). Chimeric studies involving human, rat and hagfish members of the CNT protein family have revealed that that the functional domains responsible for nucleoside selectivity and cation coupling reside within the C-terminal TM 7-13 half of the proteins (10-14).

A functional cysteine-less version of hCNT3 (hCNT3C-) has been characterized in *Xenopus* oocytes [Chapter 3 (15)], and used in Chapter 4 of this thesis to undertake substituted cysteine accessibility method (SCAM) analysis of the TM 7-8 region of the transporter. Results from these experiments identified residues of functional importance, and provided evidence of close proximity cation/nucleoside binding and translocation. The results also suggested a reversed orientation of TMs 7 and 8 in the membrane and, unexpectedly, provided evidence of novel discontinuous regions within both helices. Wild-type hCNT1 contains 20 endogenous cysteine residues, but is insensitive to inhibition by PCMBS [Appendix 1 (16)]. The present Chapter takes advantage of this observation to undertake a parallel and complementary SCAM analysis of hCNT1 TMs 7 and 8 using the wild-type protein as template to eliminate any possibility that topological results obtained for hCNT3C- were, in some way, influenced by engineering the removal of the protein's endogenous cysteine residues.

By comparing results for Na^+ -specific hCNT1 with those for Na^+- and H^+ -dependent hCNT3, it was additionally hoped that the analysis might shed light on structural features associated with the different cation-coupling characteristics of the two transporters.

Results

Wild-type hCNT1 was used as template for construction of the single cysteine mutants characterized for functional activity and PCMBS inhibition in the present Chapter. The 43 residues spanning a region between and including TMs 7 and 8 that were investigated are depicted as a schematic in Fig. 5-1.

Functional activity of single cysteine mutants – hCNT1 exclusively couples nucleoside transport to the Na^+ electrochemical gradient (6). Therefore, the functional activity of hCNT1 single cysteine mutants was determined only in Na^+-containing, H^+-reduced medium (100 mM NaCl, pH 8.5). The medium was buffered at a pH of 8.5 to enable direct comparison with the data obtained for hCNT3C- in Chapter 4. Control experiments at pH 7.5 yielded essentially identical results.

Initial rates of radiolabelled 10 μM uridine transport (± S.E.M.) for each mutant, in units of pmol/oocyte.min^{-1}, are given in Table 5-1. The uptake of 10 μM radiolabeled uridine (100 mM NaCl, pH 8.5) by oocytes expressing hCNT1 varied between experiments in the range 7 to 9 pmol/oocyte.min^{-1} (data not shown). The flux values reported in Table 5-1, and in subsequent Tables and Figures, depict mediated transport activity, defined as the difference in uptake between RNA transcript-injected and control water-injected oocytes, and are from representative experiments. In all studies reported here, uridine uptake in water-injected oocytes was < 0.02 pmol/oocyte.min^{-1} (data not shown).

All 43 hCNT1 TM 7-8 single cysteine mutants were functional (influx > 0.1 pmol/oocyte.min^{-1}) when produced in *Xenopus* oocytes (Table 5-1).

PCMBS inhibition of single cysteine mutants – Wild-type hCNT1 has previously been reported to be insensitive to inhibition by PCMBS [Appendix 1

(16)]. This enabled single cysteine mutants of hCNT1 to tested for inhibition by PCMBS in Na^+-containing, H^+-reduced medium (100 mM NaCl, pH 8.5) following 10 min exposure to 200 μM PCMBS, the same concentration of organomercurial used for hCNT3C- mutants in Chapter 4. Uptake of 10 μM radiolabeled uridine was then assayed in medium of the same composition. Exposure to PCMBS was performed on ice to minimize its diffusion across oocyte plasma membranes [Appendix 1 (16), Chapters 4, 7, 8 (17) and (18)]. In ascending numerical order of residue position, results for each mutant calculated as a percentage of mediated uridine uptake in the absence of PCMBS are presented in Fig. 5-2,. For screening purposes, a residue was considered to be PCMBS-inhibitable upon exhibiting > 20% inhibition of uridine uptake following incubation with PCMBS. Residues that were considered to be PCMBS-sensitive are highlighted in Fig. 5-2. Corresponding numerical flux values are presented in Table 5-2. A schematic of the locations of these PCMBS-inhibitable residues is presented in Fig. 5-3. Fig. 5-2 and Table 5-2 include control data for wild-type hCNT1 (unaffected by PCMBS).

In TM 7, four adjacent residues, Ser319, Gln320, Thr321 and Glu322, were PCMBS-inhibitable upon conversion to cysteine. In TM 8, six adjacent mutants (I350C, A351C, G352C, S353C, L354C and L355C) were PCMBS-inhibitable. Nearby residues Ala357 and Tyr358 were also PCMBS-inhibitable upon conversion to cysteine. A residue which localizes to the predicted intracellular loop following TM 8 (Ile363) was sensitive to PCMBS inhibition upon conversion to cysteine.

Uridine protection from PCMBS inhibition – Subsequent experiments investigated the ability of extracellular uridine (20 mM) to protect against inhibition by PCMBS for residues that were PCMBS-inhibitable. Results for each individual mutant are presented in Table 5-2, and the uridine-protectable residues are highlighted in the hCNT1 topology schematic of Fig. 5-3.

In TM 7, three residue positions exhibited uridine protection from PCMBS inhibition when converted to a cysteine (Gln320, Thr321 and Glu322). In contrast, S319C was still PCMBS-sensitive in the presence of excess uridine. In TM 8, four

residue positions were uridine-protected, all mutants (I350C, G352C, S353 and L354) exhibited full protection against PCMBS inhibition in the presence of excess uridine. In contrast, the other fourPCMBS-sensitive mutants in TM 8 were not protected by uridine (A351C, L355C, A357C and Y358C). Similarly, mutant I363C in the loop following TM 8 was not protected from PCMBS inhibition by uridine.

Na^+- mediated PCMBS inhibition of hCNT1 mutants – Of the 43 hCNT1 residue positions in the TMs 7 – 8 region that were investigated, 13 were inhibited by PCMBS (Table 5-2, Fig. 5-2). To determine if access of PCMBS to these residues required cation-induced conformational changes within the protein, each of the single cysteine mutants at these positions were re-screened for PCMBS inhibition under the original exposure condition (Na^+-containing, H^+-reduced medium) and in Na^+-free, H^+-reduced medium (100 mM ChCl pH 8.5). Fluxes of 10 μM uridine were then determined in Na^+-containing, H^+-reduced medium (Table 5-3).

All of the 13 mutants that were inhibited by PCMBS in the presence of Na^+ were also inhibited by PCMBS in Na^+-free medium (Table 5-3), indicating that PCMBS inhibition was not cation-induced. Residue position Glu322, however, showed modest (31%) inhibition by PCMBS in the absence of Na^+, with a stronger inhibition (66%) in the presence of Na^+, indicating that binding of Na^+ may induce a conformational change that increases exposure of this residue to PCMBS inhibition.

Discussion

PCMBS has been used previously to investigate individual topological features and residues of hCNT1 and hCNT3 [(14), Appendix 1 (16) and (19)]. The present systematic investigation of TMs 7 and 8 of wild-type hCNT1 confirms the corresponding SCAM analysis of the parallel region in hCNT3C- described in Chapter 4. In so doing, I have eliminated any possibility that the SCAM results obtained for hCNT3C- were influenced by engineering the removal of endogenous cysteine residues from the transporter.

Functional activity of hCNT1 mutants – Initial characterization of the hCNT1 single cysteine mutants in the present study measured uridine uptake only in Na^+-containing medium (Table 5-1). Of the 43 mutants examined, none exhibited uridine uptake values < 0.1 pmol/oocyte.min^{-1} (Table 5-1). It was possible, therefore, to test all 43 individual cysteine mutants for sensitivity to PCMBS inhibition.

PCMBS inhibition of hCNT1 mutants: transmembrane architecture and orientation of TMs 7 & 8 – To summarize the data presented in Table 5-2 and Fig. 5-2, the schematic in Fig. 5-3 highlights those TM 7 – 8 residues identified in hCNT1 as PCMBS-sensitive and uridine-protected.

In TM 7, PCMBS inhibition was evident for residues Ser319, Gln320, Thr321 and Glu322. Of these, Gln320, Thr321 and Glu322 showed uridine protection. This clustering of adjacent PCMBS-inhibitable residues is very similar to hCNT3C- (Fig. 4-5) and, again, is inconsistent with the patterning anticipated for a conventional α-helix. In TM 8, a total of six adjacent residues were sensitive to PCMBS inhibition when mutated to cysteine (Ile350, Ala351, Gly352, Ser353, Leu354 and Leu355). Of these, I350C, G352C, S353 and L354 showed uridine protection. Again, the clustering of adjacent PCMBS-sensitive was very similar to that seen for hCNT3C- (Fig. 4-5). Within the hCNT1 TM 8 region of PCMBS inhibition, Gly358 sits next to the deepest residue in the membrane at the endofacial boundary of the TM, according to the original 13 TM topology of hCNT1 shown in Fig. 5-1. Altogether, and similar to hCNT3C- (Chapter 4), the block of PCMBS-sensitive residues comprises almost the entire inner half of hCNT1 TM 8 (Fig. 5-4). It is proposed, therefore, that this pattern of inhibition supports a reversed orientation of this helix. As such, the PCMBS-inhibitable residues in TM 8 would lie exofacially within the helix, in a position more likely to be accessible to the extracellular medium and available for PCMBS binding. In agreement with this, structure-function studies of negatively charged residues in hCNT1 and hCNT3 also provide evidence for an opposite orientation of TM 7 [Appendix 1 (16) and (19)]. Other evidence supporting a reversed orientation of hCNT1 TMs 7 and 8 is that Ile363 in the putative internal loop exiting TM 8 was

sensitive to inhibition by PCMBS. Since PCMBS is membrane impermeable, it is predicted that this residue must be extracellular in order to allow access and binding of PCMBS. This residue corresponds to hCNT3C- residue Val384, which was also sensitive to PCMBS inhibition (Chapter 4) (Fig 5-4). In addition to a reversed membrane orientation, the block patterns of PCMBS inhibition seen in hCNT1 TMs 7 and 8 reinforce the conclusion reached in Chapter 4 for hCNT3C- that both transmembrane regions contain extended regions incompatible with conventional α-helical structures.

Mechanistic implications for hCNT1 – Illustrated in Fig.5-5, the pattern of PCMBS inhibition reported here for hCNT1 TMs 7 and 8 (and apparent also in the same region of hCNT3C- in Chapter 4) provides important functional evidence of extended structures resembling the discontinuous membrane helices evident in the crystal structures of the recently solved Na^+-coupled bacterial leucine, galactose and hydantoin membrane transporter proteins *Aquifex aeolicus* $LeuT_{Aa}$ (20), *Vibrio parahaemolyticus* SGLT (21), *Escherichia coli* NhaA (22), and *Microbacterium liquefaciens* NCS1 (23). In $LeuT_{Aa}$, non-traditional transmembrane α-helices are disrupted by the insertion of extended regions of polypeptide that comprise the Na^+ binding sites of the protein and, upon Na^+ binding, favour high-affinity binding of the permeant amino acid leucine (20). A similar feature is also apparent in TM 7 of the glutamate transporter homologue GltPh from *Pyrococcus horikoshii* (24). Reviewed by Screpanti and Hunte (25) and Krishnamurthy *et. al.* (26), such discontinuous membrane helices are proposed to play important mechanistic roles in ion and permeant recognition, binding and translocation in secondary active transporters.

In the case of hCNT1, previous studies have shown that residues Ser319 and Gln320 in TM 7, and Ser353 and Leu354 in TM 8, are involved in permeant selectivity and cation binding (13, 14). Confirming their central close proximity to the aqueous translocation pore, conversion of each residue to a cysteine rendered the protein sensitive to PCMBS inhibition. Both residue pairs are located within the postulated regions of helical discontinuity in the two transmembrane segments, and one of the residue positions were uridine-protected. When converted to

cysteine, the corresponding residue positions in hCNT3C- similarly exhibited sensitivity to PCMBS inhibition and uridine protection for three of the four residues. Mutation of the hCNT3C- residues also resulted in altered permeant selectivity and elevated Na^+:H^+ uridine uptake ratios (Chapter 4).

Within TM 7 of hCNT1, mutation of Glu322 results in uncoupled Na^+ currents, a property also revealed by mutation of the corresponding residue in hCNT3 [Appendix 1 (16) and (19)]. It is interpreted that this residue may form part of the inward gate of the transport vestibule. Access of PCMBS to this residue position was increased in the presence of Na^+ (Table 5-3).

The present results therefore provide further support that TMs 7 and 8 form part of a common nucleoside/cation translocation pore, and that residues contributed by these TMs have locations within or closely adjacent to the nucleoside and cation binding pockets.

Conclusions – The SCAM analysis of TMs 7 and 8 of hCNT1 presented in this Chapter reinforces that in Chapter 4 for hCNT3C- suggesting the presence of novel discontinuous regions within both TMs, indicating their reversed orientation in the membrane, and highlighting their functional importance in key cation and nucleoside binding and/or translocation events. The striking similarities revealed here between Na^+-specific hCNT1 and Na^+- and H^+ -dependent hCNT3 is contrasted with SCAM analysis of the corresponding TMs of H^+-specific *E. coli* NupC in the next Chapter.

Table 5-1. Uptake of uridine in *Xenopus* oocytes expressing hCNT1 single cysteine mutants. Influx of 10 μM ^{3}H-uridine was measured in Na^{+}-containing medium (100 mM NaCl, pH 8.5). Values are corrected for basal non-mediated uptake in control water-injected oocytes. Each value is the mean ± S.E.M. of 10-12 oocytes.

	Mediated Uridine Uptake (pmol/oocyte.min^{-1}) (100 mM NaCl, pH 8.5)		
TM 7		TM 8	
T307C	5.5 ± 0.4	V339C	5.5 ± 0.2
E308C	0.7 ± 0.1	H340C	6.0 ± 0.4
T309C	4.7 ± 0.4	V341C	4.0 ± 0.3
L310C	4.8 ± 0.3	V342C	5.9 ± 0.3
S311C	5.0 ± 0.4	M343C	4.5 ± 0.4
V312C	3.7 ± 0.2	T344C	4.8 ± 0.3
A313C	3.3 ± 0.2	G345C	3.3 ± 0.2
G314C	4.6 ± 0.4	G346C	0.5 ± 0.1
N315C	1.0 ± 0.1	Y347C	1.0 ± 0.2
I316C	2.9 ± 0.3	A348C	2.3 ± 0.4
F317C	4.9 ± 0.3	T349C	0.2 ± 0.1
V318C	4.3 ± 0.4	I350C	1.9 ± 0.2
S319C	0.9 ± 0.1	A351C	1.0 ± 0.1
Q320C	2.6 ± 0.3	G352C	3.5 ± 0.2
T321C	0.7 ± 0.1	S353C	2.2 ± 0.2
E322C	0.3 ± 0.1	L354C	1.7 ± 0.2
A323C	3.7 ± 0.3	L355C	1.8 ± 0.2
P324C	1.5 ± 0.1	G356C	0.9 ± 0.2
L325C	3.5 ± 0.2	A357C	3.2 ± 0.2
L326C	2.5 ± 0.2	Y358C	1.0 ± 0.1
I327C	3.9 ± 0.3	I359C	4.6 ± 0.2
TM 8 – 9 Loop			
I363C	2.3 ± 0.3	hCNT1	8.9 ± 0.6

Table 5-2. Effects of PCMBS on uridine uptake in *Xenopus* oocytes expressing hCNT1 single cysteine mutants. Influx of 10 μM ^{3}H-uridine was measured in Na^{+}-containing media (100 mM NaCl, pH 8.5) following 10 min incubation on ice in the absence or presence of 200 μM PCMBS or 200 μM PCMBS + 20 mM uridine in media of the same composition used to determine uptake. Values are corrected for basal non-mediated uptake in control water-injected oocytes and are presented as a percentage of mediated uridine influx in the absence of inhibitor for each individual mutant. Each value is the mean ± S.E.M. of 10-12 oocytes. The symbol * indicates substrate protection.

		Na^{+} (100 mM NaCl, pH 8.5)	
TM		+ PCMBS[a] (%)	+ PCMBS + uridine (%)
7	S319C	36 ± 3	50 ± 4
	Q320C	47 ± 5	*89 ± 7
	T321C	31 ± 2	*96 ± 7
	E322C	21 ± 1	*106 ± 9
8	I350C	8 ± 1	*96 ± 7
	A351C	46 ± 2	57 ± 4
	G352C	15 ± 2	*88 ± 7
	S353C	42 ± 3	*80 ± 4
	L354C	31 ± 3	*64 ± 3
	L355C	53 ± 6	51 ± 6
	A357C	58 ± 3	62 ± 4
	Y358C	27 ± 3	28 ± 3
8 – 9 Loop	I363C	43 ± 2	44 ± 4
Control	hCNT1	108 ± 7	88 ± 3

[a], mediated uridine influx in the absence of inhibitor is given in pmol/oocytes.min^{-1} in Table 5-1 for each of the individual mutants.

Table 5-3. Effects of Na^+ on PCMBS inhibition of hCNT1 single cysteine mutants. Influx of 10 μM ^{3}H-uridine was measured in Na^+-containing medium (100 mM NaCl, pH 8.5) following 10 min incubation on ice in the absence or presence of PCMBS in either Na^+-free or Na^+-containing medium (100 mM ChCl, pH 8.5 and 100 mM NaCl, pH 8.5, respectively). Values are corrected for basal non-mediated uptake in control water-injected oocytes and are normalized to the respective influx of uridine in the absence of inhibitor. Each value is the mean ± S.E.M. of 10-12 oocytes.

	Uptake (%) (100 mM NaCl, pH 7.5)	
	PCMBS in Na^+-free medium	PCMBS in Na^+-containing medium
TM 7		
S319C	22 ± 1	25 ± 4
Q320C	53 ± 5	46 ± 7
T321C	10 ± 2	12 ± 4
E322C	69 ± 6	34 ± 3
TM 8		
I350C	5 ± 1	7 ± 1
A351C	28 ± 3	40 ± 4
G352C	4 ± 0.4	7 ± 1
S353C	39 ± 3	38 ± 3
L354C	20 ± 2	22 ± 1
L355C	32 ± 2	26 ± 3
A357C	52 ± 4	59 ± 4
Y358C	6 ± 1	13 ± 2
TM 8-9 Loop		
I363C	27 ± 2	37 ± 2

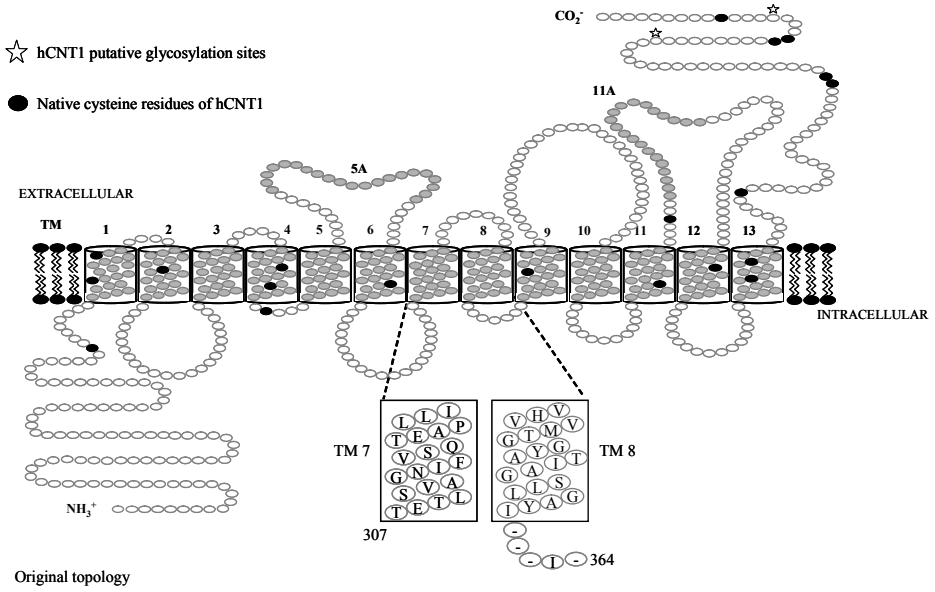

Figure 5-1. Original hCNT1 topology. Schematic of original hCNT1 (GenBank™ accession number U62968) topology with 13 TMs. Insertion of TMs 5A and 11A into the membrane was weakly predicted and will result in opposite orientations of TMs 6 - 11. The position of endogenous cysteine residues are indicated as *black* residues, and putative glycosylation sites are highlighted with a *star* symbol. Residues studied by SCAM analysis in the present Chapter are depicted in the *inset*. Some constructs were unavailable and denoted by a - symbol.

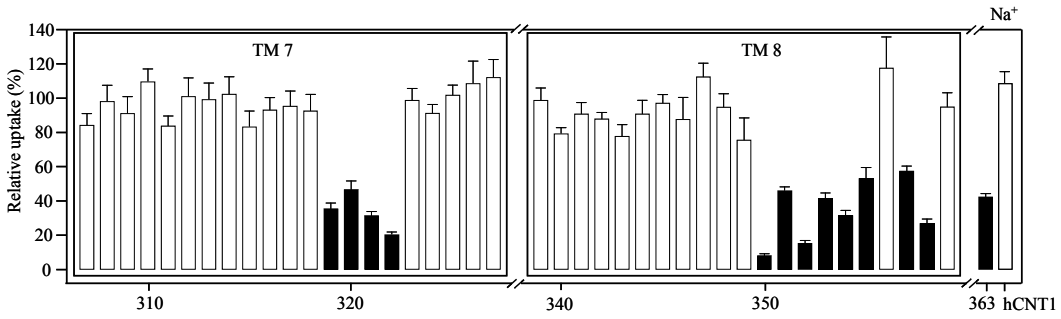

Figure 5-2. PCMBS inhibition of residues in the TM 7 – 8 region of hCNT1. Mediated influx of 10 μM radiolabeled uridine in Na^+-containing medium (100 mM NaCl, pH 8.5) was measured following 10 min incubation on ice in the same medium in the presence of 200 μM PCMBS. *Solid* columns indicate residue positions inhibited by PCMBS. Data are presented as mediated transport, calculated as uptake in RNA-injected oocytes *minus* uptake in water-injected oocytes, and are normalized to influx of uridine in the absence of inhibitor. Each value is the mean ± S.E.M. of 10-12 oocytes. hCNT1 was included as a control for all experiments. Corresponding numerical values are given in Table 5-2.

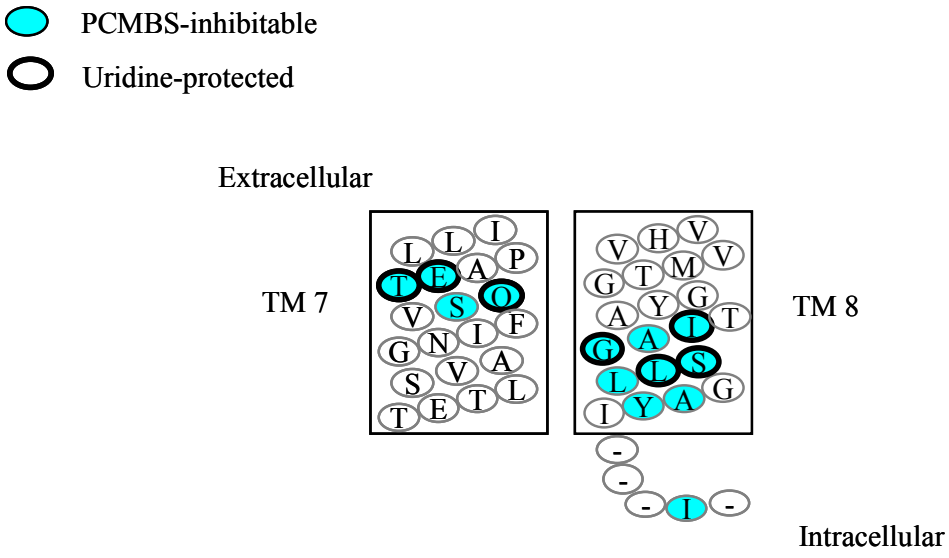

Figure 5-3. hCNT1 TM 7 – 8 region depicting PCMBS-inhibited and uridine-protected residues. hCNT1 mutants exhibiting inhibition of uridine uptake following incubation with PCMBS in Na^+-containing medium are indicated in *blue*. Residues protected from PCMBS inhibition by excess unlabeled uridine are outlined in *black*. Some constructs were unavailable and denoted by a - symbol. Corresponding numerical values are given in Table 5-2.

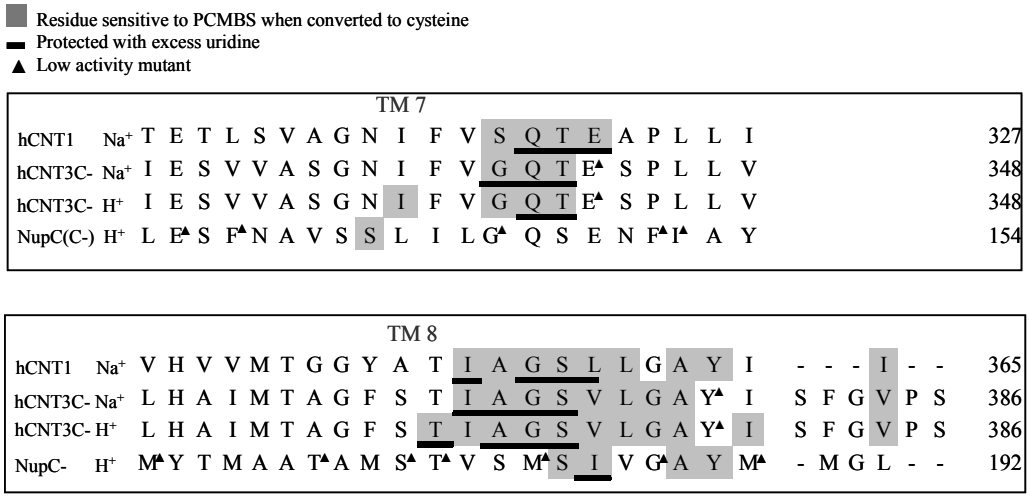

Figure 5-4. Comparison of PCMBS inhibition and substrate protection of residues in TM 7 & 8 of hCNT3C- and hCNT1. Residues sensitive to PCMBS inhibition are highlighted in grey for both hCNT1 and hCNT3C-. Those protected from PCMBS inhibition with excess 20 mM uridine are underlined. Low activity mutants are indicated by the ▲ symbol. Some constructs were unavailable and denoted by a - symbol. Corresponding numerical values for hCNT3C- are given in Chapter 4, Table 4-2, and those for hCNT1 are given in Table 5-2.

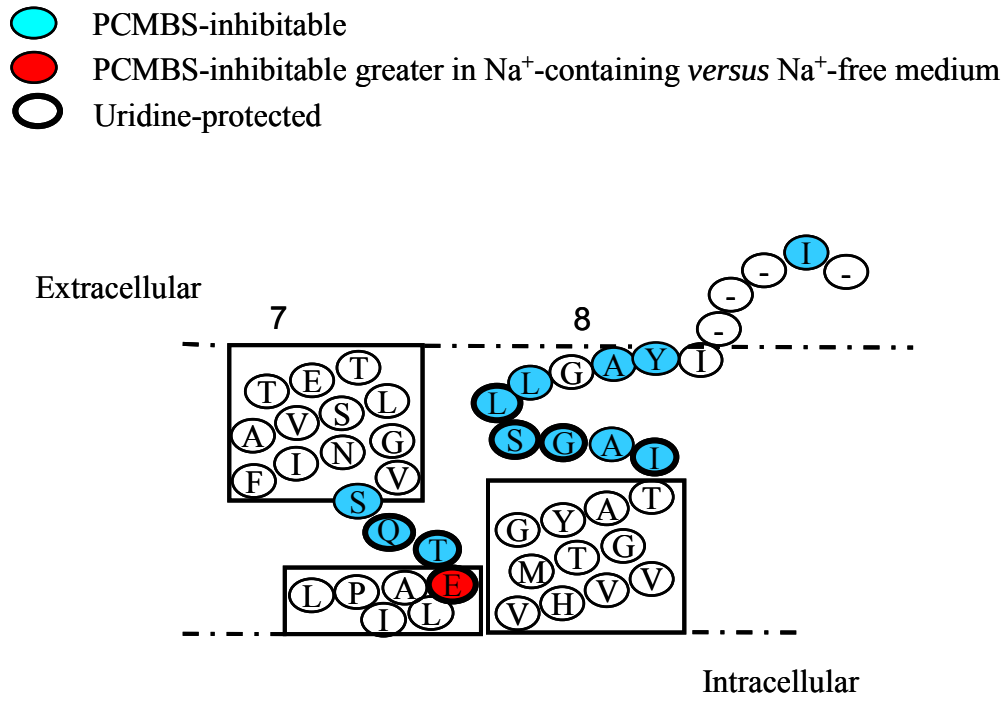

Proposed new topology

Figure 5-5. Revised topology of hCNT1 TMs 7 and 8 depicting discontinuous regions within each transmembrane segment. This schematic depicts a reversal in orientation for the TM 7 – 8 region, and non-conventional helical arrangements for both TMs. PCMBS-sensitive and uridine-protected residues are highlighted according to Figs. 5-3 and 5-4. The single residue exhibiting greater inhibition in Na^+-containing *versus* Na^+-free medium is indicated in *red*. Some constructs were unavailable and denoted by a - symbol. Corresponding numerical values are given in Tables 5-2 and 5-3.

Bibliography

1. Huang, Q. Q., Yao, S. Y. M., Ritzel, M. W. L., Paterson, A. R. P., Cass, C. E., and Young, J. D. (1994) Cloning and functional expression of a complementary DNA encoding a mammalian nucleoside transport protein. *J. Biol. Chem.* **269**: 17757-17760.

2. Che, M., Ortiz, D. F., and Arias, I. M. (1995) Primary structure and functional expression of a cDNA encoding the bile canalicular, purine-specific Na^+-nucleoside cotransporter. *J. Biol. Chem.* **270**: 13596-13599.

3. Ritzel, M. W. L., Yao, S. Y. M., Huang, M. Y., Elliot, J. F., Cass, C. E., and Young, J. D. (1997) Molecular cloning and functional expression of cDNAs encoding a human Na^+-nucleoside cotransporter (hCNT1). *Am. J. Physiol.* **272**: C707-C714.

4. Wang, J., Su, S. F., Dresser, M. J., Schaner, M. E., Washington, C. B., and Giacomini, K. M. (1997) Na^+-dependent purine nucleoside transporter from human kidney: cloning and functional characterization. *Am. J. Physiol.* **273**: F1058-F1065.

5. Ritzel, M. W. L., Yao, S. Y. M., Ng, A. M. L., Mackey, J. R., Cass, C. E., and Young, J. D. (1998) Molecular cloning, functional expression and chromosomal localization of a cDNA encoding a human Na^+/nucleoside cotransporter (hCNT2) selective for purine nucleosides and uridine. *Mol. Membr. Biol.* **15**: 203-211.

6. Smith, K. M, Ng, A. M., Yao, S. Y. M., Labedz, K. A., Knauss, E. E., Wiebe, L. I., Cass, C. E., Baldwin, S. A., Chen, X.-Z., Karpinski, E., and Young, J. D. (2004) Electrophysiological characterization of a recombinant human Na^+-coupled nucleoside transporter (hCNT1) produced in *Xenopus* oocytes. *J. Physiol.* **558**: 807-823.

7. Smith, K. M., Slugoski, M. D., Loewen, S. K., Ng, A. M., Yao, S. Y., Chen, X.-Z., Karpinski, E., Cass, C. E., Baldwin, S. A., and Young, J. D. (2005) The broadly selective human Na^+/nucleoside cotranpsorter (hCNT3) exhibits novel cation-coupled nucleoside transport characteristics. *J. Biol. Chem.* **280**: 25436-25449.

8. Smith, K. M., Slugoski, M. D., Cass, C. E., Baldwin, S. A, Karpinski, E., and Young, J. D. (2007) Cation coupling properties of human concentrative

nucleoside transporters hCNT1, hCNT2 and hCNT3. *Mol Membr Biol*. **24**: 53-64.

9. Ritzel, M. W. L., Ng, A. M. L., Yao, S. Y. M., Graham, K., Loewen, S. K., Smith, K. M., Ritzel, R. G., Mowles, D. A., Carpenter, P., Chen, X.-Z., Karpinski, E., Hyde, R. J., Baldwin, S. A., Cass, C. E., and Young, J. D. (2001) Molecular identification and characterization of novel human and mouse concentrative Na^+-nucleoside cotransporter proteins (hCNT3 and mCNT3) broadly selective for purine and pyrimidine nucleosides (system *cib*). *J. Biol. Chem.* **276**: 2914-2927.

10. Yao, S. Y., Ng, A. M., Loewen, S. K., Cass, C. E., Baldwin, S. A., and Young, J. D. (2002) An ancient prevertabrate Na^+-nucleoside cotransporter (hfCNT) from the Pacific hagfish (*Eptatretus stouti*). *Am. J. Phys. Cell Phys.* **283**: C155-C168.

11. Smith, K. M., Slugoski, M. D., Loewen, S. K., Ng, A. M., Yao, S. Y., Chen, X.-Z., Karpinski, E., Cass, C. E., Baldwin, S. A., and Young, J. D. (2005) The broadly selective human Na^+/nucleoside cotranpsorter (hCNT3) exhibits novel cation-coupled nucleoside transport characteristics. *J. Biol. Chem.* **280**: 25436-25449.

12. Wang, J., and Giacomini, K. M. (1999) Serine 318 is essential for the pyrimidine selectivity of the N2 Na^+-nucleoside transporter. *J. Biol. Chem.* **274**: 2298-2302.

13. Loewen, S. K., Ng, A. M., Yao, S. Y., Cass, C. E., Baldwin, S. A., and Young, J. D. (1999) Identification of amino acid residues responsible for the pyrimidine and purine nucleoside specificities of human concentrative Na^+ nucleoside cotransporters hCNT1 and hCNT2. *J. Biol. Chem.* **274**: 24475-24484.

14. Slugoski, M. D., Loewen, S. K., Ng, A. M., Smith, K. M., Yao, S. Y., Karpinski, E., Cass, C. E., Baldwin, S. A., and Young, J. D. (2007) Specific mutations in transmembrane helix 8 of human concentrative Na^+/nucleoside cotransporter hCNT1 affect permeant selectivity and cation coupling. *Biochemistry*. **46**: 1684-1693.

15. Slugoski, M., D., Smith, K., M., Mulinta, R., Ng, A. M. L., Yao, S. Y. M., Morrison, E. L., Lee, Q., O., T., Zhang, J., Karpinski, E., Cass, C. E., Baldwin,

S. A., and Young, J. D. (2008) A conformationally mobile cysteine residue (Cys-561) modulates Na^+ and H^+ activation of human CNT3. *J. Biol. Chem.* **283**:24922-24934.

16. Yao, S. Y. M., Ng, A. M., Slugoski, M. D., Smith, K. M., Mulinta, R., Karpinski, E., Cass, C. E., Baldwin, S. A., and Young, J. D. (2007) Conserved glutamate residues are critically involved in Na^+/nucleoside cotransport by human concentrative nucleoside transporter 1 (hCNT1). *J. Biol. Chem.* **282**: 30607-30617.

17. Slugoski, M., D., Ng, A. M. L., Yao, S. Y. M., Lin, C. C., Mulinta, R., Cass, C. E., Baldwin, S. A., and Young, J. D. (2009b) Substituted cysteine accessibility method analysis of human concentrative nucleoside transporter hCNT3 reveals a novel discontinuous region of functional importance within CNT family motif (G/A)XKX3NEFVA(Y/M/F). *J. Biol. Chem.* **284**:17281-17292.

18. Slugoski, M. D., Ng, A. M., Yao, S. Y., Smith, K. M., Lin, C. C., Zhang, J., Karpinski, E., Cass, C. E., and Baldwin, S. A., and Young, J. D. (2008) A proton-mediated conformational shift identifies a mobile pore-lining cysteine residue (Cys-561) in human concentrative nucleoside transporter 3. *J. Biol. Chem.* **283**: 8496-8507.

19. Slugoski, M., D., Smith, K., M., Ng, A. M. L., Yao, S. Y. M., Karpinski, E., Cass, C. E., Baldwin, S. A., and Young, J. D. (2009a) Conserved glutamate residues E343 and E519 provide mechanistic insights into cation/nucleoside cotransport by human concentrative nucleoside transporter 3 (hCNT3). *J. Biol. Chem.* **284**:17266-17280.

20. Yamashita, A., Singh, S. K., Kawate, T., Jin, Y., and Gouaux, E. (2005) Crystal structure of a bacterial homolgue of Na^+/Cl^--dependent neurotransmitter transporters. *Nature* **437**: 215-223.

21. Faham, S., Watanabe, A., Besserer, G. M., Cascio D., Specht, A., Hirayama, B., Wright, E. M., and Abramson, J. (2008) The crystal structure of a sodium galactose transporter reveals mechanistic insights into Na^+/sugar symport. *Science*. **321**: 810-814.

22. Hunte, C., Screpanti, E., Venturi, M., Rimon, A., Padan, E., and Michel, H. (2005) Structure of a Na^+/H^+ antiporter and insights into mechanism of action and regulation by pH. *Nature*. **435**: 1197-1202.

23. Weyand, S., Shimamura, T., Yajima, S., Suzuki, S., Mirza, O., Krusong, K., Carpenter, E. P., Rutherford, N. G., Hadden, J. M., O'Reilly, J., Ma, P., Saidijam, M., Patching, S. G., Hope, R. J., Norbertczak, H. T., Roach, P. C., Iwata, S., Henderson, P. J., and Cameron, A. D. (2008) Structure and molecular mechanism of a nucleobase-cation-symport-1 family transporter. *Science*. **322**: 709-713.

24. Yernool, D., Boudker, O., Jin, Y., and Gouaux, E. (2004) Structure of a glutamate transporter homologue from *Pyrococcus horikoshii*. *Nature* **431**: 811-818.

25. Screpanti, E., and Hunte, C. (2007) Discontinuous membrane helices in transport proteins and their correlation with function. *J. Struct. Biol.* **159**: 261-267.

26. Krishnamurthy, H., Piscitelli, C. L., and Gouaux, E. (2009) Unlocking the molecular secrets of sodium-coupled transporters. *Nature* **459**: 347- 355

Chapter 6:

Substituted Cysteine Accessibility Method Analysis of Transmembrane Domains 4 & 5 of *Escherichia coli* H^+/Nucleoside Cotransporter (NupC)

Acknowledgements and Contributions

Technologist Mrs. Mabel Ritzel constructed the single cysteine mutants. All of the cysteine-scanning functional studies were conducted by myself. Postdoctoral Fellow Dr. Shaun Loewen and Summer Student Miss Nadira Mohabir undertook the the functional characterization of NupC(C-). This research was funded by the National Cancer Institute of Canada with funds from the Canadian Cancer Society (now the Canadian Cancer Society Research Institute), Alberta Cancer Board (now the Alberta Health Services- Cancer Care), The Alberta Cancer Foundation, and by the Alberta Cancer Prevention Legacy Fund.

Introduction

NupC, a 400 amino acid residue H^+-coupled CNT family member from the inner membrane of *Escherichia coli*, lacks the first three TMs of mammalian and other eukaryote CNTs and contains 10 predicted membrane-spanning domains (1). NupC was functionally characterized following the expression of its cDNA in *Xenopus* oocytes (2). Recombinant NupC produced in oocytes resembled h/rCNT1 in nucleoside selectivity, including an ability to transport adenosine and the chemotherapeutic drugs 3'-azido-3'-deoxythymidine (AZT), 2',3'- dideoxycytidine (ddC) and 2'-deoxy-2',2'-difluorocytidine (gemcitabine), but also interacted (to a much lesser extent) with inosine and 2',3'- dideoxyinosine (ddI) (2). The apparent affinities for uridine and other physiological nucleosides were higher than those of hCNT1/3, with K_m values in the range 1-6 μM (2). NupC exhibited a hyperbolic proton-activation curve consistent with a H^+:uridine stoichiometry of 1:1 (2), and the kinetics of uridine transport measured as a function of external pH indicated an ordered transport model in which H^+ binds to the transporter first, followed by the nucleoside (2).

SCAM analysis of TM 7 and 8 of hCNT3C-, which is both Na^+- and H^+-dependent, is described in Chapter 4. Following that, SCAM analysis was undertaken for TMs 7 and 8 of exclusively Na^+-dependent hCNT1 (Chapter 5). Since *E. coli* NupC is functional in oocytes, and since the transporter contains only one internal cysteine residue, the present Chapter complements the studies of hCNT3C-/hCNT1 TMs 7 and 8 with a SCAM analysis of the corresponding TMs of cysteine-free NupC(C-) (C96A). In this way, it was hoped to explore whether the discontinuous regions observed in TMs 7 and 8 of hCNT3 and hCNT1 were are a universal feature of all CNT family members, or possibly related to the Na^+ coupling characteristics of the human proteins.

Results

NupC(C-) - The one endogenous cysteine residue present in wild-type NupC (Cys95) was replaced with either serine or alanine to produce cysteine-less NupC constructs C96S and C96A, respectively. Produced in *Xenopus* oocytes, C96S exhibited transport characteristics similar to wild-type NupC, but with lower functional acitivity resulting from a moderate ~ 3-fold increase in uridine apparent K_m, a kinetic deficit that was overcome by conversion of Cys96 instead to alanine (data not shown). In parallel with the SCAM analyses of hCNT3C- and hCNT1 presented in Chapters 4 and 5, NupC C96A [also known as NupC(C-)] was used as template for the construction of single cysteine mutants prior to scanning for functional activity and testing for inhibition by PCMBS. The 45 NupC(C-) residues spanning a region between and including TMs 4 and 5 of NupC (corresponding to hCNT1/3 TMs 7 and 8) that were investigated in the present study are highlighted in Fig. 6-1.

Functional activity of single cysteine mutants – NupC transports nucleosides using the H^+ electrochemical gradient (2). Therefore, to examine the functional activity of single cysteine mutants, uptake of 1 μM radiolabeled uridine was determined in Na^+-reduced, acidified medium (100 mM ChCl, pH 5.5). Initial rates of transport (± S.E.M.) for each mutant produced in *Xenopus* oocytes, in units of pmol/oocyte.10min^{-1}, are given in Table 6-1. The lower uridine concentration used in these experiments (1 μM *versus* 10 μM for hCNT3(C-) and hCNT1) reflects the higher apparent uridine affinity of NupC(C-) (2). Similarly, a flux time of 10-min (*versus* 1-min for hCNT3(C-) and hCNT1) was used to determine initial rates of transport because of the lower overall functional activity of the bacterial transporter. The uptake of 1 μM radiolabeled uridine (100 mM ChCl, pH 5.5) by oocytes expressing NupC(C-) varied between experiments in the range 0.4 to 0.6 pmol/oocyte.10min^{-1} (data not shown). The flux values reported in Table 6-1 and in subsequent Tables and Figures, depict mediated transport activity, defined as the difference in uptake between RNA transcript-injected and control water-injected oocytes, and are from representative experiments. In all studies reported here, uridine uptake in water-injected oocytes was < 0.02 pmol/oocyte.10min^{-1} (data not shown).

Mutants exhibiting uridine uptake values < 0.05 pmol/oocyte.10min^{-1} were excluded from further analysis (Table 6-1). Twelve out of the 45 residues investigated fell into this category (27%). These were: Glu135, Phe137, Gly146, Phe151 and Ile152, in TM 4 and Met166, Thr172, Ser175, Thr176, Met179, Gly183 and Met186 in TM 5.

PCMBS inhibition of single cysteine mutants – Previous control experiments have established the expected lack of inhibition by PCMBS for transport mediated by NupC(C-) in Na^+-free, acidified medium, a finding confirmed here in Fig. 6-2 and Table 6-2. Therefore, single cysteine mutants of NupC(C-) were tested for inhibition by PCMBS under the same conditions (100 mM ChCl, pH 5.5). After 10 min exposure to 200 μM PCMBS, uptake of 1 μM radiolabeled uridine was assayed in medium of the same composition. Exposure to PCMBS was performed on ice to minimize its diffusion across oocyte plasma membranes. In ascending numerical order of residue position, results for each mutant, calculated as a percentage of mediated uridine uptake in the absence of PCMBS, are presented in Fig. 6-2. For screening purposes, a residue was considered to be PCMBS-inhibitable upon exhibiting > 20% reduction in uridine uptake following incubation with PCMBS. Residues that were PCMBS-sensitive are highlighted in Fig. 6-2, and the corresponding numerical values are presented in Table 6-2. A schematic of the locations of these PCMBS-inhibitable residues is presented in Fig. 6-3.

In TM 4, one residue (Ser142) was PCMBS-sensitive in Na^+-reduced, acidified medium upon conversion to cysteine. In TM 5, two pairs of adjacent mutants, S180C(C-)/I181C(C-) and A184C(C-)/Y185C(C-), were PCMBS-sensitive.

Uridine protection from PCMBS inhibition – Subsequent experiments investigated the ability of extracellular uridine (20 mM) to protect against inhibition by PCMBS for residues that were PCMBS-sensitive. Results for each individual mutant are presented in Table 6-2, and the uridine-protectable residues are highlighted in the NupC topology schematics of Fig. 6-3.

S142C(C-) in TM 4 was not uridine-protected. In TM 5, only one of the four residue positions was uridine-protected, I181C(C-).

H^+- mediated PCMBS inhibition of NupC(C-) mutants – Of the 33 functional NupC(C-) mutants in the TMs 4 – 5 region investigated, 5 were inhibited by PCMBS (Table 6-2, Fig. 6-2 and Fig. 6-3). To determine if access of PCMBS to these residues required a H^+-induced conformational change within the protein, each of the single cysteine mutants at these positions were re-screened for PCMBS inhibition under the original condition (Na^+-reduced, acidified) and in Na^+-reduced, H^+-reduced medium (100 mM ChCl pH 8.5). Fluxes of 1 μM uridine were then determined under Na^+-reduced, acidified conditions (Table 6-3).

Four of the 5 mutants were inhibited by PCMBS to similar extents under both conditions, indicating that PCMBS inhibition was not H^+-induced. In marked contrast, however, Y185C(C-) in TM 5 was inhibited by PCMBS to a greater extent under acidified conditions than under H^+-reduced conditions, suggesting that, like Cys561 of hCNT3 (3), Tyr185 of NupC becomes more extracellularly accessible to PCMBS in the presence of H^+, thus reporting a H^+-dependent conformation of the protein.

Discussion

Studies from this laboratory have previously used PCMBS to investigate individual topological features and residues of human CNT family members hCNT1 and hCNT3 [(4), Appendix 1 (5) and (6)]. The present investigation of TMs 4 and 5 of *E. coli* CNT NupC(C-) extends the systematic SCAM analysis of the corresponding regions in hCNT3C- and hCNT1 reported in Chapters 4 and 5 of this thesis. Similarities and differences between the results for NupC(C-) and hCNT3(C-) and hCNT1 are apparent, all three transporters providing evidence that residues within these two TMs contribute to cation/nucleoside translocation.

Functional activity of NupC(C-) mutants – Initial characterization of the NupC(C-) single cysteine mutants in the present study measured uridine uptake in acidified (H^+-containing) medium (Table 6-1). Of the 43 mutants examined, 12

exhibited uridine uptake values < 0.05 pmol/oocyte.10min^{-1} (Table 6-1). Five were in TM 4 (E135C(C-), F137C(C-), G146C(C-), F151C(C-) and I152C(C-)), and the seven in TM 5 (M166C(C-), T172C(C-), S175C(C-), T176C(C-), M179C(C-), G183C(C-) and M186C(C-)). Consequently, these mutants were excluded from further functional analysis. Mutagenesis of NupC(C-) resulted in a higher percentage of non-functional mutants when compared to hCNT3C- or hCNT1. This may, in part, reflect production in a eukaryote heterologous expression system and the attendant lower overall transport activity exhibited by the bacterial transporter. As shown in the sequence alignment of Fig. 3-6, however, most of the "non-functional" NupC(C-) mutants cluster to the same regions of TMs shown in Chapters 4 and 5 to be functionally important for hCNT3C- and hCNT1. For hCNT3(C-), H^+-coupling appears to be generally more sensitive to mutation than Na^+-coupling and, since NupC is exclusively H^+-dependent, this may also be a contributing factor.

PCMBS inhibition of NupC(C-) mutants: topological and mechanistic implications – To summarize the data presented in Table 6-2 and Fig. 6-2, the schematics in Fig. 6-3 highlight those TMs 4 – 5 residues identified in NupC(C-) as PCMBS-sensitive and uridine-protected.

In TM 4, PCMBS inhibition is evident only for residue position Ser142, and this inhibition was not uridine protectable. This residue is not part of the cluster of adjacent residues found to be PCMBS-sensitive in hCNT3C- and hCNT1. However, it is centrally positioned in the TM (Fig. 6-4), and precedes by one position a residue in hCNT3C- (Ile337) that was sensitive to PCMBS inhibition under Na^+-reduced, acidified conditions (Chapter 4). In TM 5, two pairs of adjacent mutants, S180C(C-)/I181C(C-) and A184C(C-)/Y185C(C-), were found sensitive to PCMBS inhibition. Only I181C(C-) was protected from PCMBS inhibition by excess uridine. The corresponding residues in hCNT3C- and hCNT1 are part of the cluster of adjacent residues that were also sensitive to PCMBS inhibition (Chapters 4 and 5) (Fig. 6-4). Although these PCMBS-sensitive residues in NupC(C-) fall within the regions of proposed helical discontinuity observed in hCNT3C- and hCNT1, they are not as expansive. If

access to PCMBS and resultant transport inhibition reflects the compactness (or otherwise) of membrane-spanning regions, then TMs 4 and 5 of NupC(C-) appear more compact that the corresponding TMs 7 and 8 regions of hCNT3(C-) and hCNT1. With the caveat of potential hydrophobic mismatch resulting from insertion into a eukaryote membrane environment, it is hypothesized that the absence of major regions of discontinuity in NupC may be mechanistically related to the bacterial transporter being exclusively H^+-coupled, in contrast to its human counterparts, both of which are Na^+-dependent.

At the very least, the present results provide supporting evidence that both TMs contribute to the CNT translocation pore. Because NupC(C-) PCMBS-sensitive residues in TM 5 are predicted to be within the endofacial half of the membrane (according to the original topology of NupC shown in Fig. 6-3*A*), the data also indicate a reversed membrane orientation for both TMs (Fig. 6-3*B*). Within TM 5, PCMBS-sensitivity of one of the residues (Tyr185) reports a H^+-dependent conformation of the protein.

Conclusions – The present Chapter describes the successful use of the *Xenopus* oocyte heterologous expression system to undertake PCMBS SCAM analysis of *E. coli* NupC(C-). TMs 4 and 5 of NupC(C-), like their counterparts in hCNT1/3, contribute to a common cation/nucleoside translocation pore, and have a membrane orientation opposite to that originally predicted. More compact in terms of PCMBS inhibition than the corresponding TMs of hCNT1/3, one of the identified PCMBS-sensitive residues in TM 5, Tyr185, resembles Cys561 in TM 12 of hCNT3 (3) and senses a H^+-induced change in transporter conformation.

TABLE 6-1: **Uptake of uridine in *Xenopus* oocytes expressing NupC(C-) single cysteine mutants.** Influx of 1 μM ^{3}H-uridine was measured in Na^{+}-reduced, acidified media (100 mM ChCl, pH 5.5). Values are corrected for basal non-mediated uptake in control water-injected oocytes. Each value is the mean ± S.E.M. of 10-12 oocytes.

	Mediated Uridine Uptake (pmol/oocyte.10 min^{-1}) H^{+} (100 mM ChCl, pH 5.5)		
TM 4		TM 5	
L134C(C-)	0.18 ± 0.02	M166C(C-)	< 0.05
E135C(C-)	< 0.05	Y167C(C-)	0.10 ± 0.01
S136C(C-)	0.50 ± 0.09	T168C(C-)	0.06 ± 0.01
F137C(C-)	< 0.05	M169C(C-)	0.05 ± 0.01
N138C(C-)	0.14 ± 0.02	A170C(C-)	0.20 ± 0.04
A139C(C-)	0.11 ± 0.02	A171C(C-)	0.15 ± 0.02
V140C(C-)	0.49 ± 0.04	T172C(C-)	< 0.05
S141C(C-)	0.39 ± 0.04	A173C(C-)	0.18 ± 0.02
S142C(C-)	0.47 ± 0.06	M174C(C-)	0.11 ± 0.01
L143C(C-)	0.77 ± 0.08	S175C(C-)	< 0.05
I144C(C-)	0.18 ± 0.03	T176C(C-)	< 0.05
L145C(C-)	0.48 ± 0.05	V177C(C-)	0.10 ± 0.01
G146C(C-)	< 0.05	S178C(C-)	0.19 ± 0.02
Q147C(C-)	0.15 ± 0.02	M179C(C-)	< 0.05
S148C(C-)	0.67 ± 0.06	S180C(C-)	0.15 ± 0.02
E149C(C-)	0.10 ± 0.01	I181C(C-)	0.56 ± 0.06
N150C(C-)	1.1 ± 0.1	V182C(C-)	0.05 ± 0.01
F151C(C-)	< 0.05	G183C(C-)	< 0.05
I152C(C-)	< 0.05	A184C(C-)	0.08 ± 0.02
A153C(C-)	0.79 ± 0.10	Y185C(C-)	0.07 ± 0.01
Y154C(C-)	0.11 ± 0.03	M186C(C-)	< 0.05
TM 5 – 6 Loop			
L190C(C-)	0.26 ± 0.02		
NupC(C-)	0.64 ± 0.04		

TABLE 6-2: **Effects of PCMBS on uridine uptake in *Xenopus* oocytes expressing NupC(C-) single cysteine mutants.** Influx of 1 μM ^{3}H-uridine was measured in Na^{+}-reduced, acidified media (100 mM ChCl, pH 5.5) following 10 min incubation on ice in the absence or presence of 200 μM PCMBS or 200 μM PCMBS + 20 mM uridine in medium of the same composition used to determine uptake. Values are corrected for basal non-mediated uptake in control water-injected oocytes and are presented as a percentage of mediated uridine influx in the absence of inhibitor for each individual mutant. Each value is the mean ± S.E.M. of 10-12 oocytes. The symbol * indicates substrate protection.

		Uptake (%) (100 mM ChCl, pH 5.5)	
TM		+ PCMBS[a]	+ PCMBS + uridine
4	S142C (C-)	56 ± 4	47 ± 4
5	S180C (C-)	48 ± 9	45 ± 10
	I181C (C-)	47 ± 6	*95 ± 14
	A184C (C-)	43 ± 2	45 ± 4
	Y185C (C-)	34 ± 10	40 ± 11
Control	NupC(C-)	96 ± 1	-

[a], mediated uridine influx in the absence of inhibitor is given in pmol/oocytes.10 min^{-1} in Table 6-1 for each of the individual mutants.

TABLE 6-3: **Effects of H^+ on PCMBS inhibition of NupC(C-) single cysteine mutants.** Influx of 1 μM ^{3}H-uridine was measured in Na^+-reduced, acidified media (100 mM ChCl, pH 5.5; 10 min; 20 ºC) following 10 min incubation on ice in the absence or presence of PCMBS in either Na^+-reduced, H^+-reduced or Na^+-reduced, acidified media medium (100 mM ChCl pH 8.5, 100 mM ChCl, pH 5.5, respectively). Values are corrected for basal non-mediated uptake in control water-injected oocytes and are normalized to the respective influx of uridine in the absence of inhibitor. Each value is the mean ± S.E.M. of 10-12 oocytes.

	Uptake (%) (100 mM ChCl, pH 5.5)	
	+ PCMBS in H^+-reduced medium	+ PCMBS in acidified medium
TM 4		
S142C(C-)	39 ± 21	29 ± 7
TM 5		
S180C(C-)	53 ± 4	57 ± 5
I181C(C-)	50 ± 7	38 ± 7
A184C(C-)	11 ± 5	2 ± 3
Y185C(C-)	30 ± 6	5 ± 7

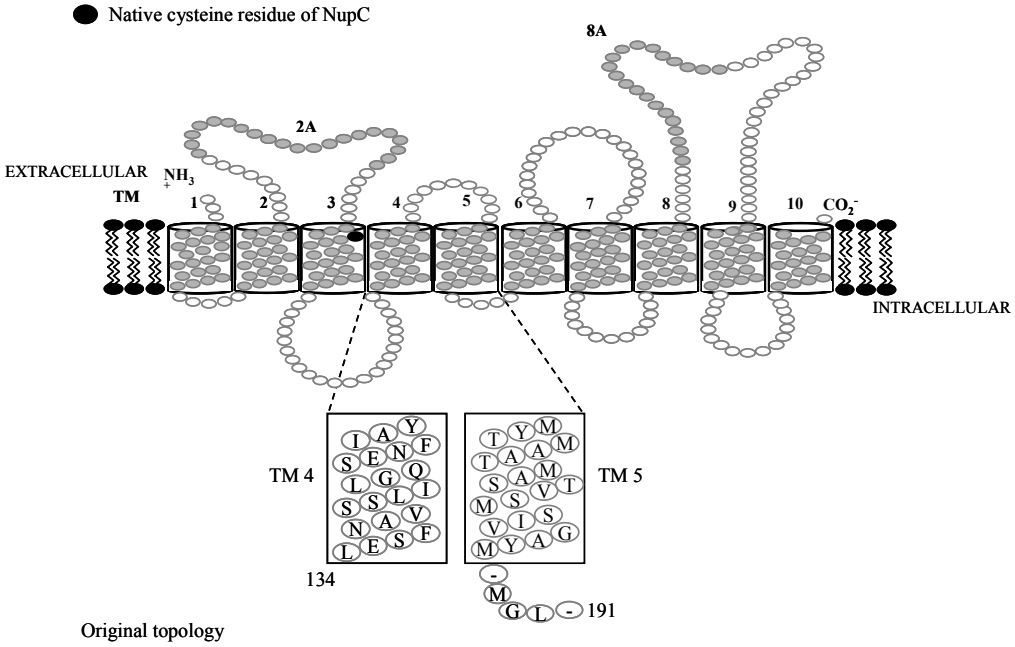

Figure 6-1. Original NupC topology. Schematic of original NupC (GenBank™ accession number NC000913) topology with 10 TMs. Insertion of TMs 2A and 8A (corresponding to hCNT1/3 TMs 5A and 11A) into the membrane will result in opposite orientations of TMs 3 - 7. The position of an endogenous cysteine residue is indicated as *black* residue. Residues studied by SCAM analysis are depicted in the *inset*. Some constructs were unavailable and denoted by a - symbol.

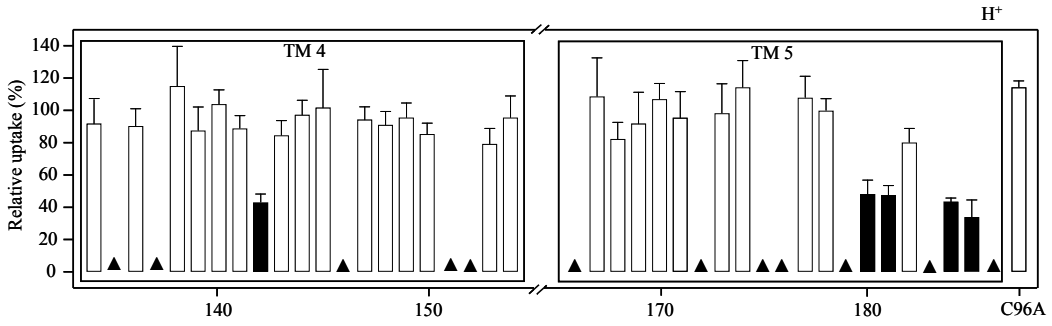

Figure 6-2. PCMBS inhibition of residues in the TM 4 – 5 region of NupC(C-). Mediated influx of 1 μM radiolabeled uridine in Na^+-reduced, acidified medium (100 mM ChCl, pH 5.5) was measured following 10 min incubation on ice in the same medium in the presence of 200 μM PCMBS. *Solid* columns indicate residue positions inhibited by PCMBS. Low activity mutants are indicated by the ▲ symbol. Data are presented as mediated transport, calculated as uptake in RNA-injected oocytes *minus* uptake in water-injected oocytes, and are normalized to influx of uridine in the absence of inhibitor. Each value is the mean ± S.E.M. of 10-12 oocytes. Control NupC(C-), also known as NupC C96A, was included as a control for all experiments. Corresponding numerical values are given in Table 6-2.

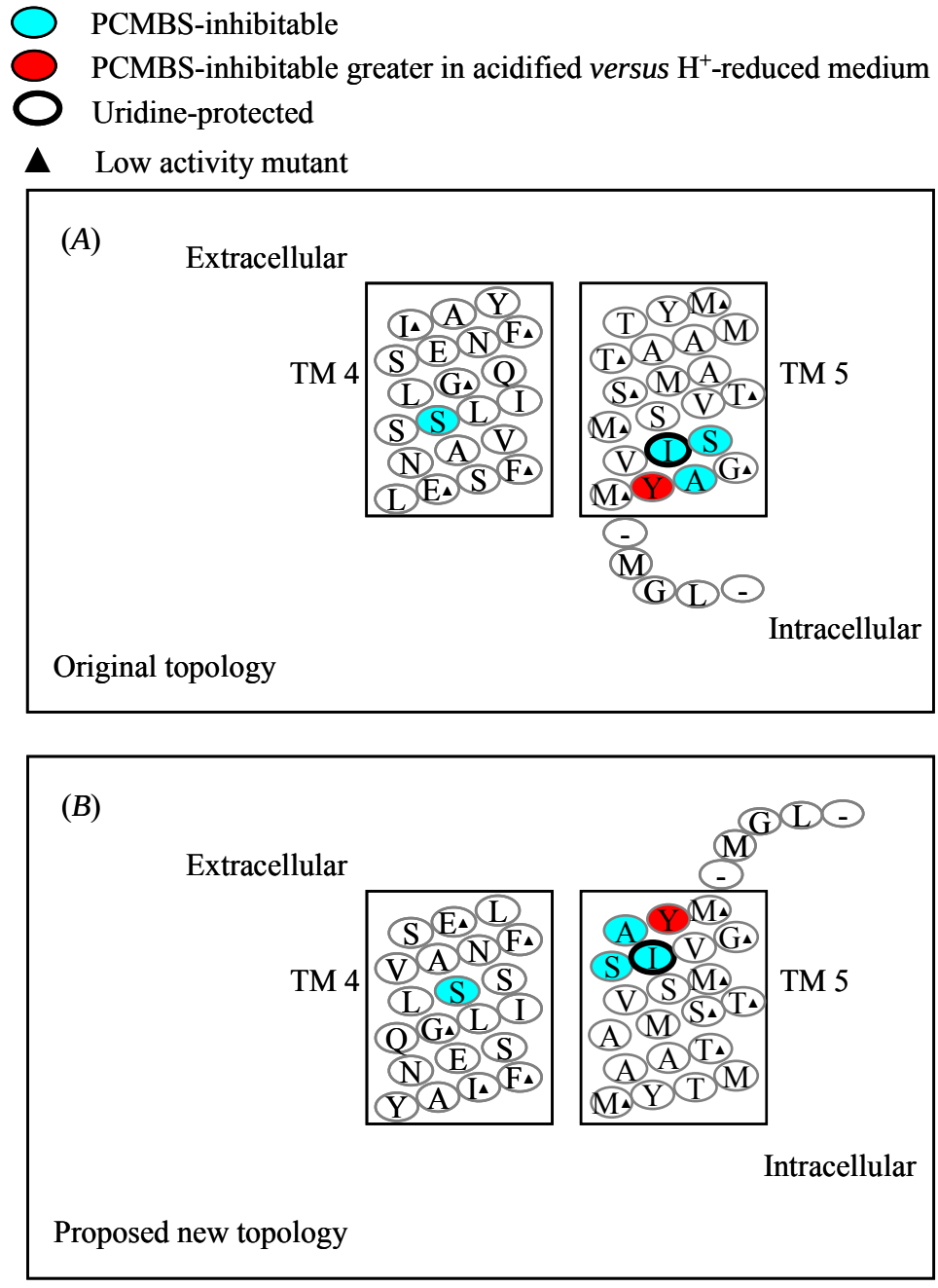
PCMBS-inhibitable
PCMBS-inhibitable greater in acidified versus H+-reduced medium
Uridine-protected
Low activity mutant
(A)
Extracellular
TM 4
TM 5
Intracellular
Original topology
(B)
Extracellular
TM 4
TM 5
Intracellular
Proposed new topology

Figure 6-3.

Figure 6-3. NupC(C-) TM 4 – 5 region depicting PCMBS-inhibited and uridine-protected residues. NupC(C-) mutants exhibiting inhibition of uridine uptake following incubation with PCMBS in both acidified and H^+-reduced media are indicated in *blue*. The single residue exhibiting greater inhibition in acidified *versus* H^+-reduced medium is indicated in *red*. The residue protected from PCMBS inhibition by excess unlabeled uridine is outlined in *black*. Low activity mutants are indicated by the ▲ symbol. Some constructs were unavailable for testing and are denoted with a - symbol.Corresponding numerical values are given in Table 6-2. *A*, original membrane topology. *B*, proposed new topology.

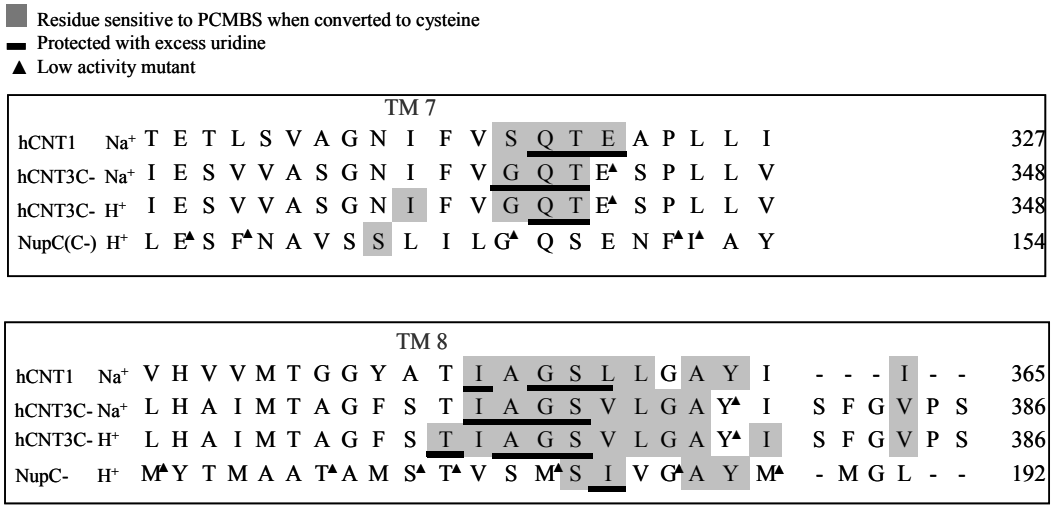

Figure 6-4. Comparison of PCMBS inhibition and substrate protection of residues in the TM 4 & 5 region of NupC with the corresponding TM 7 & 8 regions of hCNT3C- and hCNT1. Residues sensitive to PCMBS inhibition are highlighted in grey for NupC(C-), hCNT1 and hCNT3C-. Those protected from PCMBS inhibition with excess 20 mM uridine are underlined. Low activity mutants are indicated by the ▲ symbol. Some constructs were unavailable for testing and are denoted with a - symbol. Corresponding numerical values are given in Chapter 4 Table 4-2, in Chapter 5 Table 5-2, and in Table 6-2 of the present Chapter.

Bibliography

1. Craig, J. E., Zhang, Y., and Gallagher, M. P. (1994) Cloning of the nupC gene of *Escherichia coli* encoding a nucleoside transport system, and identification of an adjacent insertion element, IS 186. *Mol. Micr.* **11**: 1159-1168.

2. Loewen, S. K., Yao, S. Y., Slugoski, M. D., Mohabir, N. N., Turner, R. J., Mackey, J. R., Gallagher, M. P., Henderson, P. J., Baldwin, S. A., Cass, C. E., and Young, J. D. (2004) Transport of physiological nucleosides and anti-viral and anti-neoplastic nucleoside drugs by recombinant *Escherischia coli* nucleoside-H^+ cotransporter (NupC) produced in *Xenopus laevis* oocytes. *Mol. Membr. Biol.* **21**: 1-10.

3. Slugoski, M. D., Ng, A. M., Yao, S. Y., Smith, K. M., Lin, C. C., Zhang, J., Karpinski, E., Cass, C. E., and Baldwin, S. A., and Young, J. D. (2008) A proton-mediated conformational shift identifies a mobile pore-lining cysteine residue (Cys-561) in human concentrative nucleoside transporter 3. *J. Biol. Chem.* **283**: 8496-8507.

4. Slugoski, M. D., Loewen, S. K., Ng, A. M., Smith, K. M., Yao, S. Y., Karpinski, E., Cass, C. E., Baldwin, S. A., and Young, J. D. (2007) Specific mutations in transmembrane helix 8 of human concentrative Na^+/nucleoside cotransporter hCNT1 affect permeant selectivity and cation coupling. *Biochemistry*. **46**: 1684-1693.

5. Yao, S. Y. M., Ng, A. M., Slugoski, M. D., Smith, K. M., Mulinta, R., Karpinski, E., Cass, C. E., Baldwin, S. A., and Young, J. D. (2007) Conserved glutamate residues are critically involved in Na^+/nucleoside cotransport by human concentrative nucleoside transporter 1 (hCNT1). *J. Biol. Chem.* **282**: 30607-30617.

6. Slugoski, M., D., Smith, K., M., Ng, A. M. L., Yao, S. Y. M., Karpinski, E., Cass, C. E., Baldwin, S. A., and Young, J. D. (2009a) Conserved glutamate residues E343 and E519 provide mechanistic insights into cation/nucleoside cotransport by human concentrative nucleoside transporter 3 (hCNT3). *J. Biol. Chem.* **284**:17266-17280.

Chapter 7:

Substituted Cysteine Accessibility Method Analysis of Transmembrane Domains 9 & 10 of Human Na^+/Nucleoside Cotransporter 3 (hCNT3)

Acknowledgements and Contributions

All of the research described in this Chapter, including construction of hCNT3C- single cysteine mutants, was undertaken by myself. This research was funded by the National Cancer Institute of Canada with funds from the Canadian Cancer Society (now the Canadian Cancer Society Research Institute), Alberta Cancer Board (now the Alberta Health Services- Cancer Care), The Alberta Cancer Foundation, and by the Alberta Cancer Prevention Legacy Fund.

Introduction

In Chapters 4 to 6, I have undertaken a PCMBS SCAM analysis of hCNT3C- TMs 7 and 8, as well as the corresponding regions in hCNT1 and NupC(C-). Since previous research has emphasized the functional importance of C-terminal half of the protein in terms of interactions with both permeant and cations, the present Chapter extends the study to a parallel SCAM analysis of hCNT3C- TMs 9 and 10. The results identify further residues of functional importance, indicate close proximity cation/nucleoside binding and translocation, provide additional evidence of novel discontinuous regions within helices, and support a revised model of hCNT membrane topology.

Results

All 14 endogenous cysteine residues of hCNT3 were replaced with serine to produce the cysteine-less hCNT3 construct, hCNT3C- [(1) and Chapter 3 (2)]. hCNT3C- retained wild-type hCNT3 functional activity [Chapter 3 (2)] and, parallel with previous described studies in this thesis (Chapters 4-6), was used as a template for the construction of single cysteine mutants prior to scanning for functional activity and inhibition by PCMBS. The 92 residue positions of hCNT3C- spanning a region between and including TMs 9 and 10 that were investigated in the present study are highlighted in Fig. 7-1.

Functional activity of single cysteine mutants – hCNT3 transports nucleosides using both Na^+ and H^+ electrochemical gradients (3, 4). Therefore, to examine the functional activity of hCNT3C- single cysteine mutants, uptake of 10 μM radiolabeled uridine was determined in both Na^+-containing, H^+-reduced medium (100 mM NaCl, pH 8.5) and in Na^+-reduced, acidified medium (100 mM ChCl, pH 5.5, respectively). The Na^+-containing medium was buffered at pH 8.5 to avoid the small but significant H^+ activation of hCNT3 that occurs at pH 7.5 (4, 5). Previously, we have verified that Na^+-coupled uridine transport by hCNT3 at pH 8.5 is kinetically indistinguishable from that at pH 7.5 (5), and SCAM analysis

of the TM 7 – 8 region of hCNT3 also tested mutants for functional activity under the same conditions (Chapter 4). Initial rates of transport (± S.E.M.) for each mutant, in units of pmol/oocyte.min^{-1}, are given in Table 7-1. The uptake of 10 μM radiolabeled uridine (100 mM NaCl, pH 8.5) by oocytes expressing hCNT3C- varied between experiments in the range 2 to 4 pmol/oocyte.min^{-1} (data not shown). The flux values reported in Table 7-1, and in subsequent Tables and Figures, depict mediated transport activity, defined as the difference in uptake between RNA transcript-injected and control water-injected oocytes, and are from representative experiments. In all studies reported here, uridine uptake in water-injected oocytes was < 0.02 pmol/oocyte.min^{-1} (data not shown).

In other SCAM studies of hCNT3C- reported in this thesis, mutants exhibiting uridine uptake values < 0.1 pmol/oocyte.min^{-1} were excluded from further analysis. None of the hCNT3C- TM 9 and 10 mutants that were tested fell into this category (Table 7-1).

To facilitate comparisons between mutants, the uridine transport activity of each construct is presented as the ratio of Na^+-mediated to H^+-mediated uptake (Na^+:H^+) in Table 7-1. The corresponding Na^+:H^+ ratios of uridine uptake (10 μM) for wild-type hCNT3 and for cysteine-less hCNT3C- were ~ 1.7 and 1.0, respectively (averaged results from multiple experiments; data not shown), and were in good agreement with results of previous studies [Chapter 3 (2) and (3-5)]. Residue mutations that resulted in Na^+:H^+ ratios of uridine uptake < 0.5 and > 2.5 (Table 7-1) are highlighted in the hCNT3 topology schematic shown in Fig. 7-2.

Most of the mutants exhibited Na^+:H^+ uptake ratios similar to that of hCNT3/hCNT3C-. In contrast, mutants L389C(C-) and M395C(C-) in TM 9 presented Na^+:H^+ ratios of 5.9 and 0.4 respectively. L461C(C-) in TM 10 had a Na^+:H^+ ratio of 0.3.

PCMBS inhibition of single cysteine mutants – Wild-type hCNT3 has previously reported been to be sensitive to inhibition by PCMBS under acidic conditions only (*i.e.,* in Na^+-reduced, acidified medium) (5), there being no corresponding inhibition of the transporter in either Na^+-containing, H^+-reduced or Na^+-reduced, H^+-reduced media (5). Therefore, single cysteine mutants of

hCNT3C- were tested for inhibition by PCMBS both in Na^+-containing, H^+-reduced medium (100 mM NaCl, pH 8.5) and in Na^+-reduced, acidified medium (100 mM ChCl, pH 5.5). After 10 min exposure to 200 μM PCMBS, uptake of 10 μM radiolabeled uridine was assayed in medium of the same composition. Exposure to PCMBS was performed on ice to minimize its diffusion across oocyte plasma membranes [(5), Chapters 4 and 8 (6) and Appendix 1 (7)]. In ascending numerical order of residue position, results for each mutant calculated as a percentage of mediated uridine uptake in the absence of PCMBS are presented in Fig. 7-3. For screening purposes, a residue was considered to be PCMBS-inhibitable upon exhibiting > 20% inhibition of uridine uptake following incubation with PCMBS. Residues that were PCMBS-sensitive are highlighted in Fig. 7-3, and the corresponding numerical flux values are presented in Table 7-2. A schematic of the locations of these PCMBS-inhibitable residues is presented in Fig. 7-4. Fig. 7-3 and Table 7-2 also include control data for wild-type hCNT3 (only inhibited by PCMBS in Na^+-reduced, acidified medium) and hCNT3C- (unaffected by PCMBS either in Na^+-containing, H^+-reduced medium or in Na^+-reduced, acidified medium).

PCMBS inhibition was observed in both Na^+-containing, H^+-reduced and Na^+-reduced, acidified medium for four adjacent mutants in TM 9 (L390C(C-), T391C(C-), A392C(C-) and S393C(C-)). In close proximity to this block of residues, three additional mutants (H388C(C-), V394C(C-) and M395C(C-)) were sensitive to PCMBS inhibition only in Na^+-reduced, acidified medium. Within TM 10, two mutants (I450C(C-) and L461C(C-)) were sensitive to PCMBS inhibition only in Na^+-reduced, acidified medium.

Uridine protection of PCMBS inhibition – Subsequent experiments investigated the ability of extracellular uridine (20 mM) to protect against inhibition by PCMBS for residues that were PCMBS-inhibitable in either or both cation conditions. Results for each individual mutant are presented in Table 7-2, and the uridine-protectable residues are highlighted in the hCNT3 topology schematic of Fig. 7-4.

In TM 9, five residue positions were protected against PCMBS inhibition by uridine. V394C(C-) and M395C(C-), which were PCMBS-inhibited only in Na^+-reduced, acidified medium, showed full uridine protection, and T391C(C-) and S393C(C-), which were PCMBS-inhibited in both Na^+-containing, H^+-reduced and Na^+-reduced, acidified media were also fully uridine protected under both cation conditions. In contrast, A392C(C-), which was also PCMBS-inhibited under both cation conditions, was protected by uridine only in Na^+-containing, H^+-reduced medium. None of the PCMBS-sensitive mutants in TM 10 were protected by uridine.

H^+- mediated PCMBS inhibition of hCNT3C- – Of the 9 hCNT3C- residue positions in the TM 9 – 10 region that were PCMBS-sensitive, 4 were inhibited by PCMBS in both Na^+-containing, H^+-reduced and Na^+-reduced, acidified media, while 5 were inhibited by PCMBS in Na^+-reduced, acidified medium only (Table 7-2 and Fig. 7-4). To determine if access of PCMBS to these residues required cation-induced conformational changes within the protein, each of the single cysteine mutants at these positions were re-screened for PCMBS inhibition under the original conditions (Na^+-containing, H^+-reduced and Na^+-reduced, acidified media) and in Na^+-reduced, H^+-reduced medium (100 mM ChCl pH 8.5) and in Na^+-containing, acidified medium (100 mM NaCl pH 5.5). Fluxes of 10 μM uridine were then determined under Na^+-reduced, acidified conditions (Table 7-3).

All 4 of the mutants that were inhibited by PCMBS in both Na^+-containing, H^+-reduced and Na^+-free, acidified media were also inhibited by PCMBS in Na^+-free, H^+-reduced and Na^+-containing, acidified media (Table 7-3), indicating that PCMBS inhibition was not cation-induced. However, the five mutants that exhibited PCMBS inhibition under Na^+-reduced, acidified conditions only (H388C(C-), V394C(C-), M395C(C-) in TM 9 and I450C(C-) and L461C(C-) in TM 10) were unaffected by PCMBS under cation-reduced conditions (Na^+-free, H^+-reduced medium), but strongly inhibited by PCMBS in Na^+-containing, acidified medium. Similar to residues Ile337 in TM 7, Tyr370 in TM 8, Ile554, Tyr558 and Cys561 in TM 12 of hCNT3 [Chapters 4, 8 (6)], therefore, access of PCMBS to these residue positions reports a specific H^+-induced conformation of the transporter.

Discussion

Studies from this laboratory have previously used PCMBS to investigate individual topological features and residues of hCNT1 and hCNT3 [Appendix 1 (7) and (8, 9)]. Adding to SCAM results for the TM 7 – 8 region of hCNT3C-, presented in Chapter 4 of this thesis, the present investigation extends this analysis to hCNT3C- TMs 9 and 10 (Fig. 7-1).

Functional activity of hCNT3C- mutants – Initial characterization of the hCNT3C- single cysteine mutants in the present study measured uridine uptake in both Na^+-containing, H^+-reduced and Na^+-reduced, acidified media (Table 7-1). Of the 92 mutants examined, all retained functional activity under both cation conditions (Table 7-1).

hCNT3 couples nucleoside transport to both Na^+ and H^+ electrochemical gradients and exhibits a Na^+:H^+ ratio of uridine uptake (10 μM) of ~ 1.7 (3, 4). Similarly, hCNT3C- also mediates both Na^+- and H^+-coupled uridine transport, although the apparent K_{50} for Na^+ is increased ~ 11-fold, decreasing the Na^+:H^+ ratio of uridine uptake (10 μM) to ~ 1.0 [Chapter 3 (2)]. Table 7-1 and Fig. 7-2 highlight those residues for which mutation to cysteine in hCNT3C- resulted in Na^+:H^+ uridine uptake ratios either < 0.5 (*i.e.*, H^+-preferring) or > 2.5 (*i.e.*, Na^+-preferring). Such characteristics identified residues likely to be involved directly or indirectly in interactions with the coupling cation. Corresponding residues in the TM 7 – 8 region of the protein include Ile337, Ser330, Ser334, Gly335, Asn336, Val339, Gly340, Gln341, Ser344 and Pro345 in TM 7, Leu352 in the loop between TMs 7 and 8, and Ser369, Thr370, and Val375 in TM 8. Further analysis of the roles of these newly identified amino acids in cation coupling is in progress (Chapter 9).

PCMBS inhibition of hCNT3C- mutants: topological and mechanistic implications – To summarize the data presented in Table 7-2 and Fig. 7-3, the schematic in Fig. 7-4 highlights those TM 9 – 10 residues identified in hCNT3C- as PCMBS-sensitive and uridine-protected.

In hCNT3C- TM 9, the patterning of PCMBS inhibition paralleled that seen in TM 8 (Chapter 4), such that six adjacent residues were found to be inhibited by PCMBS when each was mutated to a cysteine (Leu390, Thr391, Ala392 and Ser393 in both cation conditions, and Val394 and Met395 in Na^+-free, acidified medium). Another residue (His388) that was also sensitive to PCMBS inhibition in Na^+-free, acidified medium was separated from the block of six consecutive PCMBS-sensitive residues by a single residue. According to the original 13 TM topology proposed for hCNTs, His388 sits deepest in the membrane at the endofacial boundary of the TM. Like TMs 7 and 8 (Chapter 4), therefore, and as shown diagrammatically in Fig. 7-5, we predict that TM 9 is reversed in its orientation, such that the PCMBS-inhibitable residues lie exofacially within the helix, in a position more likely to be accessible to the extracellular medium and available for PCMBS binding. Also similar to TMs 7 and 8, and based on the observed patterning of PCMBS inhibition, we propose that TM 9 contains a region of discontinuity within an α-helical structure (Fig. 7-5).

The SCAM analysis of TM 10, in contrast, predicts a conventional α-helix, as shown by the helical wheel projection inset in Fig. 7-5. The evidence presented in this Chapter suggests that the entire TM 7 – 10 region of the transporter, including TM 10, is in the opposite orientation (Fig. 7-5) to that proposed in the original 13 TM topology shown in Fig. 1. As will be revealed in SCAM analyses on the rest of the C-terminal half of hCNT3, TMs 11 – 13, this is made possible by reversal of TM 11 and insertion of region 11A into the membrane [Chapter 8 (6)]. Since TM 9 contains numerous residues sensitive to PCMBS inhibition and protected by uridine, some of which also have altered Na^+:H^+ uptake ratios, we predict that TM 9, similar to TMs 7 and 8 (Chapter 4), contributes to the translocation pore and nucleoside and cation binding pockets. TM 10 contained no residues for which uptake was inhibited by PCMBS by > 80%, whereas TM 7 contained two (Gly340 and Thr342) (Chapter 4), TM 8 contained five (Thr370, Ile371, Ala372, Gly373 and Val375) (Chapter 4) and TM 9 contained two (Leu390 and Ala392). In contrast, only two residues in TMs 10 were moderately

inhibited by PCMBS (Ile459 and Lys461), and neither was uridine-protected. Thus, TM 10 may be less directly involved in formation of the translocation pore than TMs 7 – 9 (Chapter 4).

PCMBS-sensitivity of three residues in TM 9 (H388C(C-), V394C(C-), M395C(C-)) and two residues in TM 10 (I450C(C-) and L461C(C-)) report a H^+-dependent conformation of the protein.

Conclusions – The present SCAM analysis of the TM 9 – 10 region of hCNT3C- completes the study of the first 4 C-terminal TMs of the protein: results for TMs 7 – 8 and 11 – 13 are presented in Chapters 4 & 8 (6). The results highlight potential functionally important residues in TMs 9 and 10. The results also support a revised topology model for hCNTs, with a reversed membrane orientation of TMs 7 – 10 and the presence of discontinuous regions within TMs 7, 8 and 9, with TM 10 adopting the conventional α-helical structure. Confirmation of this new membrane architecture comes in the next Chapter which extends the SCAM analysis to hCNT3C- TMs 11-13 [Chapter 8 (6)].

It is striking that all 50 extramembraneous residues studied in the loops between TMs 9 and 10 and that following TM 10 were PCMBS-insensitive. Also, none of the loop residues exhibited marked changes in uridine Na^+:H^+ uptake ratio. The loops between TMs 7 and 8 and between TM 9 and 10 were also relatively "silent". Instead, highlighted residue positions cluster within TMs, giving confidence that PCMBS cysteine-scanning mutagenesis as used in this thesis accurately identifies topological and other features of mechanistic importance.

Table 7-1. Na^+- and H^+-mediated uptake of uridine in *Xenopus* oocytes expressing hCNT3C- single cysteine mutants. Influx of 10 μM ^{14}C-uridine or ^{3}H-uridine was measured in both Na^+-containing, H^+-reduced and Na^+-reduced, acidified media (100 mM NaCl, pH 8.5 or 100 mM ChCl, pH 5.5, respectively). Na^+:H^+ uptake ratios which are < 0.5 or > 2.5 are highlighted with an asterisk (*). Values are corrected for basal non-mediated uptake in control water-injected oocytes. Each value is the mean ± S.E.M. of 10-12 oocytes.

	Mediated Uridine Uptake (pmol/oocyte.min^{-1})		
TM 9	Na^+ (100 mM NaCl, pH 8.5)	H^+ (100 mM ChCl, pH 5.5)	Na^+:H^+ Ratio
H388C(C-)	1.7 ± 0.4	1.4 ± 0.2	1.2
L389C(C-)	1.2 ± 0.1	0.2 ± 0.1	5.9*
L390C(C-)	1.3 ± 0.2	1.6 ± 0.4	0.8
T391C(C-)	3.7 ± 0.2	4.5 ± 0.2	0.8
A392C(C-)	1.1 ± 0.2	0.7 ± 0.1	1.5
S393C(C-)	3.3 ± 0.4	1.5 ± 0.3	2.2
V394C(C-)	4.2 ± 0.3	1.7 ± 0.2	2.4
M395C(C-)	0.6 ± 0.1	1.6 ± 0.1	0.4*
S396C(C-)	0.5 ± 0.1	0.3 ± 0.1	1.7
A397C(C-)	5.0 ± 0.4	3.3 ± 0.2	1.5
P398C(C-)	0.2 ± 0.1	0.2 ± 0.1	1.2
A399C(C-)	4.4 ± 0.5	3.0 ± 0.2	1.5
S400C(C-)	2.7 ± 0.5	1.2 ± 0.1	2.3
L401C(C-)	1.8 ± 0.1	1.6 ± 0.3	1.2
A402C(C-)	3.7 ± 0.2	3.8 ± 0.1	1.0
A403C(C-)	3.8 ± 0.1	4.2 ± 0.2	0.9
A404C(C-)	2.3 ± 0.2	1.2 ± 0.2	1.9
K405C(C-)	2.6 ± 0.2	1.5 ± 0.1	1.7
L406C(C-)	3.0 ± 0.2	3.1 ± 0.2	1.0
F407C(C-)	2.7 ± 0.2	3.3 ± 0.3	0.8
W408C(C-)	1.4 ± 0.2	1.0 ± 0.2	1.4

Table 7-1 continued

TM 9 – 10 Loop	Mediated Uridine Uptake (pmol/oocyte.min^{-1}) Na^+ (100 mM NaCl, pH 8.5)	H^+ (100 mM ChCl, pH 5.5)	Na^+:H^+ Ratio
P409C(C-)	3.1 ± 0.2	1.4 ± 0.1	2.2
E410C(C-)	1.3 ± 0.1	1.1 ± 0.1	1.3
T411C(C-)	1.6 ± 0.1	1.0 ± 0.1	1.6
E412C(C-)	1.3 ± 0.2	0.6 ± 0.1	2.4
K413C(C-)	0.8 ± 0.2	0.8 ± 0.2	1.0
P414C(C-)	0.9 ± 0.1	0.5 ± 0.1	1.7
K415C(C-)	1.4 ± 0.2	0.8 ± 0.1	1.7
I416C(C-)	1.4 ± 0.2	1.3 ± 0.2	1.1
T417C(C-)	1.9 ± 0.2	1.4 ± 0.2	1.4
L418C(C-)	1.7 ± 0.1	0.7 ± 0.1	2.5
K419C(C-)	1.5 ± 0.2	0.8 ± 0.1	1.9
N420C(C-)	1.5 ± 0.1	1.2 ± 0.1	1.3
A421C(C-)	0.6 ± 0.1	0.5 ± 0.1	1.2
M422C(C-)	0.2 ± 0.1	0.2 ± 0.1	1.0
K423C(C-)	4.0 ± 0.3	2.5 ± 0.2	1.6
M424C(C-)	1.7 ± 0.1	2.2 ± 0.1	0.8
E425C(C-)	2.3 ± 0.1	1.8 ± 0.1	1.3
S426C(C-)	2.8 ± 0.2	2.8 ± 0.1	1.0
G427C(C-)	3.5 ± 0.3	2.9 ± 0.2	1.2
D428C(C-)	3.4 ± 0.3	2.8 ± 0.1	1.2
S429C(C-)	3.3 ± 0.2	2.9 ± 0.3	1.2
G430C(C-)	2.9 ± 0.2	2.9 ± 0.1	1.0
N431C(C-)	1.4 ± 0.1	1.9 ± 0.2	0.7
L432C(C-)	2.5 ± 0.3	2.0 ± 0.2	1.3
L433C(C-)	2.8 ± 0.2	1.8 ± 0.2	1.6
E434C(C-)	2.2 ± 0.2	1.4 ± 0.1	1.6
A435C(C-)	2.9 ± 0.2	2.8 ± 0.1	1.0
A436C(C-)	2.8 ± 0.2	2.3 ± 0.1	1.2
T437C(C-)	3.5 ± 0.2	2.9 ± 0.2	1.2
Q438C(C-)	2.9 ± 0.2	2.5 ± 0.1	1.2
G439C(C-)	4.1 ± 0.5	2.6 ± 0.3	1.6
A440C(C-)	2.2 ± 0.1	1.9 ± 0.1	1.1
S441C(C-)	0.5 ± 0.1	0.5 ± 0.1	1.0

S442C(C-)	0.7 ± 0.1	0.7 ± 0.1	1.0
S443C(C-)	0.7 ± 0.1	0.5 ± 0.1	1.4
I444C(C-)	0.6 ± 0.1	0.7 ± 0.1	0.9
S445C(C-)	0.7 ± 0.1	0.7 ± 0.1	1.0

Table 7-1 continued

TM 10	Mediated Uridine Uptake (pmol/oocyte.min^{-1}) Na^+ (100 mM NaCl, pH 8.5)	H^+ (100 mM ChCl, pH 5.5)	Na^+:H^+ Ratio
L446C(C-)	1.8 ± 0.2	2.5 ± 0.2	0.7
V447C(C-)	2.7 ± 0.3	4.1 ± 0.2	0.7
A448C(C-)	2.9 ± 0.1	3.0 ± 0.2	0.9
N449C(C-)	2.9 ± 0.4	3.7 ± 0.3	0.8
I450C(C-)	1.6 ± 0.1	2.7 ± 0.2	0.6
A451C(C-)	2.5 ± 0.1	4.0 ± 0.4	0.6
V452C(C-)	2.3 ± 0.3	4.1 ± 0.2	0.6
N453C(C-)	3.2 ± 0.1	3.7 ± 0.2	0.9
L454C(C-)	1.1 ± 0.1	0.6 ± 0.1	1.7
I455C(C-)	3.2 ± 0.1	2.3 ± 0.1	1.4
A456C(C-)	1.7 ± 0.1	1.4 ± 0.1	1.2
F457C(C-)	1.4 ± 0.1	1.1 ± 0.1	1.3
L458C(C-)	2.8 ± 0.2	3.0 ± 0.2	1.0
A459C(C-)	4.5 ± 0.1	2.9 ± 0.3	1.6
L460C(C-)	3.9 ± 0.1	3.7 ± 0.3	1.0
L461C(C-)	0.9 ± 0.1	2.5 ± 0.3	0.3*
S462C(C-)	3.4 ± 0.2	3.1 ± 0.3	1.1
F463C(C-)	3.1 ± 0.2	2.6 ± 0.3	1.2
M464C(C-)	2.2 ± 0.2	2.7 ± 0.3	0.8
N465C(C-)	0.7 ± 0.1	0.5 ± 0.1	1.5
S466C(C-)	3.1 ± 0.2	2.7 ± 0.2	1.1

Table 7-1 continued

TM 10 – 11 Loop	Mediated Uridine Uptake (pmol/oocyte.min^{-1}) Na^+ (100 mM NaCl, pH 8.5)	H^+ (100 mM ChCl, pH 5.5)	Na^+:H^+ Ratio
A467C(C-)	2.0 ± 0.1	2.1 ± 0.1	0.9
L468C(C-)	0.5 ± 0.1	0.6 ± 0.1	0.8
S469C(C-)	2.7 ± 0.2	1.7 ± 0.1	1.6
W470C(C-)	0.5 ± 0.1	0.5 ± 0.1	1.0
F471C(C-)	0.5 ± 0.1	0.6 ± 0.1	0.9
G472C(C-)	16 ± 2.1	14 ± 0.8	1.1
N473C(C-)	0.8 ± 0.1	0.5 ± 0.1	1.7
M474C(C-)	0.6 ± 0.1	0.4 ± 0.1	1.6
F475C(C-)	0.7 ± 0.1	0.5 ± 0.1	1.6
D476C(C-)	0.9 ± 0.1	0.5 ± 0.1	1.8
Y477C(C-)	0.7 ± 0.1	0.5 ± 0.1	1.3
P478C(C-)	0.2 ± 0.1	0.2 ± 0.1	1.0
Q479C(C-)	0.4 ± 0.1	0.3 ± 0.1	1.3

Table 7-2. Effect of PCMBS on uridine uptake in *Xenopus* oocytes expressing hCNT3C- single cysteine mutants. Influx of 10 μM ^{14}C-uridine or ^{3}H-uridine was measured in both Na^+-containing, H^+-reduced and Na^+-reduced, acidified media (100 mM NaCl, pH 8.5 or 100 mM ChCl, pH 5.5, respectively) following 10 min incubation on ice in the absence or presence of 200 μM PCMBS or 200 μM PCMBS + 20 mM uridine in media of the same composition used to determine uptake. Values are corrected for basal non-mediated uptake in control water-injected oocytes and are presented as a percentage of mediated uridine influx in the absence of inhibitor for each individual mutant. Each value is the mean ± S.E.M. of 10-12 oocytes. The symbol * indicates substrate protection.

		Na^+ (100 mM NaCl, pH 8.5)		H^+ (100 mM ChCl, pH 5.5)	
TM		+ PCMBS[a] (%)	+ PCMBS + uridine (%)	+ PCMBS[a] (%)	+ PCMBS + uridine (%)
9	H388C(C-)	94 ± 6	94 ± 8	53 ± 6	64 ± 5
	L390C(C-)	13 ± 3	9 ± 1	24 ± 3	30 ± 3
	T391C(C-)	25 ± 2	*92 ± 8	30 ± 2	*96 ± 4
	A392C(C-)	11 ± 1	*64 ± 5	34 ± 4	35 ± 1
	S393C(C-)	21 ± 3	*101 ± 9	19 ± 1	*63 ± 4
	V394C(C-)	91 ± 10	81 ± 7	28 ± 3	*102 ± 4
	M395C(C-)	90 ± 11	107 ± 8	31 ± 2	*113 ± 7
10	I450C(C-)	116 ± 15	126 ± 12	38 ± 2	39 ± 9
	L461C(C-)	87 ± 8	100 ± 10	22 ± 2	22 ± 3
Control	hCNT3	101 ± 6	101 ± 9	20 ± 3	*104 ± 9

[a], mediated uridine influx in the absence of inhibitor is given in pmol/oocytes.min^{-1} in Table 7-1 for each of the individual mutants.

Table 7-3. Effects of cations on PCMBS inhibition of hCNT3C- single cysteine mutants. Influx of 10 μM ^{3}H-uridine was measured in Na^+-free, acidified medium (100 mM ChCl, pH 5.5) following 10 min incubation on ice in the absence or presence of PCMBS in either Na^+-free, H^+-reduced medium (100 mM ChCl, pH 8.5), Na^+-containing, H^+-reduced medium (100 mM NaCl, pH 8.5), Na^+-free, acidified medium (100 mM ChCl, pH 5.5) or Na^+-containing, acidified medium (100 mM NaCl, pH 5.5). Values are corrected for basal non-mediated uptake in control water-injected oocytes and are normalized to the respective influx of uridine in the absence of inhibitor. Each value is the mean ± S.E.M. of 10-12 oocytes.

	Uptake (%) (100 mM ChCl, pH 5.5)			
	PCMBS in Na^+-free, H^+-reduced medium	PCMBS in Na^+-containing, H^+-reduced medium	PCMBS in Na^+-free, acidified medium	PCMBS in Na^+-containing, acidified medium
<u>TM 9</u>				
H388C(C-)	85 ± 5	92 ± 7	41 ± 3	36 ± 4
L390C(C-)	43 ± 4	29 ± 3	26 ± 5	22 ± 2
T391C(C-)	15 ± 2	13 ± 1	14 ± 1	13 ± 2
A392C(C-)	31 ± 5	42 ± 6	41 ± 6	49 ± 5
S393C(C-)	37 ± 3	35 ± 4	29 ± 3	34 ± 3
V394C(C-)	60 ± 9	79 ± 6	37 ± 3	29 ± 3
M395C(C-)	97 ± 9	87 ± 5	44 ± 5	36 ± 4
<u>TM10</u>				
I450C(C-)	88 ± 11	79 ± 9	31 ± 4	29 ± 3
L461C(C-)	60 ± 3	69 ± 5	20 ± 2	19 ± 3
<u>hCNT3</u>	102 ± 6	107 ± 23	33 ± 3	54 ± 5

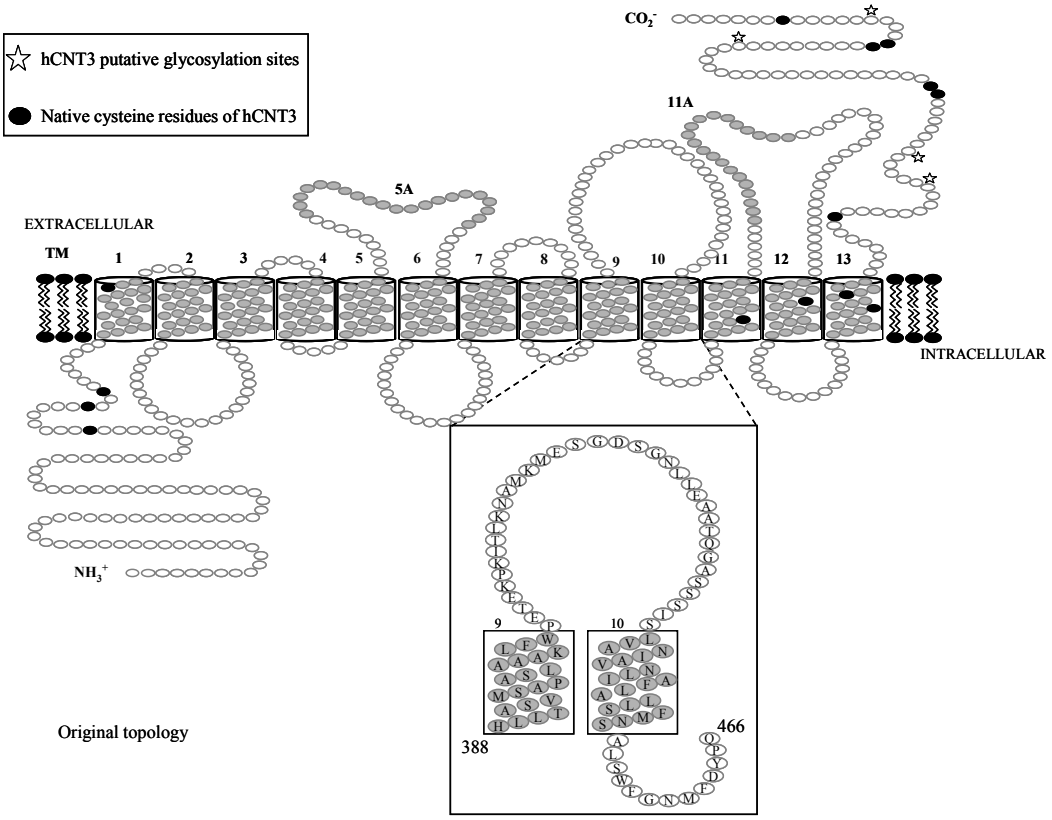

Figure 7-1. Original hCNT3 topology. Schematic of original hCNT3 (GenBank™ accession number AF305210) topology with 13 TMs. Insertion of TMs 5A and 11A into the membrane was weakly predicted and will result in opposite orientations of TMs 6 - 11. The position of endogenous cysteine residues are indicated as *black* residues, and putative glycosylation sites are highlighted with a *star* symbol. Residues studied by SCAM analysis in the present Chapter are depicted in the *inset*.

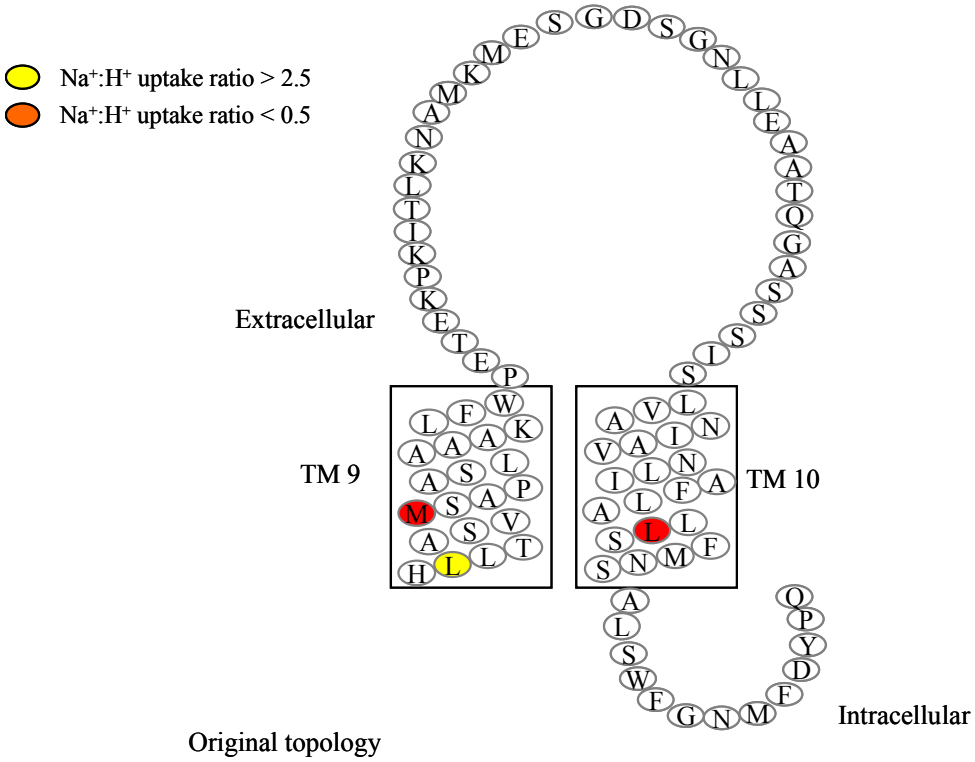

Figure 7-2. hCNT3 residues in the TM 9 - 10 region with altered Na^+:H^+ uridine uptake ratios. hCNT3C- mutants exhibiting Na^+:H^+ uridine uptake ratios > 2.5 are shown in *yellow*, and those with uptake ratios < 0.5 are shown in *orange*. Corresponding numerical values are given in Table 7-1.

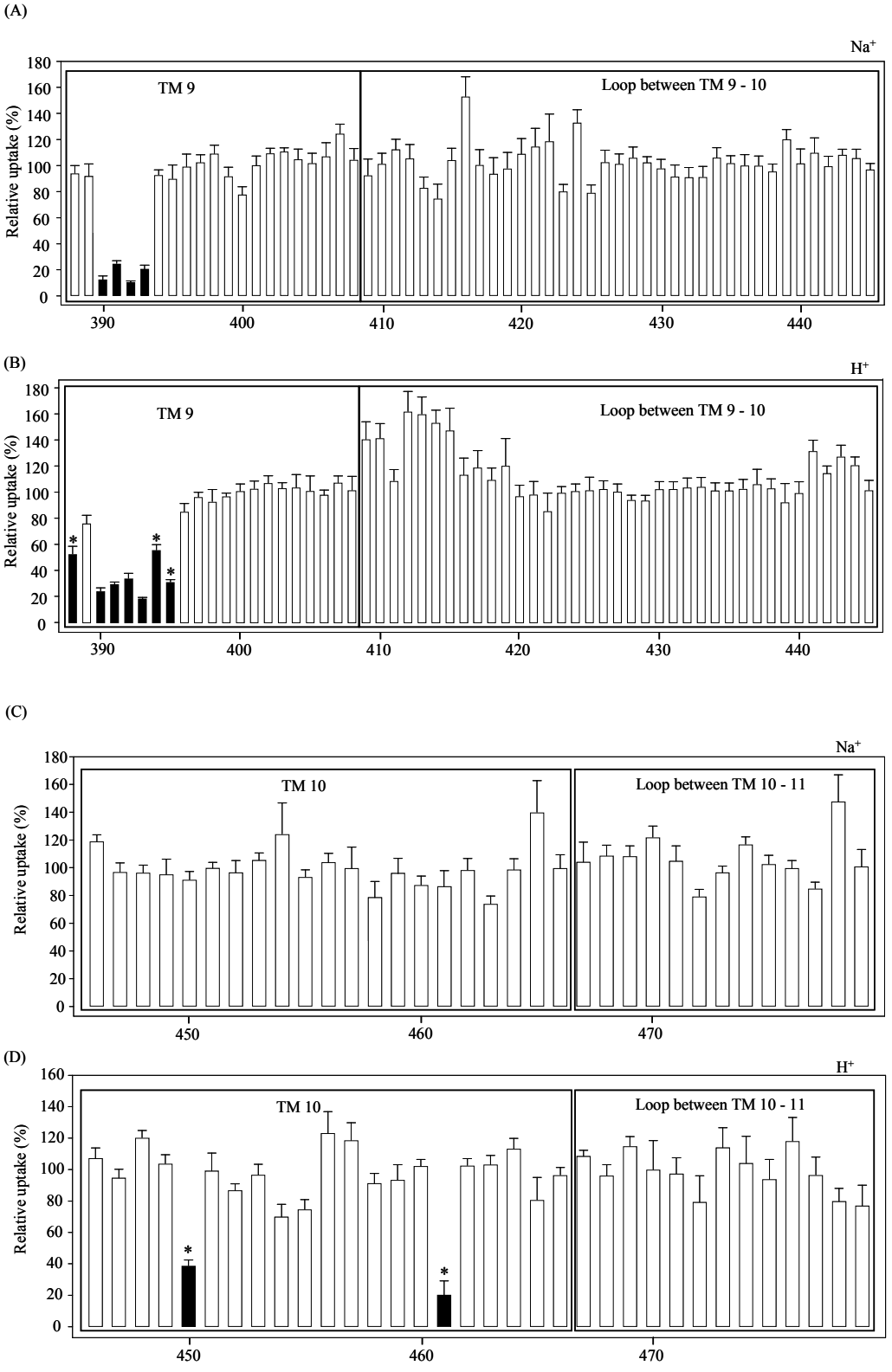
(A)
Na+
TM 9
Loop between TM 9 - 10
Relative uptake (%)
(B)
H+
TM 9
Loop between TM 9 - 10
Relative uptake (%)
(C)
Na+
TM 10
Loop between TM 10 - 11
Relative uptake (%)
(D)
H+
TM 10
Loop between TM 10 - 11
Relative uptake (%)

Figure 7-3.

Figure 7-3. PCMBS inhibition of residues in the TM 9 – 10 region of hCNT3C-. Mediated influx of 10 μM radiolabeled uridine in Na^+-containing, H^+-reduced (*A, C*) or Na^+-reduced, acidified (*B, D*) medium (100 mM NaCl, pH 8.5 or 100 mM ChCl, pH 5.5, respectively) was measured following 10 min incubation on ice in the same medium in the presence of 200 μM PCMBS. *Solid* columns indicate residue positions inhibited by PCMBS; the * symbol identifies those residues that exhibited differential inhibition by PCMBS in the two media. Data are presented as mediated transport, calculated as uptake in RNA-injected oocytes *minus* uptake in water-injected oocytes, and are normalized to influx of uridine in the absence of inhibitor. Each value is the mean ± S.E.M. of 10-12 oocytes. Control hCNT3 was included as a control for all experiments (numerical values are shown on Table 7-2). Corresponding numerical values for PCMBS-sensitive residues are also given in Table 7-2.

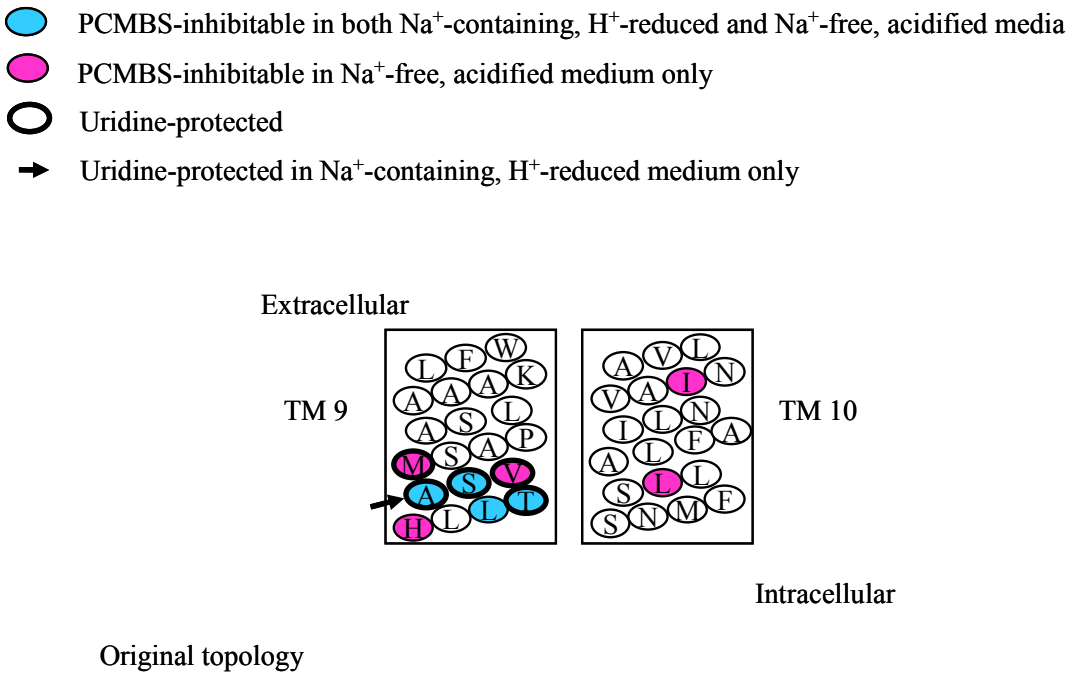

Figure 7-4. hCNT3 TM 9 – 10 region depicting PCMBS-inhibited and uridine-protected residues. hCNT3C- mutants exhibiting inhibition of uridine uptake following incubation with PCMBS in both Na^+-containing, H^+-reduced and Na^+-reduced, acidified media are indicated in *blue*, and those that were inhibited only in Na^+-reduced, acidified medium are indicated in *red*. Residues protected from PCMBS inhibition by excess unlabeled uridine are outlined in *black*. One residue, Ala392 in TM 9, which was inhibited by PCMBS in both media, but protected from that inhibition only in the presence of Na^+- containing, H^+-reduced medium are indicated by a *black arrow*. Corresponding numerical values are given in Table 7-2.

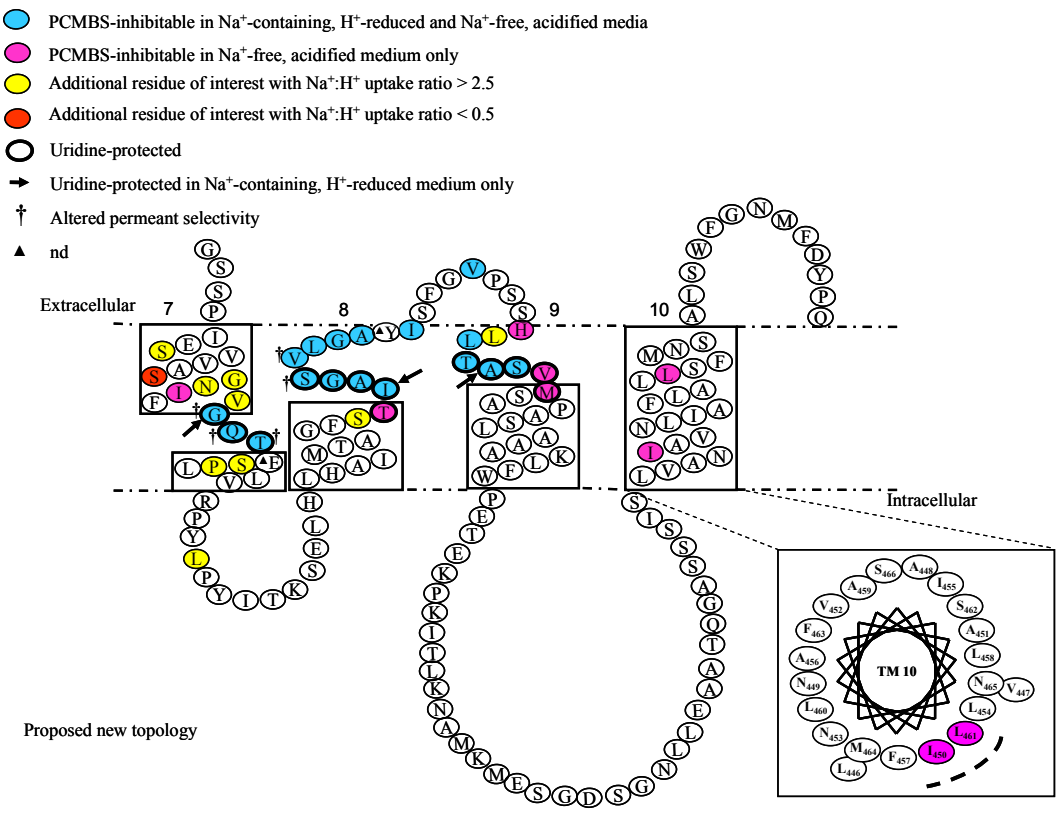

Figure 7-5. Revised topology of the hCNT3 TM 7 – 10 region depicting discontinuous regions within TM 7, 8 and 9. This schematic depicts a reversal in orientation for TM 7 – 10, and non-conventional helical arrangements for TM 7, 8 and 9. PCMBS-inhibited and uridine-protected residues, as well as additional residues of interest with Na^+:H^+ uridine uptake ratios > 2.5 or < 0.5, but not inhibited by PCMBS, are highlighted. The three residues, including Ala392 in TM 9, which were inhibited by PCMBS in both media, but were protected from that inhibition only in Na^+-containing, H^+-reduced medium are indicated by a *black arrow*. Low activity mutants are indicated by the ▲ symbol, and those with altered permeant selectivity are indicated by †. The helical wheel projection for TM 10 in the *inset* shows clustering of the two PCMBS sensitive residues to one face of the helix.

Bibliography

1. Zhang, J., Tackaberry, T., Ritzel, M. W., Raborn, T., Barron, G., Baldwin, S. A., Young, J. D., and Cass, C. E. (2006) Cysteine-accessibility analysis of transmembrane domains 11-13 of human concentrative nucleoside transporter 3. *Biochem. J.* **394**: 389-398.

2. Slugoski, M., D., Smith, K., M., Mulinta, R., Ng, A. M. L., Yao, S. Y. M., Morrison, E. L., Lee, Q., O., T., Zhang, J., Karpinski, E., Cass, C. E., Baldwin, S. A., and Young, J. D. (2008) A conformationally mobile cysteine residue (Cys-561) modulates Na^+ and H^+ activation of human CNT3. *J. Biol. Chem.* **283**:24922-24934.

3. Smith, K. M., Slugoski, M. D., Loewen, S. K., Ng, A. M., Yao, S. Y., Chen, X.-Z., Karpinski, E., Cass, C. E., Baldwin, S. A., and Young, J. D. (2005) The broadly selective human Na^+/nucleoside cotranpsorter (hCNT3) exhibits novel cation-coupled nucleoside transport characteristics. *J. Biol. Chem.* **280**: 25436-25449.

4. Smith, K. M., Slugoski, M. D., Cass, C. E., Baldwin, S. A, Karpinski, E., and Young, J. D. (2007) Cation coupling properties of human concentrative nucleoside transporters hCNT1, hCNT2 and hCNT3. *Mol Membr Biol*. **24**: 53-64.

5. Slugoski, M. D., Ng, A. M., Yao, S. Y., Smith, K. M., Lin, C. C., Zhang, J., Karpinski, E., Cass, C. E., and Baldwin, S. A., and Young, J. D. (2008) A proton-mediated conformational shift identifies a mobile pore-lining cysteine residue (Cys-561) in human concentrative nucleoside transporter 3. *J. Biol. Chem.* **283**: 8496-8507.

6. Slugoski, M., D., Ng, A. M. L., Yao, S. Y. M., Lin, C. C., Mulinta, R., Cass, C. E., Baldwin, S. A., and Young, J. D. (2009b) Substituted cysteine accessibility method analysis of human concentrative nucleoside transporter hCNT3 reveals a novel discontinuous region of functional importance within CNT family motif (G/A)XKX3NEFVA(Y/M/F). *J. Biol. Chem.* **284**:17281-17292.

7. Yao, S. Y. M., Ng, A. M., Slugoski, M. D., Smith, K. M., Mulinta, R., Karpinski, E., Cass, C. E., Baldwin, S. A., and Young, J. D. (2007) Conserved glutamate residues are critically involved in Na^+/nucleoside cotransport by human concentrative nucleoside transporter 1 (hCNT1). *J. Biol. Chem.* **282**: 30607-30617.

8. Slugoski, M. D., Loewen, S. K., Ng, A. M., Smith, K. M., Yao, S. Y., Karpinski, E., Cass, C. E., Baldwin, S. A., and Young, J. D. (2007) Specific mutations in transmembrane helix 8 of human concentrative Na^+/nucleoside cotransporter hCNT1 affect permeant selectivity and cation coupling. *Biochemistry*. **46**: 1684-1693.

9. Slugoski, M., D., Smith, K., M., Ng, A. M. L., Yao, S. Y. M., Karpinski, E., Cass, C. E., Baldwin, S. A., and Young, J. D. (2009a) Conserved glutamate residues E343 and E519 provide mechanistic insights into cation/nucleoside cotransport by human concentrative nucleoside transporter 3 (hCNT3). *J. Biol. Chem.* **284**:17266-17280.

Chapter 8:
Substituted Cysteine Accesssibility Method Analysis of Transmembrane Domains 11-13 of Human Na^+/Nucleoside Cotransporter 3 (hCNT3)*

* A version of this chapter has been published.

Slugoski, M., D., Ng, A. M. L., Yao, S. Y. M., Lin, C. C., Mulinta, R., Cass, C. E., Baldwin, S. A., and Young, J. D. (2009b) Substituted cysteine accessibility method analysis of human concentrative nucleoside transporter hCNT3 reveals a novel discontinuous region of functional importance within CNT family motif (G/A)XKX3NEFVA(Y/M/F). *J. Biol. Chem.* **284**:17281-17292.

Acknowledgements and Contributions

Graduate Student Dr. Melissa D. Slugoski was the principle author and investigator of this study. I contributed to the functional characterization of hCNT3C- TM 11-13 mutants and to the design and interpretation of experiments. Technologist Mrs. Amy M. L. Ng was involved in construction of the single cysteine mutants and, together with Dr. Sylvia Y. M. Yao and Summer Student Colin C. Lin, assisted with their functional characterization. Drs. Carol E. Cass and Stephen A. Baldwin are collaborative principal investigators who assisted with research funding and manuscript preparation. This research was funded by the National Cancer Institute of Canada with funds from the Canadian Cancer Society (now the Canadian Cancer Society Research Institute), Alberta Cancer Board (now the Alberta Health Services- Cancer Care), The Alberta Cancer Foundation, and by the Alberta Cancer Prevention Legacy Fund.

Introduction

Current models of concentrative nucleoside transporter (CNT) topology have 13 putative transmembrane domains (TMs) (1-4). Two additional TMs (designated 5A and 11A) are weakly predicted by computer algorithms and immunocytochemical experiments with site-specific antibodies, and studies of native and introduced glycosylation sites have confirmed an intracellular N-terminus and an extracellular C-terminus (3). Chimeric studies involving human (h) CNTs and hagfish (hf) CNT, a CNT from the ancient marine prevertebrate the Pacific hagfish *Eptatretus stouti*, have revealed that the functional domains responsible for CNT nucleoside selectivity and cation coupling reside within the C-terminal TM 7 - 13 half of the protein (5, 6). In contrast to mammalian and other eukaryotic CNTs, NupC, a H^+-coupled CNT family member from *Escherichia coli*, lacks TMs 1 - 3, but otherwise shares a similar membrane topology (7).

A functional cysteine-less version of hCNT3 has been generated by mutagenesis of endogenous cysteine residues to serine, resulting in the cysteine-less construct hCNT3C- employed originally in a yeast expression system for substituted cysteine accessibility method (SCAM) analysis of TMs 11, 12 and 13 using methanethiosulfonate (MTS) reagents (8). Subsequently, hCNT3C- was characterized in the *Xenopus laevis* oocyte expression system [Chapter 3 (9)], and SCAM analysis projects undertaken with the alternative thiol-specific reagent *p*-chloromercuribenzene sulfonate (PCMBS) to investigate the TM 7 – 10 region of the protein (Chapters 4 and 7). Continuing the investigation of hCNT3 C-terminal membrane topology and function, the present Chapter reports PCMBS SCAM results for the TM 11 - 13 part of the protein, including loop regions linking the putative TMs not previously studied using MTS reagents. This completes SCAM analysis of the entire C-terminal half of hCNT3, a region encompassing 289 consecutive amino acid residue positions.

In previous structure/function studies of the hCNT3 TM 11-13 region, a cluster of conformationally mobile residue positions in TM 12 (Ile554, Tyr558 and

Cys561) was identified which exhibits H^+-activated inhibition by PCMBS, with uridine protection evident for Tyr558 and Cys561 (10). Located deeper within the plane of the membrane, other uridine-protectable residue positions in TM 12 are PCMBS-sensitive in both H^+- and Na^+-containing medium (10). Also in previous studies, hCNT3 Glu519 and the corresponding residue in hCNT1 (Glu498) in region TM 11A were identified as having key roles in permeant and cation binding and translocation [(11) and Appendix 1 (12)]; additionally, hCNT3 E519C showed inhibition of uridine uptake by PCMBS (11). Mechanistically, this residue is proposed to be a direct participant in cation coupling via the common hCNT3 Na^+/H^+-binding site that, in other CNTs, is either Na^+-specific (e.g. hCNT1) or H^+-specific (e.g. NupC) (11). The present results identify other residues of functional importance in this region of the protein, confirm the predicted α-helical structures of TMs 11, 12 and 13, and provide evidence for a novel membrane-associated conformation for the TM 11A region. These findings strongly support a revised topology model for CNTs.

Results

All 14 endogenous cysteine residues of hCNT3 were replaced with serine to produce hCNT3C-, a cysteine-less hCNT3 construct [Chapter 3 (9)]. hCNT3C- retained wild-type hCNT3 functional activity, but with an increased K_{50} value for Na^+ activation [Chapter 3 (9)]. In parallel with previous studies of TMs 7-10 (Chapters 4 and 7), hCNT3C- was used as a template for the construction of single cysteine mutants prior to scanning for functional activity and inhibition by PCMBS. The 133 residues spanning a region between and including TMs 11 - 13 that were investigated in the present study are highlighted in Fig. 8-1.

Functional activity of single cysteine mutants – hCNT3 transports nucleosides using both Na^+ and H^+ electrochemical gradients (6, 13). Therefore, to examine the functional activity of single cysteine mutants, uptake of 10 μM radiolabeled uridine was determined in both Na^+-containing, H^+-reduced and Na^+-reduced, acidified medium (100 mM NaCl, pH 8.5 and 100 mM ChCl, pH 5.5,

respectively). Na^+-containing medium was buffered at a pH of 8.5 to avoid the small, but significant, amount of hCNT3 H^+-activation that occurs at pH 7.5 (6, 13). Previously, Na^+-coupled uridine transport by hCNT3 at pH 8.5 was verified to be kinetically indistinguishable from that at pH 7.5 [Chapter 3 (9)]. Initial rates of transport (± SEM) for each mutant, in units of pmol/oocyte.min^{-1}, are given in Table 8-1. The uptake of 10 μM radiolabeled uridine (100 mM NaCl, pH 8.5) by oocytes expressing hCNT3C- showed expected variation between experiments and ranged from 2 and 4 pmol/oocyte.min^{-1} (data not shown). The flux values reported in Table 8-1, and in subsequent Tables and Figures, depict mediated transport activity, defined as the difference in uptake between RNA transcript-injected and control water-injected oocytes, and are from representative experiments. In all of the studies reported here, uridine uptake in water-injected oocytes was < 0.02 pmol/oocyte.min^{-1} under all conditions tested (data not shown).

Mutants exhibiting uridine uptake values < 0.1 pmol/oocyte.min^{-1} were excluded from further analysis (Table 8-1). Only nine out of the 133 residues investigated fell into this category (6.8%) and in every case, the mutation to cysteine resulted in a protein with low functional activity both in Na^+- and H^+-containing media (100 mM NaCl, pH 8.5 and 100 mM ChCl, pH 5.5, respectively). The nine amino acids were: Met496 and Gly498 in TM 11, Glu519 in TM 11A, Phe563 and Ser568 in TM 12, and Arg593, Ala594, Ala606 and Gly610 in TM 13. Cell surface labeling with sulfo-NHS-LC-biotin and immobilized streptavidin resin were used to distinguish cell surface proteins from those associated with the total (plasma + intracellular) membranes. Three of the nine mutants (residues Gly498, Phe563, and Ser568) that exhibited low levels of functional activity were present at cell surfaces in amounts and with electrophoretic mobilities similar to hCNT3C- (data not shown). The others were truncated (Met496) or present at cell surfaces in reduced amounts (residues Glu519, Arg593, Ala594, Ala606, and Gly610) (data not shown).

To facilitate comparisons between the remaining 124 mutants, the uridine transport activity of each construct is also presented as a Na^+:H^+ uptake ratio (Table 8-1). Corresponding Na^+:H^+ ratios of uridine uptake (10 μM) for wild-type

hCNT3 and cysteine-less hCNT3C- were ~ 1.7 and 1.0, respectively (averaged results from multiple experiments; data not shown) and are in good agreement with previous studies [6, Chapter 3 (9), 13]. Residue mutations which resulted in Na^+:H^+ ratios of uridine uptake < 0.5 and > 2.5 (Table 8-1) are highlighted in the hCNT3 topology schematic shown in Fig. 8-2.

All mutants in TM 11, TM 13 and in the loop between TMs 12 and 13 exhibited Na^+:H^+ uptake ratios similar to hCNT3/hCNT3C-. In contrast, mutant Y558C(C-) in TM 12 presented a Na^+:H^+ ratio of 0.2 and three other TM 12 mutants exhibited Na^+:H^+ ratios > 2.5 (A564C(C-), N565C(C-) and I566C(C-) with ratios equal to 5.0, 3.3 and 2.6, respectively).

A cluster of residues with altered cation-coupling characteristics was also evident in the loop between TMs 11 and 12. Mutation of residue Tyr513 to cysteine resulted in a Na^+:H^+ uptake ratio of 0.4 and the more numerous residues whose mutation to cysteine resulted in Na^+:H^+ ratios > 2.5 were Gly512 (3.9), Lys514 (7.9), Phe516 (3.1), Ala522 (7.0), Glu524 (2.6) and His525 (2.7). All seven of these residues lie within the predicted TM 11A and, more specifically, five are located within the conserved CNT family (G/A)*X*K*X*$_3$NEFVA(Y/M/F) motif. In hCNT3, this motif corresponds to residues GYKTFFNEFVAY, which span the region from Gly512 to Tyr523. Although the transport activity of E519C(C-) was < 0.1 pmol/oocyte.min^{-1} and therefore not analyzed in the present study, the transport activity of two Glu519 mutants in a wild-type hCNT3 background (E519D and E519C) was previously characterized (11). Both of these mutants displayed robust transport of uridine in the presence of Na^+, but only low (E519D) or not detectable (E519C) levels of transport activity in Na^+-free, acidified medium (11).

PCMBS inhibition of single cysteine mutants – Wild-type hCNT3 and mutants bearing single cysteine residues at any of three TM 12 positions (Ile554, Tyr558 and Cys561) were previously reported to be sensitive to inhibition by PCMBS under acidic conditions only (*ie*. in Na^+-free, acidified medium) (10). Previous control experiments have also established lack of inhibition by PCMBS for transport mediated by hCNT3C- in both Na^+-containing, H^+-reduced and Na^+-free, acidified media (10). Therefore, single cysteine mutants of hCNT3C- were tested for

inhibition by PCMBS both in Na^+-containing, H^+-reduced medium (100 mM NaCl, pH 8.5) and in Na^+-free, acidified medium (100 mM ChCl, pH 5.5). After 10 min exposure to 200 μM PCMBS, uptake of 10 μM radiolabeled uridine was assayed in medium of the same composition (10, 14). Exposure to PCMBS was performed on ice to minimize any possibility of diffusion or other movement across oocytes plasma membranes (10, 14). Results for each individual mutant calculated as a percentage of mediated uridine uptake in the absence of PCMBS are presented in Fig. 8-3 (TM regions) and Fig. 8-4 (loop regions). For screening purposes, a residue was considered PCMBS-inhibitable upon exhibiting >20% inhibition of uridine uptake following incubation with PCMBS. Residues that were PCMBS-inhibitable are highlighted in Figs. 8-3 and 8-4, and the corresponding numerical values are presented in Table 8-2. A schematic of the locations of these PCMBS-inhibitable residues is presented in Fig. 8-5.

In TM 11, three residues, Phe482, Ser487 and Met491, were PCMBS-inhibitable in both Na^+-containing, H^+-reduced and Na^+-free, acidified medium upon mutation to cysteine. Flanking Phe482, mutants E483C(C-) and L484C(C-) were PCMBS-inhibitable only in Na^+-containing, H^+-reduced medium, whereas L480C(C-) was PCMBS-inhibitable only in Na^+-free, acidified medium. As described previously (10), and as also shown here, TM 12 contains four residues (Thr557, Asn565, Gly567 and Ile571) that, upon mutation to cysteine, were PCMBS-inhibitable in both cation conditions and three (Ile554, Tyr558 and Ser561) that were only PCMBS-inhibitable when tested in Na^+-free, acidified medium. In TM 13, three mutants (A601C(C-), A609C(C-) and L612C(C-)) were PCMBS-sensitive in both cation conditions.

Inhibition of an introduced cysteine residue by PCMBS was previously described for E519C in hCNT3 TM 11A (11). Scanning of the loop between TMs 11 and 12, which includes TM 11A, revealed additional PCMBS-inhibitable residues. Upon conversion to cysteine, residues Met506, Tyr513, Phe516, Phe517, Asn518, Phe520, Val521, Tyr523 and Leu526 were PCMBS-inhibitable under both cation conditions. Additionally, PCMBS inhibition was observed for Ala522 in Na^+-containing, H^+-reduced medium, and for Ala508, Gly512 and Gln545 it was

observed only in Na^+-free, acidified medium. Of these 13 residues, 11 lie within the TM 11A region, and nine lie within the CNT family (G/A)*X*K*X*$_3$NEFVA(Y/M/F) motif. In contrast, none of the residues in the TM 12 - 13 loop, when converted to cysteine in hCNT3C-, were inhibitable by PCMBS under either cation condition.

Uridine protection of PCMBS inhibition – Subsequent experiments investigated the ability of extracellular uridine (20 mM) to protect against inhibition by PCMBS for residues which were PCMBS-inhibitable in either or both cation conditions. Results for each individual mutant are presented in Table 8-2 as a percentage of mediated uridine uptake in the absence of PCMBS, and uridine-protectable residues are highlighted in the hCNT3 topology schematic of Fig. 8-5.

In TM 11, three residues exhibited uridine protection from PCMBS inhibition. L480C(C-), which was PCMBS-inhibitable only in Na^+-free, acidified medium, demonstrated full protection against that inhibition, and F482C(C-), which was PCMBS-inhibitable in both Na^+-containing, H^+-reduced and Na^+-free, acidified media was also fully protectable under both cation conditions. In contrast, M491C(C-), which was also PCMBS-inhibitable under both cation conditions, was partially protectable only in Na^+-containing, H^+-reduced medium. As previously described (10), five of the seven PCMBS-inhibitable mutants in TM 12 exhibited uridine protection. These were N565C(C-), G567C(C-) and I571C(C-) which were PCMBS-inhibitable in both cation conditions, and Y558C(C-) and S561C(C-) which were PCMBS-inhibitable only in Na^+-free, acidified medium. Except for Y558C(C-), the four other TM 12 mutants exhibited full protection against PCMBS inhibition. Of the three mutants in TM 13 which were PCMBS-inhibitable under both cation conditions, L612C(C-) and A609C(C-) were fully and partially protectable, respectively, by extracellular uridine under both cation conditions.

In the TM 11 - 12 loop, only one mutant inhibitable by PCMBS under both cation conditions, F516C(C-), also exhibited uridine protection under both cation conditions. Y523C(C-) and L526C(C-), which were PCMBS-inhibitable under both cation conditions, were only protectable in Na^+-containing, H^+-reduced medium. A508C(C-) and G512C(C-), which were PCMBS-inhibitable only in Na^+-free, acidified medium, and A522C(C-), which was PCMBS-inhibitable in Na^+-

containing, H^+-reduced medium, also showed uridine protection under the same cation conditions. All six of the uridine-protectable residues in the TM 11 - 12 loop are located in TM 11A and four of these reside within the CNT family (G/A)*X*K*X*$_3$NEFVA(Y/M/F) motif.

Discussion

Building upon results from TMs 7-10 of hCNT3 presented in Chapters 4 and 7, the present Chapter reports a parallel PCMBS SCAM analysis of the TM 11-13 region of hCNT3C- and, in so doing, completes a cysteine-scanning mutagenesis study of the entire C-terminal half of the transporter.

Functional activity of hCNT3C- mutants – Initial characterization of the hCNT3C- single cysteine mutants investigated in the present study measured uridine uptake in both Na^+-containing, H^+-reduced and Na^+-free, acidified media (Table 8-1). Of the 133 mutants examined, nine exhibited uridine uptake values < 0.1 pmol/oocyte.min^{-1} under both cation conditions (Table 8-1). Two of these mutants were in TM 11 (M496C(C-) and G498C(C-)), one in TM 11A (E519C(C-)), two in TM 12 (F563C(C-) and S568C(C-)) and four in TM 13 (R593C(C-), A594C(C-), A606C(C-) and G610C(C-)). M496C(C-), G498C(C-), F563C(C-), and S568C(C-) were present at cell surfaces, suggesting loss of intrinsic transport capability. M496C(C-) was truncated, consistent with proteolytic cleavage to a lower molecular weight species. The other five exhibited reduced quantities in plasma membranes. All nine mutants were excluded from further functional analysis.

The previous MTS study that examined TMs 11, 12 and 13 in yeast also identified the majority of these same residues, upon mutation to cysteine, to be non-functional (Met496, Gly498, Phe563, Ala594 and Ala606) or to exhibit low levels of transport activity (Ser568, Arg593 and Gly610) (8). In addition, G598C(C-) was non-functional and I485C(C-), L595C(C-) and F603C(C-) exhibited low transport activities in yeast (8). Cell surface processing experiments by immunofluorescence and confocal microscopy found all of these mutants,

except G498C(C-) and L595C(C-), to be present at the yeast cell surface in similar abundance to the wild-type protein (8). Common to both studies, therefore, the following amino acids have potentially important roles in hCNT3 structure and/or function: Phe563 and Ser568 in TM 12 and Arg593, Ala594, Ala606, and Gly610 in TM 13. In the yeast expression system, mutants M496C(C-) and G598C(C-) were rescued by conversion to alanine (M496A(C-) and G598A(C-), respectively), whereas G498C(C-) and F563C(C-) were not (8). Although broadly similar in overall profile, the observed differences in the functional activity of some mutants indicates the existence of variations in processing, expression and/or conformation of the mature proteins at the cell surface in the *Xenopus* oocyte and yeast expression systems.

hCNT3 couples nucleoside transport to both Na^+ and H^+ electrochemical gradients and exhibits a Na^+/H^+ ratio of uridine uptake (10 μM) of ~ 1.7 (6, 13). Similarly, hCNT3C- also mediates both Na^+- and H^+-coupled uridine transport, although the apparent K_{50} for Na^+ is increased ~ 11-fold, decreasing the Na^+/H^+ ratio of uridine uptake (10 μM) to ~ 1.0 [Chapter 3 (9)]. Table 8-1 and Fig. 8-2 highlight those residues for which mutation to cysteine in hCNT3C- resulted in Na^+/H^+ uridine uptake ratios either < 0.5 (*ie.* H^+-preferring) or > 2.5 (*ie.* Na^+-preferring). Such mutants identified residues likely to be involved directly or indirectly in interactions with the coupling cation. The locations of these residues correspond well with regions of the protein shown in other studies to be important for hCNT cation interactions.

In a previous investigations, mutation of hCNT3 Cys561, a conformationally sensitive TM 12 residue located at the Na^+/H^+ boundary of extracellularly accessible residues, influenced interactions with coupling the two coupling cations (Na^+ and H^+) differently (10). In good agreement with a role for TM 12 in cation interactions, mutation to cysteine in hCNT3C- resulted in Na^+/H^+ ratios of uridine uptake < 0.5 for residue Tyr558 (*ie.* H^+-preferring) and > 2.5 for residues Ala564, Asn565 and Ile566 (*ie.* Na^+-preferring). Also in a previous study, the hCNT3 TM 11A residue Glu519 was demonstrated to be an important determinant of Na^+/H^+ coupling to the conserved CNT cation binding site that in

other family members interacts exclusively with either Na^+ or H^+ (11). In the present investigation, mutation to cysteine in hCNT3C- resulted in Na^+/H^+ ratios of uridine uptake < 0.5 for residue Tyr513 and > 2.5 for residues Gly512, Lys514, Phe516, Ala522, Glu524 and His525 in the TM 11 - 12 loop, all of which also reside within TM 11A. Thus, the present results expand this role(s) of hCNT3 Glu519 (TM 11A) and Cys561 (TM 12) in cation binding and/or translocation to other adjacent residues in the same regions of the protein. Further analysis of the roles of these newly characterized amino acids in cation coupling is in progress (Chapter 9).

PCMBS inhibition of hCNTC- mutants: transmembrane architecture and transmembrane orientation of TMs 11-13 – To summarize the data presented in Table 8-2 and Figs. 8-3 and 8-4, the schematic in Fig. 8-5 highlights those residues identified in hCNT3C- as PCMBS-sensitive and uridine-protectable. In agreement with previous predictions (3, 8), the pattern of PCMBS inhibition evident within TMs 11, 12 and 13 supports a conventional membrane-spanning α-helical architecture for these regions because affected residues, in general, cluster on one face of each of the helices. To more clearly demonstrate this, α-helical wheel projections for each of the TMs are presented in Fig. 8-6, although it is appreciated that the true structures of these regions of the protein may differ from the perfect α-helices illustrated (see also Ref. 10 for a *space-filling representation* of TM 12)..

In TM 11, PCMBS inhibition is evident for residues Gly483 and Leu484 in Na^+-containing, H^+-reduced medium only; Leu480 in Na^+-free, acidified medium only; and Phe482, Ser487 and Met491 in both cation conditions. Of these, Leu480 (Na^+-free, acidified only), Phe482 (both cation conditions) and Met491 (Na^+-containing, H^+-reduced only) showed uridine protection. In the previous study in yeast, inhibition by MTS reagents for Leu480 and Ser487 in Na^+-containing, H^+-reduced medium was partly protected by uridine (8). In the current 13 TM model of hCNT3 topology, the six PCMBS-inhibitable residues in TM 11 span a central to deep region within the helix, including the last putative residue (Leu480) of the helix (Fig. 8-5). Uridine protection was evident for residues located at both ends of this region (Met491 and Leu480), a pattern of inhibition supporting the reversed

orientation of this helix. As such, the majority of PCMBS-inhibitable residues would lie exofacially within the helix in a position more likely to be accessible to the extracellular medium and available for PCMBS binding. Five of the six PCMBS-inhibitable residues cluster to one face of the helix (Fig. 8-6), consistent with an α-helical structure. Residue Phe482, however, resides on a separate face of the helix. A reversed orientation of TM 11, as predicted by the revised new model of hCNT3 membrane topology (Fig. 8-1 *inset*), would place residue Phe482 at the exofacial boundary of the TM in a position potentially in contact with the external medium and accessible to PCMBS despite its location in a different face within the helix relative to the other PCMBS-inhibitable residues.

As previously reported (10), three residues in TM 12 (Ile554, Tyr558 and Ser561) show PCMBS inhibition only in Na^+-free, acidified medium and four additional residues (Thr557, Asn565, Gly567 and Ile571) showed PCMBS inhibition under both cation conditions (Fig. 8-5). Of the seven PCMBS-sensitive residues identified in TM 12, five (Tyr558, Ser561, Asn565, Gly567 and Ile571) showed uridine protection. In good agreement with these results, the yeast study also identified Thr557, Asn565, Gly567 and Ile571 as MTS-sensitive in Na^+-containing, H^+-reduced medium, and these four residues exhibited varying degrees of uridine protection (8). In addition to residing in the extracellular facing, exofacial half of the helix, the residues inhibitable by PCMBS only in Na^+-free, acidified medium cluster to one quadrant of the helix surface, whereas those that were reactive under both cation conditions span a region that is deeper within the helix and extends over a wider aspect of the helix face (Figs. 8-5 and 8-6). Consistent with a conventional α-helical structure for TM 12, all of the PCMBS-accessible residues nevertheless reside within one-half of the helix surface. TM 12 Cys561 is the residue responsible for PCMBS inhibition of wild-type hCNT3 (10), which occurred under acidified conditions only, and therefore reported a specific conformational change associated with H^+ binding (10). Adjacent residues Ile554 and Tyr558 reported the same H^+-mediated conformational transition. Unlike TM 11, the longitudinal dispersal of PCMBS-sensitive residues shown in Fig. 8-5 for TM 12 suggests that the helix is presented in its correct transmembrane orientation. Nevertheless, the finding that

residue Ile571 showed clear evidence of PCMBS inhibition and uridine protection (Table 8-2) indicates that the hCNT3 translocation pore penetrates deep within the membrane.

Although no TM 13 residues were reported as MTS-sensitive (8), the present Chapter identified Ala601, Ala609 and Leu612 as PCMBS-sensitive under both cation conditions. Uridine protection from PCMBS inhibition was evident for the two most exofacially located residues, Ala609 and Leu612 (Fig. 8-5). Supporting an α-helical structure for TM 13, these three residues cluster to one face of the helix (Fig. 8-6). Similar to TM 12, but unlike TM 11, the predicted location of Ala601, Ala609 and Leu612 within the extracellular half of the membrane (Fig. 8-5) provided evidence that TM 13 is correctly oriented in both the 13 TM and the newly revised topology models of hCNT3 membrane architecture (Fig. 8-1). Consistent with previous findings for rat CNT1 (3), our demonstration that all hCNT3 glycosylation sites are confined to the C-terminal end affords additional supporting evidence in this regard [Chapter 3 (9)].

PCMBS inhibition of hCNT3C- mutants: transmembrane architecture and orientation of TM 11A – The TM 11 - 12 loop, encompassing TM 11A, revealed an unexpected and novel pattern of reactivity to PCMBS (Table 8-2 and Figs. 8-4 and 8-5). Fourteen of the 52 residues in this region showed inhibition by PCMBS upon conversion to cysteine in hCNT3C-, including residue Ala522 only in Na^+-containing, H^+-reduced medium; Ala508, Gly512 and Gln545 only in Na^+-free, acidified medium; and Met506, Tyr513, Phe516, Phe517, Asn518, Phe520, Val521, Tyr523 and Leu526 under both cation conditions. Partial or complete uridine protection from PCMBS inhibition was evident for six of the residues: Ala522 and Tyr523 only in Na^+-containing, H^+-reduced medium; Ala508 and Gly512 only in Na^+-free, acidified medium; and Phe516 and Leu526 under both cation conditions. Together, the results suggested that this region is critically involved in the transport mechanism of hCNT3 and predicted at least a portion is membrane-associated, either in the form of a re-entrant loop or as part of a transmembrane domain. The majority of the PCMBS-sensitive residues reside within the previously predicted membrane domain TM 11A. One exception is Met506, for which the corresponding

hCNT3C- mutant showed PCMBS inhibition under both cation conditions and is positioned immediately adjacent to the TM 11A region. It is possible that the putative boundary of TM 11A includes Met506 within the membrane-associated region. The other exception is Gln545, which is separated from putative TMs 11A and 12 by 17 and 8 residues, respectively (Fig. 8-5). Q545C(C-) showed robust PCMBS inhibition only in Na^+-free, acidified medium and was not uridine-protected. Centrally positioned in the putative exofacial loop region linking TMs 11A and 12 (Fig. 8-1 *inset* and Fig. 8-5), residue Gln545 is unlikely to be membrane-associated, but may nevertheless reside in sufficiently close proximity to the exofacial aspect of translocation pore that binding of PCMBS interferes with hCNT3 cotransport activity. Since Q545C(C-) was inhibited by PCMBS only in Na^+-free, acidified medium, it may be similar to Cys561, reporting a specific H^+-induced conformation of the transporter.

The overall pattern of PCMBS reactivity in putative TM 11A measured by transport inhibition suggested that this region, or at least part of it, differs from the traditional α-helical structure of membrane-associated TMs. Within the conserved CNT family (G/A)*X*K*X*$_3$NEFVA(Y/M/F) motif of TM 11A, a sequence of eight consecutive residues, extending from Phe516 to Tyr523, were PCMBS-sensitive upon conversion to cysteine in under both cation conditions, the only exceptions being Glu519, which showed low levels of uridine transport activity, and Ala522, which showed PCMBS inhibition only in Na^+-containing, H^+-reduced medium. In the wild-type hCNT3 background, mutant E519C exhibited Na^+-specific nucleoside transport activity and was PCMBS-sensitive in the presence of Na^+ (11). Within this region of eight PCMBS-inhibitable residues, three (Phe516, Ala522 and Tyr523) were uridine-protectable. Flanking either end of this block of PCMBS-sensitive residues, and especially noticeable in the first part of the TM adjacent to Met506, the pattern of PCMBS inhibition showed evidence of periodicity consistent with small segments of α-helical content. TM 11A therefore has characteristics of a pore-lining discontinuous helix in which the majority of the residues comprising central conserved (G/A)*X*K*X*$_3$NEFVA(Y/M/F) motif, including the key glutamate residue Glu519, adopt a relaxed, extended and possibly mobile conformation within the

translocation pore which allows PCMBS binding to most of the residues within the motif. Block patterns of PCMBS reactivity also occur in TMs 7, 8 and 9 (Chapters 4 and 7).

As such, the pattern of PCMBS inhibition reported here for TM 11A [and apparent also in TMs 7 – 9 (Chapters 4 and 7)] provides functional evidence of extended structures resembling the discontinuous membrane helices evident in crystal structures of the recently solved Na^+-coupled bacterial leucine, galactose, and hydantoin membrane transport proteins *Aquifex aeolicus*, $LeuT_{Aa}$ (15), *Vibrio parahemeolyticus* SGLT (16), and *Microbacterium liquefaciens* NCS1 (17). In $LeuT_{Aa}$, non-traditional transmembrane α-helices are disrupted by the insertion of extended regions of polypeptide that comprise the Na^+ binding sites of the protein and, upon Na^+ binding, favor high-affinity binding of the permeant amino acid leucine (15). A similar feature is also apparent in TM 7 of the glutamate transporter homologue Glt_{Ph} from *Pyrococcus horikoshii* (18). Reviewed by Screpanti and Hunte (19) and Krishnamurthy (20), such discontinuous membrane helices are proposed to play important mechanistic roles in ion and permeant recognition, binding, and translocation in secondary active transporters. In the case of TM 11A in hCNT3, the centrally positioned glutamate residue Glu519, which resides in the conserved (G/A)*X*K*X*$_3$NEFVA(Y/M/F) motif, plays a critical and possibly direct role in cation coupling/binding that is probably common to all CNT family members (11). Separated only by 26 amino acids, membrane-associated TM 11A is likely to lie within the translocation pore in close proximity to TM 12, which our lab has previously shown to undergo cation-dependent conformational changes (10).

Overall topological and mechanistic implications for hCNT3 – Although the pattern of PCMBS-inhibitable and uridine-protectable residues in TMs 12 and 13 supports the current α-helical orientation of these regions, a reversed orientation similar to TMs 7-10 (Chapters 4 and 7), is more plausible for TM 11. In this scenario, membrane-associated TM 11A would be membrane-spanning rather than a re-entrant loop (see schematic in Fig. 8-7). This is in good agreement with earlier predictions for TMs 5A and 11A as potentially membrane-spanning (3), as shown in

the *inset* of Fig. 8-1. Previously, SCAM analysis of TMs 11 – 13 revealed MTS-sensitive residues buried deep within the TM 11 helix (8). Thus, the present study in this Chapter expands upon these earlier findings and provides solid experimental evidence to support the original hypothesis of an additional TM 11A. As shown in Fig. 8-1 (*inset*), insertion of both TMs 5A and 11A through the membrane bilayer would result in opposite orientation for TMs 6 – 11. In agreement with this, a recent structure-function study of negatively charged residues in hCNT1 has provided evidence for an opposite orientation for TM 7 [Appendix 1 (12)]. Full PCMBS SCAM analysis of hCNT3C- TMs 7 – 10 was performed in Chapters 4 and 7 and confirms their opposite orientation, findings supported by parallel studies of hCNT1 TMs 7/8 (Chapter 5) and *E. coli* NupC TMs 4/5 (Chapter 6). Therefore, the cumulative evidence presented in this thesis favors a revised model of hCNT3 membrane architecture (Fig. 8-1).

PCMBS-inhibitable and uridine-protectable residues were identified in TMs 7, 8, 9, 11, 11A, 12 and 13, thereby placing aspects of all seven regions within, or in close proximity to, the permeant translocation pathway of hCNT3. At the very least, all of the residues inhibited by PCMBS must be solvent-accessible from the extracellular medium and in a location where PCMBS binding compromises transport activity. Serving as a control for the present experiments, the putative intracellular loops between TMs 9 – 10 (Chapter 7) and 12 – 13 showed no inhibition by PCMBS despite robust functional activity of all of the mutants. Quantitatively, the study in this Chapter showed residues with the most severe inhibition by PCMBS located in TMs 11A and 12, and not TMs 11 and 13 (Table 8-2). For example, TMs 11 and 13 contained no residues where uptake was inhibited by PCMBS by > 80%, whereas TM 11A contained six (Phe516, Phe517, Asn518, Phe520, Tyr523 and Leu526) and TM 12 contained three (Thr557, Tyr558 and Gly567). Furthermore, the five of these residues that were uridine-protectable (Phe516, Tyr523, Leu526, Tyr558 and Gly567) were fully protected by extracellular uridine (Table 8-2). This strongly implicated these two TMs in formation of key functional regions of the translocation pore and supports results of previous studies identifying important residues in TMs 11A [11 and Appendix 1 (12)] and 12 (10).

Additionally, residues which altered the Na^+/H^+ ratio of uridine uptake were also located in TM 11A and 12 (Fig. 8-7). In contrast, residues in TMs 11 and 13 were inhibited by PCMBS to a lesser extent, and of the five residues that were uridine-protectable, two (Met491 in TM 11 and Ala609 in TM 13) were only partially protected by extracellular uridine (Table 8-2). Similarly, only two hCNT3C-residues in TM 11 (Leu480 and Ser487) and no residues in TM 13 were identified as inhibitable by MTS reagents in the yeast study, and those mutants also displayed only partial inhibition and protection (8). Together with the observation that PCMBS-accessible residues were more exofacially located in TMs 11 and 13 than in TMs 11A and 12 (Fig. 8-7), these findings suggested that TMs 11 and 13 may be less directly involved in formation of the translocation pore than TMs 11A and 12. Some cases of PCMBS-inhibition and/or uridine-protection may, for example, be secondary indirect effects of cation- or permeant-induced conformational changes, rather than indicators of close-proximity interaction with cation or nucleoside binding domains.

The present study in this Chapter also contributed to two further insights into hCNT3 structure and function. The first relates to cation-dependent conformations adopted by the exofacially-facing form of the protein. In contrast to Na^+-specific hCNT1 and hCNT2, hCNT3 mediates both Na^+- and H^+-coupled nucleoside cotransport (1, 2, 4, 6, 13, 21). The cation/nucleoside stoichiometry for hCNT3 H^+-coupled transport is 1:1, compared to 2:1 for Na^+ and, when both cations are present, charge/uptake experiments suggest that hCNT3 binds one Na^+ and one H^+ (6, 13). The nucleoside and nucleoside drug selectivity pattern of hCNT3 in the presence of H^+ also differs from that in the presence of Na^+ (4, 6). Previously, mutation of hCNT3 Cys561 in TM 12 was reported to alter Na^+ and H^+ kinetics and, together with Tyr558 and Ile554, form a face of the helix which becomes extracellularly accessible to PCMBS only in the presence of H^+ (Fig. 8-6), thus reporting a H^+-dependent conformation of the protein [Chapter 3 (9), 10]. Building upon these observations, the different patterns of residues exhibiting PCMBS inhibition and uridine protection in Na^+-containing, H^+-reduced medium only *versus* Na^+-free, acidified medium only *versus* both media provided strong additional support for the

existence of multiple Na^+- and/or H^+-induced conformational states of hCNT3 (Table 8-2 and Fig. 8-5), some of which, like the H^+-specific TM 12 Ile554/Tyr558/Cys561 cluster, involve subdomains within TMs. Other potential conformational differences are even more subtle. The arrows in Figs. 8-5 and 8-7, for example, identify residues in TMs 11 and 11A which were PCMBS-sensitive in both media, but were uridine-protected only in Na^+-containing, H^+-reduced medium.

Second, the present studies in this Chapter support the concept of central closely adjacent cation-nucleoside binding domains within a common cation/nucleoside translocation pore. Similar to TMs 7, 8 (Chapter 4), 9 (Chapter 7) and 12 (10), TM 11A contains residues deep within the membrane that are PCMBS-inhibitable and uridine-protectable. Met491, a centrally positioned residue in TM 11, also shares this phenotype. In good agreement with this, other cation transporters for which high resolution molecular structures have been solved, including $LeuT_{Aa}$ (15) and Glt_{Ph} (18), also exhibit central cation and permeant binding domains.

Conclusions – This SCAM analysis of the TM 11-13 region of hCNT3 supports a revised topology model for hCNTs, with the insertion of TM 11A as a membrane-spanning discontinuous helix, and completes a PCMBS cysteine-scanning mutagenesis study of the whole C-terminal half of the transporter. Confirmation of this new membrane architecture will come from extension of the analysis to TMs in the N-terminal half of the protein, including TM 5A. Additionally, this Chapter highlights the functional importance of residues in TMs 11A and 12 in key cation and nucleoside binding and/or translocation events.

Table 8-1. Na^+- and H^+-mediated uptake of uridine in *Xenopus* oocytes expressing hCNT3C- single cysteine mutants. Influx of 10 μM ^{3}H-uridine was measured in both Na^+-containing and H^+-containing medium (100 mM NaCl, pH 8.5 or 100 mM ChCl, pH 5.5, respectively). Na^+:H^+ uptake ratios which are < 0.5 or > 2.5 are highlighted with an asterisk (*). Values are corrected for basal non-mediated uptake in control water-injected oocytes. Each value is the mean ± SEM of 10 - 12 oocytes.

	Mediated Uridine Uptake (pmol/oocyte.min^{-1})		
TM 11	Na^+ (100 mM NaCl, pH 8.5)	H^+ (100 mM ChCl, pH 5.5)	Na^+:H^+ Ratio
L480C(C-)	0.9 ± 0.1	1.1 ± 0.2	0.8
S481C(C-)	1.2 ± 0.1	0.7 ± 0.1	1.7
F482C(C-)	0.8 ± 0.1	0.7 ± 0.1	1.1
E483C(C-)	0.6 ± 0.1	0.2 ± 0.1	2.5
L484C(C-)	2.6 ± 0.5	2.7 ± 0.3	1.0
I485C(C-)[b]	2.0 ± 0.3	1.4 ± 0.1	1.4
S486C(C-)	3.9 ± 0.4	2.6 ± 0.2	1.5
S487C(C-)	1.4 ± 0.2	1.7 ± 0.2	0.8
Y488C(C-)	2.3 ± 0.2	1.1 ± 0.1	2.2
I489C(C-)	2.3 ± 0.2	2.5 ± 0.3	0.9
F490C(C-)	0.9 ± 0.2	0.4 ± 0.1	2.4
M491C(C-)	2.5 ± 0.3	2.7 ± 0.3	0.9
P492C(C-)	1.0 ± 0.1	0.8 ± 0.1	1.3
F493C(C-)	3.6 ± 0.4	2.3 ± 0.2	1.6
S494C(C-)	0.7 ± 0.1	1.0 ± 0.1	0.8
F495C(C-)	1.6 ± 0.3	1.7 ± 0.2	0.9
M496C(C-)[a]	< 0.1	< 0.1	-
M497C(C-)	2.0 ± 0.2	3.0 ± 0.2	0.7
G498C(C-)[a]	< 0.1	< 0.1	-
V499C(C-)	1.8 ± 0.3	3.0 ± 0.3	0.7
E500C(C-)	4.8 ± 0.3	4. 3 ± 0.3	1.1

Table 8-1 continued

TM 11 - 12 loop	Mediated Uridine Uptake (pmol/oocyte.min^{-1})		Na^+:H^+ Ratio
	Na^+ (100 mM NaCl, pH 8.5)	H^+ (100 mM ChCl, pH 5.5)	
W501C(C-)	3.1 ± 0.6	1.3 ± 0.3	2.4
Q502C(C-)	4.1 ± 0.5	3.5 ± 0.2	1.2
D503C(C-)	2.2 ± 0.2	1.3 ± 0.1	1.7
S504C(C-)	1.7 ± 0.3	1.8 ± 0.2	1.0
F505C(C-)	3.9 ± 0.4	2.9 ± 0.3	1.4
M506C(C-)	2.0 ± 0.2	2.2 ± 0.2	0.9
V507C(C-)	5.0 ± 0.3	5.8 ± 0.4	0.9
A508C(C-)	2.0 ± 0.3	1.3 ± 0.2	1.5
R509C(C-)	6.8 ± 0.3	4.2 ± 0.3	1.6
L510C(C-)	5.4 ± 0.3	5.9 ± 0.4	0.9
I511C(C-)	3.4 ± 0.3	3.7 ± 0.3	0.9
G512C(C-)	1.4 ± 0.2	0.4 ± 0.1	3.9*
Y513C(C-)	1.4 ± 0.1	3.2 ± 0.4	0.4*
K514C(C-)	1.1 ± 0.2	0.1 ± 0.1	7.9*
T515C(C-)	1.9 ± 0.3	2.1 ± 0.2	0.9
F516C(C-)	4.8 ± 0.4	1.5 ± 0.1	3.1*
F517C(C-)	0.3 ± 0.1	0.4 ± 0.1	0.6
N518C(C-)	3.8 ± 0.4	1.6 ± 0.2	2.3
E519C(C-)	< 0.1	< 0.1	-
F520C(C-)	1.2 ± 0.1	1.7 ± 0.1	0.7
V521C(C-)	2.1 ± 0.2	1.0 ± 0.1	2.1
A522C(C-)	1.8 ± 0.1	0.3 ± 0.1	7.0*
Y523C(C-)	1.2 ± 0.2	0.5 ± 0.1	2.5
E524C(C-)	2.7 ± 0.2	1.0 ± 0.1	2.6*
H525C(C-)	4.2 ± 0.4	1.6 ± 0.2	2.7*
L526C(C-)	4.0 ± 0.4	5.5 ± 0.6	0.7
S527C(C-)	2.3 ± 0.2	2.5 ± 0.2	0.9
K528C(C-)	4.0 ± 0.4	4.0 ± 0.2	1.0
W529C(C-)	3.2 ± 0.2	4.5 ± 0.3	0.7
I530C(C-)	3.5 ± 0.4	2.5 ± 0.2	1.4
H531C(C-)	4.5 ± 0.4	3.8 ± 0.2	1.2
L532C(C-)	3.2 ± 0.3	3.6 ± 0.4	0.9

R533C(C-)	4.2 ± 0.4	3.5 ± 0.3	1.2
K534C(C-)	3.8 ± 0.2	4.3 ± 0.2	0.9

Table 8-1 continued

TM 11 - 12 loop	Mediated Uridine Uptake (pmol/oocyte.min^{-1})		Na^+:H^+ Ratio
	Na^+ (100 mM NaCl, pH 8.5)	H^+ (100 mM ChCl, pH 5.5)	
E535C(C-)	2.5 ± 0.3	1.6 ± 0.1	1.6
G536C(C-)	4.0 ± 0.4	4.1 ± 0.3	1.0
G537C(C-)	3.9 ± 0.3	4.5 ± 0.4	0.9
P538C(C-)	4.3 ± 0.3	3.9 ± 0.3	1.1
K539C(C-)	4.1 ± 0.2	4.6 ± 0.5	0.9
F540C(C-)	3.8 ± 0.3	4.7 ± 0.5	0.8
V541C(C-)	4.1 ± 0.4	4.4 ± 0.4	0.9
N542C(C-)	5.0 ± 0.3	4.8 ± 0.5	1.0
G543C(C-)	5.0 ± 0.2	5.6 ± 0.4	0.9
V544C(C-)	4.3 ± 0.4	5.3 ± 0.3	0.8
Q545C(C-)	3.3 ± 0.1	5.1 ± 0.3	0.7
Q546C(C-)	3.3 ± 0.3	4.7 ± 0.3	0.7
Y547C(C-)	3.5 ± 0.2	4.2 ± 0.4	0.8
I548C(C-)	3.3 ± 0.2	4.4 ± 0.1	0.8
S549C(C-)	3.6 ± 0.2	5.0 ± 0.3	0.7
I550C(C-)	3.6 ± 0.2	4.7 ± 0.4	0.8
R551C(C-)	1.4 ± 0.1	1.4 ± 0.2	1.0
S552C(C-)	3.7 ± 0.2	5.2 ± 0.4	0.7
E553C(C-)	3.7 ± 0.3	5.2 ± 0.6	0.7

Table 8-1 continued

TM 12	Mediated Uridine Uptake (pmol/oocyte.min^{-1}) Na^+ (100 mM NaCl, pH 8.5)	H^+ (100 mM ChCl, pH 5.5)	Na^+:H^+ Ratio
I554C(C-)	2.0 ± 0.3	1.5 ± 0.2	1.3
I555C(C-)	1.9 ± 0.2	2.1 ± 0.2	0.9
A556C(C-)	1.5 ± 0.3	1.5 ± 0.1	1.0
T557C(C-)	2.7 ± 0.3	1.9 ± 0.1	1.4
Y558C(C-)	0.1 ± 0.1	0.5 ± 0.1	0.2*
A559C(C-)	0.8 ± 0.1	1.0 ± 0.1	0.8
L560C(C-)	2.1 ± 0.3	2.1 ± 0.3	1.0
S561C(C-)	2.4 ± 0.4	3.6 ± 0.2	0.7
G562C(C-)	0.8 ± 0.2	0.5 ± 0.1	1.5
F563C(C-)[a]	< 0.1	< 0.1	-
A564C(C-)	0.5 ± 0.1	0.1 ± 0.1	5.0*
N565C(C-)	2.6 ± 0.4	0.8 ± 0.1	3.3*
I566C(C-)	0.9 ± 0.2	0.4 ± 0.1	2.6*
G567C(C-)	1.4 ± 0.3	0.9 ± 0.1	1.6
S568C(C-)[b]	< 0.1	< 0.1	-
L569C(C-)	1.8 ± 0.3	1.5 ± 0.2	1.1
G570C(C-)	1.1 ± 0.2	0.7 ± 0.1	1.6
I571C(C-)	3.2 ± 0.4	1.4 ± 0.1	2.3
V572C(C-)	3.3 ± 0.3	2.0 ± 0.2	1.7
I573C(C-)	3.8 ± 0.5	1.8 ± 0.2	2.1
G574C(C-)	0.2 ± 0.1	0.1 ± 0.1	1.4

Table 8-1 continued

TM 12 - 13 Loop	Mediated Uridine Uptake (pmol/oocyte.min^{-1})		Na^+:H^+ Ratio
	Na^+ (100 mM NaCl, pH 8.5)	H^+ (100 mM ChCl, pH 5.5)	
G575C(C-)	4.6 ± 0.6	3.5 ± 0.3	1.3
L576C(C-)	2.9 ± 0.3	1.7 ± 0.2	1.8
T577C(C-)	3.9 ± 0.5	3.1 ± 0.3	1.2
S578C(C-)	3.7 ± 0.3	3.5 ± 0.2	1.1
M579C(C-)	4.2 ± 0.3	2.9 ± 0.3	1.5
A580C(C-)	4.1 ± 0.3	3.5 ± 0.3	1.2
P581C(C-)	0.6 ± 0.1	0.2 ± 0.1	2.5
S582C(C-)	4.4 ± 0.5	5.7 ± 0.3	0.8
R583C(C-)	1.6 ± 0.3	1.0 ± 0.1	1.7
K584C(C-)	2.3 ± 0.4	1.7 ± 0.2	1.3
R585C(C-)	3.7 ± 0.5	2.2 ± 0.2	1.7
D586C(C-)	4.9 ± 0.4	3.0 ± 0.4	1.6
I587C(C-)	1.2 ± 0.2	1.2 ± 0.1	1.0
A588C(C-)	2.1 ± 0.2	2.7 ± 0.2	0.8
S589C(C-)	3.4 ± 0.4	3.9 ± 0.4	0.9
G590C(C-)	3.5 ± 0.5	3.3 ± 0.2	1.1
A591C(C-)	1.9 ± 0.3	1.9 ± 0.2	1.0

Table 8-1 continued

TM 13	Mediated Uridine Uptake (pmol/oocyte.min^{-1}) Na^+ (100 mM NaCl, pH 8.5)	Mediated Uridine Uptake (pmol/oocyte.min^{-1}) H^+ (100 mM ChCl, pH 5.5)	Na^+:H^+ Ratio
V592C(C-)	2.0 ± 0.3	1.9 ± 0.2	1.1
R593C(C-)[b]	< 0.1	< 0.1	-
A594C(C-)[a]	< 0.1	< 0.1	-
L595C(C-)[b]	1.4 ± 0.2	1.3 ± 0.1	1.0
I596C(C-)	0.8 ± 0.1	1.1 ± 0.3	0.7
A597C(C-)	2.4 ± 0.3	3.6 ± 0.3	0.7
G598C(C-)[a]	0.8 ± 0.1	1.6 ± 0.3	0.5
T599C(C-)	2.6 ± 0.3	3.0 ± 0.3	0.9
V600C(C-)	2.2 ± 0.2	2.3 ± 0.2	1.0
A601C(C-)	0.4 ± 0.1	0.6 ± 0.1	0.6
S602C(C-)	4.2 ± 0.4	2.1 ± 0.2	2.0
F603C(C-)[b]	3.0 ± 0.4	2.4 ± 0.3	1.3
M604C(C-)	0.7 ± 0.2	0.6 ± 0.1	1.1
T605C(C-)	1.0 ± 0.2	1.7 ± 0.3	0.6
A606C(C-)[a]	< 0.1	< 0.1	-
S607C(C-)	1.8 ± 0.1	1.5 ± 0.2	1.2
I608C(C-)	1.3 ± 0.2	1.8 ± 0.2	0.7
A609C(C-)	0.8 ± 0.1	0.5 ± 0.1	1.6
G610C(C-)[b]	< 0.1	< 0.1	-
I611C(C-)	1.6 ± 0.3	1.7 ± 0.2	1.0
L612C(C-)	2.2 ± 0.2	2.0 ± 0.3	1.1

[a], previously identified as non-functional (7); [b], previously identified as low-functioning (7).

Table 8-2. Effect of PCMBS on uridine uptake in *Xenopus* oocytes expressing hCNT3C- single cysteine mutants. Influx of 10 μM ^{3}H-uridine was measured in both Na^+-containing and H^+-containing medium (100 mM NaCl, pH 8.5 or 100 mM ChCl, pH 5.5, respectively) following 10 min incubation on ice in the absence or presence of 200 μM PCMBS or 200 μM PCMBS + 20 mM uridine in media of the same composition used to determine uptake (*i.e.* containing Na^+ or H^+, as indicated). Values are corrected for basal non-mediated uptake in control water-injected oocytes and are presented as a percentage of mediated uridine influx in the absence of inhibitor for each individual mutant. Each value is the mean ± SEM of 10 - 12 oocytes.

		Na^+ (100 mM NaCl, pH 8.5)		H^+ (100 mM ChCl, pH 5.5)	
TM		+ PCMBS[a] (%)	+ PCMBS + uridine (%)	+ PCMBS[a] (%)	+ PCMBS + uridine (%)
11	L480C(C-)[b]	110 ± 20	90 ± 20	53 ± 8	91 ± 10
	F482C(C-)	39 ± 7	91 ± 20	59 ± 8	98 ± 10
	E483C(C-)	52 ± 6	42 ± 10	94 ± 20	85 ± 10
	L484C(C-)	48 ± 5	57 ± 8	95 ± 10	86 ± 7
	S487C(C-)[b]	47 ± 7	45 ± 5	48 ± 10	68 ± 5
	M491C(C-)	38 ± 4	70 ± 7	60 ± 3	65 ± 7
11 - 12 loop	M506C(C-)	21 ± 5	21 ± 5	37 ± 3	37 ± 3
	A508C(C-)	86 ± 10	78 ± 10	37 ± 6	94 ± 20
	G512C(C-)	70 ± 10	92 ± 20	54 ± 10	83 ± 10
	Y513C(C-)	45 ± 4	44 ± 6	60 ± 9	62 ± 6
	F516C(C-)	9 ± 1	100 ± 10	11 ± 2	73 ± 7
	F517C(C-)	12 ± 3	10 ± 3	16 ± 3	20 ± 3
	N518C(C-)	6 ± 1	9 ± 1	5 ± 1	7 ± 1
	F520C(C-)	26 ± 3	17 ± 3	5 ± 1	12 ± 2
	V521C(C-)	26 ± 3	18 ± 2	35 ± 6	27 ± 3
	A522C(C-)	30 ± 5	100 ± 10	90 ± 9	110 ± 10
	Y523C(C-)	10 ± 1	77 ± 20	3 ± 2	3 ± 1
	L526C(C-)	26 ± 4	120 ± 10	10 ± 2	35 ± 6
	Q545C(C-)	83 ± 8	81 ± 7	47 ± 3	40 ± 3

Table 8-2 continued

TM		Na^+ (100 mM NaCl, pH 8.5)		H^+ (100 mM ChCl, pH 5.5)	
		+ PCMBS[a] (%)	+ PCMBS + uridine (%)	+ PCMBS[a] (%)	+ PCMBS + uridine (%)
12	I554C(C-)	98 ± 20	93 ± 8	52 ± 6	67 ± 9
	T557C(C-)[b]	7 ± 1	16 ± 2	22 ± 2	33 ± 2
	Y558C(C-)	92 ± 20	100 ± 20	19 ± 3	71 ± 10
	S561C(C-)	100 ± 20	99 ± 9	54 ± 5	94 ± 8
	N565C(C-)[b]	37 ± 5	110 ± 10	46 ± 9	110 ± 20
	G567C(C-)[b]	17 ± 4	97 ± 20	14 ± 5	94 ± 20
	I571C(C-)[b]	44 ± 8	85 ± 9	30 ± 3	90 ± 8
13	A601C(C-)	57 ± 7	43 ± 8	29 ± 5	29 ± 3
	A609C(C-)	55 ± 5	69 ± 9	60 ± 6	76 ± 10
	L612C(C-)	48 ± 5	100 ± 9	59 ± 3	86 ± 5

[a], mediated uridine influx in the absence of inhibitor is given in pmol/oocytes.min^{-1} in Table 8-1 for each of the individual mutants; [b], previously identified as MTS-sensitive residues (7).

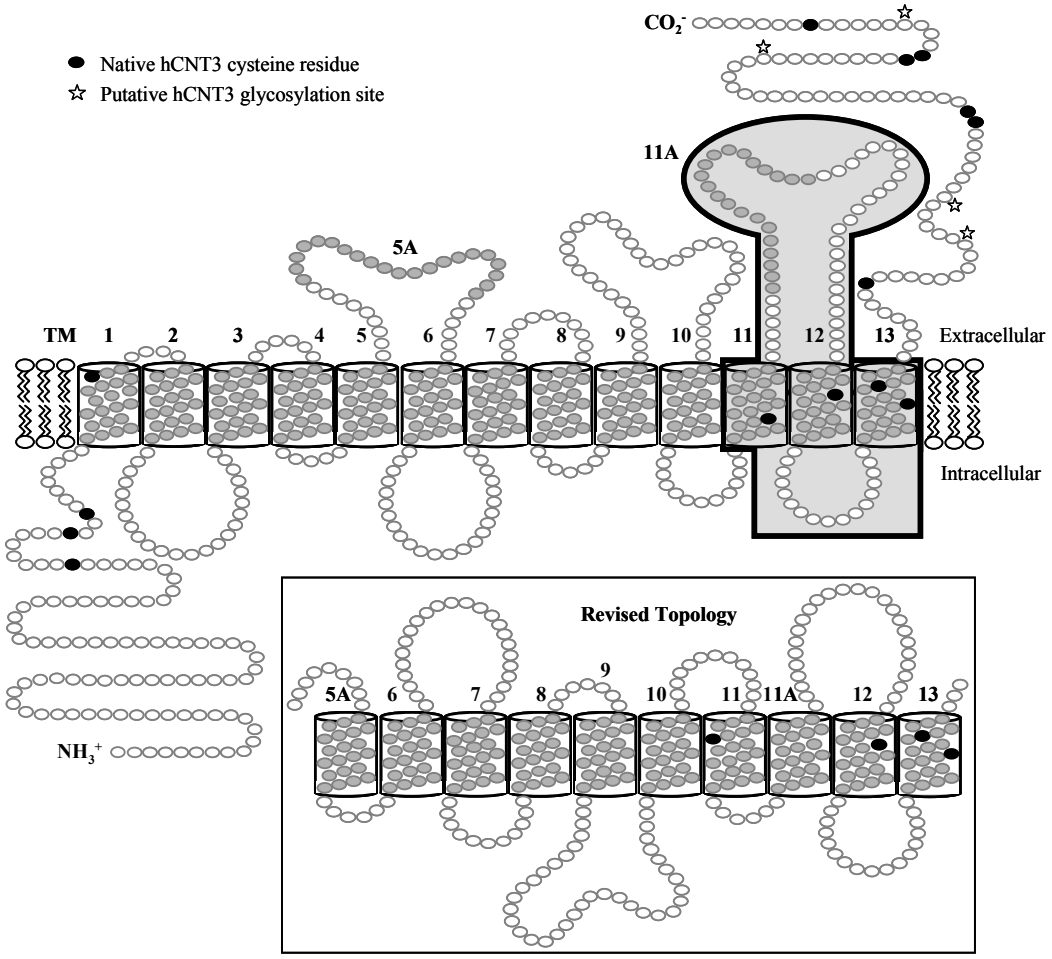

Figure 8-1. Alternative models of hCNT3 topology. Schematic of proposed hCNT3 (GenBank™ accession number AF305210) topology with either 13 TMs or revised topology. Insertion of TMs 5A and 11A into the membrane, resulting in a revised architecture and opposite orientations of TMs 6 - 11, is depicted in the *inset*. The position of endogenous cysteine residues are indicated as *black* residues, and putative glycosylation sites are highlighted with a *star* symbol. Residues studied by SCAM analysis are highlighted with a *grey* box.

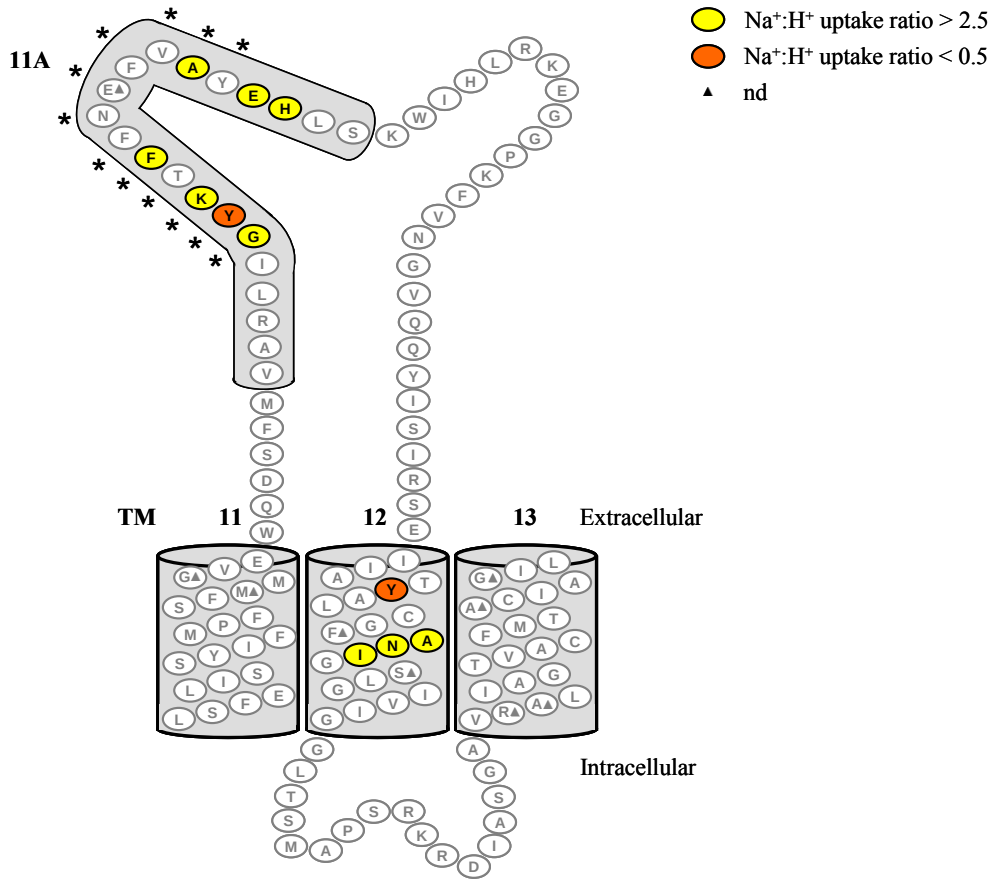

Figure 8-2. hCNT3 TMs 11 - 13 depicting residues with altered Na^+:H^+ uridine uptake ratios. hCNT3C- mutants exhibiting Na^+:H^+ uridine uptake ratios > 2.5 are indicated in *yellow*, and those with uptake ratios < 0.5 are shown in *orange* (Table 8-1). The * symbol represents residues which form the conserved CNT family (G/A)*X*K*X*$_3$NEFVA(Y/M/F) motif. Low activity mutants with uridine transport rates < 0.1 pmol/oocyte.min^{-1} in both Na^+- and H^+-containing transport media (100 mM NaCl, pH 8.5 and ChCl, pH 5.5, respectively) are indicated by the ▲ symbol. Corresponding numerical values are given in Table 8-1.

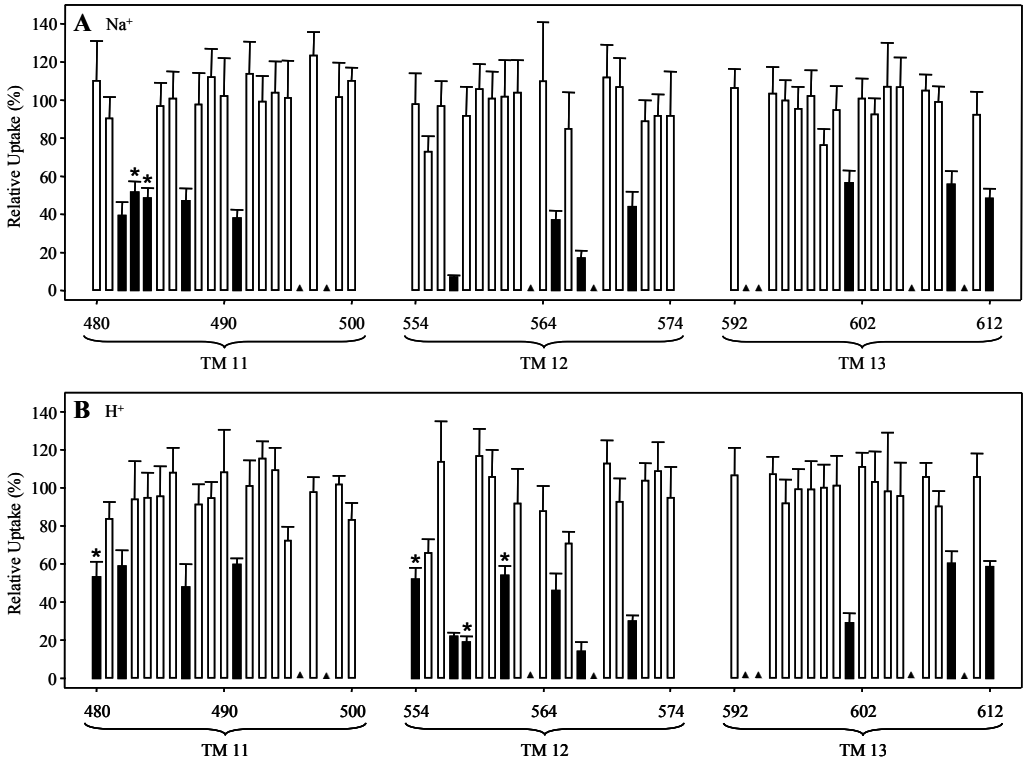

Figure 8-3. PCMBS inhibition of residues in hCNT3C- TMs 11, 12 and 13. Mediated influx of 10 μM radiolabeled uridine in Na^+-containing (*A*) or H^+-containing (*B*) medium (100 mM NaCl, pH 8.5 or 100 mM ChCl, pH 5.5, respectively) was measured following 10 min incubation on ice in Na^+- or H^+-containing medium (*A* or *B*, respectively) in the presence of 200 μM PCMBS. *Solid* columns indicate residue positions inhibited by PCMBS; the * symbol identifies those residues which exhibit differential inhibition by PCMBS in the two media. Low activity mutants where inhibition was not determined are indicated by the ▲ symbol. Data are presented as mediated transport, calculated as uptake in RNA-injected oocytes *minus* uptake in water-injected oocytes, and are normalized to the respective influx of uridine in the absence of inhibitor. Each value is the mean ± SEM of 10 - 12 oocytes.

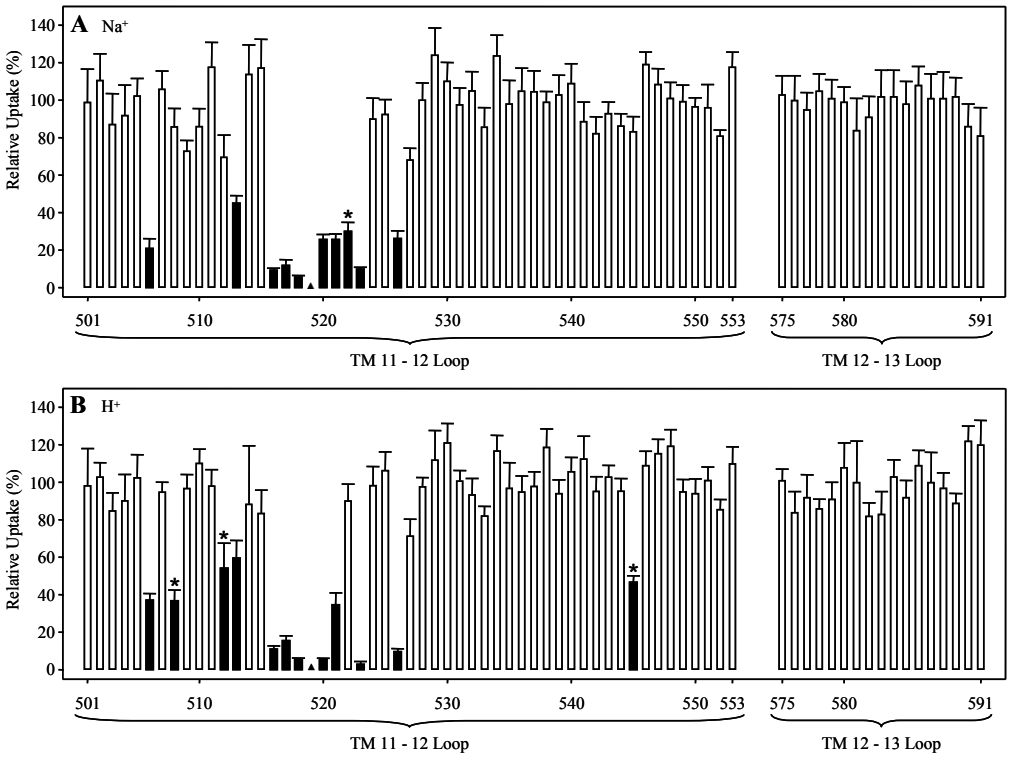

Figure 8-4. PCMBS inhibition of residues in hCNT3C- loop regions between TMs 11 and 12, and TMs 12 and 13. Mediated influx of 10 μM radiolabeled uridine in Na^+-containing (*A*) or H^+-containing (*B*) medium (100 mM NaCl, pH 8.5 or 100 mM ChCl, pH 5.5, respectively) was measured following 10 min incubation on ice in Na^+- or H^+-containing medium (*A* or *B*, respectively) in the presence of 200 μM PCMBS. *Solid* columns indicate residue positions inhibited by PCMBS; the * symbol identifies those residues which exhibit differential inhibition to PCMBS in the two media. Low activity mutants where inhibition was not determined are indicated by the ▲ symbol. Data are presented as mediated transport, calculated as uptake in RNA-injected oocytes *minus* uptake in water-injected oocytes, and are normalized to the respective influx of uridine in the absence of inhibitor. Each value is the mean ± SEM of 10 - 12 oocytes.

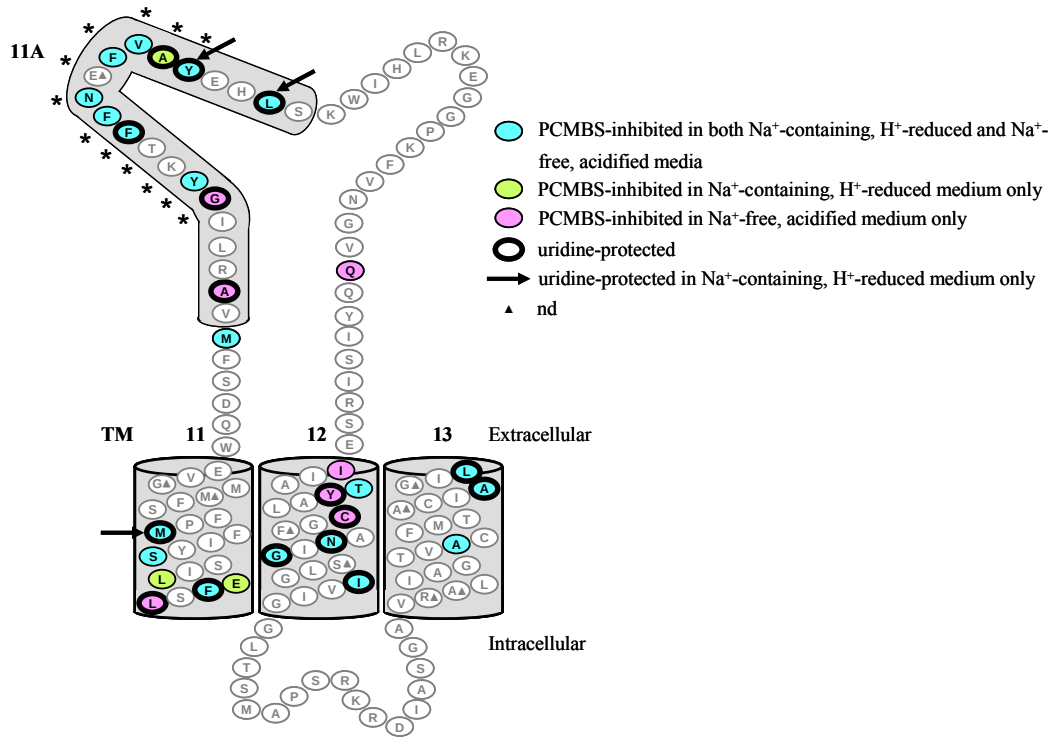

Figure 8-5. hCNT3 TMs 11 - 13 depicting PCMBS-inhibited and uridine-protected residues. hCNT3C- mutants exhibiting inhibition of uridine uptake following incubation with PCMBS in both Na^+- and H^+-containing transport medium are indicated in *blue*, those inhibited in Na^+-containing transport medium only are indicated in *green* and those inhibited in H^+-containing transport medium only are indicated in *pink*. Residues protected from PCMBS inhibition by excess unlabeled uridine are outlined in *black*. The three residues, Met491 in TM 11, Tyr523 and Leu526 in TM 11A, which were inhibited by PCMBS in both Na^+- and H^+-containing medium, but protected from that inhibition only in the presence of Na^+ are indicated by a *black arrow*. The * symbol represents residues which form the conserved CNT family (G/A)*X*KK*X*$_3$NEFVA(Y/M/F) motif. Low activity mutants are indicated by the ▲ symbol. Corresponding numerical values are given in Table 8-2.

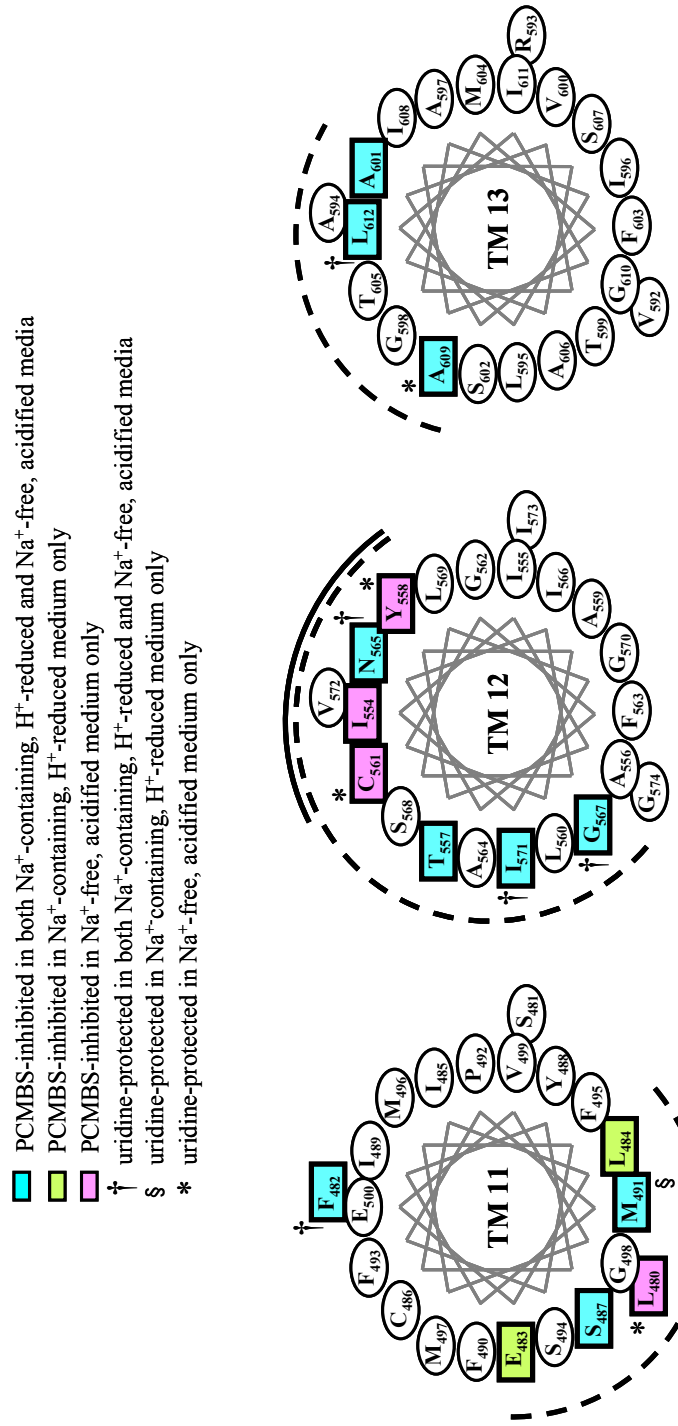
PCMBS-inhibited in both Na+-containing, H+-reduced and Na+-free, acidified media
PCMBS-inhibited in Na+-containing, H+-reduced medium only
PCMBS-inhibited in Na+-free, acidified medium only
† uridine-protected in both Na+-containing, H+-reduced and Na+-free, acidified media
§ uridine-protected in Na+-containing, H+-reduced medium only
* uridine-protected in Na+-free, acidified medium only
TM 11
TM 12
TM 13

Figure 8-6.

Figure 8-6. Helical wheel projections of hCNT3 TMs 11, 12 and 13. The helical wheel projections, as viewed from the extracellular side of the membrane, highlight in *blue* the locations of hCNT3 residues which are inhibited by PCMBS in both Na^+- and H^+-containing media, in *green* those residues inhibited in Na^+-containing medium only and in *pink* those inhibited in H^+-containing medium only. Those residues for which uridine-protection was evident in both Na^+-containing, H^+-reduced and Na^+-free, acidified transport media or in Na^+-containing, H^+-reduced medium only or in Na^+-free, acidified medium only, are indicated by the symbols †, § and *, respectively. Corresponding numerical values are given in Table 8-2.

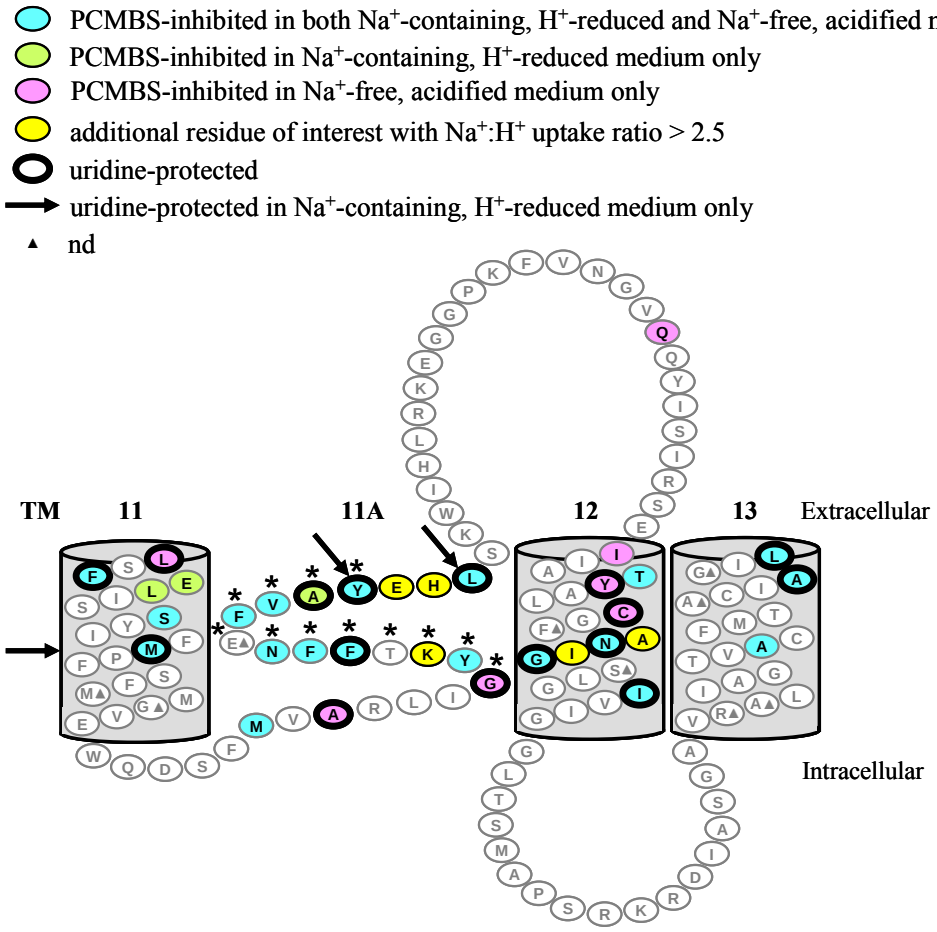
PCMBS-inhibited in both Na+-containing, H+-reduced and Na+-free, acidified media
PCMBS-inhibited in Na+-containing, H+-reduced medium only
PCMBS-inhibited in Na+-free, acidified medium only
additional residue of interest with Na+:H+ uptake ratio > 2.5
uridine-protected
uridine-protected in Na+-containing, H+-reduced medium only
nd
TM
11
11A
12
13
Extracellular
Intracellular

Figure 8-7.

Figure 8-7. Revised hCNT3 TM 11 - 13 topology depicting TM 11A as membrane-spanning. This schematic depicts insertion of TM 11A as membrane-spanning, thus reversing the orientation of TM 11. For illustrative purposes, the endofacial boundary of helix 11A, as illustrated in Figs. 8-1, 8-2 and 8-5, has been shifted by one residue to include the residue Met506. PCMBS-inhibited and uridine-protected residues as well as additional residues of interest with Na^+:H^+ uridine uptake ratios > 2.5, but not inhibited by PCMBS are highlighted according to Figs. 8-5 and 8-2, respectively. Two residues, Tyr^{513} in TM 11A and Tyr558 in TM 12, which exhibited Na^+:H^+ uridine uptake ratios < 0.5 were also PCMBS-inhibited and are only indicated as such. The three residues, Met491 in TM 11, and Tyr523 and Leu526 in TM 11A, which were inhibited by PCMBS in both Na^+- and H^+-containing medium, but protected from that inhibition only in the presence of Na^+ are indicated by a *black arrow*. The * symbol represents residues which form the conserved CNT family (G/A)*X*KX_3NEFVA(Y/M/F) motif. Low activity mutants are indicated by the ▲ symbol. Corresponding numerical values are given in Tables 8-1 and 8-2.

Bibliography

1. Ritzel, M. W. L., Yao, S. Y. M., Huang, M. Y., Elliott, J. F., Cass, C. E., and Young, J. D. (1997) Molecular cloning and functional expression of cDNAs encoding a human Na^+-nucleoside cotransporter (hCNT1). *Am. J. Physiol*. **272**: C707-C714.

2. Ritzel, M. W. L., Yao, S. Y. M., Ng, A. M. L., Mackey, J. R., Cass, C. E., and Young, J. D. (1998) Molecular cloning, functional expression and chromosomal localization of a cDNA encoding a human Na^+/nucleoside cotransporter (hCNT2) selective for purine nucleosides and uridine. *Mol. Membr. Biol*. **15**: 203-211.

3. Hamilton, S. R., Yao, S. Y. M., Ingram, J. C., Hadden, D. A., Ritzel, M. W. L., Gallagher, M. P., Henderson, P. J. F., Cass, C. E., Young, J. D., and Baldwin, S. A. (2001) Subcellular distribution and membrane topology of the mammalian concentrative nucleoside transporter rCNT1. *J. Biol. Chem.* **276**: 27981-27988.

4. Ritzel, M. W. L., Ng, A. M. L., Yao, S. Y. M., Graham, K., Loewen, S. K., Smith, K. M., Ritzel, R. G., Mowles, D. A., Carpenter, P., Chen, X.-Z., Karpinski, E., Hyde, R. J., Baldwin, S. A., Cass, C. E., and Young, J. D. (2001) Molecular identification and characterization of novel human and mouse concentrative Na^+-nucleoside cotransporter proteins (hCNT3 and mCNT3) broadly selective for purine and pyrimidine nucleosides (system *cib*). *J. Biol. Chem*. **276**: 2914-2927.

5. Yao, S. Y. M., Ng, A. M. L., Loewen, S. K., Cass, C. E., Baldwin, S. A., and Young, J. D. (2002) An ancient prevertabrate Na^+-nucleoside cotransporter (hfCNT) from the Pacific hagfish (*Eptatretus stouti*). *Am. J. Physiol. Cell Physiol*. **283**: C155-C168.

6. Smith, K. M., Slugoski, M. D., Loewen, S. K., Ng, A. M., Yao, S. Y., Chen, X.-Z., Karpinski, E., Cass, C. E., Baldwin, S. A., and Young, J. D. (2005) The broadly selective human Na^+/nucleoside cotranpsorter (hCNT3) exhibits novel cation-coupled nucleoside transport characteristics. *J. Biol. Chem.* **280**: 25436-25449.

7. Craig, J. E., Zhang, Y., and Gallagher, M. P. (1994) Cloning of the nupC gene of *Escherichia coli* encoding a nucleoside transport system, and

identification of an adjacent insertion element, IS 186. *Mol. Microbiol.* **11**: 1159-1168.

8. Zhang, J., Tackaberry, T., Ritzel, M. W., Raborn, T., Barron, G., Baldwin, S. A., Young, J. D., and Cass, C. E. (2006) Cysteine-accessibility analysis of transmembrane domains 11-13 of human concentrative nucleoside transporter 3. *Biochem. J.* **394**: 389-398.

9. Slugoski, M. D., Smith, K. M., Mulinta, R., Ng, A. M. L., Yao, S. Y. M., Morrison, E. L., Lee, Q. O. T., Zhang, J., Karpinski, E., Cass, C. E., Baldwin, S. A., and Young, J. D. (2008) A conformationally mobile cysteine residue (C561) modulates Na^+- and H^+-activation of human concentrative nucleoside transporter 3 (hCNT3). *J. Biol. Chem.* **283**: 24922-24934.

10. Slugoski, M. D., Ng, A. M., Yao, S. Y., Smith, K. M., Lin, C. C., Zhang, J., Karpinski, E., Cass, C. E., and Baldwin, S. A., and Young, J. D. (2008) A proton-mediated conformational shift identifies a mobile pore-lining cysteine residue (Cys-561) in human concentrative nucleoside transporter 3. *J. Biol. Chem.* **283**: 8496-8507.

11. Slugoski, M. D., Smith, K. M., Ng, A. M. L., Yao, S. Y. M., Karpinski, E., Cass, C. E., Baldwin, S. A., and Young, J. D. (2009a) Conserved glutamate residues E343 and E519 provide mechanistic insights into cation/nucleoside cotransport by human concentrative nucleoside transporter 3 (hCNT3). *J. Biol. Chem.* **284**:17266-17280.

12. Yao, S. Y. M., Ng, A. M., Slugoski, M. D., Smith, K. M., Mulinta, R., Karpinski, E., Cass, C. E., Baldwin, S. A., and Young, J. D. (2007) Conserved glutamate residues are critically involved in Na^+/nucleoside cotransport by human concentrative nucleoside transporter 1 (hCNT1). *J. Biol. Chem.* **282**: 30607-30617.

13. Smith, K. M., Slugoski, M. D., Cass, C. E., Baldwin, S. A., Karpinski, E., and Young, J. D. (2007) Cation coupling properties of human concentrative nucleoside transporters hCNT1, hCNT2 and hCNT3. *Mol. Membr. Biol*. **24**: 53-64.

14. Yao, S. Y. M., Sundaram, M., Chomey, E. G., Cass, C. E., Baldwin, S. A., and Young, J. D. (2001) Identification of Cys_{140} in helix 4 as an exofacial

cysteine residue within the substrate-translocation channel of rat equilibrative nitrobenzylthioninosine (NBMPR)-insensitive (ENT2) nucleoside transporter rENT2. *Biochem. J.* **353**: 387-393.

15. Yamashita, A., Singh, S. K., Kawate, T., Jin, Y., and Gouaux, E. (2005) Crystal structure of a bacterial homologue of Na^+/Cl^--dependent neurotransmitter transporter. *Nature* **437**: 215-223.

16. Faham, S., Watanabe, A., Besserer, G. M., Cascio D., Specht, A., Hirayama, B., Wright, E. M., and Abramson, J. (2008) The crystal structure of a sodium galactose transporter reveals mechanistic insights into Na^+/sugar symport. *Science*. **321**: 810-814.

17. Weyand, S., Shimamura, T., Yajima, S., Suzuki, S., Mirza, O., Krusong, K., Carpenter, E. P., Rutherford, N. G., Hadden, J. M., O'Reilly, J., Ma, P., Saidijam, M., Patching, S. G., Hope, R. J., Norbertczak, H. T., Roach, P. C., Iwata, S., Henderson, P. J., and Cameron, A. D. (2008) Structure and molecular mechanism of a nucleobase-cation-symport-1 family transporter. *Science*. **322**: 709-713.

18. Yernool, D., Boudker, O., Jin, Y., and Gouaux, E. (2004) Structure of a glutamate transporter homologue from *Pyrococcus horikoshii*. *Nature* **431**: 811-818.

19. Screpanti, E., and Hunte, C. (2007) Discontinuous membrane helices in transport proteins and their correlation with function. *J. Struct. Biol.* **159**: 261-267.

20. Krishnamurthy, H., Piscitelli, C. L., and Gouaux, E. (2009) Unlocking the molecular secrets of sodium-coupled transporters. *Nature* **459**: 347- 355.

21. Smith, K. M., Ng, A. M. L., Yao, S. Y. M., Labedz, K. A., Knaus, E. E., Wiebe, L. I., Cass, C. E., Baldwin, S. A., Chen, X.-Z., Karpinski, E., and Young, J. D. (2004) Electrophysiological characterization of a recombinant human Na^+-coupled nucleoside transporter (hCNT1) produced in *Xenopus* oocytes. *J. Physiol.* **558**: 807-823.

Chapter 9:

General Discussion

Synopsis

In mammalian cells, two major protein families mediate nucleoside transport processes: the equilibrative nucleoside transporters family (ENTs) and the concentrative nucleoside transporters family (CNTs). The proteins in these separate families are structurally unrelated and, to date, there are four characterized human ENT members (hENT 1-4) and three human CNT members (hCNT 1-3) (1-3). The first mammalian nucleoside transport protein to be identified at the molecular level was rCNT1 from rat jejunum (4). However, most studies of nucleoside transporter structure and function have focused on ENTs, and it is only relatively recently that corresponding investigation of CNTs has commenced. CNTs are predominantly located in specialized cells such as intestine, kidney and liver epithelia, and are postulated to play important physiological and pharmacological roles in the absorption, secretion, distribution and elimination of nucleosides and anticancer and antiviral nucleoside drugs (5-7). Some studies suggested that CNT3 has a possible role in intracellular nucleoside trafficking due to its apparent intracellular localization in some cells (7, 8). hCNT1-3 correspond to the three major concentrative nucleoside transport processes of mammalian cells and tissues (9, 10), and their functional diversity provides unique opportunities to elucidate the structural and molecular mechanisms underlying cation-nucleoside membrane cotransport.

Human and other mammalian CNTs are capable of coupling inwardly directed nucleoside accumulation to the electrochemical gradient of Na^+ (and, in the case of CNT3, H^+). Previously, the kinetic characterization of wild-type CNTs has established a basic understanding of the functional properties of the proteins (4, 11-17). Building upon this foundation, corresponding molecular studies of CNTs have employed two complementary strategies. In the first, chimeric studies and multiple sequence alignments between CNT family members have guided site-directed mutagenesis studies to locate and characterize individual amino acid residues of mechanistic importance (17-20). In the second, substituted cysteine accessibility method (SCAM) analyses have been initiated (21, 22) to

systematically explore CNT topology and uncover additional residues of functional significance. The structure-function studies of recombinant wild-type and mutant hCNT family members in *Xenopus laevis* presented in Chapters 3 (23), 4, 6, 7, 8 (24) and Appendix 1 (published as ref. 25) of this thesis describe my contributions to our current understanding of CNT membrane architecture and the molecular mechanisms underlying nucleoside and cation binding and translocation.

Within the mammalian CNT family of proteins, there are two distinct phylogenetic subfamilies. In humans, hCNT1 and hCNT2 belong to one subfamily, while hCNT3 belongs to another. All three hCNTs are capable of Na^+/nucleoside cotransport. hCNT1 and hCNT2 are selective for pyrimidine and purine nucleosides, respectively, with a Na^+ to nucleoside coupling stoichiometry of 1:1 (15). hCNT3 is broadly selective for both pyrimidine and purine nucleosides and, unlike hCNT1/2, the Na^+/nucleoside coupling ratio is 2:1 (17). Also different from hCNT1/2, hCNT3 has been shown to be capable of transporting nucleosides in the presence of H^+ (17). Binding of Na^+ and/or H^+ increases the transporter's affinity for the co-transported nucleoside, and there is evidence that only one of the two hCNT3 Na^+-binding sites is shared by H^+ (15, 17). H^+-coupled hCNT3 does not transport guanosine, 3'-azido-3'-deoxythymidine (zidovudine; AZT) or 2', 3'-dideoxycytidine (zalcitabine; ddC) (17), demonstrating that Na^+- and H^+-bound versions of hCNT3 have significantly different conformations of the nucleoside binding pocket and/or translocation pore. Chimeric studies between hCNT1 and hCNT3 have located hCNT3-specific cation interactions to the C-terminal half of hCNT3, setting the stage for site-directed mutagenesis and SCAM experiments to identify the residues involved.

A functional cysteine-less version of hCNT3 (hCNT3C-) has been generated by mutagenesis of endogenous cysteine residues to serine, and initially investigated in the yeast expression system for SCAM analysis of TMs 11, 12 and 13 using methanesulfonate (MTS) reagents (21). Subsequently, hCNT3C- has also been characterized in the *Xenopus* oocytes expression system [Chapter 3 (23)]. In the hCNT3C- construct, all 14 endogenous cysteine residues of wild-type

hCNT3 were converted to serine. hCNT3C- was processed to the oocyte cell surface in amounts similar to wild-type hCNT3, suggesting that the engineered transporter had undergone proper protein folding. Confirming this, hCNT3C- exhibited hCNT3-like functional properties, but with a decrease in apparent affinity for Na^+ that was not apparent for H^+. Identical to wild-type hCNT3, the stoichiometry of cation:uridine coupling was 2:1 for Na^+ and 1:1 for H^+. Site-directed mutagenesis of both wild-type hCNT3 and hCNT3C- identified Cys561 in TM 12 as the residue responsible for the altered Na^+-binding phenotype. When the alternative amino acids threonine, valine and isoleucine were each substituted into position Cys561, H^+-dependent nucleoside transport activity was greatly diminished. In a previous analysis, the same residue was shown to be located in a mobile TM 12 region of the CNT translocation pore in a position within, or closely adjacent to, the nucleoside binding pocket, such that access of PCMBS to this residue reports a specific H^+-induced conformational state of the protein (22). Chapter 3 (23) provides further evidence to show that Cys561 is located in a position important for cation binding and/or translocation. Additionally, the results presented in this Chapter validated hCNT3C- as a template suitable for SCAM analysis of hCNT3.

The current topological model for hCNTs is a protein with 13 putative α-helical TM domains, with intracellular and extracellular N- and C-termini, respectively. The studies of Chapters 4 – 8 and Appendix 1 (25) provide strong evidence instead for an alternative membrane architecture, at least for the C-terminal half of hCNTs. In the absence of a crystal structure, valuable information on a membrane protein's structure can be gained from SCAM analysis using thiol reactive reagents such as *p*-chloromercuribenzene sulfonate (PCMBS). In the first series of SCAM experiments described in this thesis, individual single cysteine residues were sequentially introduced into putative TMs 7 and 8 of hCNT3C-, inclusive of extramembranous bridging loops, followed by heterologous expression in *Xenopus* oocytes and probing for reactivity to PCMBS (Chapter 4).

In previous studies of hCNT1, it was shown that putative TMs 7 and 8 contained two pairs of adjacent residues of functional importance. Mutation of hCNT1 TM 7 residues Ser319 and Gln320 to the corresponding residues of hCNT2 (Gly and Met, respectively) produced a protein that was hCNT3-like in permeant selectivity (19). Simultaneous mutation of Ser353 and Leu354 in TM 8 to the corresponding residues of hCNT2 (Thr and Val, respectively) in turn switched the protein to a purine nucleoside-preferring hCNT2-like phenotype (19). Single mutation of hCNT1 Ser353 to Thr in putative TM 8 resulted in decreased cytidine transport efficiency, and additional mutation of Leu354 to Val (S353T/L354V) resulted in a novel uridine-preferring transport phenotype (20). In addition, single mutation Leu354 to Val increased the apparent affinity of hCNT1 for both Na+ and Li^+ (20). These studies indicated that residues within putative TMs 7 and 8 play key roles in nucleoside specificity and cation coupling. Both hCNT1 TM 8 residues exhibited uridine-protectable inhibition by PCMBS, suggesting that they occupy positions within or closely adjacent to a commom cation/nucleoside translocation pore (20). Also studied were highly conserved TM 7 Glu residues Glu308 and Glu322 (hCNT1) [Appendix 1 (25)] and Glu343 (hCNT3) (26). These residues were also found to play key roles in cation/nucleoside cotransport. Thus, mutation of Glu308 or Glu322 of hCNT1 to its neutral amino acid equivalent (Gln) or alternative acidic amino acid replacement (Asp), decreased the apparent affinities for both Na^+ and uridine, with correspondingly diminished Na^+ and uridine V_{max} values [Appendix 1 (25)]. hCNT1 Glu322 additionally exhibited uridine-gated uncoupled Na^+ transport when converted to Gln, and uridine-protected inhibition by PCMBS and MTSEA when converted to cysteine [Appendix 1 (25)]. Corresponding mutation of the equivalent hCNT3 residue Glu343 had similar effects (26). Located deep within the translocation pore, Glu322 of hCNT1 and Glu343 of hCNT3 may form part of the inward gate of the transporter vestibule [Appendix 1 (25) and (26)]. The SCAM study of hCNT3C- TMs 7 and 8 presented in Chapter 4 (i) confirmed the functional importance of these transmembrane regions in both permeant and cation binding and/or translocation, (ii) supported an alternative hCNT C-terminal

topology, and (iii) provided evidence of discontinuous/extended regions within predicted hCNT helical transmembrane domains.

Following the results obtained for hCNT3C-, a parallel SCAM analysis of TMs 7 and 8 of Na^+-specific hCNT1 also revealed the presence of discontinuous/extended regions within the two predicted membrane-spanning regions (Chapter 5). Wild-type hCNT1 was shown not to be sensitive to PCMBS inhibition [(20) and Appendix 1 (25)], and so site-specific insertion of individual cysteine residues into TMs 7 and 8 was undertaken using wild-type hCNT1 as template. The close correspondence in results obtained for hCNT3C- and wild-type hCNT1 eliminated the (unlikely) possibility that the block patterns of PCMBS inhibition seen in hCNT3C- TMs 7 and 8 were artifacts of an altered structure of the engineered transporter. Studies in Chapter 6 also scanned the same region of *E. coli* H^+-coupled NupC/C96A (TMs 4 and 5) for PCMBS inhibition. Here, too, the smaller number of residues affected by PCMBS were localized within the same regions affected by PCMBS in hCNT1 and hCNT3C-. Different from hCNT3C- and hCNT1, however, was the absence of large block patterns of PCMBS inhibition (please see below, Topology). The SCAM analysis of hCNT1 (Chapter 5) also supported the proposed inversion of TMs 7 and 8 of hCNT3C- (Chapter 4), thereby exposing residue Val384 (hCNT3C-) and Ile363 (hCNT1), originally located within a putative internal loop, to the extracellular medium for PCMBS reaction and inhibition. This inversion also exposed the block of PCMBS-inhibitable residues in TM 8 of hCNT1 and hCNT3C- exofacially within the helix, in a position more likely to be accessible to the extracellular medium and available for PCMBS binding. This being the case, an inversion of TM 7 of hCNT1 and hCNT3C- is also highly probable.

SCAM analysis of the next two putative transmembrane regions of hCNT3C- (TMs 9 and 10) is reported in Chapter 7. Closely matching the discontinuous regions of TMs 7 and 8 and, in particular, mirroring almost exactly the findings for TM 8, there was block PCMBS inhibition of adjacent residues within putative TM 9 that similarly clustered towards the endofacial side of the membrane suggesting, again, the probable inversion of this region in the

topological model. Unlike TMs 7, 8 and 9, however, putative TM 10 was predicted to be a conventional α-helix. Taken together, the sum of the evidence presented in Chapters 4 – 7 suggests that the entire TMs 7 – 10 region of the transporter is in an orientation (Fig. 9-1, *inset*) opposite to that proposed in the original 13 TM topology of the transporter shown in Fig. 9-1.

The reversed orientation of TMs 7 – 10 is made possible by the reversal of TM 11 and by insertion of region 11A into the membrane, as predicted by the SCAM analysis of TMs 11 – 13 of hCNT3C- presented in Chapter 8 (24). In parallel site-directed mutagenesis studies, residues in TM 11A [Appendix 1 (25) and (26)] and in TM 12 (22) have been shown to play important roles in permeant and cation binding and/or translocation in hCNTs. For example, conversion of Glu519 in region TM 11A of hCNT3 to cysteine resulted in a shift in Na^+:nucleoside stoichiometry from 2:1 to 1:1, loss of H^+-dependent transport, as well as altered nucleoside selectivity, suggesting that this residue plays a direct role in Na^+/nucleoside and H^+/nucleoside cotransport (26). TM 12 is the region of the transporter containing conformationally-mobile Cys561. The SCAM study of Chapter 8 (24) elaborates the functional importance of TMs 11A and TM 12, supports the currently defined designation of TMs 11, 12 and 13 as membrane-spanning α-helices, and identifies a novel membrane-associated topology for TM 11A and the highly conserved CNT family motif (G/A)XKX$_3$NEFVA(Y/M/F) that it contains. That motif, like the previously described regions within TMs 7, 8 and 9, exhibited PCMBS inhibition characteristics consistent with an extended non-helical conformation. For TMs 7 and 11A, the discontinuous regions appeared bracketed by normal regions of α-helical structure. Those in TMs 8 and 9, in contrast, occupied the entire exofacial half of the predicted membrane-spanning regions.

Chapters 4-8 therefore provide novel and important insights into CNT membrane architecture and function. The relationship of these findings to the molecular mechanisms of CNT cation/nucleoside transport, and to the structure and function of other cotransporter families is further discussed below.

Molecular Mechanisms of CNT Cation/Nucleoside Cotransport

TMs Involved in Interactions with Nucleosides

Mammalian CNT1 and CNT2 family members are primarily pyrimidine nucleoside- and purine nucleoside-selective, respectively, although both mediate the transport of uridine and adenosine (2, 3). In contrast, CNT3 subfamily members are broadly selective for both pyrimidine and purine nucleosides (10, 17). Non-mammalian CNT family members also exhibit varied nucleoside selectivities. For example, the CNT family member from *E. coli*, NupC, is pyrimidine nucleoside-selective, but also transports adenosine and, to a lesser extent, inosine (27).

Scanning of the C-terminal half of hCNT3C- for uridine protection from PCMBS inhibition revealed the following residues to be potentially located within, or closely adjacent to, the nucleoside binding pocket: TM 7 (Gly340, Gln341, Thr342) (Chapter 4); TM 8 (Thr370, Ile371, Ala372, Gly373, Ser374) [Chapter 4]; TM 9 (Thr391, Ala392, Ser393, Val394, Met395) [Chapter 7]; TM 11 (Leu480, Phe482, Met491) [Chapter 8 (24)]; TM 11A (A508, Gly512, Phe516, Ala522, Tyr523, Leu526) [Chapter 8 (24)]; TM 12 (Tyr558, Cys561, Asn565, Gly567, Ile571) [Chapter 8 (24)]; and TM 13 (Ala609, Leu612) [(22) and Chapter 8 (24)] (Fig. 9-2). Parallel results were obtained for hCNT1 TMs 7 and 8 [Chapter 5 and Appendix 1 (25)]. Taken together, and with the caveat that some of the influences may be indirect, these findings provide evidence for the potential involvement of TMs 7, 8, 9, 11, 11A, 12 and 13 in the formation of the translocation pore and association with the CNT nucleoside binding pocket. Related studies from previous CNT structure-function studies also support these findings. For example, an hCNT3/1 chimera demonstrated that the C-terminal half of the protein contained functional domains responsible for nucleoside permeant selectivity (17), such that the mutant hCNT3 protein with TMs 7-13 replaced by hCNT1 exhibited hCNT1-like permeant selectivity. Within this region of the protein, residue pairs Ser319/Gln320 and Ser 353/Leu354 in TMs 7 and 8 of hCNT1, respectively, and

a corresponding TM 7 residue in CaCNT (Ser328), were shown to influence interactions with permeant (19, 28). For example, simultaneous mutation of hCNT1 Ser319/Gln320 and Ser353/Leu354 to the corresponding residues in hCNT2 resulted in a mutant protein that was purine nucleoside-selective, and hence hCNT2-like. Mutation of hCNT1 TM 7 residues Ser319/Gln320 alone generated a protein with broad hCNT3-like nucleoside selectivity (19), while mutation of TM 8 residues Ser353/Leu354 alone resulted in a protein with unique uridine-selective transport characteristics (20). Corresponding studies in hCNT1 investigating highly conserved glutamate residues in TMs 7 (Glu308 and Glu322) and TM 11A (Glu498) revealed changes in uridine transport kinetics when these residues were mutated to the equivalent neutral amino acid, Gln [Appendix 1 (25)]. Parallel analysis of the same residues in hCNT3 showed that mutation of Glu343 to Cys or Gln resulted in a protein impaired in guanosine transport and, in the case of E343C, also reduced in thymidine and inosine transport activity (26). In Na^+-free, acidified medium, hCNT3 E343Q and E343C showed increased influx of adenosine, thymidine and cytidine (E343Q) or adenosine and thymidine alone (E343C) (26). In contrast, restoration of the negative charge (mutant E343D) resulted in wild-type Na^+- and H^+-coupled nucleoside selectivity (26). In the case of hCNT3 Glu519 in TM 11A, mutation to Cys resulted in reduced influx of purine nucleosides (adenosine, guanosine and inosine), whereas charge replacement (mutant E519D) restored wild-type transport selectivity (26).

In the present thesis, residues in TMs 7 to 10, which were thought to be potentially located within, or closely adjacent to, the nucleoside binding pocket, were further tested for potential roles in permeant selectivity (Chapters 4 and 7). Five Cys-mutants in TMs 7 and 8 showed significantly different nucleoside uptake profiles compared to hCNT3 and hCNT3C- (Chapter 4). These were: G340C(C-), Q341C(C-), T342C(C-), S374C(C-) and V375C(C-) [Chapter 4]. Residues Gly340, Gln341, Ser374 and Val375 in hCNT3 correspond to the two adjacent pairs of TM 7 and 8 residues in hCNT1 that have previously been shown to determine the differences in permeant selectivity between that transporter and hCNT2 (19, 20). The present results therefore reinforce the suggestion that TM 7

and 8 of CNTs are very likely to form part of the translocation pore, and that residues within these regions play important roles in permeant selectivity and/or translocation.

PCMBS-inhibitable and uridine-protectable residues were identified in TMs 7 to 13 of hCNT3 [Chapters 4, 7 and 8 (24)], thereby placing aspects of these regions within or in close proximity to the permeant translocation pathway of the protein. At the very least, all of the residues inhibited by PCMBS must be solvent-accessible from the extracellular medium and in a location where PCMBS binding compromises transport activity. Quantitatively, the residues showing the most severe inhibition by PCMBS were located in TMs 7, 8, 9, 11A and 12 and not in TMs 10, 11 and 13 [Chapters 4, 7 and 8 (24)]. For example, TMs 10, 11 and 13 contained no residues for which uptake was inhibited by PCMBS by >80%, whereas TM 7 contained one (Gly340), TM 8 had four (Thr370, Ile371, Ala372, Gly373 and Val375), TM 9 had two (Leu390 and Ala392), TM 11A had six (Phe516, Phe517, Asn518, Phe520, Tyr 523 and Leu526) and TM 12 had three (Thr557, Tyr558 and Gly567) [Chapters 4, 7 and 8 (24)]. Furthermore, the PCMBS-sensitive residues in TMs 7, 8, 9, 11A and 12 reported modest to full protection with excellular uridine, while none of those in TMs 10, 11 and 13 exhibited full uridine protection [Chapters 4, 7 and 8 (24)]. Supporting previous mutagenesis studies in TMs 7, 8 [(19, 20), Appendix 1 (25) and (26)], 11A [Appendix 1 (25) and 26] and 12 (22), the present findings strongly implicate the same five TMs in formation of key functional regions of the translocation pore. Additionally, as discussed below, residues that altered the Na^+/H^+ ratio of uridine uptake were also primarily located in TMs 7, 8, 9, 10, 11A and 12 [Chapters 4, 7, 8 (24)]. TMs 10, 11 and 13 may therefore be less directly involved in the formation of the translocation pore than TMs 7, 8, 9, 11A and 12. Some cases of PCMBS inhibition and/or uridine protection may, for example, be secondary indirect effects of cation- or permeant-induced conformational changes rather than indicators of close proximity interaction with cation or nucleoside binding domains.

In summary, therefore, TMs 7, 8, 9, 11A and 12 were shown to be the most important in the binding and/or translocation of permeant.

TMs Involved in Interactions with Cations

Different CNT family members exhibit different cation coupling characteristics. hCNT1 and hCNT2, for example, are largely Na^+-specific with a 1:1 Na^+:nucleoside coupling stoichiometry (16). hCNT3, in contrast, is able to couple nucleoside uptake to Na^+ and/or H^+, with Na^+:nucleoside and H^+:nucleoside coupling ratios of 2:1 and 1:1, respectively (16, 17). Another member of the CNT3 subfamily, hfCNT, exhibits only Na^+-dependent transport of nucleosides with a 2:1 Na^+:nucleoside stoichiometry (18). CNT family members that are exclusively H^+-dependent include *C. albicans* CaCNT (28) and *E. coli* NupC (27). Like hCNT3, the CaCNT H^+:nucleoside coupling ratio is 1:1 (28). For wild-type hCNT3, but not hCNT1/2, Li^+ is able to substitute for Na^+ (16, 17).

The same hCNT3/1 chimeric protein used to establish the role of the C-terminal half of the transporter in permeant selectivity was also used to demonstrate that this region of the protein contained key determinants of cation coupling (17). Thus, the mutant protein was Na^+-dependent, and H^+-independent, with a hyperbolic Na^+-activation curve yielding a Hill coefficient consistent to a Na^+/nucleoside coupling stoichiometry of 1:1 (17). Site-directed mutagenesis studies have subsequently pinpointed several key TMs and residues with roles in cation coupling. For example, mutation of a single amino acid in TM 8 of hCNT1 (Leu354) to the corresponding residue in hCNT2 (Val) increased the transporter's apparent affinity for Li^+, thus displaying a hCNT3-like phenotype (20). The same mutation also increased the transporter's apparent affinity for Na^+ (20). Other studies investigated negatively charged residues in hCNT1 TM 7 (Glu308 and Glu322) and TM 11A (Glu498), and showed that their mutation resulted in altered cation kinetics [Appendix 1 (25)]. For example, mutation of Glu308 or Glu322 to Gln or Asp, resulted in a substantially decreased apparent affinity for Na^+, with E308Q, E322D and E322Q also showing major reductions in V_{max}^{Na+} values

compared to wild-type hCNT1 [Appendix 1 (25)]. Interestingly, mutant E322Q also exhibited features consistent with uncoupled Na^+ transport, whereby low Na^+-dependent uridine transport activity was associated with disproportionately high uridine-induced Na^+ currents, giving variable Na^+/nucleoside charge:flux ratios in excess of the expected wild-type value of 1:1 [Appendix 1 (25)]. It is interpreted that this residue may form part of the inward gate of the transport vestibule [Appendix 1 (25)]. Evidence of close proximity of this residue to the site of Na^+ binding is the finding that hCNT1 mutant E322C was partly protected from PCMBS inhibition by the absence of Na^+ (Chapter 5). In the case of TM 11A residue Glu498, mutation to Asp resulted in a marked reduction in V_{max}^{Na+} [Appendix 1 (25)]. Together, these studies of hCNT1 suggest key roles for residues in TM 7 and 11A in cation binding and/or translocation. Notably, hCNT1 Glu498 is centrally positioned within the conserved CNT family motif (G/A)XKX_3N**E**FVA(Y/M/F). In hCNT3, the corresponding TM 7 and 11A Glu residues have also been strongly implicated in interactions with cations (26). For example, cysteine substitution of Glu519 leads to loss of H^+-dependence and a decrease in Na^+:uridine stoichiometry from 2:1 to 1:1 (26). Glu519, therefore, is specifically linked to (and may be a direct participant in) the hCNT3 cation binding site common to Na^+ and H^+. Since Glu519 is conserved in all CNTs, it is hypothesized that the shared (primary) Na^+/H^+ site of hCNT3 corresponds to the Na^+-specific site of hCNT1/2 and the H^+-specific site of NupC/CaCNT. Corresponding to Glu322 in TM 7 of hCNT1, mutation of Glu343 of hCNT3 also resulted in altered Na^+-dependent (and H^+- dependent) transport function (26). hCNT3 E343Q and E343C, for example, exhibited very low affinities for Na^+, while E343D had a modest decrease in apparent K_{50} value for Na^+, but a marked decrease in V_{max}. All three mutants displayed minimal H^+-dependent uridine uptake (26). Also similar to hCNT1 Glu322, E343C exhibited partially uncoupled transport characteristics consistent with a potential gating function within the common solute/cation translocation pore [Appendix 1 (25) and (26)]. Also in hCNT3, mutation of Cys561 in TM 12 to Ser caused a decreased affinity of hCNT3C- for Na^+, while other residue substitutions at this position (C561T,

C561V and C561I) displayed decreased rates of H^+-mediated transport [Chapter 3 (23)].

SCAM analysis of hCNT3C- TMs 7 – 13 expanded the role of Cys561 to include a cluster of conformationally-sensitive residues in TM 12 that were accessed by PCMBS under acidic conditions [(22) and Chapter 8 (24)] and also revealed multiple additional residues with differential sensitivity to PCMBS in Na^+-containing, H^+-reduced and/or Na^+-free, acidified media (Fig. 9-2). Residues which were sensitive to PCMBS inhibition only in Na^+-free, acidified medium were found in TM 7 (Ile337) [Chapter 4], TM 8 (Thr370) [Chapter 4], TM 9 (His388, Val394 and Met395) [Chapter 7], TM 10 (Ile450 and Leu471) [Chapter 7], TM 11 (Leu480) [Chapter 8 (24)], TM 11A (Ala508 and Gly512) [Chapter 8 (24)], the loop between TMs 11A – 12 (Gln545) [Chapter 8 (24)] and TM 12 (Ile554, and, Tyr558 and Cys561) [22, Chapter 8 (24)]. Three different residues were sensitive to PCMBS inhibition only in Na^+-containing, H^+-reduced medium: Glu483 and Leu484 in TM 11, and, Ala522 in TM 11A. Also exhibiting a greater PCMBS inhibition under acidified conditions than under H^+-reduced conditions was mutant Y185C(C-) in NupC(C-) (Chapter 6), suggesting that, like Cys561 of hCNT3, Tyr185 of NupC becomes more extracellularly accessible to PCMBS in the presence of H^+, thus reporting a H^+-dependent conformation of the protein (Chapter 6). The corresponding residue in TM 8 of hCNT3C-, Tyr379, was present at cell surfaces in reduced amounts but non-functional when converted to cysteine, and thus was not characterized further in this thesis (Chapter 4). Additionally, a number of hCNT3C- mutants exhibited altered Na^+: H^+ uridine uptake ratios, suggesting potential roles for these residues in cation coupling [Chapters 4, 7 and 8 (24)]. These included residues in TM 7 (Ser330, Ser334, Gly335, Asn336, Ile337, Val339, Gly340, Gln341, Ser344 and Pro345) [Chapter 4], the loop between TMs 7 – 8 (Leu352) [Chapter 4], TM 8 (Ser369, Thr370, and Val375) [Chapter 4], TM 9 (Leu389 and Met395) [Chapter 7], TM 10 (Leu461) [Chapter 7], TM 11A (Gly512, Tyr513, Lys514, Phe516, Ala522, Glu524 and His525) [Chapter 8 (24)] and TM 12 (Tyr558, Ala564, Asn565 and Ile566) [22, Chapter 8 (24)]. Similar to the findings for uridine protection against PCMBS

inhibition, therefore, TMs 7, 8, 9, 11A and 12 contain multiple residues that play key roles in CNT-cation interactions and/or report cation-induced conformational states of the protein.

Putative Mechanisms of CNT Cation/Nucleoside Cotransport

For hCNT1/3, sodium and/or protons bind to the transporter first, increasing the affinity for nucleoside, which then binds second (15-17). Fast (τ_{fast}) and slow (τ_{slow}) rate constants have been isolated from hCNT1/3 presteady-state currents: τ_{fast} (10-16 msec) was independent of Na^+ concentration, and likely corresponds to reorientation of the empty carrier; τ_{slow} (50-80 msec) was observed only in the presence of sodium and is hypothesized to be a composite rate constant of rapid sodium binding and slower sodium-induced conformational transitions within the protein [(29) and Dr. K. Smith, unpublished data]. Similar to the mammalian GAT1 sodium-dependent GABA transporter (30–36), a postulated mechanism for hCNT3 that, with modification, serves as a potential cotransport model for all CNTs, predicts that an occlusion step (or other slow conformational change) is associated with binding of two sodium ions to hCNT3, one to the primary (E519-associated) sodium (or proton) site, and the second to an auxiliary sodium-specific site. Nucleoside then binds, followed by transport: τ_{slow} approximates the hCNT1/3 turnover rate of 10 uridine molecules transported per protein per sec at -50 mV, so that the cation-induced conformational change may be the overall rate-limiting step of transport. The contributions of the research described in this thesis were (i) to provide topological context to the model, (ii) to add to the accumulating body of evidence that, similar to the recently solved crystal structures of LacY (37), $LeuT_{Aa}$ (38) and Glt_{Ph} (39, 40), there is close-proximity of cation/permeant binding and transport within a common translocation pore, (iii) to locate residues that potentially sense and report specific cation-induced conformational states within the translocation cycle, and (iv) identify residues potentially involved in nucleoside and cation binding and/or translocation. Exemplifying this is the new revised membrane architecture for

CNTs discussed further in the next Section. Also of especial note is the relatively small but likely important sub-group of PCMBS-sensitive residues that exhibited both uridine-protection and altered Na^+:H^+ ratios of uridine uptake (*i.e.,* that are potentially involved in cation interactions while simultaneously being involved in and/or located in close proximity to the nucleoside binding pocket). These include TM 7 residues Gly340 and Gln341, TM 8 residue Thr370, TM 9 residue Met395, TM 11A residues Gly512, Phe516 and Ala522, and TM 12 residues Tyr558 and Asn565 [Chapters 4, 7 and 8 (24)].

Topology

Hydropathy profiles of mammalian CNTs initially suggested the presence of 14 potential TMs (4, 11, 13). Further topological studies utilizing antipeptide antibodies and glycosylation analysis in conjunction with analysis of a larger grouping of CNT sequences using a more comprehensive array of computer algorithisms revised the putative model of CNT topology to 13 TMs (5) (Fig. 9.1). Two additional membrane spanning regions (TMs 5A and 11A) were also weakly predicted by the computer algorithms (5). Evidence presented in this thesis, together with data from other recent studies (*e.g.* 20, 26, 41), support a revision to the 13 TM topology model for mammalian and other eukaryote CNTs in which the TM 11A region (and possibly also TM 5A) are membrane-spanning (Fig. 9.1). In particular, SCAM analyses of TMs 7 to 11 revealed this region of the protein to have an orientation opposite to that predicted in the current putative 13 TM model (Chapters 4 to 8). For example, a single residue in the putative internal loop between TMs 8 and 9 of hCNT3C- (Val384), and the corresponding residue in hCNT1 (Ile363), were strongly PCMBS-sensitive and resulted in marked transport inhibition when converted to Cys (Chapters 4 and 5). Since PCMBS is membrane impermeable, this residue must be accessible from the extracellular medium and thus supports the opposite orientation of TMs 7 to 11. Furthermore, SCAM analysis of hCNT3 TM 11A demonstrated that nine amino acids, including Glu519, were reactive to PCMBS and four were nucleoside protectable

[Chapter 8 (24)]. TM 11A contains the highly conserved motif (G/A)XKX$_3$NEFVA(Y/M/F), which is common to all CNT family members (5). This motif directly contributes to cation coupling (26) suggesting, in conjunction with the present findings, that it is highly likely to be membrane-associated and form part of the CNT translocation pore. It is more likely to be a transmembrane domain than a re-entrant loop, given that two additional TMs (putative 5A and 11A) are needed to preserve the exofacial location of the glycosylated C-terminus of the protein. Supporting evidence that the TM 11A region is membrane spanning comes from parallel topological studies of *E. coli* NupC examining the susceptibilities of single cysteine mutants in intact and lysed bacteria to modification by membrane-impermeant Oregon green malemide and ethyltrimethylammonium methanethiosulfonate (41). Together, the results provide strong support for a new revised membrane architecture for the TM 7 – 13 region (C-terminal half) of hCNT3.

SCAM analyses also revealed unexpected block patterns of PCMBS reactivity in the TMs 7, 8, 9 and 11A regions of hCNT3C- [Chapters 4, 7 and 8 (24)], thus providing the first evidence of novel discontinuous/extended regions within putative CNT transmembrane α-helices. The block patterns of PCMBS inhibition observed in TMs 7 and 8 of hCNT3C- (Chapter 4) were reproduced in hCNT1 (Chapter 5). In marked contrast, TMs 10, 11, 12 and 13 exhibited conventional periodic patterns of PCMBS inhibition, with affecting residues generally aligning to one face of each of the helices [Chapters 7 and 8 (24)]. The extended regions of PCMBS inhibition evident in the present studies are interpreted as functional evidence of discontinuous membrane helices similar to those revealed in crystal structures of recently solved bacterial membrane cotransport proteins. For instance, the crystal structure of the bacterial *A. aeolicus* Na^+/Cl^--dependent leucine amino acid transporter ($LeuT_{Aa}$) has two transmembrane α-helices disrupted by insertions of extended regions of polypeptide (38). These extended regions are adjacent contributing parts of the two Na^+ binding sites of the protein. Upon binding of Na^+, the area is stabilized to

favor high-affinity binding of leucine in close proximity to the two Na^+ cations (38). Indeed, one of the two Na^+ ions directly contributes to leucine binding. The $LeuT_{Aa}$ proposed mechanism of transport consists of a three-state model with extracellular and intracellular gates which allow alternate access to otherwise occluded Na^+ and leucine binding sites from either side of the membrane bilayer (38). In $LeuT_{Aa}$, the discontinuous regions also serve as the flexible hinge to facilitate the required conformational changes (38). Other crystal structures with observable discontinuous regions within transmembrane α-helices include the nucleobase cation symporter from *M. liquefaciens* (Mhp1), the Na^+/galactose symporter from *V. parahaemolyticus* (vSGLT) and the Na^+/H^+ exchanger from *E. coli* (NhaA) (42-44). In the *Pyrococcus horikoshii* (Glt_{Ph}) glutamate transporter, discontinuous regions within α-helical structures take the form of flexible hinges within a hairpin-like conformation in a re-entrant loop or non-transmembrane helix (39, 40). In the case of hCNT3, SCAM analysis predicts TM 11A to be membrane spanning and, thus, more similar to $LeuT_{Aa}$ than Glt_{Ph} [Chapter 8 (24)].

The mechanistic roles of discontinuous membrane helices in ion recognition, binding and translocation in secondary active transporters have recently been reviewed (45, 46). The functional identification of such extended regions of polypeptide in hCNT3C- TMs 7, 8 (Chapter 4), 9 (Chapter 7) and 11A [Chapter 8 (24)] strongly supports the central role of these TMs in formation of the CNT nucleoside/cation binding pocket(s) and common translocation pore. Additional support for such an arrangement of these TMs within the protein, and for the additional contributions from TMs 11 and 12 to the translocation pore, stems from the other SCAM and site-directed mutagenesis studies previously discussed in this Chapter. Structurally and functionally, a number of features deserve additional comment and consideration. For example, the discontinuous region in TM 7 occupies a central position within the membrane, whereas those in TMs 8 and 9 occupy matching symmetrical locations in the outward-facing half of the membrane (Fig. 9.2). Additionally, new TM 11A is in close proximity to conformationally mobile TM 12. Also shown in the new proposed topology of the C-terminal half of hCNT in Fig. 9-2, TMs 9 and 10 are separated by a relatively

long 37 amino acid cytoplasmic loop that, if flexible, may enable TMs 7/8/9 and 11A/12 to come together to form the translocation pore in a manner that facilitates conformational transitions within the cation/nucleoside translocation cycle. It is also noteworthy from Fig. 9.2 that those residues potentially involved in cation interactions, while simultaneously being involved in, and/or located in close proximity to the nucleoside binding pocket (TM 7 residues Gly340 and Gln341, TM 8 residue Thr370, TM 9 residue Met395, TM 11A residues Gly512, Phe516 and Ala522, and TM 12 residues Tyr558 and Asn565), localize in the protein to the approximate centre of the lipid bilayer. This provides a level of confidence that the hCNT3 C-terminal membrane architecture described in this thesis may approximate the actual topology of the protein, and is in accord with pre-steady state electrophysiological experiments suggesting that Na^+ binds to hCNT1 and hCNT3 ~ 40% within the membrane electric field, which is approximately midway across the membrane (15, 17, 29). Finally, the block patterns of PCMBS inhibition seen in hCNT3C- and hCNT1 (Chapters 4 and 5) were not seen in NupC (Chapter 6). Potentially, this may be related to the fact that hCNT1/3 are Na^+-coupled while NupC is exclusively H^+-dependent.

Future Directions

The structure-function studies presented in this thesis have contributed to the current understanding of CNT-mediated nucleoside transport. Some residues and regions have been highlighted as important or potentially important for cation/nucleoside binding and/or cotransport. As well, the studies have also revealed a novel topological organization for the C-terminal half of CNT family members. However, there remain many unanswered questions.

Within hCNT3, SCAM analysis with PCMBS has only yet been applied to TMs 7 – 13, leaving the entire N-terminal half (TMs 1 – 6) of the protein, including potential new TM 5A, uncharacterized. Furthermore, the use of alternative thiol reactive reagents to explore key architectural features and topographical highlights of the protein will be beneficial. For example, the MTS

reagents MTSET and MTSES are positively and negatively charged, respectively, and, like PCMBS, are membrane impermeable. MTSEA, in contrast, is neutral at physiological pH and therefore membrane permeable. Also varying in size (MTSEA < MTSES < MTSET) their use on preselected mutants will not only provide information on pore-lining residues complementary to that already obtained by PCMBS, but also provide information on outward- and inward-facing aspects of the translocation pore, the location and identity of residues within the nucleoside binding site, and the character of the permeability barrier (47). Membrane permeable *N*-ethyl maleimide (NEM) will also be useful in this regard (47). Topological information can also be provided by labeling studies with biotin malemide derivatives which are unreactive towards membrane-embedded cysteine residues, and thus map TM helix boundaries (47-50). This is important because the transporter crystal structures determined thus far reveal extensive variation in TM length ranging, in the case of the *E. coli* glycerol-3-phosphate transporter (GlpT), from 18-38 residues (51). TM boundaries may also change during transport (52, 53). When hCNT3 membrane architecture is more established, helix proximity arrangements and conformational changes in these distances can be studied in oocytes by introduction of pairs of cysteine residues into TMs predicted to be adjacent in the folded protein. The nearness of such residues is then tested by oxidative cross-linking (54) and/or by use of bi-functional cross-linking agents (52, 55, 56). For example, initial candidates for this type of experiment would be TMs 7 and 11A, both of which contain identified Glu residues involved in Na^+/nucleoside and H^+/nucleoside cotransport [Appendix 1 (25) and (26)], and both of which contain additional residues exhibiting uridine-protection against PCMBS inhibition, suggesting their close proximity to the nucleoside binding pocket [Chapters 4 and 8 (24)]. In addition, helix proximity arrangements and conformational changes can be analyzed in oocytes using dual-probe FRET/LRET (fluorescence/luminescence resonance energy transfer) studies to measure intramolecular (Å-scale) distances between selected amino acid positions within the protein (57, 58-62). Single probe epifluorescent microscopy in oocytes, although less powerful, is also capable of

providing information on conformational changes during transport, especially when used in conjunction with electrophysiology (63-65). The experiments described in this thesis provide a rich resource of residue positions potentially amenable to this type of analysis.

Similarly, this thesis has generated an extensive resource of functionally-modified mutants for follow-up analysis using site-directed mutagenesis (to introduce other amino acid side chain substitutions of varying size, shape, hydrophobicity and charge) in combination with kinetic/functional assessment in oocytes to reveal the structural and mechanistic basis for the initial phenotype change. For example, SCAM analysis studies in this thesis have identified a subset of hCNT3C- mutants (Table 9-1) which display substantially altered Na^+ and H^+ dependence, suggesting that they could be involved in cation coupling. Experiments are in progress to further characterize these mutants in detail. As a first step towards this, each of the mutants has been recreated in the wild-type hCNT3 background and re-tested for Na^+- and H^+-dependence. This was undertaken because the hCNT3C- protein has altered affinity for Na^+. Of the 28 hCNT3 mutants tested in Table 9-1, 9 promising candidates with markedly altered Na^+- and/or H^+-dependence were identified. Experiments are now underway to investigate the detailed Na^+ and H^+ activation characteristics and cation coupling stoichiometries of these mutants. Initial results have identified at least 2 mutants with major defects in cation coupling (hCNT3 N336C and G340C).

Obtaining crystal structures of membrane transporter proteins has proven to be difficult, and only relatively recently have a number of bacterial membrane transporter structures been solved, including LacY (37), $LeuT_{Aa}$ (38), Glt_{Ph} (39), Mhp1 (42), vSGLT (43) and NhaA (44). Acquiring the crystal structure for a CNT would generate a high-resolution image of the structure of this family of transporters and provide a map for future structure-function analyses. From a clinical and pharmacologic perspective, this would also pave the way for development of designer permeants and inhibitors. For CNTs, the focus of current efforts in this laboratory, in collaboration with colleagues in the UK, is to obtain 2D and 3D crystal structures of NupC. Even in the absence of a crystal structure,

however, the studies undertaken in my thesis and suggested here in "Future Directions" have the potential to define in substantial detail the 3D structure and molecular mechanisms of human cation/nucleoside cotransporters.

Table 9-1. Further characterization of cysteine mutants with altered Na^+:H^+ uridine uptake ratios.

Cys-mutants	Na^+ : H^+ ratio (hCNT3C-)	Na^+ : H^+ ratio (hCNT3)	K_{50}^{Na+} (mM) (hCNT3)	V_{max}^{Na+} (pmol/ oocyte. min^{-1}) (hCNT3)	K_{50}^{H+} (nM) (hCNT3)	V_{max}^{H+} (pmol/ oocytes.min^{-1}) (hCNT3)
TM 7						
S330C	2.7	1.5	-	-	-	-
S334C	0.3	0.5	6.8 ± 0.7	1.1 ± 0.1	1766 ± 265	1.58 ± 0.06
	3.5	2.3	-	-	-	-
G335C	6.5	18.9	836 ± 4450	6.7 ± 14	7.8 ± 6.0	0.27 ± 0.03
N336C	0.4	1.3	-	-	-	-
I337C	2.9	2.2	-	-	-	-
V339C	10.2	11.2	3.1 ± 0.4	0.7 ± 0.1	4.3 ± 3.2	0.26 ± 0.02
G340C	4.6	2.0	-	-	-	-
Q341C	9.4	3.1	-	-	-	-
S344C	9.2	1.3	-	-	-	-
P345C						
Loop 7-8						
L352C	4.5	1.9	-	-	-	-
TM 8						
S369C	2.9	6.4	16.3 ± 2.4	2.8 ± 0.2	901 ± 234	1.85 ± 0.11
T370C	0.2	1.5	-	-	-	-
V375C	8.0	2.2	-	-	-	-
TM 9						
L389C	5.9	23.8	68.7 ± 51.3	2.0 ± 1.0	747 ± 227	0.20 ± 0.01
M395C	0.4	0.9	12.8 ± 2.4	1.9 ± 0.2	192 ± 82	1.70 ± 0.14
TM 10						
L461	0.3	1.0	-	-	-	-
TM 11A						
G512C	3.9	1.7	-	-	-	-
Y513C	0.4	1.1	-	-	-	-
K514C	7.9	0.7	nd	nd	nd	nd
F516C	3.1	1.7	-	-	-	-
A522C	7.0	4.3	10 ± 0.6	2.8 ± 0.1	190 ± 101	0.68 ± 0.07
E524C	2.6	1.6	-	-	-	-
H525C	2.7	2.1	-	-	-	-
TM 12						
Y558C	0.2	1.3	-	-	-	-
A564C	5.0	4.6	7.5 ± 2.9	3.0 ± 0.5	1679±1002	0.45 ± 0.06
N565C	3.3	2.8	-	-	-	-

Table 9-1 continued

Cys-mutants	$Na^+ : H^+$ ratio (hCNT3C-)	$Na^+ : H^+$ ratio (hCNT3)	K_{50}^{Na+} (mM) (hCNT3)	V_{max}^{Na+} (pmol/ oocytes. min^{-1}) (hCNT3)	K_{50}^{H+} (nM) (hCNT3)	V_{max}^{H+} (pmol/ oocytes.min^{-1}) (hCNT3)
I566C	2.6	2.8	-	-	-	-
hCNT3	1.7		10.7 ± 1.6	2.4 ± 0.1	414 ± 118	3.84 ± 0.23
hCNT3C-	1.0		-	-	-	-

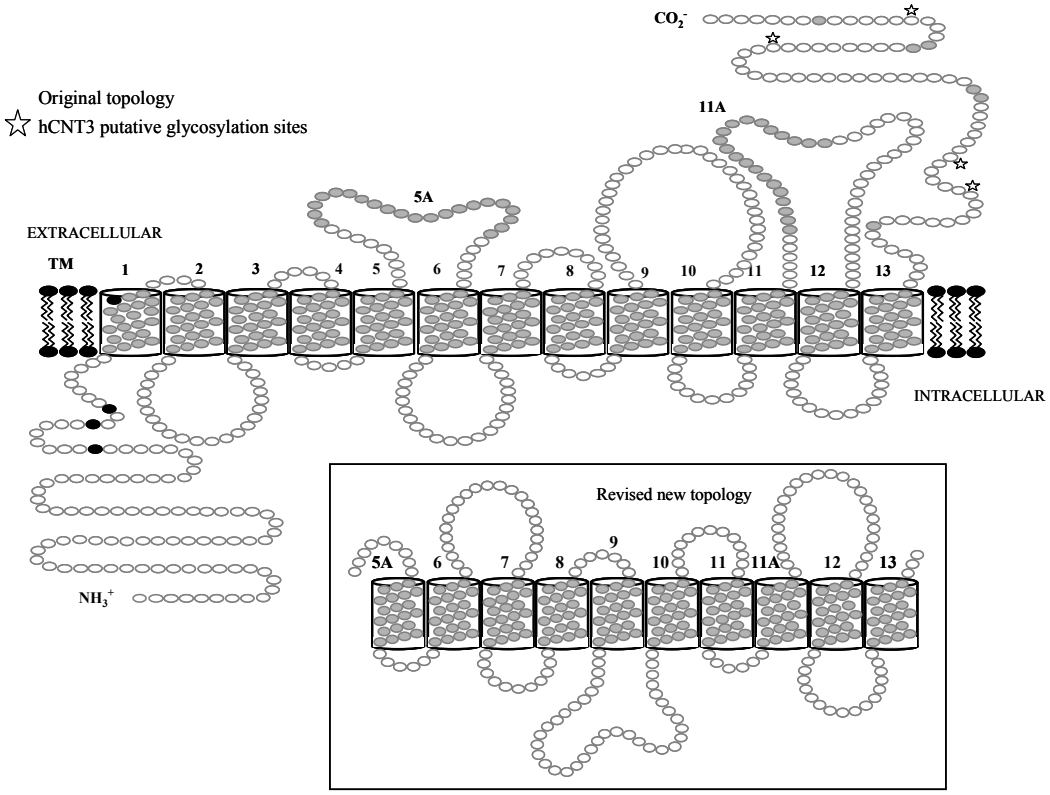

Figure 9-1. Putative 13 TM and proposed new CNT topology models. Predicted transmembrane domains 5A and 11A are marked. Inset shows the opposite orientation of TMs 7 – 11, with the insertions of 5A and 11A, in the proposed new topology of the C-terminal half of CNTs.

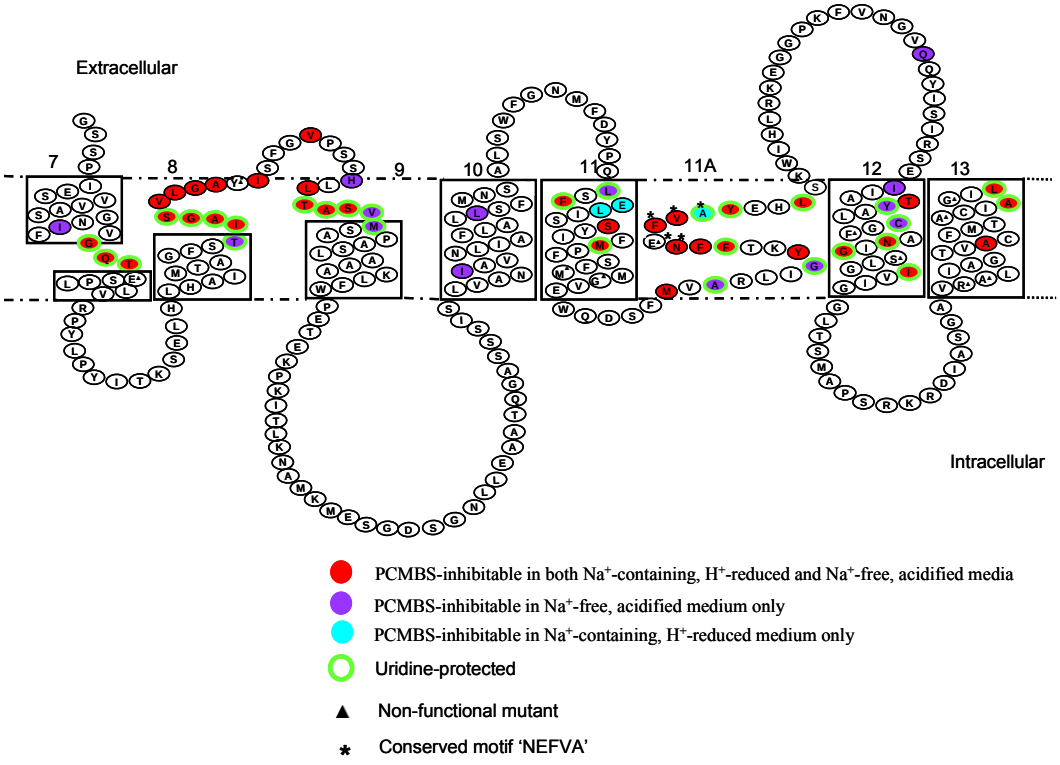

Figure 9-2. Proposed C-terminal topology of hCNT3. Putative transmembrane helices are numbered 7 to 13, with TMs 7, 8, 9 and 11A containing discontinuous regions. Residues in hCNT3C- sensitive to PCMBS inhibition when converted to Cys and protected by uridine are indicated.

Bibliography

1. Young, J. D., Yao, S. Y. M., Sun, L., Cass, C. E., and Baldwin, S. A. (2008) The ENT family of nucleoside and nucleobase transporter proteins. *Xenobiotica*. **38**: 995-1021.

2. Gray, J. H., Owen, R. P., and Giacomini, K. M. (2004) The concentrative nucleoside transporter family, SLC28. *Pflugers Arch.* **447**: 728-734.

3. Zhang, J., Visser, F., King, K. M., Baldwin, S. A., Young, J. D., and Cass, C. E. (2007) The role of nucleoside transporters in cancer chemotherapy with nucleoside drugs. *Cancer Metastasis Rev.* **26**: 85-110.

4. Huang, Q. Q., Yao, S. Y. M., Ritzel, M. W. L., Paterson, A. R. P., Cass, C. E., and Young, J. D. (1994) Cloning and functional expression of a complementary DNA encoding a mammalian nucleoside transport protein. *J. Biol. Chem.* **269**: 17757-17760.

5. Hamilton, S. R., Yao, S. Y., Ingram, J. C., Hadden, D. A., Ritzel, M. W., Gallagher, M. P., Henderson, P. J., Cass, C. E., Young, J. D., and Baldwin, S. A. (2001) Subcellular distribution and membrane topology of the mammalian concentrative Na^+-nucleoside cotransporter, rCNT1. *J. Biol. Chem.* **276**: 27981-27988.

6. Elwi, A. N., Damaraju, V. L., Baldwin, S. A., Young, J. D., Sawyer, M. B., and Cass, C. E. (2006) Renal nucleoside transporters: physiological and clinical implications. *Biochem. Cell. Biol.* **84**: 844-858.

7. Damaraju, V. L., Elwi, A. N., Hunter, C., Carpenter, P., Santos, C., Barron, G. M., Sun, X., Baldwin, S. A., Young, J. D., Mackey, J. R., Sawyer, M. B., and Cass, C. E. (2007) Localization of broadly selective equilibrative and concentrative nucleoside transporters, hENT1 and hCNT3, in human kidney. *Am. J. Physiol. Renal Physiol.* **293**: F200-F211.

8. Mackey, J. R., Galmarini, C. M., Graham, K. A., Joy, A. A., Delmer, A., Dabbagh, L., Glubrecht, D., Jewell, L. D., Lai, R., Lang, T., Hanson, J., Young, J. D., Merle-Béral, H., Binet, J. L., Cass, C. E., and Dumontet, C. (2005) Quantitative analysis of nucleoside transporter and metabolism gene expression in chronic lymphocytic leukemia (CLL): identification of fludarabine-densitive and -insensitive populations. *Blood* **105**: 767-774.

9. Cass, C. E. (1995) Nucleoside transport, in *Drug Transport in Antimicrobial and Anticancer Chemotherapy* (Georgopapadakou, N. H., Ed.), pp 403-451, Marcel Deker, New York.

10. Griffith, D. A., and Jarvis, S. M. (1996) Nucleoside and nucleobase transport systems of mammalian cells. *Biochim. Biophys. Acta* **1286**: 153-181.

11. Che, M., Ortiz, D. F., and Arias, I. M. (1995) Primary structure and functional expression of a cDNA encoding the bile canalicular, purine-specific Na^+-nucleoside cotransporter. *J. Biol. Chem.* **270**, 13596-13599.

12. Ritzel, M. W. L., Yao, S. Y. M., Huang, M. Y., Elliot, J. F., Cass, C. E., and Young, J. D. (1997) Molecular cloning and functional expression of cDNAs encoding a human Na^+-nucleoside cotransporter (hCNT1). *Am. J. Physiol.* **272**: C707-C714.

13. Wang, J., Su, S. F., Dresser, M. J., Schaner, M. E., Washington, C. B., and Giacomini, K. M. (1997) Na^+-dependent purine nucleoside transporter from human kidney: cloning and functional characterization. *Am. J. Physiol.* **273**: F1058-F1065.

14. Ritzel, M. W. L., Yao, S. Y. M., Ng, A. M. L., Mackey, J. R., Cass, C. E., and Young, J. D. (1998) Molecular cloning, functional expression and chromosomal localization of a cDNA encoding a human Na^+/nucleoside cotransporter (hCNT2) selective for purine nucleosides and uridine. *Mol. Membr. Biol.* **15**: 203-211.

15. Smith, K. M., Ng, A. M., Yao, S. Y. M., Labedz, K. A., Knauss, E. E., Wiebe, L. I., Cass, C. E., Baldwin, S. A., Chen, X.-Z., Karpinski, E., and Young, J. D. (2004) Electrophysiological characterization of a recombinant human Na^+-coupled nucleoside transporter (hCNT1) produced in *Xenopus* oocytes. *J. Physiol.* **558**: 807-823.

16. Smith, K. M., Slugoski, M. D., Cass, C. E., Baldwin, S. A., Karpinski, E., and Young, J. D. (2007) Cation coupling properties of human concentrative nucleoside transporters hCNT1, hCNT2 and hCNT3. *Mol. Membr. Biol.* **24**: 53-64.

17. Smith, K. M., Slugoski, M. D., Loewen, S. K., Ng, A. M., Yao, S. Y., Chen, X. Z., Karpinski, E., Cass, C. E., Baldwin, S. A., and Young, J. D. (2005) The broadly selective human Na^+/nucleoside cotransporter (hCNT3) exhibits novel cation-coupled nucleoside transport characteristics. *J. Biol. Chem*. **280**: 25436-25449.

18. Yao, S. Y., Ng, A. M., Loewen, S. K., Cass, C. E., Baldwin, S. A., and Young, J. D. (2002) An ancient prevertabrate Na^+-nucleoside cotransporter (hfCNT) from the Pacific hagfish (*Eptatretus stouti*). *Am. J. Phys. Cell Phys.* **283**: C155-C168.

19. Loewen, S. K., Ng, A. M., Yao, S. Y., Cass, C. E., Baldwin, S. A., and Young, J. D. (1999) Identification of amino acid residues responsible for the pyrimidine and purine nucleoside specificities of human concentrative Na^+ nucleoside cotransporters hCNT1 and hCNT2. *J. Biol. Chem.* **274**: 24475-24484.

20. Slugoski, M. D., Loewen, S. K., Ng, A. M., Smith, K. M., Yao, S. Y., Karpinski, E., Cass, C. E., Baldwin, S. A., and Young, J. D. (2007) Specific mutations in transmembrane helix 8 of human concentrative Na+/nucleoside cotransporter hCNT1 affect permeant selectivity and cation coupling. *Biochem*. **46**: 1684-1693.

21. Zhang, J., Tackaberry, T., Ritzel, M. W., Raborn, T., Barron, G., Baldwin, S. A., Young, J. D., and Cass, C. E. (2006) Cysteine-accessibility analysis of transmembrane domains 11-13 of human concentrative nucleoside transporter 3. *Biochem. J.* **394**: 389-398.

22. Slugoski, M. D., Ng, A. M. L., Yao, S. Y., Smith, K. M., Lin, C. C., Zhang, J., Karpinski, E., Cass, C. E., Baldwin, S. A., and Young, J. D. (2008) A proton-mediated conformational shift identifies a mobile pore-lining cysteine residue (Cys-561) in human concentrative nucleoside transporter 3. *J. Biol. Chem*. **283**: 8496-8507.

23. Slugoski, M. D., Smith, K. M., Mulinta, R., Ng, A. M. L., Yao, S. Y. M., Morrison, E. L., Lee, Q., O., T., Zhang, J., Karpinski, E., Cass, C. E., Baldwin, S. A., and Young, J. D. (2008) A conformationally mobile cysteine residue (Cys-561) modulates Na^+ and H^+ activation of human CNT3. *J. Biol. Chem.* **283**:24922-24934.

24. Slugoski, M. D., Ng, A. M. L., Yao, S. Y. M., Lin, C. C., Mulinta, R., Cass, C. E., Baldwin, S. A., and Young, J. D. (2009b) Substituted cysteine accessibility method analysis of human concentrative nucleoside transporter hCNT3 reveals a novel discontinuous region of functional importance within CNT family motif (G/A)XKX3NEFVA(Y/M/F). *J. Biol. Chem.* **284**:17281-17292.

25. Yao, S. Y. M., Ng, A. M., Slugoski, M. D., Smith, K. M., Mulinta, R., Karpinski, E., Cass, C. E., Baldwin, S. A., and Young, J. D. (2007) Conserved glutamate residues are critically involved in Na^+/nucleoside cotransport by human concentrative nucleoside transporter 1 (hCNT1). *J. Biol. Chem.* **282**: 30607-30617.

26. Slugoski, M. D., Smith, K. M., Ng, A. M. L., Yao, S. Y. M., Karpinski, E., Cass, C. E., Baldwin, S. A., and Young, J. D. (2009a) Conserved glutamate residues E343 and E519 provide mechanistic insights into cation/nucleoside cotransport by human concentrative nucleoside transporter 3 (hCNT3). *J. Biol. Chem.* **284**:17266-17280.

27. Loewen, S. K., Yao, S. Y., Slugoski, M. D., Mohabir, N. N., Turner, R. J., Mackey, J. R., Gallagher, M. P., Henderson, P. J., Baldwin, S. A., Cass, C. E., and Young, J. D. (2004) Transport of physiological nucleosides and anti-viral and anti-neoplastic nucleoside drugs by recombinant *Escherischia coli* nucleoside-H^+ cotransporter (NupC) produced in *Xenopus laevis* oocytes. *Mol. Membr. Biol.* **21**: 1-10.

28. Slugoski, M. D., Loewen, S. K., Ng, A. M., Baldwin, S. A., Cass, C. E., and Young, J. D. (2004) Allelic isoforms of the H^+/nucleoside co-transporters (CaCNT) from Candida albicans reveal separate high- and low-affinity transport systems for nucleosides. *Yeast.* **21**: 1269-1277.

29. Smith, K. M., Cass, C. E., Baldwin, S. A., Karpinski, E., and Young, J. D. (2008) Presteady-state currents of human concentrative nucleoside transporter 3 (hCNT3). *J. Physiol.* (submission pending).

30. Mager, S., Naeve, J., Quick, M., Labarca, C., Davidson, N. and Lester, H.A. (1993) Steady states, charge movements, and rates for a cloned GABA transporter expressed in *Xenopus* oocytes. *Neuron* **10**:177-188.

31. Mager, S., Kleinberger-Doron, N., Kehset, G.I., Davidson, N., Kanner, B.I. and Lester, H.A. (1996) Ion binding and permeation at the GABA transporter GAT1. *J Neurosci* **16**: 5405-5414.

32. Mager, S., Cao, Y. and Lester, H.A. (1998) Measurement of transient currents from neurotransmitter transporters expressed in *Xenopus* oocytes. *Methods Enzymol.* **296**:551-566.

33. Galli, A., DeFelice, L.J., Duke, B.J., Moore, K.R. and Blakely, R.D. (1995) Sodium-dependent norepinephrine-induced currents in norepinephrine-transporter-transfected HEK-293 cells blocked by cocaine and antidepressants. *J. Exp. Biol.* **198**:2197-2212.

34. Hilgemann, D.W. and Lu, C. GAT1 (GABA: Na^+:Cl^-) cotransport function. (1999) Database reconstruction with an alternating access model. *J. Gen. Physiol.* 114459-475.

35. Lu, C.-C. and Hilgemann, D.W. GAT1 (GABA: Na^+:Cl^-) cotransport function. (1999) Kinetic studies in giant *Xenopus* oocyte membrane patches. *J. Gen. Physiol.* 114:445-447

36. Fesce, R., Giovannardi, S., Bidna, F., Bossi, E. and Peres, A. (2002) The relation between charge movement and transport-associated currents in the rat GABA cotransporter rGAT1. *J. Physiol.* **545**:739-750.

37. Abramson, J., Smirnova, I., Kasho, V., Verner, G., Kaback, H. R., and Iwata, S. (2003) Structure and mechanism of the lactose permease of *Escherichia coli*. *Science* **301**: 610-605.

38. Yamashita, A., Singh, S. K., Kawate, T., Jin, Y., and Gouaux, E. (2005) Crystal structure of a bacterial homologue of Na^+/Cl^--dependent neurotransmitter transporters. *Nature* **437**: 215-223.

39. Yernool, D., Boudker, O., Jin, Y., and Gouaux, E. (2004) Structure of a glutamate transporter homologue from *Pyrococcus horikoshii*. *Nature* **431**: 811-818.

40. Boudker, O., Ryan, R. M., Yernool, D., Shimamoto, K., and Gouaux, E. (2007) Coupling substrate and ion binding to extracellular gate of a sodium-dependent aspartate transporter. *Nature* **445**: 387-393.

41. Xie, H., Sun, L., Hadden, D. A., Mulinta, R., Loewen, S. K., Ingram, J. C., Litherland, G. L., Gallagher, M. P., Henderson, P. J. F., Cass, C. E., Young, J. D., and Baldwin, S. A. (2008) Structure/function relationships in the *Escherichia coli* nucleoside transport protein NupC, a paradigm for the concentrative nucleoside transporter (CNT) family. *Mol. Microbiol.* (submission pending).

42. Weyand, S., Shimamura, T., Yajima, S., Suzuki, S., Mirza, O., Krusong, K., Carpenter, E. P., Rutherford, N. G., Hadden, J. M., O'Reilly, J., Ma, P., Saidijam, M., Patching, S. G., Hope, R. J., Norbertczak, H. T., Roach, P. C. J., Iwata, S., Henderson P. J. F., and Cameron, A. D. (2008) Structure and molecular mechanism of a nucleobase-cation-symport-1 family transporter. *Science*. **322**: 709- 713.

43. Faham, S., Watanabe, A., Besserer, G. M., Cascio, D., Specht, A., Hirayama, B. A., Wright, E. M., and Abramson, J. (2008) The crystal structure of a sodium galactose transporter reveals mechanistic insights into Na^+/sugar symport. *Science*. **321**: 810-814.

44. Hunte, C., Screpanti, E., Venturi, M., Rimon, A., Padan, E., and Michel, H. (2005) Structure of a Na^+/H^+ antiporter and insights into mechanism of action and regulation by pH. *Nature*. **435**: 1197-1202.

45. Screpanti, E., and Hunte, C. (2007) Discontinuous membrane helices in transport proteins and their correlation with function. *J. Struct. Biol.* **159**: 261-267.

46. Krishnamurthy, H., Piscitelli, C. L., and Gouaux, E. (2009) Unlocking the molecular secrets of sodium-coupled transporters. *Nature* **459**: 347- 355.

47. Zhu, Q., and Casey, J. R. (2007) Topology of transmembrane proteins by scanning cysteine accessibility mutagenesis methodology. *Methods*. **41**: 439-450.

48. Mueckler, M. and Makepeace, C. (2004) Analysis of transmembrane segment 8 of the GLUT1 glucose transporter by cysteine-scanning

mutagenesis and substituted cysteine accessibility. *J. Biol. Chem.* **279**: 10494-10499.

49. Fujinaga, J., Tang, X.B. and Casey, J.R. (1999) Topology of the membrane domain of human erythrocyte anion exchange protein, AE1. *J. Biol. Chem.* **274**: 6626-6633.

50. Tang, X.B., Kovacs, M., Sterling, D. and Casey, J.R. (1999) Identification of residues lining the translocation pore of human AE1 plasma membrane anion exchange protein. *J. Biol. Chem.* **274**: 3557-3564.

51. Huang, Y., Lemieux, M.J., Song, J., Auer, M. and Wang, D.N. (2003) Structure and mechanism of the glycerol-3-phosphate transporter from *Escherichia coli*. *Science* **301**:616-620.

52. Elliott, D.J., Neale, E.J., Aziz, Q., Dunham, J.P., Munsey, T.S., Hunter, M. and Sivaprasadarao, A. (2004) Molecular mechanism of voltage sensor movements in a potassium channel. *EMBO J*. **23**:4717-4726.

53. Neale, E.J., Rong, H., Cockcroft, C.J. and Sivaprasadarao, A. (2007) Mapping the membrane-aqueous border for the voltage-sensing domain of a potassium channel. *J. Biol. Chem*. **282**:37597-37604 .

54. Wu, J.H. and Kaback, H.R. (1996) A general method for determining helix packing in membrane proteins *in situ* – helices I and II are close to helix VII in the lactose permease of *Escherichia coli*. *Proc. Natl. Acad. Sci. USA* **93**:14498-14502.

55. Neale, E.J., Elliott, D.J.S., Hunter, M. and Sivaprasadarao, A. (2003) Evidence for intersubunit interactions between S4 and S5 transmembrane segments of the shaker potassium channel. *J. Biol. Chem*. **278**:29079-29085.

56. Sun, J.Z. and Kaback H.R. (1997) Proximity of periplasmic loops in the lactose permease of *Escherichia coli* determined by site-directed cross-linking. *Biochem.* **36**:11959-11965.

57. Cha, A., Snyder, G.E., Selvin, P.R. and Bezanilla, F. (1999) Atomic scale movement of the voltage-sensing region in a potassium channel measure via spectroscopy. *Nature* **402**:809-813.

58. Koch, H.P. and Larsson, H.P. (2005) Small-scale molecular motions accomplish glutamate uptake in human glutamate transporters. *J. Neurosci.* **25**:1730-1736.

59. Soragna, A., Bossi, E., Giovannardi, S., Pisani, R. and Peres, A. (2005) Functionally independent subunits in the oligomeric structure of the GABA cotransporter rGAT1. *Cell Mol Life Sci* **62**:2877-2885.

60. Bossi, E., Soragna, A., Miszner, A., Giovannardi, S., Frangione, V. and Peres, A. (2007) Oligomeric structure of the neutral amino acid transporters KAAT1 and CAATCH1. *Am J Physiol Cell Physiol* **292**:C1379-1387.

61. Pedersen, M., Carmosino, M. and Forbush, B. (2008) Intramolecular and intermolecular fluorescence resonance energy transfer in fluorescent protein-tagged Na-K-Cl cotransporter (NKCC1). Sensitivity to regulatory conformational change and cell volume. *J Biol Chem* **283**:2663-2674.

62. Posson, D. J. and Selvin, P. R. (2008) Extent of voltage sensor movement during gating of Shaker K^+ channels. *Neuron* **59**:98-109.

63. Loo, D. D., Hirayama B. A., Gallardo E. M., Lam J. T., Turk E., and Wright E. M. (1998) Conformational changes couple Na^+ and glucose transport. *Proc Nat. Acad Sci USA* **95**:7789–7794.

64. Larsson H.P., Tzingounis A. V., Koch H. P., and Kavanaugh M. P. (2004) Fluorometric measurements of conformational changes in glutamate transporters. *Proc Nat. Acad Sci USA* **101**:3951-3956.

65. Gagnon D. G., Frindel C., and Lapointe J. Y. (2007) Voltage-clamp fluorometry in the local environment of the Na^+/glucose cotransporter. *Biophys J* **92**:2403-2411.

Appendix 1:

Conserved glutamate residues are critically involved in Na^+/nucleoside cotransport by human concentrative nucleoside transporter 1 (hCNT1)

***** This appendix has been published.

Yao, S. Y. M., Ng, A. M., Slugoski, M. D., Smith, K. M., Mulinta, R., Karpinski, E., Cass, C. E., Baldwin, S. A., and Young, J. D. (2007) Conserved glutamate residues are critically involved in Na^+/nucleoside cotransport by human concentrative nucleoside transporter 1 (hCNT1). *J. Biol. Chem.* **282**: 30607-30617.

THE JOURNAL OF BIOLOGICAL CHEMISTRY VOL. 282, NO. 42, pp. 30607–30617, October 19, 2007

Conserved Glutamate Residues Are Critically Involved in Na^+/Nucleoside Cotransport by Human Concentrative Nucleoside Transporter 1 (hCNT1)*

Received for publication, April 18, 2007, and in revised form, August 16, 2007 Published, JBC Papers in Press, August 17, 2007, DOI 10.1074/jbc.M703285200

Sylvia Y. M. Yao[‡], Amy M. L. Ng[‡], Melissa D. Slugoski[‡1], Kyla M. Smith[‡], Ras Mulinta[‡], Edward Karpinski[‡], Carol E. Cass[§¶2], Stephen A. Baldwin[‖], and James D. Young[‡3]

From the Membrane Protein Research Group, Departments of [‡]Physiology and [§]Oncology, University of Alberta and [¶]Cross Cancer Institute, Edmonton, Alberta T6G 2H7, Canada and the [‖]Astbury Centre for Structural Molecular Biology, Institute of Membrane and Systems Biology, University of Leeds, Leeds LS2 9JT, United Kingdom

Human concentrative nucleoside transporter 1 (hCNT1), the first discovered of three human members of the SLC28 (CNT) protein family, is a Na^+/nucleoside cotransporter with 650 amino acids. The potential functional roles of 10 conserved aspartate and glutamate residues in hCNT1 were investigated by site-directed mutagenesis and heterologous expression in *Xenopus* oocytes. Initially, each of the 10 residues was replaced by the corresponding neutral amino acid (asparagine or glutamine). Five of the resulting mutants showed unchanged Na^+-dependent uridine transport activity (D172N, E338Q, E389Q, E413Q, and D565N) and were not investigated further. Three were retained in intracellular membranes (D482N, E498Q, and E532Q) and thus could not be assessed functionally. The remaining two (E308Q and E322Q) were present in normal quantities at cell surfaces but exhibited low intrinsic transport activities. Charge replacement with the alternate acidic amino acid enabled correct processing of D482E and E498D, but not of E532D, to cell surfaces and also yielded partially functional E308D and E322D. Relative to wild-type hCNT1, only D482E exhibited normal transport kinetics, whereas E308D, E308Q, E322D, E322Q, and E498D displayed increased K_{50}^{Na+} and/or $K_m^{uridine}$ values and diminished V_{max}^{Na+} and $V_{max}^{uridine}$ values. E322Q additionally exhibited uridine-gated uncoupled Na^+ transport. Together, these findings demonstrate roles for Glu-308, Glu-322, and Glu-498 in Na^+/nucleoside cotransport and suggest locations within a common cation/nucleoside translocation pore. Glu-322, the residue having the greatest influence on hCNT1 transport function, exhibited uridine-protected inhibition by *p*-chloromercuriphenyl sulfonate and 2-aminoethyl methanethiosulfonate when converted to cysteine.

Most nucleosides, including nucleoside analogs with antineoplastic and/or antiviral activity, are hydrophilic molecules that require specialized plasma membrane nucleoside transporter (NT)[4] proteins for uptake into or release from cells (1–3). NT-mediated transport is a critical determinant of nucleoside and nucleotide metabolism and, for nucleoside drugs, their pharmacologic actions (3–5). By regulating adenosine availability to cell-surface purinoreceptors, NTs also profoundly affect neurotransmission, vascular tone, and other physiological processes (5, 6). Two structurally unrelated families of integral membrane proteins exist in human and other mammalian cells as follows: the SLC28 concentrative nucleoside transporter (CNT) family, and the SLC29 equilibrative nucleoside transporter (ENT) family (3, 6–8). ENTs are normally present in most, possibly all, cell types (8). CNTs, in contrast, are found predominantly in intestinal and renal epithelia and other specialized cells, suggesting important roles in absorption, secretion, distribution, and elimination of nucleosides and nucleoside drugs (1–4, 6, 7).

In humans (h), hCNT1 and hCNT2 are pyrimidine nucleoside-selective and purine nucleoside-selective, respectively, whereas hCNT3 transports both pyrimidine and purine nucleosides (9–11). Together, these proteins and their orthologs account for the three major concentrative nucleoside transport processes of human and other mammalian cells. Nonmammalian members of the CNT protein family that have been characterized include hfCNT from the ancient marine prevertebrate the Pacific hagfish *Eptatretus stouti* (12), CaCNT from the pathogenic yeast *Candida albicans* (13), CeCNT3 from the nematode *Caenorhabditis elegans* (14), and NupC from the bacterium *Escherichia coli* (15). hCNT1, hCNT2, and hfCNT are predominantly Na^+-coupled nucleoside transporters, whereas hCNT3 can utilize electrochemical gradients of either Na^+ or H^+ to accumulate nucleosides within cells (12, 16–18). CaCNT, CeCNT3, and NupC function exclusively as H^+/nucleoside cotransporters (13–15). Na^+/nucleoside coupling sto-

* This work was supported in part by the National Cancer Institute of Canada, the Canadian Cancer Society, and the Alberta Cancer Board. The costs of publication of this article were defrayed in part by the payment of page charges. This article must therefore be hereby marked "*advertisement*" in accordance with 18 U.S.C. Section 1734 solely to indicate this fact.
[1] Supported by a studentship from the Alberta Heritage Foundation for Medical Research.
[2] Holds a Canada Research Chair in Oncology at the University of Alberta.
[3] Heritage Scientist of the Alberta Heritage Foundation for Medical Research. To whom correspondence and reprint requests should be addressed: Dept. of Physiology, 7-55 Medical Sciences Bldg., University of Alberta, Edmonton, Alberta T6G 2H7, Canada. Tel.: 780-492-5895; Fax: 780-492-7566; E-mail: james.young@ualberta.ca.

[4] The abbreviations used are: NT, nucleoside transporter; CNT, concentrative nucleoside transporter; ENT, equilibrative nucleoside transporter; MTS, methanethiosulfonate; MTSEA, 2-aminoethyl methanethiosulfonate hydrobromide; MTSES, sodium (2-sulfonatoethyl) methanethiosulfonate; MTSET, [(triethylammonium)ethyl] methanethiosulfonate bromide; PCMBS, sodium *p*-chloromercuriphenyl sulfonate; TM, putative transmembrane helix; h, human.

ichiometries are 1:1 for hCNT1 and hCNT2 and 2:1 for hCNT3 and hfCNT (12, 16–19). H^+/nucleoside coupling ratios for hCNT3 and CaCNT are both 1:1 (13, 17–19).

Although considerable progress has been made in molecular studies of ENT proteins (6, 8), studies of structurally and functionally important residues within the CNT protein family are still at an early stage. Topological investigations suggest that hCNT1–3 and other eukaryote CNT family members have a 13 (or possibly 15)-transmembrane helix (TM) architecture, and multiple alignments reveal strong sequence similarities within the C-terminal half of the proteins (20). Prokaryote CNTs lack the first three TMs of their eukaryote counterparts, and functional expression of N-terminally truncated human/rat CNT1 in *Xenopus* oocytes has established that the first three TMs are not required for Na^+-dependent uridine transport activity (20). Consistent with these findings, chimeric studies between hCNT1 and hfCNT (12) and between hCNT1 and hCNT3 (17) have demonstrated that residues involved in Na^+- and H^+-coupling reside in the C-terminal half of the protein.

In hCNT1, two sets of adjacent residues in TM 7 and 8 have been identified (Ser-319/Gln-320 and Ser-353/Leu-354) that, when converted to the corresponding residues in hCNT2, change the nucleoside specificity of the transporter from CNT1-type to CNT2-type (21). Mutation of Ser-319 in TM 7 of hCNT1 to glycine was sufficient to enable transport of purine nucleosides, whereas mutation of the adjacent residue Gln-320 to methionine (which had no effect on its own) augmented this transport. The additional mutation of Ser-353 in TM 8 of hCNT1 to threonine converted S319G/Q320M from broadly selective (CNT3-type) to purine nucleoside-selective (CNT2-type) but with relatively low adenosine transport activity. Further mutation of Leu-354 to valine increased the adenosine transport capability of S319G/Q320M/S353T, producing a full CNT2-type phenotype. Residues in both TMs 7 and 8 therefore play key roles in determining hCNT1/2 nucleoside selectivities. Confirming this, the double TM 8 mutant (S353T/L354V) was recently shown to exhibit a unique uridine-preferring transport phenotype (22). Mutation of Leu-354 alone markedly increased the affinity of the transporter for Na^+ and Li^+, demonstrating that TM 8 also has a role in cation coupling (22).

Although negatively charged amino acid residues play key functional and structural roles in a broad spectrum of mammalian and bacterial cation-coupled transporters (23–33), essentially nothing is known about their roles in CNTs. Using hCNT1 as the template, we report here the consequences of individually mutating 10 aspartate and glutamate residues that are highly conserved in mammalian CNTs. We identified three residues (Glu-308, Glu-322, and Glu-498) with roles in CNT Na^+ and nucleoside binding and translocation.

EXPERIMENTAL PROCEDURES

Site-directed Mutagenesis and DNA Sequencing—hCNT1 cDNA (GenBank™ accession number U62968) in the *Xenopus* expression vector pGEM-HE (34) provided the template for construction of hCNT1 mutants by the oligonucleotide-directed technique (35), using reagents from the QuikChange® site-directed mutagenesis kit (Stratagene) according to the manufacturer's directions. Constructs were sequenced in both directions by *Taq* dye deoxy terminator cycle sequencing to ensure that only the correct mutation had been introduced.

Production of Wild-type and Mutant hCNT1 Proteins in Xenopus Oocytes—hCNT1 cDNAs were transcribed with T7 polymerase and expressed in oocytes of *Xenopus laevis* by standard procedures (36). Healthy defolliculated stage VI oocytes were microinjected with 10 nl of water or 10 nl of water containing RNA transcript (1 ng/nl) and incubated in modified Barth's medium at 18 °C for 72 h prior to the assay of transport activity.

Flux Assays—Transport was traced using $^{14}C/^{3}H$-labeled nucleosides at 1 μCi/ml. Flux measurements were performed at room temperature (20 °C) as described previously (36, 37). Briefly, groups of 12 oocytes were incubated in 200 μl of transport medium containing either 100 mM NaCl or choline chloride and 2 mM KCl, 1 mM $CaCl_2$, 1 mM $MgCl_2$, and 10 mM HEPES, pH 7.5. Unless otherwise indicated, the uridine concentration was 10 μM. At the end of the incubation period, extracellular label was removed by six rapid washes in ice-cold Na^+-free (choline chloride) transport medium, and individual oocytes were dissolved in 1% (w/v) SDS for quantitation of oocyte-associated radioactivity by liquid scintillation counting (LS 6000 IC; Beckman). Initial rates of transport (influx) were determined using an incubation period of 1 min, except for mutants E322Q and E322D, which had low transport activity and required a longer incubation time (5 min) to achieve cellular uptake comparable with that of wild-type hCNT1 and the other mutants. In PCMBS inhibition studies, oocytes were pretreated with PCMBS (0.1 mM) on ice for 30 min and then washed five times with ice-cold transport medium to remove excess organomercurial before the assay of transport activity. Corresponding pretreatment with the MTS reagents MTSEA, MTSES, and MTSET (2.5, 10, and 1 mM, respectively) was performed at room temperature for 5 min. To demonstrate substrate protection, unlabeled uridine (20 mM) was included along with inhibitor during the preincubation step (38). The flux values shown are means ± S.E. of 10–12 oocytes, and each experiment was performed at least twice on different batches of cells. Kinetic (K_m, K_{50}, V_{max}, and Hill coefficient) parameters (±S.E.) were determined using SigmaPlot software (Jandel Scientific). Statistical significance of the reported data sets was evaluated using *t* tests.

Electrophysiology—Steady-state and presteady-state currents were measured using the two-microelectrode voltage clamp as described previously (16).

Na^+/Nucleoside Stoichiometry—Coupling ratios were determined by direct charge/flux measurements (16, 17, 19).

Isolation of Membranes and Immunoblotting—Total membranes (plasma + intracellular membranes) and purified plasma membranes were isolated by centrifugation from groups of 100 oocytes at 4 °C in the presence of protease inhibitors as described previously (39, 40). Colloidal silica (Sigma) was used to increase the gravitational density of plasma membranes and enhance their yield and purity (40). Protein was determined by the bicinchoninic acid protein assay (Pierce) using bovine serum albumin as standard.

For immunoblotting, oocyte membranes (1 μg of plasma membrane protein or total membrane protein) were resolved

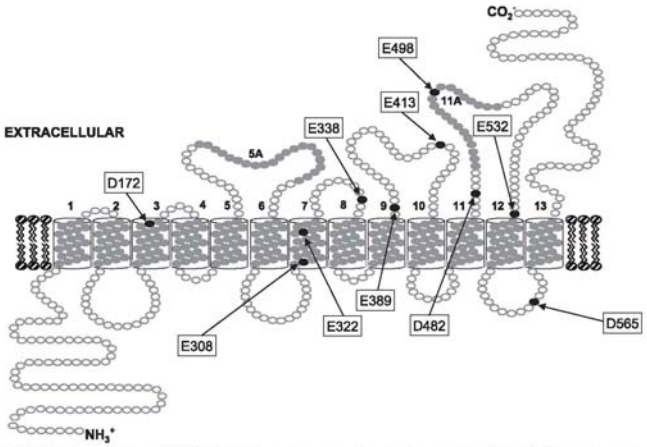

FIGURE 1. **Topological model of hCNT1.** Membrane-spanning α-helices predicted from bioinformatic analyses of currently identified CNT family members are numbered *1–13* (strongly predicted) and *5A* and *11A* (weakly predicted). Highly conserved acidic amino acid residues are indicated with *filled circles*.

TABLE 1

Uridine uptake by wild-type hCNT1 and mutants expressed in *Xenopus* oocytes

Oocytes producing recombinant hCNT1 and hCNT1 mutants were incubated in transport medium with or without Na^+ at 20 °C as described under "Experimental Procedures." Each value is the mean ± S.E. from 10 to 12 oocytes. For influx in the presence of Na^+, significant differences in mediated uridine uptake ($p < 0.05$) compared with wild-type hCNT1 are indicated by *.

	Mediated uridine uptake		Protein expression[a]
	Na^+ medium	Na^+-free medium	
	pmol/oocyte·min^{-1}		
hCNT1	5.0 ± 0.7	0.06 ± 0.01	+
D172N	4.9 ± 0.4	0.12 ± 0.02	ND[b]
E308Q	0.7 ± 0.1*	<0.01	+
E322Q	0.2 ± 0.1*	<0.01	+
E338Q	4.7 ± 0.6	0.03 ± 0.01	ND
E389Q	3.8 ± 0.3	0.05 ± 0.01	ND
E413Q	5.4 ± 0.6	0.07 ± 0.02	ND
D482N	0.1 ± 0.1*	<0.01	−
E498Q	<0.01*	<0.01	−
E532Q	<0.01*	<0.01	−
D565N	5.4 ± 0.5	0.08 ± 0.02	ND

[a] Relative expression in the plasma membrane is from Fig. 3.
[b] ND indicates not determined.

on 12% SDS-polyacrylamide gels (41). The electrophoresed proteins were transferred to polyvinylidene difluoride membranes and probed with affinity-purified anti-hCNT1-(31–55) polyclonal antibodies (22). Blots were then incubated with horseradish peroxidase-conjugated anti-rabbit antibodies (Amersham Biosciences) and developed with enhanced chemiluminescence reagents (Amersham Biosciences).

RESULTS

Residues Identified for Mutagenesis—In this study, we employed site-directed mutagenesis and heterologous expression in *Xenopus* oocytes to analyze the roles of hCNT1 acidic amino acid residues. The locations of the residues selected for study are shown in Fig. 1.

hCNT1 contains 51 aspartate and glutamate residues. Of these, 10 are conserved in other mammalian CNT family members and were included in the present analysis (hCNT1 residues Asp-172, Glu-308, Glu-322, Glu-338, Glu-389, Glu-413, Asp-482, Glu-498, Glu-532, and Asp-565). All but one (Asp-172) were located in the C-terminal half of the protein. In initial mutagenesis experiments, each of the 10 hCNT1 aspartate and glutamate residues were individually replaced by the corresponding neutral amino acids (asparagine or glutamine, respectively). All mutations were verified by sequencing the entire coding region of the double-stranded plasmid DNA in both directions. Except for the desired base changes, all sequences were identical to wild-type hCNT1.

Uridine Uptake and Cell-surface Expression of Wild-type hCNT1 and Mutants—The hCNT1 mutant transporters were expressed in *Xenopus* oocytes and assayed for uridine transport activity (10 μM uridine influx, 1 min fluxes) in the presence and absence of Na^+ as described under "Experimental Procedures." Representative values for mediated uridine uptake, corrected for basal nonmediated uptake in control water-injected oocytes, are presented in Table 1. Five of the mutants (D172N, E338Q, E389Q, E413Q, and D565N) exhibited >75% of wild-type Na^+-dependent transport activity and were not investigated further. In contrast, substitution of Glu-308 reduced transport activity by almost 90%, whereas mutation of E322Q, D482N, E498Q, and E532Q resulted in >99% loss of uridine transport activity. The time course of uridine uptake by wild-type hCNT1 shown in Fig. 2*A* demonstrates that the measured fluxes corresponded to initial rates of transport. Fig. 2*A* also demonstrates the absence of uridine uptake in water-injected oocytes.

Cell-surface expression of mutants E308Q, E322Q, D482N, E498Q, and E532Q was investigated by immunoblotting of purified oocyte plasma membranes using polyclonal antibodies (22) directed against amino acid residues 31–55 at the N terminus of the protein (Fig. 3*A*). Wild-type hCNT1 and transporters with mutations at positions 308 and 322 were present in similar amounts, indicating that these single amino acid substitutions resulted in loss of intrinsic hCNT1 transport activity without altering surface quantities in the oocyte plasma membrane. Antibody specificity was confirmed by lack of immunoreactivity in membranes prepared from control water-injected oocytes. Unlike E308Q and E322Q, very little plasma membrane immunoreactivity was detected for the transporters having mutations at positions 482, 498, and 532, indicating that the lack of transport activity was associated with reduced cell-surface expression.

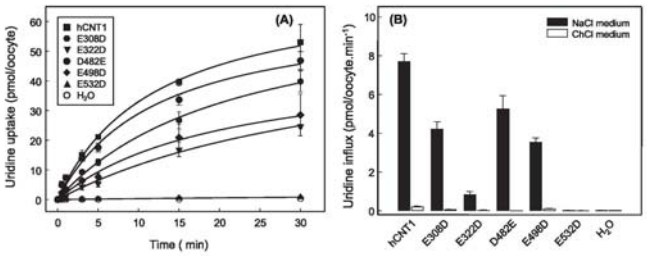

FIGURE 2. **Expression of wild-type hCNT1 and mutants in *Xenopus* oocytes.** Oocytes were injected with 10 ng of RNA transcripts or water alone and incubated for 3 days. *A*, time courses of radiolabeled uridine uptake by wild-type hCNT1 and mutants (10 μM, 20 °C). *B*, initial rates of radiolabeled uridine uptake (10 μM, 20 °C) measured in the presence or absence of Na^+ in the incubation medium. H_2O, control water-injected oocytes. Each value is the mean ± S.E. from 10 to 12 oocytes.

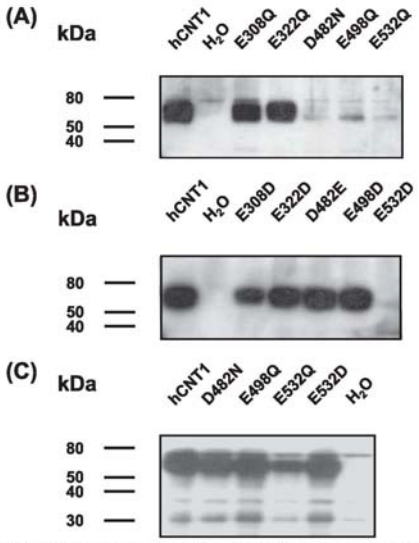

FIGURE 3. **Immunoblot analysis of wild-type hCNT1 and mutants.** Plasma membranes (1 μg of protein) (*A* and *B*) and total membranes (1 μg of protein) (*C*) were obtained from oocytes producing wild-type hCNT1 and hCNT1 mutants. Membranes were subjected to SDS-PAGE and transferred to polyvinylidene difluoride membranes for immunoblotting with anti-hCNT1-(31–55) antibody. The positions of molecular weight standards are shown on the *left*. H_2O, membranes from control water-injected oocytes. *Blots A–C* are from different gels.

In a second round of mutagenesis experiments, Glu-308, Glu-322, Asp-482, Glu-498, and Glu-532 of hCNT1 were replaced by the alternative negatively charged amino acid (*i.e.* glutamate to aspartate or aspartate to glutamate). Time courses of uridine accumulation in the presence of Na^+ and the initial rate of uridine uptake in the presence and absence of Na^+ by E308D, E322D, D482E, E498D, and E532D produced in *Xenopus* oocytes are shown in Fig. 2*A*. Relative to the corresponding asparagine and glutamine mutations (Table 1), oocytes expressing E308D, D482E, or E498D exhibited higher uridine transport activities with fluxes that were broadly similar to those of wild-type hCNT1. E322D, in contrast, displayed only partial transport activity. In all cases, uridine uptake was Na^+-dependent (Fig. 2*B*). Transport was also concentrative because the 15- and 30-min uptake values exceeded the initial extracellular uridine concentration of 10 μM (Fig. 2*A*), assuming an intracellular water volume of 1 μl (36, 37). Immunological analysis revealed that low activity E322D was present in normal quantities at the cell surfaces (Fig. 3*B*), demonstrating that its low transport activity was not because of defective insertion and/or stability of the transporter in oocyte plasma membranes. Unlike the other positions, hCNT1 with Glu-532 substituted by aspartate (E532D) lacked functional activity (Fig. 2, *A* and *B*) and remained undetectable at the cell surface by immunoblotting (Fig. 3*B*). The immunoblots shown in Fig. 3*C* demonstrated that oocyte total membranes (plasma + intracellular membranes) contained mutants D482N, E498Q, E532Q, and E532D, indicating that the "no activity" mutants were present within cells, confirming improper targeting to the plasma membrane.

Kinetic Characterization of Wild-type hCNT1 and Mutants—To further elucidate the effects of individual replacement of amino acids Glu-308, Glu-322, Asp-482, and Glu-498 on hCNT1 transport function, mutants E308D, E308Q, E322D, E322Q, D482E, E498D, and wild-type hCNT1 were characterized for Na^+ activation and uridine concentration dependence kinetics. Na^+ activation was investigated by measuring 10 μM uridine influx as a function of Na^+ concentration (Fig. 4), whereas the concentration dependence of uridine uptake was determined at a saturating concentration (100 mM) of Na^+ (Fig. 5). Kinetic parameters derived from these data, including measures of apparent Na^+ affinities (K_{50}^{Na+}), apparent uridine affinities ($K_m^{uridine}$), and maximal rates of transport (V_{max}^{Na+} and $V_{max}^{uridine}$) are summarized in Table 2.

In agreement with previous studies (16, 18), the rate of uridine transport by oocytes expressing wild-type hCNT1 increased markedly as the Na^+ concentration was increased from 0 to 100 mM and was essentially saturated at Na^+ concentrations above 40 mM. In contrast, rates of uridine transport by oocytes producing E308Q, E322D, or E322Q did not reach saturation, even at the highest concentration of Na^+ (100 mM) (Fig. 4). Hill-type analysis of the data yielded an apparent K_{50}^{Na+} value of 8.2 mM for wild-type hCNT1 compared with 20 mM for E308D and >40 mM for E308Q, E322D, and E322Q. E308Q, E322D, and E322Q also showed major reductions in V_{max}^{Na+} values (<1 pmol/oocyte·min^{-1}, compared with 5.6 pmol/oocyte·min^{-1} for wild-type hCNT1). V_{max}^{Na+}:K_{50}^{Na+} ratios (a measure of transport efficiency) were 0.68 for wild-type hCNT1, 0.17 for E308D, and <0.03 for E308Q, E322D, and

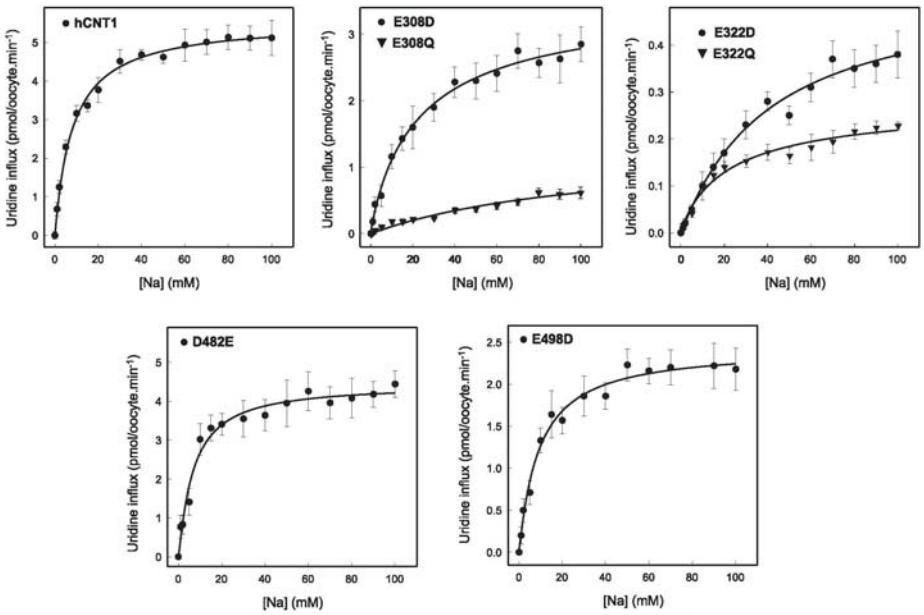

FIGURE 4. **Sodium activation kinetics of wild-type hCNT1 and mutants.** Initial rates of transporter-mediated radiolabeled uridine uptake (10 μM, 20 °C) were measured in transport media containing 0–100 mM NaCl, using choline chloride to maintain isosmolality. Each value is the mean ± S.E. from 10 to 12 oocytes. Mediated transport was calculated as uptake in RNA-injected oocytes *minus* uptake in oocytes injected with water alone. Kinetic parameters derived from the data are presented in Table 2.

E322Q. In the absence of Na^+, uridine uptake by all mutants was close to zero, indicating an absence of measurable slippage (uncoupled, Na^+-independent uridine uptake). As also shown in Fig. 4 and summarized in Table 2, D482E and E498D exhibited Na^+ activation kinetics broadly similar to those of wild-type hCNT1. In the case of E498D, however, there was a noticeable reduction in the V_{max}^{Na+} values (2.5 pmol/oocyte·min^{-1}), leading to a corresponding decrease in the V_{max}^{Na+}:K_{50}^{Na+} ratio (0.26). Where measurable (hCNT1, E308D, D482E, and E498D), Hill coefficients were consistent with a Na^+:uridine coupling ratio of 1:1 (16, 18, 19).

To minimize the potential effects of altered Na^+ apparent affinity on uridine kinetic parameters, experiments to investigate uridine transport kinetics were undertaken at the maximum possible Na^+ concentration of 100 mM. As shown in Fig. 5 and summarized in Table 2, only D482E exhibited uridine transport kinetics similar to those of wild-type hCNT1 ($K_m^{uridine}$ 26 and 29 μM, $V_{max}^{uridine}$ 18 and 19 pmol/oocyte·min^{-1}, and $V_{max}^{uridine}$:$K_m^{uridine}$ ratios 0.69 and 0.66, respectively). All other mutants exhibited reduced apparent affinities for uridine and/or decreases in $V_{max}^{uridine}$ values. Mutants with increased $K_m^{uridine}$ values were E308D (108 μM), E308Q (46 μM), E322Q (79 μM), and E498D (64 μM), and dramatic reductions in $V_{max}^{uridine}$ values were seen for E308Q, E322D, and E322Q (3.8, 1.8 ,and 1.2 pmol/oocyte·min^{-1}, respectively). Compared with a value of 0.66 for wild-type hCNT1, $V_{max}^{uridine}$:$K_m^{uridine}$ ratios ranged from 0.18 and 0.25 for E308D and E498D, respectively, to 0.08, 0.06, and 0.02 for E308Q, E322D, and E322Q, respectively. The nucleoside selectivities of E308D, E322D, D482E, and E498D were identical to wild-type hCNT1 (Table 3).

Electrophysiological Characterization of Wild-type hCNT1 and Mutants—In steady-state electrophysiological experiments (16), all mutants (E308D, E308Q, E322D, E322Q, D482E, and E498D) were confirmed to mediate uridine-induced Na^+ inward currents (Fig. 6*A*). No currents were detected in the absence of Na^+ or in control water-injected oocytes. Measured in the same batch of oocytes on the same day, there was excellent correlation between the magnitudes of the currents recorded and the corresponding Na^+-dependent fluxes of radiolabeled uridine (Fig. 6*B*). The one exception was mutant E322Q, which exhibited an elevated uridine-induced Na^+ current disproportionate to its very low Na^+-dependent uridine transport activity (compare, for example, E322D and E322Q in Fig. 6, *A* and *B*).

In parallel presteady-state electrophysiological experiments performed in the absence of uridine, oocytes producing wild-type hCNT1 and mutants E308D, E308Q, E322D, and E322Q

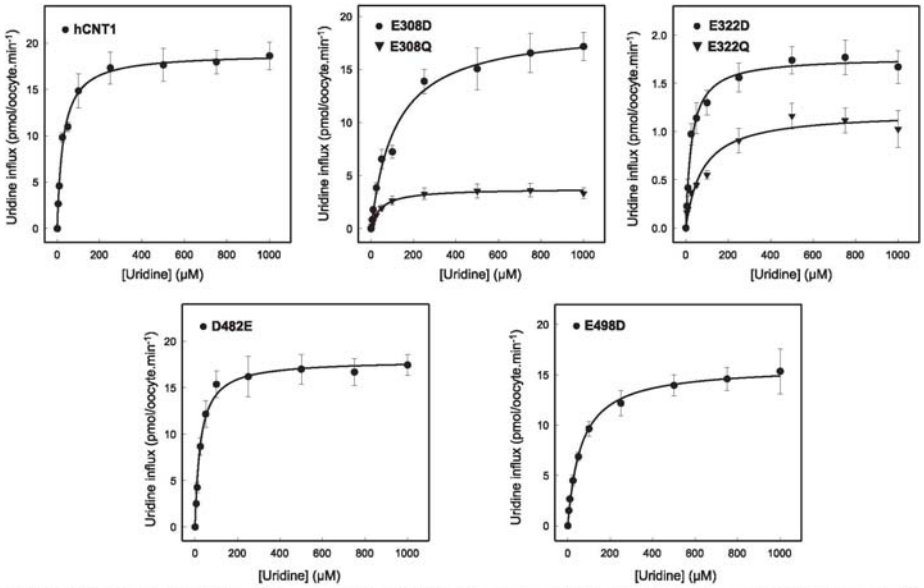

FIGURE 5. **Uridine kinetics of wild-type hCNT1 and mutants.** Initial rates of transporter-mediated radiolabeled uridine uptake (20 °C) were measured in transport medium containing 100 mM NaCl. Each value is the mean ± S.E. from 10 to 12 oocytes. Mediated transport was calculated as uptake in RNA-injected oocytes *minus* uptake in oocytes injected with water alone. Kinetic parameters derived from the data are presented in Table 2.

TABLE 2

Kinetic properties of wild-type hCNT1 and mutants

Significant differences in kinetic parameters ($p < 0.05$) compared with wild-type hCNT1 are indicated by *.

	Na^+ activation[a]				Uridine kinetics[b]		
	K_{50}^{Na+}	V_{max}^{Na+}	Hill coefficient	$V_{max}^{Na+}:K_{50}^{Na+}$ ratio	$K_m^{uridine}$	$V_{max}^{uridine}$	$V_{max}^{uridine}:K_m^{uridine}$ ratio
	mM	pmol/oocyte·min^{-1}			μM	pmol/oocyte·min^{-1}	
hCNT1	8.2 ± 0.1	5.6 ± 0.1	0.8 ± 0.1	0.68	29 ± 3	19 ± 1	0.66
E308D	20 ± 2*	3.3 ± 0.1*	1.2 ± 0.1	0.17	108 ± 12*	19 ± 1	0.18
E308Q	>40*	<1*		<0.03	46 ± 4*	3.8 ± 0.1*	0.08
E322D	>40*	<1*		<0.03	28 ± 3	1.8 ± 0.1*	0.06
E322Q	>40*	<1*		<0.03	79 ± 18*	1.2 ± 0.1*	0.02
D482E	7.2 ± 1.0	4.6 ± 0.2	0.8 ± 0.1	0.64	26 ± 2	18 ± 1	0.69
E498D	9.5 ± 1.1	2.5 ± 0.1*	0.9 ± 0.1	0.26	64 ± 4*	16 ± 1	0.25

[a] Data are from Fig. 4.
[b] Data are from Fig. 5.

were voltage-clamped at a holding potential (V_h) of −50 mV, and presteady-state currents were activated by voltage steps to a series of test potentials (V_t) (Fig. 7, *A* and *B*). In agreement with previous studies (16), current relaxations that were largely eliminated upon removal of external Na^+ were observed for wild-type hCNT1. Presteady-state currents were greatly reduced in mutant E322D and absent from mutants E308Q, E308D, E322Q, and control water-injected oocytes.

Na^+:Nucleoside Coupling Ratios of Wild-type hCNT1 and Mutants—The Na^+/uridine coupling stoichiometries of wild-type hCNT1 and mutants E308Q and E322Q were determined by simultaneously measuring Na^+ currents and radiolabeled uridine uptake under voltage-clamp conditions. The linear correlations between integrated uridine-dependent charge and radiolabeled uridine accumulation measured in Na^+-containing transport medium (100 mM) gave calculated Na^+/nucleoside coupling ratios of 0.88 ± 0.06 and 0.82 ± 0.03 for hCNT1 and E308Q, respectively (Fig. 8, *A* and *B*). Consistent with E322Q functioning as a partially uncoupled uridine-gated Na^+ channel, there was no correlation between Na^+ current and radiolabeled uridine uptake, charge:flux ratios for individual E322Q-producing oocytes ranging from 5 to 74 (Fig. 8*C*).

PCMBS and MTS Inhibition of Uridine Transport by Wild-type hCNT1 and Mutants—Residues lining the translocation pore can be identified through the use of hydrophilic thiol-reactive reagents such as *p*-chloromercuribenzene sulfonate

TABLE 3

Nucleoside uptake by wild-type hCNT1 and mutants expressed in *Xenopus* oocytes

Oocytes producing recombinant hCNT1 and hCNT1 mutants were incubated with different radiolabeled nucleosides (10 μM) in NaCl transport medium at 20 °C as described under "Experimental Procedures." Each value is corrected for basal uptake in control water-injected oocytes and is the mean ± S.E. from 10 to 12 oocytes. Significant differences in mediated nucleoside uptake ($p < 0.05$) compared with wild-type hCNT1 are indicated by *. To permit a side-by-side comparison of pyrimidine and purine nucleoside uptake, all fluxes were determined using a 5-min incubation interval.

	Mediated uptake					
	Uridine	Cytidine	Thymidine	Adenosine	Guanosine	Inosine
	pmol/oocyte·5 min^{-1}					
hCNT1	9.6 ± 0.1	4.0 ± 0.3	5.6 ± 0.7	0.14 ± 0.06	<0.01	<0.01
E308D	6.2 ± 1.1*	2.2 ± 0.3*	5.0 ± 0.5	0.20 ± 0.13	<0.01	<0.01
E322D	1.2 ± 0.2*	0.2 ± 0.02*	1.3 ± 0.2*	0.13 ± 0.08	<0.01	<0.01
D482E	12 ± 1	4.6 ± 0.9	7.4 ± 0.8	0.16 ± 0.03	<0.01	<0.01
E498D	7.6 ± 0.7	3.1 ± 0.4	4.1 ± 0.4	0.05 ± 0.02	<0.01	<0.01

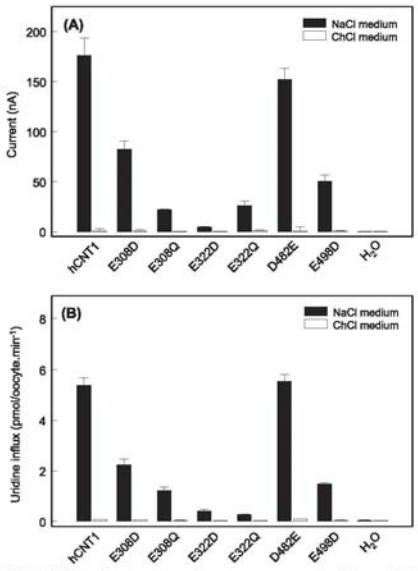

FIGURE 6. **Uridine-induced steady-state currents of wild-type hCNT1 and mutants.** Oocytes were injected with 10 ng of RNA transcripts or water alone and incubated for 3 days. *A*, averaged inward currents in hCNT1- and mutant-producing oocytes perfused with 1 mM uridine in the presence or absence of 100 mM Na^+ in the incubation medium. Each value is the mean ± S.E. from five oocytes. No currents were observed in control water-injected oocytes. *B*, initial rates of radiolabeled uridine uptake (10 μM, 20 °C) measured in the presence or absence of 100 mM Na^+ in the incubation medium. H_2O, control water-injected oocytes. Each value is the mean ± S.E. from 10 to 12 oocytes.

(PCMBS) and methanethiosulfonate (MTS) derivatives (22, 38, 42–45). Thus, a final series of mutagenesis experiments was undertaken in which hCNT1 acidic amino acid residues Glu-308, Glu-322, Asp-482, Glu-498, and Glu-532 were individually replaced by cysteine. Consistent with our other studies of these positions, substitution of Asp-482, Glu-498, and Glu-532 with cysteine yielded transporters that were nonfunctional in oocytes (data not shown) and could not be investigated further. Relative to wild-type hCNT1, however, mutants E308C and E322C showed reduced but measurable influx of uridine (Fig. 9*A*). Both were present in oocyte plasma membranes in amounts similar to those of wild-type hCNT1 (Fig. 9*B*). Although wild-type hCNT1 contains 20 endogenous cysteine residues, and consistent with results of previous studies (38), there was no change in hCNT1-mediated uridine uptake following incubation with membrane-impermeant PCMBS at a concentration of 0.1 mM (Fig. 9*A*). PCMBS exposure also had no measurable effect on E308C transport activity. In contrast, uridine uptake by E322C was strongly inhibited by PCMBS, and the presence of extracellular uridine (20 mM) protected the transporter against this inhibition (Fig. 9*A*).

Fig. 10 extends this analysis by showing the corresponding inhibitory effects of three MTS reagents with different sizes (MTSEA < MTSES < MTSET), charges (MTSEA and MTSES, negatively charged; MTSET, positively charged), and membrane permeabilities (MTSEA, membrane-permeable; MTSES and MTSET, membrane-impermeable). Reflecting their different reactivities with thiol groups, MTSEA, MTSES, and MTSET were tested on wild-type hCNT1 and mutants E308C and E322C at concentrations of 2.5, 10, and 1 mM, respectively. Only MTSEA gave significant inhibition, and only E322C was affected (Fig. 10*A*). Like PCMBS, addition of uridine (20 mM) to the extracellular medium protected E322C against MTSEA inhibition (Fig. 10*B*).

DISCUSSION

As shown in Fig. 1 for hCNT1, current models of hCNT topology have 13 putative TMs (9–11, 20). Computer algorithms also weakly predict two additional potential transmembrane regions, designated in Fig. 1 as TMs *5A* and *11A* (20). Location of the N and C termini as intracellular and extracellular, respectively, derives from immunocytochemical experiments with site-specific antibodies, and from studies of native and introduced glycosylation sites (20). Cytoplasmic exposure of the loop linking TMs 4 and 5 has been similarly confirmed (20). Both a 13 TM and 15 TM membrane architecture are consistent with these landmarks. Initial substituted cysteine accessibility method analyses of TMs 11, 12, and 13 of a functional cysteine-free version of a human CNT3 (hCNT3C−) using MTS reagents (46), as well as other published structure/function studies (*e.g.* 21, 22), are also consistent with both models. TMs 1–3 of human and rat CNT1 are not required for Na^+-dependent uridine transport activity (20).

The present study identified five conserved acidic amino acid residues of Na^+/nucleoside cotransporter hCNT1 (Glu-308,

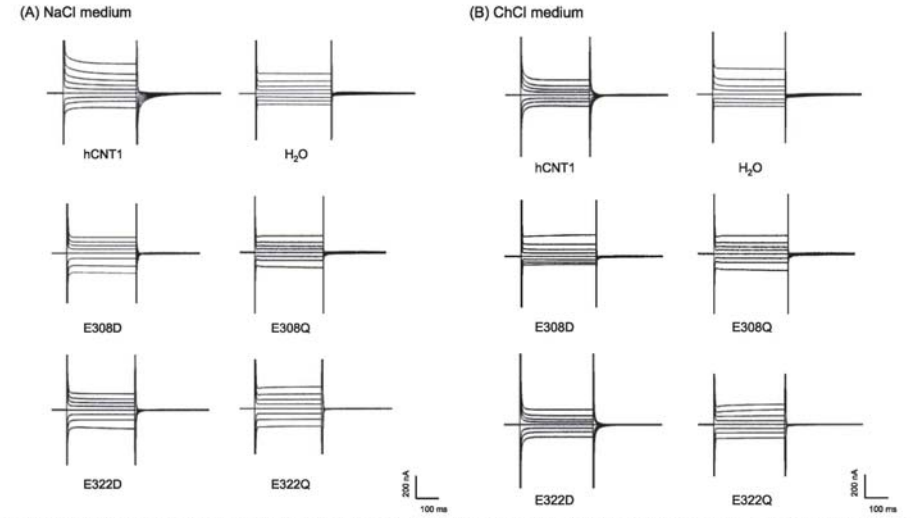

FIGURE 7. **Wild-type hCNT1 and mutant presteady-state currents elicited by voltage pulse.** The oocyte membrane was held at a holding potential (V_h) of −50 mV and stepped to a range of test potentials (V_t) from −125 to +50 mM (25-mV increments). *A*, NaCl transport medium; *B*, choline chloride transport medium.

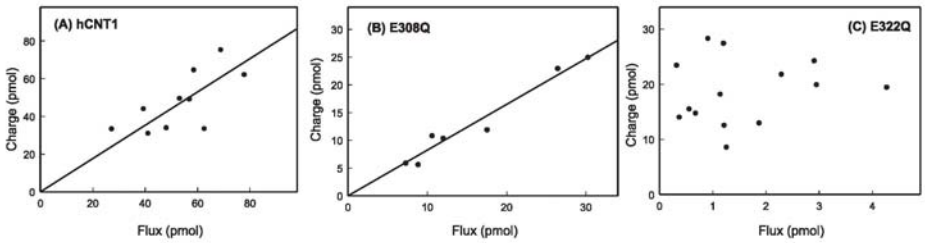

FIGURE 8. **Stoichiometry of wild-type hCNT1, E308Q, and E322Q.** Oocytes were clamped at V_h of −50 mV and perfused with 200 μM [^{3}H]uridine. Integration of the uridine-evoked current over the uptake period (1 min) yielded the charge moved, which was converted to picomoles and plotted against radiolabeled uridine uptake (pmol) in the same oocyte. The experiment was performed in 10, 7, and 14 individual oocytes for wild-type hCNT1 (*A*), E308Q (*B*), and E322Q (*C*), respectively. Nucleoside-induced current was obtained as the difference between base-line current and the inward nucleoside-induced current. Radiolabeled fluxes were corrected for basal nonmediated uridine uptake in oocytes injected with water alone. The slope (± S.E.) of the linear fits (Na^+ /nucleoside coupling ratio) for wild-type hCNT1 and mutant E308Q are indicated by the *straight lines*.

Glu-322, Asp-482, Glu-498, and Glu-532) whose mutation to the corresponding neutral amino acid (glutamine or asparagine) dramatically reduced transport activity of the recombinant protein produced in *Xenopus* oocytes. All are situated in the C-terminal half of the protein, a region previously implicated in both nucleoside and cation translocation (12, 17, 21). Glu-308 and Glu-322 are located in predicted TM 7; Asp-482 is adjacent to the extracellular face of TM 11; Glu-498 is located in the middle of TM11A; and Glu-532 is on the extracellular boundary of TM 12 (Fig. 1). Although TM 7 mutants E308Q and E322Q targeted normally to cell surfaces, their impaired intrinsic transport activities suggested key roles for both glutamate residues in hCNT1-mediated transport. D482N, E498Q, and E532Q, in contrast, were retained in intracellular membranes. Mutant E532D, in which the negative charge of Glu-532 was replaced with aspartate, was also retained in intracellular membranes, implying an absolute requirement of this glutamate residue to achieve normal cell-surface levels. The predicted location of Glu-532 on the immediate extramembranous surface of TM 12 (Fig. 1) suggests that it may be necessary for the anchoring and/or correct membrane configuration of this TM. Replacement of Asp-482 with glutamate, and Glu-498 with aspartate, in contrast, yielded normal processing to cell surfaces and resulted in uridine fluxes broadly similar to those of wild-type hCNT1. The functional activities of TM 7 mutants E308Q and E322Q were also partially restored by replacement

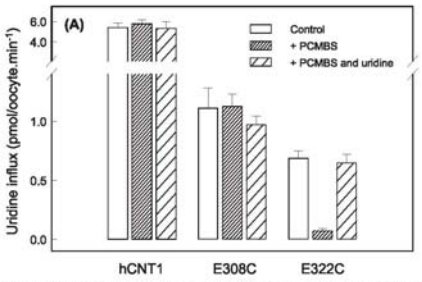

FIGURE 9. **PCMBS inhibition of wild-type hCNT1, E308C, and E322C.** *A*, oocytes producing wild-type hCNT1 or mutants E308C or E322C were incubated with or without PCMBS (0.1 mM) in NaCl transport medium at 1 °C in the absence or presence of unlabeled uridine (20 mM). After 30 min, excess PCMBS and uridine were removed by washing in ice-cold medium. Initial rates of uridine uptake were then determined (10 μM) at 20 °C. Each value is the mean ± S.E. from 10 to 12 oocytes and was corrected by subtraction of the corresponding basal uptake value in control water-injected oocytes. *B*, immunoblot analysis of plasma membranes (1 μg of protein) from oocytes producing wild-type hCNT1, E308C, or E322C. Plasma membranes were subjected to SDS-PAGE and transferred to polyvinylidene difluoride membranes for immunoblotting with anti-hCNT1-(31–55) antibodies. The positions of molecular weight standards are shown on the *left*. H_2O, membranes from control water-injected oocytes.

of Glu-308 and Glu-322 with aspartate. Because E532Q failed to translocate to cell surfaces, it was not possible to investigate its functional properties. Subsequent kinetic experiments therefore focused on mutants E308D, E308Q, E322D, E322Q, D482E, and E498D.

Residues Asp-482 and Glu-498—Relative to wild-type hCNT1, replacement of Asp-482 with glutamate (mutant D482E) resulted in no change in V_{max}^{Na+}, $V_{max}^{uridine}$, K_{50}^{Na+}, or $K_m^{uridine}$, indicating that this residue is unlikely to have a mechanistic role in hCNT1 Na^+/nucleoside cotransport. Mutation of Glu-498 to aspartate (mutant E498D), however, led to a >50% reduction in V_{max}^{Na+} and an almost 2-fold increase in the $K_m^{uridine}$ value such that both the V_{max}^{Na+}:K_{50}^{Na+} and $V_{max}^{uridine}$:$K_m^{uridine}$ ratios were reduced relative to those of wild-type hCNT1. Although substitution of Glu-498 with glutamine would be predicted to exhibit more marked changes in transport function, mutant E498Q was not processed to cell surfaces and thus could not be characterized. Consistent with a key role for Glu-498, it is centrally positioned in the most highly conserved sequence motif in the entire CNT family (G/A)XKX_3NEFVA(Y/M/F). Mutation of Glu-519, the residue in hCNT3 that corresponds to hCNT1 Glu-498, impaired both the Na^+/nucleoside and H^+/nucleoside transport activities of the transporter.[5]

As illustrated in Fig. 1, Glu-498 and the conserved motif of which it is a part are located in a region of the protein that is potentially exofacial (in the loop linking TMs 11 and 12) or membrane-associated (TM 11A). The functional significance of Glu-498 revealed by this study favors the latter possibility. If TM 11A is transmembrane (as opposed to a re-entrant loop), there is the likelihood that the TM 5A region is also transmembrane (to preserve the experimentally determined endofacial and exofacial locations of the N and C termini of the protein, respectively). A consequence of this is that the central TM 6–11 region of the protein may be in an orientation opposite to that shown in Fig. 1 (please see below).

Residues Glu-308 and Glu-322—Effects on hCNT1 transport kinetics were also apparent by mutation of Glu-308 and Glu-322. In the presence of a saturating concentration of Na^+, substitution of Glu-308 by aspartate (mutant E308D) resulted in an almost 4-fold increase in $K_m^{uridine}$ with no change in $V_{max}^{uridine}$. A 3-fold increase in K_{50}^{Na+} combined with a modest reduction in V_{max}^{Na+} was also observed. Therefore, both V_{max}^{Na+}:K_{50}^{Na+} and $V_{max}^{uridine}$:$K_m^{uridine}$ ratios of the transporter were affected. More pronounced kinetic effects were apparent for E308Q and E322D/E322Q, a consistent feature of these mutants being a dramatic reduction in apparent affinities for Na^+ (increase in K_{50}^{Na+}) as well as V_{max}^{Na+} and $V_{max}^{uridine}$ values. Two of the mutants (E308Q and E322Q) also exhibited reductions in apparent affinities for uridine (increase in $K_m^{uridine}$). As a result, V_{max}^{Na+}:K_{50}^{Na+} and $V_{max}^{uridine}$:$K_m^{uridine}$ ratios were severely compromised, indicating critical roles for Glu-308 and Glu-322 in cation and nucleoside binding and/or translocation. Because removal of the carboxylate groups at these positions (mutants E308Q and E322Q) still allowed residual Na^+-dependent uridine transport activity, albeit with very low kinetic efficiency, electrostatic interactions involving Glu-308 and Glu-322 must not in themselves be obligatory for function.

Similar to the proposed roles of Asp-187 in the *E. coli* PutP Na^+/proline transporter (27), Glu-269 and Glu-325 of *E. coli* LacY H^+-coupled lactose permease (24, 25, 47), and Asp-369 and Asp-404 of the *Aquifex aeolicus* $LeuT_{Aa}$ Na^+/Cl^--dependent leucine transporter (48), the profound and complementary effects of hCNT1 Glu-308 and Glu-322 mutations on both V_{max}^{Na+} and $V_{max}^{uridine}$ values suggest that these residues may facilitate conformational transitions within the Na^+/nucleoside transport cycle. As indicated by the observed effects of Glu-308 and Glu-322 mutations on binding affinities for Na^+ and uridine, secondary roles in cation and nucleoside binding are also possible. Examples where this occurs in other transporters include Asp-55 of PutP (26), and glutamate and aspartate residues in the *E. coli* MelB Na^+/melibiose and GlpT glycerol 3-phosphate transporters (23, 49), the mammalian NaDC-1 Na^+/dicarboxylate transporter (28), the Na^+/H^+-coupled EAAC1 glutamate transporter (30), the NHE1 Na^+/H^+ exchanger (31), and the Na^+/Cl^--dependent dopamine transporter (32). As hypothesized for Glu-325 of LacY (33), individual acidic amino residues can accommodate interrelated functions in both conformational transitions and cation/solute binding. The functional consequence of removal of the carboxyl group of LacY Glu-325 is a reduction in the lactose

[5] S. Y. M. Yao, A. M. L. Ng, M. D. Slugoski, K. M. Smith, R. Mulinta, E. Karpinski, C. E. Cass, S. A. Baldwin, and J. D. Young, unpublished observations.

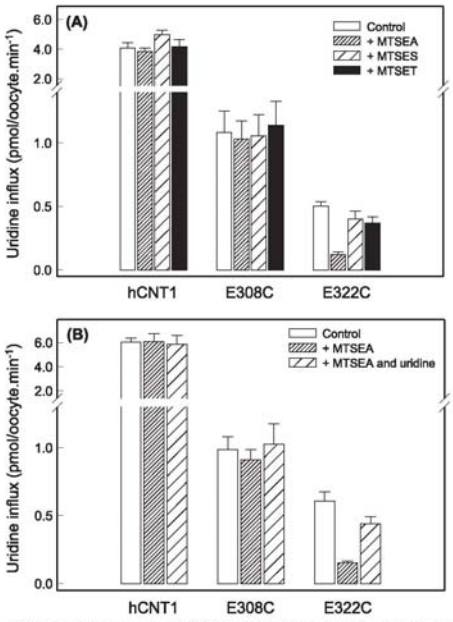

FIGURE 10. **MTS reagent inhibition of wild-type hCNT1, E308C, and E322C.** *A*, oocytes producing wild-type hCNT1 or mutants E308C or E322C were incubated with or without MTSEA (2.5 mM), MTSES (10 mM), or MTSET (1 mM) in NaCl transport medium at 20 °C. After 5 min, excess MTS reagents were removed by washing in ice-cold medium. Initial rates of uridine uptake were then determined (10 μM) at 20 °C. *B*, protection from MTSEA inhibition by uridine. Oocytes producing wild-type hCNT1 or mutants E308C or E322C were incubated with or without MTSEA (2.5 mM) in NaCl transport medium at 20 °C in the absence or presence of unlabeled uridine (20 mM). After 5 min, excess MTSEA and uridine were removed by washing in ice-cold medium. Initial rates of uridine uptake were then determined (10 μM) at 20 °C. Each value is the mean ± S.E. from 10 to 12 oocytes and was corrected by subtraction of the corresponding basal uptake value in control water-injected oocytes.

transport V_{max}:K_m ratio with the major effect on V_{max} (50), a kinetic outcome similar to that seen here for mutation of hCNT1 residues Glu-308 and Glu-322.

Mutant E308Q retained the wild-type Na^+/nucleoside coupling ratio of 1:1. In addition to possessing low level Na^+-dependent uridine transport activity, however, and different from E308Q, mutant E322Q also exhibited features consistent with uncoupled Na^+ transport. This was manifest by disproportionately high uridine-induced Na^+ currents causing variable Na^+/nucleoside charge:flux ratios in excess of the expected wild-type value of 1:1. Residues of other transporters where mutation causes channel-like behavior include Asp-204 of the human SGLT1 and Asn-177 of the rat 5-hydroxytryptamine transporter (51–52).

Glu-308 and Glu-322 are both located on the putative hydrophilic surface of TM 7 (21). This surface also includes the residues Asn-315 and Ser-319 (previously shown to determine

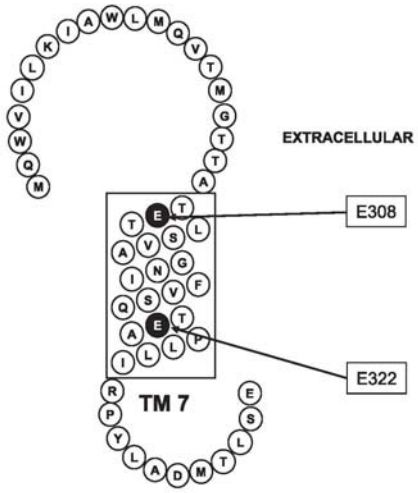

FIGURE 11. **Topological model of TM7 of hCNT1.** Residues Glu-308 and Glu-322 are indicated with *filled circles*. Helix orientation is that predicted by a 15-TM membrane architecture.

hCNT1/2 nucleoside selectivities) (21). The present results further strengthen the functional importance of TM 7 and suggest that the helix face containing these four residues lines a common Na^+/nucleoside translocation pore. TM 8 is also likely to be pore-lining (22). In TM 7, Glu-322 is located close to its extracellular aspect according to the putative 13-TM topology model shown in Fig. 1, but it would be close to its intracellular aspect if TMs 6–11 were in the opposite orientation as predicted by the alternate 15-TM models of hCNT3 topology. When converted to cysteine (mutant E322C), this residue was accessible to membrane-impermeant PCMBS added to the extracellular medium, which resulted in marked transport inhibition that was prevented by externally applied uridine. Supporting the pore-lining location of Glu-322, the corresponding residue in a cysteine-free version of hCNT3 (hCNT3C−) (46), when converted to cysteine, also resulted in PCMBS inhibition of uridine uptake.[5] The smallest of the MTS reagents tested (MTSEA) was also inhibitory against hCNT1 E322C. As with PCMBS, externally applied uridine protected the transporter against MTSEA inhibition. Therefore, Glu-322 evidently lies within the permeant translocation channel in a position with restricted access that is occluded by uridine. Potentially located deep inside the translocation channel in a position within or in close proximity below the uridine binding pocket, this is more consistent with the TM 7 orientation shown in Fig. 11 (15-TM model) than with that in Fig. 1 (13-TM model). Lack of a corresponding effect of PCMBS and MTS reagents on uridine transport by E308C may reflect the more external location of this residue within the translocation vestibule (Fig. 11). Possibly, therefore, Glu-308 and Glu-322 may include parts of the extracellular and internal gates of the transporter, respectively,

a function supported by the channel-like behavior of mutant E322Q revealed by steady-state currents, and by the potential gating function of negatively charged residues within the common cation/solute translocation pore of the recently solved three-dimensional crystal structure of *A. aeolicus* $LeuT_{Aa}$ (48). In the latter protein, negatively charged residues stabilize the transporter in a closed conformation that occludes closely associated Na^+ and leucine-binding sites halfway across the membrane bilayer. Similar to the mammalian GAT1 Na^+/Cl^--dependent γ-aminobutyric acid transporter (53, 54), a member of the same protein family as $LeuT_{Aa}$, hCNT1 (and hCNT3) presteady-state currents largely reflect binding and potential occlusion of extracellular Na^+.[5] Consistent with a gating function for residues Glu-308 and Glu-322, their mutation markedly impaired hCNT1 presteady-state currents.

Conclusions—The present results for hCNT1 suggest close proximity integration of cation/solute binding and transport within a common cation/permeant translocation pore, and reveal important roles for three postulated intramembranous glutamate residues (Glu-308, Glu-322, and Glu-498) in cation/nucleoside translocation. Setting the stage for additional future substituted cysteine accessibility method and other analyses of hCNT structure and function, the findings favor a revised 15-TM model of hCNT1 membrane architecture.

REFERENCES

1. Cass, C. E. (1995) in *Drug Transport in Antimicrobial and Anticancer Chemotherapy* (Georgopapadakou, N. H., ed) pp. 403–451, Marcel Dekker, Inc., New York
2. Griffith, D. A., and Jarvis, S. M. (1996) *Biochim. Biophys. Acta* **1286,** 153–181
3. Young, J. D., Cheeseman, C. I., Mackey, J. R., Cass, C. E., and Baldwin, S. A. (2000) *Curr. Top. Membr.* **50,** 329–378
4. Damaraju, V. L., Damaraju, S., Young, J. D., Baldwin, S. A., Mackey, J., Sawyer, M. B., and Cass, C. E. (2003) *Oncogene* **22,** 7524–7536
5. Latini, S., and Pedata, F. (2001) *J. Neurochem.* **79,** 463–484
6. King, A. E., Ackley, M. A., Cass, C. E., Young, J. D., and Baldwin, S. A. (2006) *Trends Pharmacol. Sci.* **27,** 416–425
7. Gray, J. H., Owen, R. P., and Giacomini, K. M. (2004) *Pfluegers Arch.* **447,** 728–734
8. Baldwin, S. A., Beal, P. R., Yao, S. Y. M., King, A. E., Cass, C. E., and Young, J. D. (2004) *Pfluegers Arch.* **447,** 735–743
9. Ritzel, M. W. L., Yao, S. Y. M., Huang, M. Y., Elliott, J. F., Cass, C. E., and Young, J. D. (1997) *Am. J. Physiol.* **272,** C707–C714
10. Ritzel, M. W. L., Yao, S. Y. M., Ng, A. M. L., Mackey, J. R., Cass, C. E., and Young, J. D. (1998) *Mol. Membr. Biol.* **15,** 203–211
11. Ritzel, M. W. L., Ng, A. M. L., Yao, S. Y. M., Graham, K., Loewen, S. K., Smith, K. M., Ritzel, R. G., Mowles, D. A., Carpenter, P., Chen, X. Z., Karpinski, E., Hyde, R. J., Baldwin, S. A., Cass, C. E., and Young, J. D. (2001) *J. Biol. Chem.* **276,** 2914–2927
12. Yao, S. Y. M., Ng, A. M. L., Loewen, S. K., Cass, C. E., Baldwin, S. A., and Young, J. D. (2002) *Am. J. Physiol.* **283,** C155–C168
13. Loewen, S. K., Ng, A. M. L., Mohabir, N. N., Baldwin, S. A., Cass, C. E., Young, J. D. (2003) *Yeast* **20,** 661–675
14. Xiao, G., Wang, J., Tangen, T., and Giacomini, K. M. (2001) *Mol. Pharmacol.* **59,** 339–348
15. Loewen, S. K., Yao, S. Y. M., Slugoski, M. D., Mohabir, N. N., Turner, R. J., Mackey, J. R., Weiner, J. H., Gallagher, M. P., Henderson, P. J., Baldwin, S. A., Cass, C. E., and Young, J. D. (2004) *Mol. Membr. Biol.* **21,** 1–10
16. Smith, K. M., Ng, A. M. L., Yao, S. Y. M., Labedz, K. A., Knaus, E. E., Wiebe, L. I., Cass, C. E., Baldwin, S. A., Chen, X. Z., Karpinski, E., and Young, J. D. (2004) *J. Physiol. (Lond.)* **558,** 807–823
17. Smith, K. M., Slugoski, M. D., Loewen, S. K., Ng, A. M. L., Yao, S. Y. M., Chen, X.-Z., Karpinski, E., Cass, C. E., Baldwin, S. A., and Young, J. D. (2005) *J. Biol. Chem.* **280,** 25436–25449
18. Ritzel, M. W. L., Ng, A. M. L., Yao, S. Y. M., Graham, K., Loewen, S. K., Smith, K. M., Hyde, R. J., Karpinski, E., Cass, C. E., Baldwin, S. A., and Young, J. D. (2001) *Mol. Membr. Biol.* **18,** 65–72
19. Smith, K. M., Slugoski, M. D., Cass, C. E., Baldwin, S. A., Karpinski, E., and Young, J. D. (2007) *Mol. Membr. Biol.* **24,** 53–64
20. Hamilton, S. R., Yao, S. Y. M., Ingram, J. C., Hadden, D. A., Ritzel, M. W. L., Gallagher, M. P., Henderson, P. J. F., Cass, C. E., Young, J. D., and Baldwin, S. A. (2001) *J. Biol. Chem.* **276,** 27981–27988
21. Loewen, S. K., Ng, A. M. L., Yao, S. Y. M., Cass, C. E., Baldwin, S. A., and Young, J. D. (1999) *J. Biol. Chem.* **274,** 24475–24484
22. Slugoski, M. D., Loewen, S. K., Ng, A. M. L., Smith, K. M., Yao, S. Y. M., Karpinski, E., Cass, C. E., Baldwin, S. A., and Young, J. D. (2007) *Biochemistry* **46,** 1684–1693
23. Pourcher, T., Zani, M. L., and Leblanc, G. (1993) *J. Biol. Chem.* **268,** 3209–3215
24. Franco, P. J., and Brooker, R. J. (1994) *J. Biol. Chem.* **269,** 7379–7386
25. Kaback, H. R. (1997) *Proc. Natl. Acad. Sci. U. S. A.* **94,** 5508–5543
26. Quick, M., and Jung, H. (1997) *Biochemistry* **36,** 4631–4636
27. Quick, M., and Jung, H. (1998) *Biochemistry* **37,** 13800–13806
28. Griffith, D. A., and Pajor, A. M. (1999) *Biochemistry* **38,** 7524–7531
29. Pirch, T., Quick, M., Nietschke, M., Langkamp, M., and Jung, H. (2002) *J. Biol. Chem.* **277,** 8790–8796
30. Grewer, C., Watzke, N., Rauen, T., and Bicho, A. (2003) *J. Biol. Chem.* **278,** 2585–2592
31. Noel, J., Germain, D., and Vadnais, J. (2003) *Biochemistry* **42,** 15361–15368
32. Chen, N., Rickey, J., Berfield, J. L., and Reith, M. E. (2004) *J. Biol. Chem.* **279,** 5508–5519
33. Abramson, J., Smirnova, I., Kasho, V., Verner, G., Kaback, H. R., and Iwata, S. (2003) *Science* **301,** 610–615
34. Liman, E. R., Tytgat, J., and Hess, P. (1992) *Neuron* **9,** 861–871
35. Kirsch, R. D., and Joly, E. (1998) *Nucleic Acids Res.* **26,** 1848–1850
36. Yao, S. Y. M., Cass, C. E., and Young, J. D. (2000) in *Membrane Transport: A Practical Approach* (Baldwin, S. A., ed) pp. 47–78, Oxford University Press, Oxford
37. Huang, Q. Q., Yao, S. Y. M., Ritzel, M. W., Paterson, A. R., Cass, C. E., and Young, J. D. (1994) *J. Biol. Chem.* **269,** 17757–17760
38. Yao, S. Y. M., Sundaram, M., Chomey, E. G., Cass, C. E., Baldwin, S. A., and Young, J. D. (2001) *Biochem. J.* **353,** 387–393
39. Sundaram, M., Yao, S. Y. M., Ingram, J. C., Berry, Z. A., Abidi, F., Cass, C. E., Baldwin, S. A., and Young, J. D. (2001) *J. Biol. Chem.* **276,** 45270–45272
40. Kamsteeg, E.-J., and Deen, P. M. T. (2001) *Biochim. Biophys. Res. Commun.* **282,** 683–690
41. Laemmli, U. K. (1970) *Nature* **227,** 680–685
42. Rothstein, A. (1970) *Curr. Top. Membr. Transp.* **1,** 135–176
43. Yan, R. T., and Maloney, P. C. (1993) *Cell* **75,** 37–44
44. Yan, R. T., and Maloney, P. C. (1995) *Proc. Natl. Acad. Sci. U. S. A.* **92,** 5973–5976
45. Zhu, Q., and Casey, J. R. (2007) *Methods (San Diego)* **41,** 439–450
46. Zhang, J., Tackaberry, B., Ritzel, M. W., Raborn, T., Baldwin, S. A., Young, J. D., and Carol, C. E. (2006) *Biochem. J.* **394,** 389–398
47. Kaback, H. R. (2005) *C. R. Biologies* **328,** 557–567
48. Yamashita, A., Singh, S. K., Kawate, T., Jin, Y., and Gouaux, E. (2005) *Nature* **437,** 215–223
49. Huang, Y., Lemieux, M. J., Song, J., Auer, M., and Wang, D. N. (2003) *Science* **301,** 616–620
50. Weinglass, A. B., Smirnova, I. N., and Kaback, H. R. (2001) *Biochemistry* **40,** 769–776
51. Quick, M., Loo, D. D. F., and Wright, E. M. (2001) *J. Biol. Chem.* **276,** 1728–1734
52. Lin, F., Lester, H. A., and Marger, S. (1996) *Biophys. J.* **71,** 3126–3135
53. Lu, C.-C., and Hilgemann, D. W. (1999) *J. Gen. Physiol.* **114,** 445–457
54. Hilgemann, D. W., and Lu, C.-C. (1999) *J. Gen. Physiol* **114,** 459–475